Improving the buildings envelopes energy performance using aerogel-based insulating mineral rendering

Mohamad Ibrahim

ParisTech
INSTITUT DES SCIENCES ET TECHNOLOGIES
PARIS INSTITUTE OF TECHNOLOGY

MINES ParisTech

École doctorale n° 432 : Sciences et Métiers de l'Ingénieur

Doctorat ParisTech

T H È S E

pour obtenir le grade de docteur délivré par

l'École nationale supérieure des mines de Paris

Spécialité " Énergétique "

présentée et soutenue publiquement par

Mohamad IBRAHIM

Le 19 Décembre 2014

Improving the building envelopes energy performance using aerogel-based insulating mineral rendering

Etude de l'amélioration de la performance énergétique de bâtiments due à l'emploi d'enduit minéral à fort pouvoir isolant

Directeurs de thèse : **Patrick ACHARD et Etienne WURTZ**

Jury

Mme Monika WOLOSZYN, Professeur, Université de Savoie	Rapporteur
M. Olaf ADAN, Professeur, Technische Universiteit Eindhoven	Rapporteur
Mme Evelyne PRAT, Docteur, Directeur R&D, Société Parex Group	Examinateur
M. Daniel QUENARD, Docteur, Responsable Division Enveloppes et Matériaux innovants, CSTB	Examinateur
M. Pascal Henry BIWOLE, Maitre de conférence, Université de Nice Sophia Antipolis	Examinateur
M. Etienne WURTZ, Directeur de Recherche CNRS, CEA/INES	Examinateur
M. Patrick ACHARD, Directeur de Recherche, Mines-ParisTech	Examinateur

T H È S E

MINES ParisTech
Centre Procédés, Energies Renouvelables et Systèmes Energétiques (PERSEE)
1 rue Claude Daunesse, 06904 Sophia Antipolis, France

TO MY FAMILY ...

Acknowledgement

First and foremost, I want to express my sincere gratitude to my advisors Pr. Patrick ACHARD and Pr. Etienne WURTZ for the help and dedicated support during the past three years. It has been an honor to be their Ph.D student. Without their help and encouragement, this work would not have been achieved.

I would like to thank Dr. Pascal H. BIWOLE for all his valuable contribution and for being a member of my thesis committee.

I would also like to express my appreciation and my thanks to Pr. Monika WOLOSZYN, Pr. Olaf ADAN, Dr. Evelyne PRAT, and Dr. Daniel QUENARD for their advice and constructive criticism and for reviewing my thesis as members of my thesis committee.

I would like to acknowledge the support and help of all the colleagues and all the staff members of the PERSEE research center at Mines ParisTech. I would like also to thank all the members at the National Solar Energy Institute (INES) for their help, support, contribution, and valuable discussions. I was really fortunate to have worked in these two professional and friendly environments, Mines ParisTech and INES.

Many thanks to all the partners of PAREX.it project: Parex Group, ARMINES, CEA, LOCIE, CSTB, PCAS, and Wienerberger, with special thanks to the FUI financial support and the financial support of PAREX group.

Special thanks go to my friends who supported me during all the period of my study.

Last but not least, I would like to express my deepest gratitude to my parents and my brothers for the continuous support and encouragement during all my studies.

Contents

Nomenclature

Latin Letters

Notation	*unit*	*significance*
A	*m²*	*area*
ach	*h^{-1}*	*air changes per hour*
CC	*-*	*cloudiness coefficient*
CS	*€*	*cost savings*
cp	*J/(kg.K)*	*specific heat*
D	*m*	*diameter*
D_{φ}	*kg/(m.s)*	*liquid conduction coefficient*
f	*-*	*decrement factor*
F	*-*	*view factor*
h	*W/(m².K)*	*heat transfer coefficient*
h_v	*J*	*latent heat of vaporization*
H	*J*	*enthalpy*
HDD	*deg.day*	*heating degree day*
I	*W/m²*	*solar irradiation*
k	*W/(m.K)*	*thermal conductivity*
$\dot{m}$	*kg/s*	*mass flow rate*
Nu	*-*	*Nusselt number*
N	*year*	*lifetime*
P	*Pa*	*pressure*
PP	*year*	*payback period*
Pr	*-*	*Prandtl number*
Q	*J*	*energy consumption*
q	*W/m²*	*heat flux*
R	*(m²K)/W*	*thermal resistance*
Re	*-*	*Reynolds number*
r	*m*	*radius*
r	*-*	*solar reflectivity*
T	*K*	*temperature*

t	*s*	*time*
U	*W/(m²K)*	*heat transfer coefficient*
v	*m/s*	*velocity*
V	m^3	*molume*
w	kg/m^3	*moisture content*
x, y, z	*m*	*spacial coordinates*

Greek Letters

Notation	*unit*	*significance*
α	-	*solar absorptivity*
β	*kg/(m² s Pa)*	*water vapour transfer coefficient*
ρ	kg/m^3	*density*
σ	$kg/(s^3 K^4)$	*Stefan-Boltzmann constant*
φ	-	*relative humidity*
$\emptyset$	*h*	*time lag*
η	*%*	*efficiency*
ε	-	*emissivity*
δ_p	*kg/(m s Pa)*	*Water vapour permeability*
τ	-	*Solar transmissivity*
Δt	*s*	*time step*
Δx	*m*	*thickness*
ΔR	*W/m²*	*long-wave radiation exchange*

Subscripts and Superscripts

Notation	*significance*
a	*air*
abs	*absorber*
c	*convective*
cv	*Control volume*
dp	*dew point*
e	*east*
f	*fluid*
g	*glass*
gr	*ground*
h	*heating*
i , j	*node position*
in	*inside*
l	*layer*
n	*north*
MRT	*Mean radiant temperature*
mm	*Mean monthly*
out	*outside*
r	*radiative*
rm	*Running mean*
s	*south*
sat	*saturation*
w	*water*
w	*west*

Notations

Notation	*significance*
ABC	*Aerogel-Based Coating – In all the manuscript, we use the word "coating" to refer to a "rendering" or a "mortar" having a certain thickness*
C	*concrete*
CR	*Condensation risk*
cH	*Continuous heating*
DR	*Dryness rate*
EPS	*Expanded polysyrene*
GW	*Glass wool*
HB	*Hollow blocks*
iH	*Intermittent heating*
MG	*Mold growth*
N	*north*
nH	*No heating*
PWF	*Present worth factor*
R	*Rain (driving rain)*
SW	*South-west*
SHGF	*Solar heat gain coefficient*
TCI	*Thermal comfort index*
WALS	*Wall active loop system*
1D (2D)	*One (two)-dimensional*

List of Figures

List of Tables

GENERAL INTRODUCTION

According to experts from GIEC (Groupement International d'expert sur l'Evolution du Climat), it is almost certain that global warming observed over the past century is linked to greenhouse gas emissions produced by the human activities. To limit the aggravation of this phenomenon, the countries must reduce their greenhouse gas emissions. All business sectors are concerned, but the building sector requires a special attention because, according to a report on energy trends in buildings (Enerdata 2012), the building sector consumed about 41% of total final energy requirements in Europe in 2010. It is the largest end-use sector, followed by transport (32%), industry (24%) and agriculture (2%). The final energy consumption of buildings has increased by around 1% per year since 1990 (Enerdata 2012).

In France, the building sector is the largest consumer of energy and accounts for about 43% of the total energy consumption (ADEME 2014). This energy consumption contributes to producing around 25% of CO_2 emissions. Energy consumption from the building sector has increased by about 30% over the past 30 years due to the increase in new constructions (UNEP 2012). France has already adopted the objective of reducing its energy consumption and greenhouse gas emissions by a factor of four to five by the year 2050 as a part of its national strategy for sustainable development introduced in June 2003, and it's Climate Plan introduced in July 2004. The new thermal regulations (French RT 2012) limit the annual primary energy consumption for new buildings to 50 kWh/m^2. Also, the share of renewable energy in proportion to the total energy consumption must increase from 10% (as of 2009) to 23% by 2020.

The building sector offers significant potential for improved energy efficiency through the use of high-performance insulation and energy-efficient systems. For existing buildings, renovation has a high priority in many countries, including France, because these buildings represent a high proportion of energy consumption and they will be present for decades to come. Until the year 2009, the residential building sector in France counted around 32.2 million housing units with an annual energy consumption of about 494 TWh (ADEME 2009). Several studies (Verbeeck 2005, Enkvist 2007, EEW 2013) showed that the most efficient way to curb the energy consumption in the building sector (new and existing) remains the reduction of the heat losses by improving the insulation of the building envelope. For retrofitting and even for new buildings in cities, the thickness of internal or external insulation layers becomes a major issue of concern.

Nowadays, there is a growing interest in the so-called super-insulating materials, such as Aerogels. The unique properties of aerogels offer many new applications in buildings. Their extraordinary low thermal conductivity as well as their optical transparency allows their use for insulating building facades and insulating window panes.

The objectives of this work are to enhance the thermal behavior and to foster energy efficiency of buildings through the use of a newly developed aerogel-based insulating coating (rendering) as well as the use of renewable energy sources, specifically solar energy. We examine the thermal behavior of buildings having the new aerogel-based insulating coating on the external facades. This includes its effect on the building's energy load and thermal comfort for different building construction types and in various climates. We examine the effect of the coating on time lag and decrement factor for different wall types. Also, we study the effect of this coating on limiting the heat losses through thermal bridges. The impact of the coating is scrutinized not only from a thermal perspective but also from a hygrothermal one. Through the modeling of the coupled heat and moisture transfer in different wall structures, the risk of condensation and mold growth are examined. Another objective is to propose an assisting heating system to decrease the heating demand and enhance thermal comfort. We propose a system to take advantage of the solar radiation falling on the south facade and transfer this energy to the north facade through water pipes embedded in the aerogel coating.

The thesis is composed of four chapters. The first chapter starts with a brief description of the various heat transfer exchange processes between the building and its environment and some factors influencing the building's thermal behavior. Then, we present some state-of-the-art thermal comfort models. After that, we provide a brief history on the evolution of the construction and energy performance of the houses in France since before the World War 2 till the last decade. We move to present the characteristics of a newly developed silica-aerogel-based insulating coating after showing the importance of using aerogel based materials in the building sector. This chapter ends by showing some of the mathematical models used in determining the heat flows in a building as well as presenting a few whole building energy simulation tools.

The second chapter deals with developing all the mathematical and numerical models needed for this study. It starts with modeling the one-dimensional heat transfer in a multilayer wall

structure. This latter is extended to model the two-dimensional heat transfer in a multilayer wall structure to examine the impact of applying the coating on thermal bridges heat losses. Also, the one-dimensional hygrothermal (heat and moisture) model is constructed using the commercial software WUFI®. To show the impact of the coating on energy load and thermal comfort, a full-scale house thermal model is built using EnergyPlus. Finally, chapter two ends with explaining the concepts of the proposed assisting heating system (wall active water loop system). The mathematical model of this system is also presented.

The third chapter deals with all experiments done to validate the different numerical models. We have conducted three experiments. The first one is a test cell located in Sophia Antipolis. The second is a full-scale two-story house located in Chambery. The third experiment (in Chambery) is related to the newly proposed assisting heating system.

Last but not least, the fourth chapter presents all the simulation results. It provides clear recommendations on the feasibility of installing this aerogel-based coating, firstly, alone and, secondly, as insulation associated with an active water loop system.

*Résumé de l'introduction en Fran*çais

Selon une étude réalisée par les experts du Groupement International d'expert sur l'évolution du Climat (GIEC), il est devenu certain que le réchauffement climatique est lié aux émissions de gaz à effet de serre, dues aux activités humaines. Afin de limiter ce phénomène, les pays doivent diminuer de nombreuses activités qui interviennent dans l'augmentation de la concentration des gaz à effet de serre dans l'atmosphère terrestre. Tous les secteurs de métier sont concernés par cet acte, surtout le secteur de la construction des bâtiments. En effet et selon une étude publiée dans Enerdata en 2012, le domaine de la construction consomme près de 41 % de l'énergie totale requise en Europe en 2010. Ce secteur est classé en premier sur l'échelle de la consommation en énergie, devant le transport avec 32 % de consommation, l'industrie (24 %) et l'agriculture, 2%. La consommation énergétique totale par les bâtiments évolue de 1% chaque année depuis 1990 et de 2,4% pour l'électricité (Enerdata, 2012).

En France, le secteur de la construction est le plus grand consommateur d'énergie, occupant une tranche de 43% de la consommation totale énergétique (ADEME, 2014), ce qui entraine 25% des émissions de CO2. La consommation énergétique du secteur de la construction a augmenté de 30% durant ces 30 dernières années, du fait des constructions modernes (UNEP, 2012). L'objectif de la France est de réussir à réduire son taux en consommation en énergie à un facteur de 4 ou 5 en 2050. Cet objectif fait partie de la stratégie nationale pour un développement durable introduite en Juin 2003. Les nouvelles régulations thermiques adoptées limitent la consommation annuelle en énergie primaire des nouvelles constructions à 50KWh/m^2 (RT 2012). De plus, ceci est conjugué avec une augmentation du recours aux énergies renouvelables, avec une part passant de 10% (2009) à 23% en 2020, par rapport à la consommation énergétique totale.

Le secteur de la construction offre un potentiel significatif pour améliorer l'efficacité énergétique en utilisant des systèmes énergétiques efficaces et une isolation de haute performance. Pour les bâtiments existants, leur rénovation est devenue une grande priorité pour certains pays, y compris la France, puisqu'ils représentent une proportion élevée de l'énergie consommée et seront présents, en termes de construction, pour le prochain siècle. Jusqu'à l'année 2009, la construction résidentielle comptait près de 32.2 millions de maisons avec un niveau de consommation en énergie annuelle qui a atteint les 494 TWh (ADEME, 2009). Des études

(Verbeeck 2005, Enkvist 2007, EEW 2013) ont montré que la solution la plus efficace pour contrôler la consommation énergétique du secteur de la construction (anciens et nouveaux bâtiments) est de réduire la perte énergétique en améliorant l'isolation externe installée. L'amélioration de la performance thermique courante de l'enveloppe des bâtiments est essentielle pour réduire la demande en énergie requise pour les constructions. Pour la réhabilitation et même pour les nouveaux bâtiments, l'épaisseur des couches de l'isolation externe et interne est devenue un problème. Aujourd'hui, il y a un intérêt majeur pour l'utilisation des matériaux dits super-isolants, comme les aérogels. Les aérogels présentent des propriétés uniques qui s'avèrent très intéressantes et qui doivent être prise en compte dans les nouvelles règles des constructions. En effet, avec leur transparence optique et leur très faible conductivité thermique, les aérogels peuvent être utilisés dans l'isolation des façades opaques et des parties vitrées.

L'objectif de ce travail est d'étudier l'amélioration du comportement thermique et l'économie d'énergie possible des bâtiments par l'utilisation de nouveaux enduits isolants à base d'aérogel et aussi d' énergies renouvelables, notamment l'énergie solaire. La thèse est composée de quatre chapitres. Le premier chapitre introduit le concept de la construction et le comportement thermique. Le deuxième chapitre décrit les modèles mathématiques et numériques utilisés pour cette étude. Le troisième explique toutes les expériences qui ont été faites pour valider les modèles numériques. Enfin, le dernier chapitre présente les résultats de la simulation.

CHAPTER 1

BACKGROUND ON BUILDING CONSTRUCTION, AEROGEL-BASED INSULATION, ENERGY MODELING AND SIMULATION

Chapter 1
Background on Building Construction, Aerogel-Based Insulation, Energy Modeling and Simulation

Chapter Contents

1. Buildings: Complex Dynamic Systems

1.1. Introduction

A building can be seen to be like a box, protecting its contents from climatic conditions. Its envelope acts like an exchanger, gaining and releasing heat to the environment. It is crucial to know how to design an energy efficient envelope by examining its effect on the thermal performance of the building in order to improve the comfort of its occupants while consuming as little energy as possible.

Thermal performance of buildings refers to the heat exchange processes that occur between the building and its surroundings. This enables us to estimate the cooling and heating loads of the building, and as a result, to make proper selection and sizing of the various heating, ventilation, and air-conditioning (HVAC) systems needed to maintain thermal comfort during air-conditioning periods. For non-air-conditioned spaces, this would allow us to calculate the indoor air and operative temperatures which help estimate the duration of uncomfortable periods.

Heat is exchanged between the building and its surrounding environment through different means (Fig. 1.1). One way is heat conduction through the walls, roofs, floors, etc. Another way is convection from different surfaces. Solar radiation is absorbed by the building internal surfaces after penetrating through windows. Also, heat is added to the space from the various internal sources such as occupants, lights, equipment, etc. Air flow from or to the space through infiltration and ventilation contributes to bringing or removing heat.

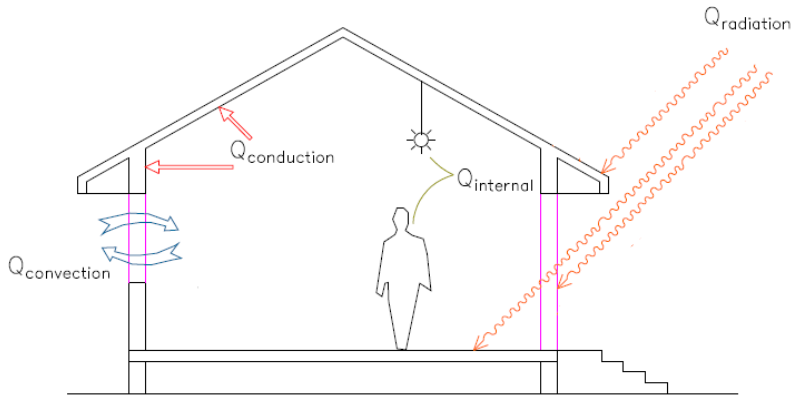

Fig. 1.1: Examples of heat exchange processes between a building and the environment

1.2. Factors Affecting the Building's Thermal Response

Many factors affect the thermal performance or response of a building. Among these are: thermal insulation, thermal mass associated with natural ventilation, and solar gains.

1.2.1. Thermal Insulation

According to Cadiergues (1986), a well-insulated wall reduces the heat losses to the outside during the cold season and reduces the transmitted heat to the inside during the day in the hot season. It also prevents condensation in the wall through avoiding the too low temperatures. Besides, it improves thermal comfort by preventing the too hot or too cold thermal sensation near the walls due to radiative exchange.

On the other side, a well-insulated envelope may lead to overheating in hot summers where the absorbed solar radiation during the day (entering through windows) may be trapped inside without being able to be released to the outside.

The position of insulation plays an important role in the dynamic thermal behaviour of exterior walls. Different construction types exist:

- insulation at the outside wall surface
- insulation at the inside wall surface
- insulation at the middle of the wall
- insulation is distributed within the wall structure

Generally, insulation materials are not dense; thus, they cannot store a large amount of heat per unit volume. This leads to fast response to the imposed driving forces. Tsilingiris (2006) showed that for intermittently conditioned spaces, the thermal insulation performs better when installed at the interior wall side. Due to its low thermal capacitance, when the heating cycle begins, there is a rapid increase of room temperature up to the desired thermostat setting level. Conversely, Kossecka and Kosny (1998) showed that for a continuously heated and/or cooled building, the best solution from an energy point of view is placing insulation at the exterior wall surface.

1.2.2. Thermal Mass Associated with Natural Ventilation

During the winter season, thermal inertia absorbs and stores the excess heat due to solar radiation during the day and releases it at a later time in the night when it gets colder outside.

During summer nights, when the outside air temperature is lower than the temperature inside the building, it is possible to apply natural ventilation. The ventilated air promotes convection and dissipation of the heat stored in the envelope to the outside. This strategy allows reducing the peak energy loads of the building; thus, reducing the required size of the HVAC system. In the non air-conditioned buildings, it helps to dampen strong fluctuations of the exterior temperature and to maintain the inner surface temperatures fairly at a constant temperature irrespective of fluctuating outer surface temperature. Also, thermal mass can delay the heat penetrating into the indoor space to a later time more desirable for occupants.

However, the improvement of summer thermal comfort by adopting thermal inertia and natural ventilation depends on the climate. The contribution of thermal inertia varies greatly depending on the nature of the external stresses cycles to which the building is subjected (Givoni 1994, Roucoult 1999).

Two parameters are defined: time lag and decrement factor (Fig. 1.2). Time lag is the time it takes for the heat wave to propagate from the outer surface to the inner surface of the wall and the decrement factor is the decreasing ratio of its amplitude. These are calculated as following:

$$time\ lag\ , \emptyset = t_{in,max} - t_{out,max} \quad or \quad \emptyset = t_{in,min} - t_{out,min} \tag{1.1}$$

$$decrement\ factor, f = \frac{A_1}{A_2} = \frac{T_{in,max} - T_{in,min}}{T_{out,max} - T_{out,min}} \tag{1.2}$$

where $t_{in,max}$ and $t_{out,max}$ represent the time when the inside and outside surface temperatures are at their maximums, respectively. $t_{in,min}$ and $t_{out,min}$ represent the time when the inside and outside surface temperatures are at their minimums, respectively. $T_{in,max}$, $T_{in,min}$, $T_{out,max}$, and $T_{out,min}$ are the maximum and minimum inner wall surface temperatures and the maximum and minimum outer wall surface temperatures, respectively.

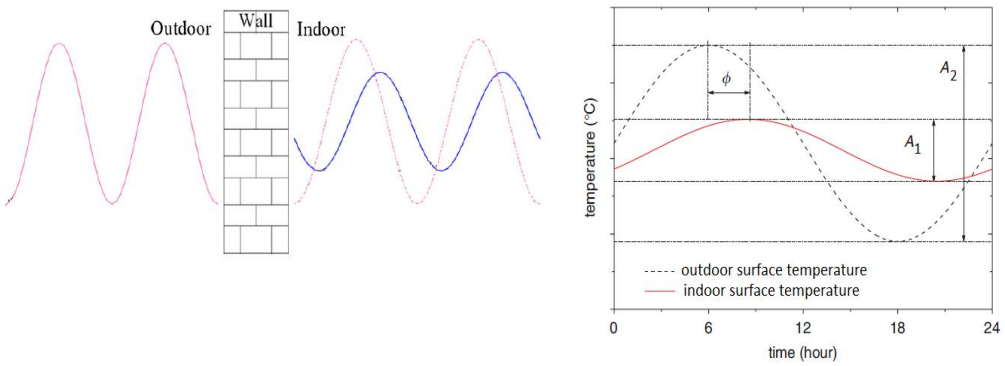

Fig. 1.2: Time lag and decrement factor

Extensive research was carried out dealing with wall heat flux and temperature time lag and decrement factor. Most of these studies dealt with optimizing the properties and distribution of the different material layers in a wall/roof to increase time lag and to decrease decrement factor (Asan and Sancaktar 1998, Asan 2000, Ulgen 2002, Kontoleon 2008, Kaska and Yumrutas 2008, Kaska and Yumrutas 2009, Sun et al. 2013).

1.2.3. Solar Radiation

Solar radiation incident on building facades contributes in two ways. The first one is the solar radiation absorbed by the exterior opaque surfaces then transmitted to the inside. Dexter and Bickle (1978) indicate that the efficiency of a building exterior surface is its ability to collect solar radiation and transmit it to the inside. For climates where the heating season is dominant, it is more important to have higher efficiency. For climates where the cooling season is dominant, it is more important to have less efficiency. The second way is the direct solar gains through windows. Solar radiation passes through the wall glazing surfaces to be absorbed by the interior room surfaces (especially the floor). Part of this energy is transmitted directly to the indoor air and another part is absorbed to be transmitted at a later time of the day. It is crucial to optimize the sizes of the windows, their glazing properties, their orientation, and their interior and exterior shading devices. In cold winters, it is important to benefit from the passive solar gains through the windows. In hot summers, it is important to decrease the solar gains to prevent overheating.

1.3. Thermal Comfort

1.3.1. Introduction

The ISO Standard 7730 (ISO 2005) defines thermal comfort as the mental condition that expresses satisfaction with the thermal environment. A lot of factors affect the occupants' thermal comfort, such as room temperature, humidity, air velocity, etc. Extensive research has been done trying to model thermal comfort within spaces. Most practitioners refer to standards such as ASHRAE Standard 55 (ASHRAE 2010) and ISO Standard 7730 (ISO 2005) to estimate thermal comfort. These standards are based primarily on mathematical models developed by Fanger and his colleagues on the basis of laboratory studies (Fanger 1970).

1.3.2. Simple Models

The easiest way is to use the indoor air temperature as an indicator to assess thermal comfort. This method calculates the number of hours during which the indoor air temperature exceeds a certain comfort value (for example, 26°C or 27°C in summer). Alternatively, the operative temperature could be used to account for radiative heat exchange between the occupants and the different room surfaces.

1.3.3. Conventional Models

Throughout the last few decades, a lot of research has been carried out to develop a mathematical model that predicts thermal sensation and comfort of occupants. Three thermal comfort models are widely used: Fanger model (Fanger 1970), Pierce two-node model (Gagge et al. 1970 and Gagge et al. 1986), and KSU model (Azer and Hsu 1977). All three models are related to heat balance equations of the human body and a thermal sensation scale. Some environmental variables (air temperature, mean radiant temperature, relative humidity, and air velocity) as well as human factors (metabolic rate and clothing insulation) are used to predict thermal comfort levels.

Fanger obtained his mathematical model of thermal comfort by conducting experiments in a climatic chamber. Participants wore standard clothing and performed standard activities while subjected to different thermal environments. They recorded their thermal sensation using a 7 point scale varying between -3 to +3 where 0 represents neutrality. Positive numbers represent warm/hot environment whereas negative numbers represent cool/cold environment.

Using correlated data from the experiments and taking all major human body heat losses, the model was developed using the predicted mean vote (PMV) index calculated using equation (1.3). For a thermally comfortable environmental, PMV should lie between -0.5 and 0.5.

$$PMV = (0.303e^{-0.036M} + 0.028) * (H - L) \quad (1.3)$$

where:

H is the internal heat production rate per unit area (W/m^2)
L is the energy loss from body (W/m^2)
M is the metabolic rate per unit area (W/m^2)

The Pierce Two-Node Model (Gagge et al. 1970, Gagge et al. 1986) divides the human body into two parts: core and skin. Heat balance equations are developed. Thermal sensation, measured using a similar scale as that of Fanger, is then calculated to assess thermal comfort.

The KSU model (Azer and Hsu 1977) is similar to the Pierce Two-Node model except that there is a variation in the heat balance calculation between the core and the skin in cold environment and a variation of the skin wettedness in warm environment. Berglund (1978) shows further details about the theoretical background of these models.

1.3.4. Adaptive Models

The PMV method for calculation of thermal comfort has faced a lot of criticism. The main point is that the PMV approach is derived from laboratory tests under steady state conditions. Some publications say that this approach could be misleading when used to predict thermal comfort (Humphreys et al. 2002, Stoops et al. 2004, Jokl et al. 2007). Most remarks say that the PMV does not take into consideration the effect of adaptation: psychological, physiological, and behavioral adaptation. Hence, several researchers prefer estimating thermal comfort using adaptive models. However, these latter are intended to be used in naturally ventilated buildings.

1.3.4.1. Adaptive Comfort Model Based on ASHRAE Standard 55-2010

This model relates the indoor comfort temperature (operative temperature) to the mean monthly outdoor air temperature. It defines two regions (as shown in Fig. 1.3) where 80% and 90% of occupants are satisfied.

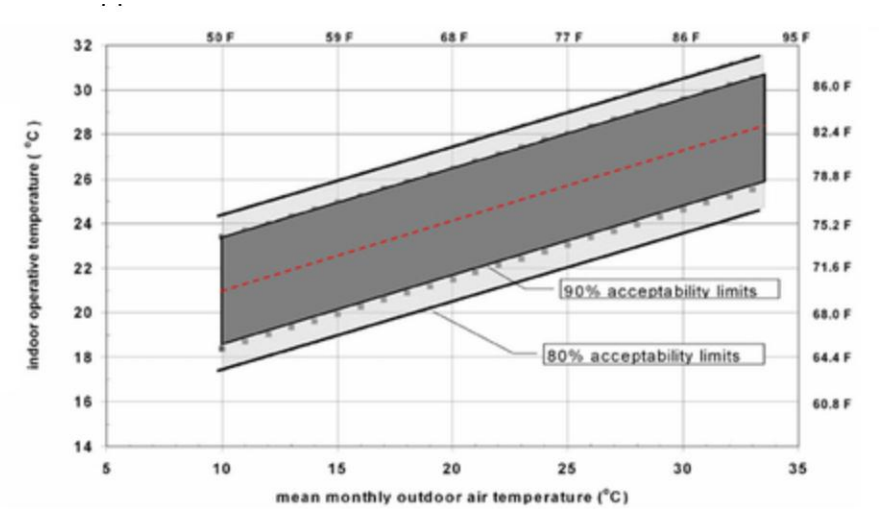

Fig. 1.3: Adaptive thermal comfort region according to ASHARE Standard 55

The red line (comfort temperatures), and the 90% and 80% acceptability limits of Fig. 1.3 have equations (1.4-a), (1.4-b), and (1.4-c), respectively.

$$T_{op} = 0.31*T_{o,mm} + 17.8 \quad (1.4\text{-a})$$

$$T_{op} = 0.31*T_{o,mm} + 17.8 \pm 2.5 \text{ (90\% acceptability)} \quad (1.4\text{-b})$$

$$T_{op} = 0.31*T_{o,mm} + 17.8 \pm 3.5 \text{ (80\% acceptability)} \quad (1.4\text{-c})$$

where:

T_{op} is the operative temperature (°C)
$T_{o,mm}$ is the monthly mean outdoor air dry-bulb temperature (°C).

1.3.4.2. Adaptive Comfort Model Based on EN Standard 15251-2007

This model is similar to that of ASHRAE standard but it relates the operative temperature to the weekly outdoor mean temperatures as shown in Fig. 1.4. It defines three acceptability regions: 90%, 80%, and 65% acceptability.

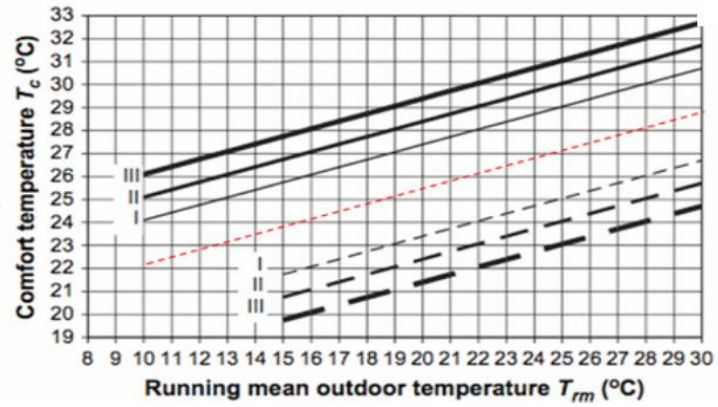

Fig. 1.4: Adaptive thermal comfort region according to EN Standard15251

The red line (comfort temperatures), and the 90%, 80%, and 65% acceptability limits of Fig. 1.4 have equations (1.5-a), (1.5-b), (1.5-c), and (1.5-d), respectively.

$T_{op} = 0.33*T_{o,rm} + 18.8$ (1.5-a)
$T_{op} = 0.33*T_{o,rm} + 18.8 \pm 2$ (90% acceptability) (1.5-b)
$T_{op} = 0.33*T_{o,rm} + 18.8 \pm 3$ (80% acceptability) (1.5-c)
$T_{op} = 0.33*T_{o,rm} + 18.8 \pm 4$ (65% acceptability) (1.5-d)

where:

T_{op} is the operative temperature (°C)

$T_{o,rm}$ is the running mean outdoor air dry-bulb temperature (°C) of the previous 7-day daily mean outdoor air dry-bulb temperatures.

1. Building Construction and Energy Performance Evolution

1.1. Introduction

Until the year 2009, the residential building sector in France counted around 32.2 million housing units with an annual energy consumption of about 494 TWh (ADEME 2009, Chiffres clés du batiment,). Figure 1.5 shows the number of individual and collective houses for three significant periods in building construction for the different climatic zones of France (FILOCOM 2009, taxe d'habitation,).

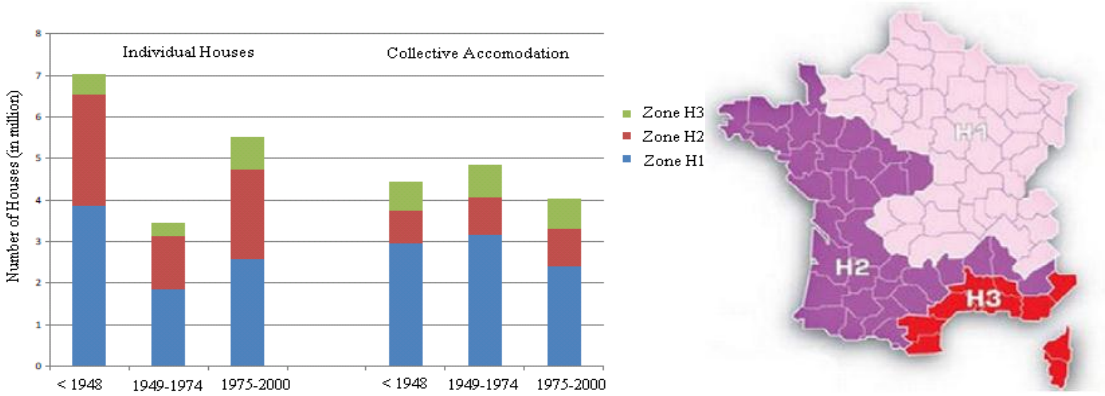

Fig. 1.5: Number of housing units in France per climatic region (source: FILOCOM 2009, taxe d'habitation)

In the Building Sector, space heating and domestic hot water remain the most important energy users, as presented in Fig. 1.6 (IEA 2007, Energy Use in the New Millennium - Trends in IEA Countries). Since the first oil crisis, the implementation of building thermal regulations (RT 1974) through a combination of higher efficiencies of equipment and improved thermal performance of the building envelope has led to a significant reduction in the per capita energy requirement for space heating.

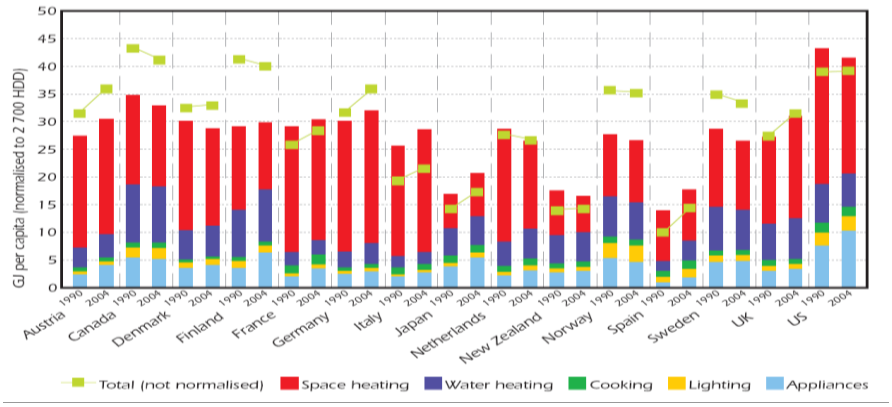

Fig. 1.6: Household energy use per capita (source: IEA 2007, Energy Use in the New Millennium -Trends in IEA Countries)

In most industrialized countries, new buildings will only contribute between 10% to 20% additional energy consumption by 2050 whereas more than 80% of the energy consumption will be influenced by the existing building stock and 75% of current buildings will still be standing in 2050.

1.2. History of Construction in France[1]

1.2.1. Traditional Way till the World War 2

This period can be divided into two periods: the first one (before 1914) includes the old buildings where the construction was based on local materials such as millstone, with little professionalized implementation. The second period (1914-1948) represents the period where some manufactured materials started to be used in building construction such as cement, solid brick, interlocking tiles, etc.

Fig. 1.7: Traditional houses before World War 2

These houses consume around 214kWh/m² (final end-use energy) per year for space heating. Exterior walls are composed mainly of one of the following materials: stone rubble (sandstone, limestone, granite…), mud-brick, solid bricks, timbered structure with soil, brick, or mixed filling. For the ceiling and roof, the construction is wood. Windows are simple glazed with wooden joinery, and the window-to-wall ratio is around 10%. No specific thermal insulation is used.

1.2.2. Construction Strategy after the World War 2

At the end of the World War 2 (WW2), there was an urgent need to rebuild the devastated country. For many, traditional tools and techniques seem somewhat obsolete; they cannot meet the very important and urgent reconstruction needs. Thus, during the reconstruction period, it was vital to experience different construction techniques. Here came the necessity to apply the methods used in industry to the building construction sector: serial, mass, and standard production (construction). That was then called "Building Industrialization".

[1] Reference: " DHUP (2007), Typologie des bâtiments d'habitation en France, " and " DHUP (2011), Etude socio-technico-economique du gisement de travaux de rénovation énergétique dans le secteur immobilier résidentiel, " as reported by "Analyse Détaillée du Parc Résidentiel Existant, Report 2009".

Prefabricated homes were the solution because their construction was rapid and standard. For individual houses, the construction material for exterior walls was hollow concrete blocks or hollow bricks. For collective (community) houses, the construction material was reinforced concrete.

Fig. 1.8: Prefabricated houses

For the houses constructed between the years 1948 and 1967, the space heating energy consumption is approximately 226 kWh/(m².year). The ceiling, floor and roof are composed of wood with interlocked tiles or asphalt shingles. Windows are simple glazed and the window-to-wall ratio varies between 20-27%. No specific thermal insulation is used.

For the houses constructed between the years 1968 and 1974, the space heating energy consumption is approximately 177 kWh/(m².year). The ceiling and roof are composed of wood with interlocked tiles or concrete shingles as final coating. It's in these years where insulation started to enter the building industry; however, its implementation was still low. Some of these houses have insulation (4-10cm glass wool) below the ceiling or below the pitched roof. The floor is composed of concrete slab or terracotta. Two types of window glazing are used: simple or double, and the window-to-wall ratio is approximately 37%. In general, no specific thermal insulation is used in the exterior walls.

1.2.3. Interior Insulation: A Reaction after the Oil Crisis in 1970

After the increase in oil prices in 1970, the French government set a policy encouraging energy conservation by improving the performance and efficiency of heating systems and by using thermal insulation in the building fabric. In 1974, the first thermal regulation (RT 1974) was launched forcing buildings to have thermal insulation. Also, the petrochemical industry diversified its markets by producing large amounts of glass wool insulation and polystyrene facilitating the entry of insulation into the building sector.

Fig. 1.9: Houses after 1974

For this period, we distinguish two periods: the first one is between 1975 and 1981, and the second is between 1982 and 1989. Houses in the first period (1975-1981) have exterior walls composed of either masonry blocks, hollow bricks, or stone, with thermal insulation having an R-value of 2.3 (m².K)/W. Energy consumption for space heating is approximately 142 kWh/(m².year). The ceiling/roof is composed of wood with cement finishing. Also, thermal insulation (R = 4.8(m².K)/W) is added below the pitched roof. Windows are simple or double glazed and the window-to-wall ratio is around 25%. The floor is composed of concrete slab or terracotta with thermal insulation (R=1 (m².K)/W).

The majority of the houses in the second period (1982-1989) have exterior walls composed of concrete hollow blocks (67%) with interior insulation having an R-value of 2.4 (m².K)/W. Others (15%) have walls composed of hollow bricks with interior insulation. In addition, other materials are also used such as solid bricks, wood, cellular concrete. Energy consumption for space heating is approximately 106 kWh/(m².year). The ceiling/roof has insulation of R = 4.8(m².K)/W. Windows are simple or double glazed and the window-to-wall ratio is around 25%. The floor is composed of concrete slab or terracotta with thermal insulation having an R-value of 0.8 (m².K)/W for ground floor or R=1.9 (m².K)/W for crawl spaces.

1.2.4. Exterior Insulation: The New Approach

For homes built after 1990, exterior walls are, majorly, composed of concrete blocks with thermal insulation having an R-value of 3 (m².K)/W. New types of hollow bricks (such as brick-monomur) are also used possessing a higher energetic performance than those used in previous periods. Ceilings and roofs have thermal insulation of R-value = 6 (m².K)/W. Floors also have thermal insulation (R = 3 (m².K)/W) below the concrete slab. The installed windows were at first simple glazed, and then became double glazed. The window-to-wall ratio is around 20%. Energy consumption for space heating is approximately 95 kWh/(m².year).

During these last two decades, the rehabilitation of existing buildings introduced the concept of exterior insulation. It is difficult to choose between interior and exterior insulation. Moreover, thermal regulations in force today still don’t recommend on the best way to insulate buildings. This technique of building insulation has its advantages and its drawbacks.

1.2.4.1. Advantages of Using Exterior Insulation

- reduces heat losses through thermal bridges
- enhances thermal comfort through increasing the thermal inertia near the inside of the living space
- preserves the usable area of the living space
- conducts the work without the necessity for inhabitants' displacement (for existing buildings); thus, facilitates rehabilitation
- decreases the possibility of condensation
- avoids polluting the interior air due to the insulating materials used
- modifies/improves the aesthetic of buildings (especially old ones; not convenient with some ornamented or heritage buildings)

1.2.4.2. Drawbacks of Using Exterior Insulation

- causes a problem when balconies and parapets are present
- high inner thermal inertia may not be suitable in some cases (intermittent heating/cooling)
- should be protected from outside conditions
- more difficult to install than interior insulation
- can't be used when ornamented or heritage facades are to be preserved

1.2.5. Summary

Table 1.1 summarizes the construction types of French houses since before the WW2 till the last decade.

Table 1.1 : Houses' Construction in France during the different periods

		period					
		< 1948	1948 - 1967	1968-1974	1975-1981	1982-1989	1990-2000
Space Heating	Final energy use for space heating	214 (kWh/m²/year)	226 (kWh/m²/year)	177 (kWh/m²/year)	142 (kWh/m²/year)	106 (kWh/m²/year)	95 (kWh/m²/year)
Opaque wall	Construction	- Stone rubble: (such as sandstone, limestone, granite…) - mud-brick - solid bricks - timbered structure with soil, brick, or mixed filling	- hollow concrete blocks - hollow bricks - reinforced concrete	-hollow concrete blocks - hollow bricks - reinforced concrete	-masonry blocks -cellular concrete -hollow brick - stone	- concrete hollow blocks (67% of houses) - hollow bricks (15%)	- concrete blocks - more energy efficient hollow bricks (such as brick monomur)
	Thermal Insulation	No	No	No	R = 2.3 (m².K)/W	R = 2.4 (m².K)/W	R = 3 (m².K)/W
Roof/ceiling	Construction	wood with a final coating based on local materials	wood with interlocked tiles or asphalt shingles	wood with interlocked tiles or concrete shingles	wood with cement finishing (	wood with cement finishing (	Concrete insulated beam
	Thermal Insulation	No	No	Some houses start to have insulation (4-10cm glass wool)	R = 4.8 (m².K)/W)	R = 4.8 (m².K)/W)	R = 6 (m².K)/W)
Floor	Construction	Wood (on arcs) or slab on ground	Wood	concrete slab or terracotta	concrete slab or terracota	concrete slab or terracota	Concrete slab
	Thermal Insulation	No	No	No	R= 1 (m².K)/W)	R = 0.8 (m².K)/W for ground floor or R=1.9 (m².K)/W for crawl spaces.	R = 3 (m².K)/W)
Window	Construction	Simple glazed	Simple glazed	Simple / Double	Simple / Double	Simple / Double	Simple then Double
	Window to wall ratio	10 %	20 - 27%	37 %	25 %	25%	20%

2. Aerogel-Based Insulating Materials: Building Applications

2.1. Introduction

The strict new thermal regulations and the notion of the net zero energy building (nZEB) ensure that new buildings do not place additional burden upon energy resources. For existing buildings, as shown in the previous section, renovation has a high priority in many countries, and France is one of them, because these buildings represent such a high proportion of energy consumption and they will be present for decades to come. Several studies (Verbeeck and Hens 2004, Enkvist et al. 2007, Energy Efficiency Watch Final Report 2013) have shown that the most efficient way to curb the energy consumption in the building sector (new and existing) remain the reduction of the heat losses by improving the insulation of the building envelope. A step beyond the current thermal performance of building envelope is essential to realize the intended energy reduction in buildings. For retrofitting and even for new buildings in cities, the thickness of internal or external insulation layers becomes a major issue of concern. Therefore, there is a growing interest in the so-called super-insulating materials, such as Aerogels.

Silica aerogels are silica-based dried gels having very low weight and excellent thermal insulation performance (Bisson et al. 2004). Specifically, they have high porosity (80-99.8%), low density (3 kg/m^3), and low thermal conductivity (0.014 $W/m^{-1}.K^{-1}$), (Soleimani Dorcheh A. 2008). Silica Aerogels are an innovative alternative to traditional insulation due to their high thermal performance, although the costs of the material remain high for cost-sensitive industries such as the building industry. Research is continuing to improve the insulation performance and to decrease the production costs of aerogels. The unique properties of aerogels offer many new applications in buildings (TAASIS 2011). The extraordinary low thermal conductivity of aerogels as well as its optical transparency allows its use for insulating building facades and insulating window panes. Two different types of silica aerogel-based insulating materials are being used in the building sector. The first type is the opaque silica aerogels-based materials and the second one is the translucent materials.

2.2. Opaque Composite Silica Aerogel-Based Materials

Aerogel blankets/panels are used to insulate building walls, grounds, attics, etc. Aspen Aerogels Inc. (Northborough, MA, US) has developed an insulation blanket based on silica aerogels, Spaceloft® (www.aerogel.com/products /pdf/Spaceloft_MSDS.pdf). It has a thermal conductivity of 0.0131 W/(m.K). Spaceloft® was used to convert an old mill house in Switzerland into an energy saving passive house (Fig. 1.10). A 9mm thickness layer was used externally and internally on the walls and also internally on the floors. The U-value of the walls improved from 1 W/(m^2K) to 0.2 W/(m^2K) (Case study, www.aerogel.com /markets/Case_Study_House_Renovation_web.pdf).

Fig. 1.10: Aspen aerogel insulation for retrofitting of an old brick dwelling

Due to its small thickness, Spaceloft® can be installed on interior walls of buildings preserving the area of the occupied spaces. A case study was done in the United Kingdom where a number of governmental housing units were retrofitted by adding Spaceloft® insulation layer at the interior wall surfaces (Case study, www.aerogel.com/ markets/Case_Study_Interior_Wall_web.pdf). A 44% reduction in the U-value, a 900 kWh/year energy reduction, and a 400 kg/year reduction in carbon emissions were obtained.

In a typical building, the framing is not insulated, resulting in heat losses through the studs. Spaceloft® insulation decreases heat loss through thermal bridges and improves thermal performance up to 40% in steel studs and up to 15% in wood studs. Fig. 1.11 shows the reduction in the thermal bridges heat losses between the ground floor un-insulated frames and the top floor insulated frames (Case study, www.aerogel.com/markets /Case _Study_Framing_web.pdf).

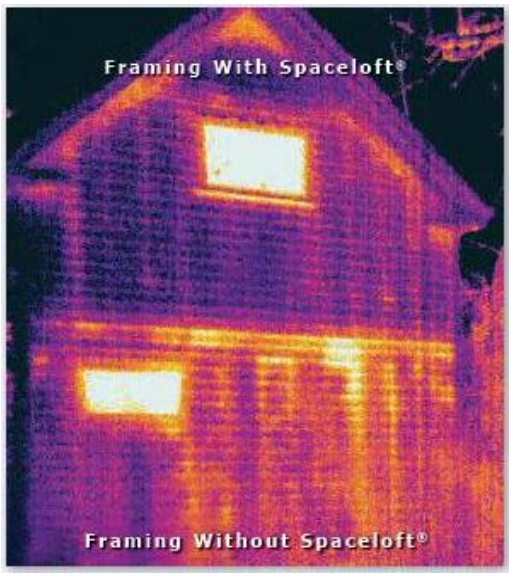

Fig. 1.11 : A thermographic image of a timber wall where the studs of the top floor are insulated with a thin layer of aerogel insulation whereas the ground floor is not

In another study, thermal performances and experimental tests were performed on walls and roofs using aerogel insulation (Kosny et al. 2007). Hot box measurements on wall assemblies containing aerogels showed that the R-value of wood framed walls is improved by 9% and that of a steel framed wall by 29%. Finite difference simulations performed on steel-framed wall assemblies using 0.6cm thick aerogel strips showed that aerogel can help in reducing the internal surface temperature differences between the center of the cavity and the stud location from 3.2ºC to only 0.4ºC. For roof structures, hot box measurements performed on the fastened metal roof insulated with aerogel strips showed an increase in the overall roof R-value by about 14%.

2.3. Translucent Silica Aerogel-Based Materials

Another type of silica aerogel-based materials which are used in buildings is the translucent insulation materials. These materials have the advantage to combine a low thermal conductivity along with high transmittance of solar energy and daylighting. Research has been conducted in the last decade on the development of highly insulating windows based on granular aerogels and monolithic aerogels (Pajonk 1998). A new glazing element based on granular silica aerogel was developed at ZAE Bayern, Germany (Reim et al. 2002, Reim et al. 2005). The glazing consists of 16mm double skin sheet made of polymethylmethacrylate filled with granular silica aerogels separated by two gaps filled with krypton or argon and installing glass panes at the ends (Fig. 1.12). Two types of granular silica aerogels are used: semi-transparent spheres and highly translucent granulates. Three window systems were developed. The first is a daylighting system by applying a low-e coating (emissivity = 0.08) on the panes. A total solar transmittance between 0.33 and 0.45, and a U-value having a range of 0.44-0.56 W/(m^2K) were obtained. The second system is a sun protecting system developed by applying a lower emissivity (0.03) to the glass panes. A U-value of 0.37-0.47 W/(m^2K), a visible transmittance of the range of 0.19 and 0.38, and a solar transmittance between 0.17 and 0.23 were achieved. The third is a solar collector by placing a heat exchanger between a layer of aerogels and two glass panes. When

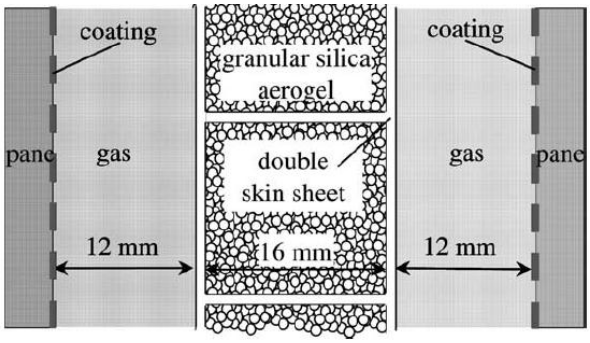

Fig. 1.12: Cross-section through the granular aerogel based glazing

compared to a traditional flat-plate solar collector, the collector using aerogel granules has a reduction in heat losses of about 40% and has a 3 cm smaller system thickness.

In a project supported by the European Union, in which our lab was one of the partners, a monolithic aerogel based window was developed (Fig. 1.13) (Jensen et al. 2004). They obtained a total heat transfer coefficient for the window (U-value) of 0.66 W/(m^2K) and a solar transmittance of 0.85 using a 13.5mm thick monolithic aerogel. Vacuum glazing technology was also used in developing this window.

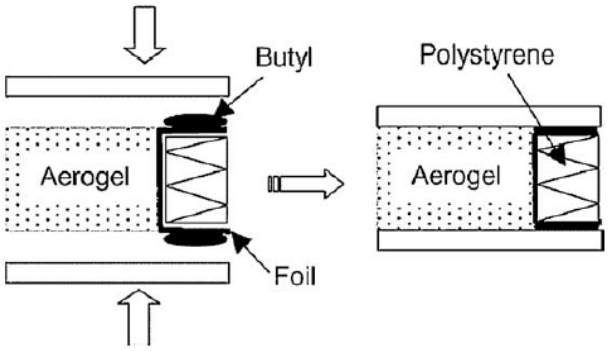

Fig. 1.13: cross-section of the monolithic aerogel based evacuated glazing

This U-value can be lowered when using more thickness of aerogel, and at the same time keeping the solar transmittance more than 0.75. A case study was done for the Danish climate, where a triple glazed window filled with argon was replaced by this aerogel based window for a house built according to the passive house standards. Energy savings of about 19 and 34% were achieved for 13.5 and 20mm aerogel thickness, respectively.

2.4. Life Cycle Assessment

Dowson et. al. (2012) investigated the life cycle assessment of silica aerogels. The mass of raw materials and electricity used for the production of 1 m^3 of silica aerogel are determined to estimate the energy costs as well as the CO_2 burden during the manufacturing process. Then, this is compared to energy savings and CO_2 emission reduction when a single glazed window is retrofitted by a translucent aerogel window over a 15 years product lifespan to see if the resulting operational savings can pay back the costs of aerogel production. Results showed that the payback period for the production cost and its CO_2 burden is within 0.3 and 1.9 years. However, the end of life processing impact, such as recycling, reusing, land filling etc., and also transport costs were not taken into consideration in this study. Also, this study is limited to the production of only 1 m^3 of silica aerogel; thus, on a full scale (mass production), the results may not reflect

accurately the energy cost and the CO_2 emission. Despite these factors, results have demonstrated that aerogel can provide a measurable benefit over its life cycle.

Huang (2012) has studied the feasibility of using silica aerogels in buildings. The energy saving potential of silica aerogel used as building insulations is calculated by using the life cycle cost analysis. Results showed that silica aerogel can reduce the annual heat losses of a non-insulated building by around 51%. Moreover, it can reduce about half of the annual heating costs when compared with other insulation materials. However, the cost of silica aerogel-based materials is higher than other traditional insulation materials. The payback time is estimated to be 3.54 years for aerogel materials which is longer than the other competitive solutions (0.22 years for expanded polystyrene, 0.07 years for extruded polystyrene).

2.5. The New Aerogel-Based Coating

Baetens et al. (2011), Cuce et al. (2014), and Koebl et al. (2012) conducted a review on the knowledge of aerogel insulation in general and for building applications in particular. All these presented a review of aerogel-based panels, blankets, and glazing systems. However, a very limited number of studies exist on aerogel-based thermal insulating plasters. Barbero et al. (2014) provided an overall analysis of thermal insulating plasters in the European market. They concluded that innovative solutions for thermal insulating plasters based on materials with pore size in nanometer range, such as aerogel, could make a significant contribution to this field, reaching higher level of thermal performance and reducing the needed thickness. Additionally, successful approaches will have the ability to be used on both new and existing buildings, using techniques that are familiar to today's construction industry. According to the authors, thermal insulating plasters have the advantage of being applied on non-aligned, out of square, or, even, curved areas. They are flexible and can be suitable for any architectural and design solutions. Their easy application on the facades facilitates the rehabilitation of existing buildings. Researchers at EMPA Building Technologies Laboratory (EMPA, www.empa.ch) compared several insulating plasters found in the market today with the aerogel plaster (see Fig. 1.14) and concluded that the thermal conductivity of the aerogel plaster is significantly lower than that of the other plasters.

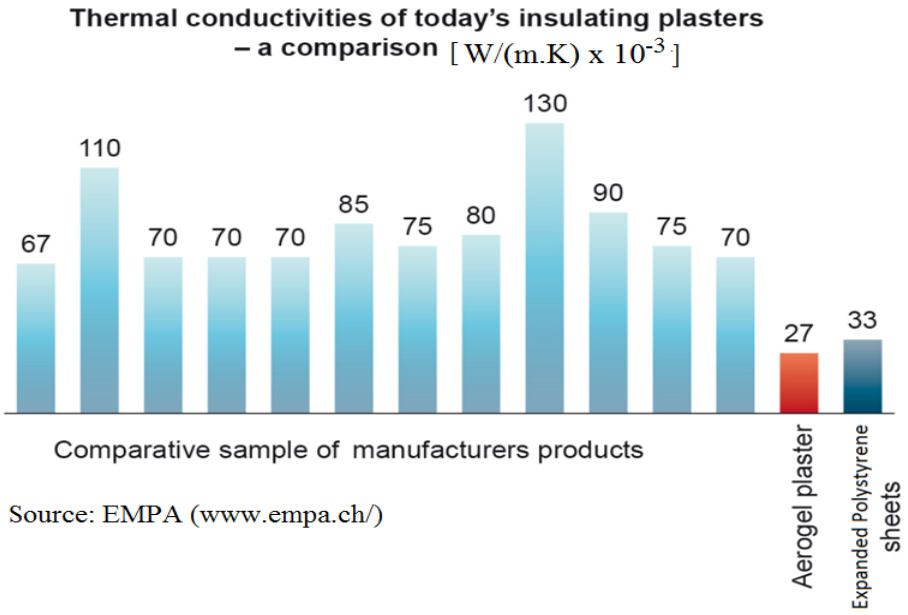

Fig. 1.14 : Thermal conductivity of today's insulating plasters and the aerogel plaster

An innovative insulating coating or rendering based on the (super)-insulating materials silica aerogels has been developed (Fig. 1.15) possessing a low thermal conductivity (Achard et al., WIPO Patent WO/083174, 2011). The invention is a foam of mortar that can be applied to the external wall surfaces of a building to produce a thermally insulating coating. It consists of water, a mineral and/or organic hydraulic binder, insulating filler comprising a powder or granules of hydrophobic silica xerogel, structuralizing filler (option), and additives (option).

Fig. 1.15 : The new aerogel-based insulating coating (rendering)

The aerogel granules are an industrial product manufactured separately in a specialized plant. Thus, the mortar is made from these aerogel grains that somehow replace the sand used in conventional mortar. The latter is prepared industrially as a dry composition by mixing all the above mentioned components and then the mix is stored in bags and transported to the site for

use. Then, on site, the product is mixed with water in order to obtain a paste with a viscosity suitable for the application, for example by spraying, on the building's exterior surface.

This coating has been developed mainly for exterior wall surface applications. The coating thermo-physical characteristics are presented in Table 1.2. They are measured at the Scientific and Technical Center of Buildings (CSTB). Its thermal conductivity is measured by means of guarded hot plate and heat flow meter according to the NF EN standard 12667. Its specific heat is measured by means of differential scanning calorimeter (DSC) according to NF EN 1159-3 standard. Its density is measured according to the NF EN 1602 standard. Its vapour diffusion resistance factor is measured using the Cup method according the NF EN ISO 12572 standard.

Table 1.2: Thermo-physical properties of the new Aerogel-based Insulating Coating

Thermal conductivity (W/m.K)	0.0268
Specific heat (J/kg.K)	990
Density (kg/m^3)	156 (dry)
Vapour diffusion resistance factor (-)	4.25 (average)
Water absorption coefficient (kg/m^2.s$^{1/2}$)	0.184

Until the time of writing this thesis, the thermal conductivity of this new aerogel-based coating (ABC) is 0.0268 W/(m.K) which is better compared to that of traditional insulation (See Table 1.3). Moreover, the volumetric heat capacitance ($\rho * cp$) is much higher than that of traditional insulation.

Table 1.3: Thermal conductivity of some traditional insulation products (source: M. Koebel, A. Rigaccci, P. Achard, Aerogels for Superinsulation: A synoptic view, Chapter 26, p 611, in "Aerogels Handbook (2011), editors: M. Aegerter, N. Leventis, and M. Koebel".

Insulation Product	Chemical Composition	Thermal Conductivity (W.m^{-1}.K^{-1})
Mineral wool	Inorganic oxides	0.034 – 0.045
Glass wool	Silicon dioxide	0.031 – 0.043
Foam glass	Silicon dioxide	0.038 – 0.050
Expanded Polystyrene	Polymer foam	0.029 – 0.055
Extruded Polystyrene	Polymer foam	0.029 – 0.048

The rendering's application on the building facades is rather easy. It is done through direct spraying onto the facade manually (using the ordinary techniques well-known by builders, such as traditional plastering) or using a plastering machine. This has an advantage over traditional insulations especially for building retrofit cases. Traditional insulation needs a plane surface to be

applied on. Furthermore, adjustment, gluing and even fastening by means of dowels is also needed. Insulation materials are often manufactured in precise dimensions; this can lead to discontinuity in thermal insulation. In this sense, the new coating takes advantage over traditional insulation: its application is simple, allows a continuous thermal insulation, and adheres directly to the masonry without leaving hollow gaps where moisture could form. This type of rendering can also be used to limit heat losses through thermal bridges. It can be easily applied to places where existing solutions of external insulation are technically difficult to apply especially for buildings. The new aerogel-based coating can be used in new and existing buildings. For old buildings, it provides not only a better thermal performance but also a decoration for exterior deteriorated facades. Thanks to its mineral basis, the new rendering is very similar to the traditional building materials (e.g. masonry facades), and this makes it ideal for use on old buildings.

In contrary, since this coating is based on silica aerogels, its production cost remains high relative to other existing insulation materials which will increase the payback period as illustrated in the previous section (Huang 2012). Furthermore, its mechanical properties are still not sufficient enough, so there is a need to add a reinforcing mesh.

In a recent research (Stahl et al. 2012, Guizzardi 2014), a new kind of rendering based on silica aerogels granulates, very similar to the one we are presenting, has been developed possessing a thermal conductivity of 0.025 W/(m.K) and a density of around 200 kg/m^3. It contains a purely mineral and cement-free binder. It can be applied to walls both manually or by the aid of a plastering machine.

3. Building Energy Mathematical Models

3.1. Introduction

Buildings are in dynamic interaction with the outside environment. Also, they are influenced by the behavior of occupants. All this creates a complex heat transfer phenomenon through the building. It is vital to create mathematical models for the energy transfer in the building, and then use simulation to predict its energy behavior. Several techniques are available for estimating the energy performance of buildings. Some of them are simple and provide information on the average load or temperature, on a monthly or annual basis. Others are

complex and require more detailed input information. However, the latter perform a more accurate analysis and provide results on an hourly or daily basis. These techniques can be classified under steady state methods or dynamic methods.

3.2. Simple Steady State Models

In the years before computers, it was necessary to find a calculation method based on fewer data, and fewer calculations. Static models use steady state equations to model the heat transfer between the indoor and the outdoor environments. There is always a balance between the heat flux at the exterior surface and the interior surface of the building envelope. Thus, static models are intended mainly to estimate peak heating/cooling loads and select the HVAC sizes. The heat balance for the heating season is given in equation (1.6) (Richalet 1991):

$$Q = L(T_{in} - T_{out}) - A_s * I \quad (1.6)$$

where:

Q is the power of the heating system (W)
L is the building heat loss coefficient (W/°C)
T_{in} , T_{out} are the indoor and outdoor air temperatures, respectively (°C)
A_s is equivalent south surface area (m²)
I is global solar radiation falling on a south wall (W/m²)

Another method is to use the degree-day method. This latter is the summation of temperature differences between a reference temperature and the outdoor air temperature over time. The reference temperature is known as the base temperature which, for buildings, is a balance point temperature, i.e. the outdoor temperature at which the heating (or cooling) systems do not need to run in order to maintain comfort conditions. Then, the energy consumption of the heating/cooling system is proportional to the degrees-days. The energy demand for a building in the heating season can be expressed as equation (1.7) (Sarak and Satman 2003):

$$Q = UA * HDD_y * 86400 \quad (1.7)$$

where:

Q is the annual heating energy demand (J)
UA is the overall heat transfer coefficient for the building (W/°C)
HDD_y is the yearly heating degree-days (°C.day)

These methods can be used to have a quick and rough estimation of the heating and cooling loads of the building through the estimation of its static heat losses/gains. However, they are based on simple assumptions and don't take the transient behavior into consideration. By being fast, these methods sacrifice accuracy in the energy predictions. In addition, they are unable to accurately predict energy impacts of features that have large hourly fluctuations.

3.3. Dynamic Models

The second method of energy modeling, the detailed method, performs a whole-building heat transfer calculation every hour (or even sub-hour) of the year. With the currently available microprocessor speeds, it is viable to use detailed energy simulation models. It accounts for exact sun angles, cloud cover, wind, temperature, and humidity. In doing so, the method can also account for effects of thermal time lag and thermal storage in the building's interior. Using these detailed calculations, one can study the effects of internal thermal mass, solar shading devices, thermostatic controls, daylighting dimmers occupancy sensors, and any other parameter that responds to hourly stimuli.

3.3.1. Detailed Complex Models

In these models, a detailed energy balance is written for all the building elements. Some of these elements (such as walls, roof, etc.) are decomposed into elementary control volumes where the energy balance for each of these volumes is solved after setting the adequate boundary conditions. Equation (1.8) represents the energy balance within a control volume element (Zayane 2011):

$$\rho_{cv} Cp_{cv} V_{cv} \frac{\partial T_{cv}}{\partial t} = \sum_k \emptyset(t) + P(t) \qquad (1.8)$$

where:

$(\rho\ Cp)_{cv}$ is the volumetric heat capacitance of the control volume (J/(m^{3}K))
V is the volume (m^3)
T is the temperature of the control volume element (K)
t is time (s)
$\emptyset$ is the heat fluxes at the control volume boundaries (W)
P is the outside thermal stresses (W)

3.3.2. Reduced-Order Models

Model reduction techniques attempt to simulate the building performance with a reduced set of equations without deteriorating, significantly, the quality of the simulation results. This enables a computer simulation with reduced numerical expenses. This is an important requirement of a dynamic model, especially for its use in real-time control.

The detailed heat balance equations in a building can be written in a state-space form as shown in equation (1.9):

$$\begin{cases} \dot{T} = AT + BU \\ Y = CT + DU \end{cases} \tag{1.9}$$

where T is the state vector of dimension n, U is the input vector, and Y is the output vector. A, B, C, and D are matrices.

The objective of model reduction using state-space representation is to replace equation (1.9) by a similar representation, involving other four matrices A_r , B_r , C_r , D_r as shown in equation (1.10).

$$\begin{cases} \dot{x} = A_r x + B_r U \\ y = C_r T + D_r U \end{cases} \tag{1.10}$$

The new state vector "x" is a reduced state vector of dimension m ($m << n$). "y" is the new output vector, which must approach as near as possible the original vector "Y ". DAUTIN (1997) presents in details different techniques used to reach these reduced-order equations.

Among the reduced-order methods are the Electric Circuits Equivalent Models. These methods make an analogy between the heat transfer in buildings and electric circuits (RC, R2C2, R3C2…), (Laret 1980, Roux 1984, Marti and Rignac 1991). Heat flux is treated as electric current, temperature as voltage, imposed heat flux as current generator, heat capacitance as electric condenser, etc. Resistor–capacitor (RC) networks are commonly used for constructing a reduced order model of the transient heat flow through a solid surface, such as a wall. The resistances and capacitances are carefully chosen to model the combined effect of conduction between the air masses separated by the surface, as well as long wave radiation and convection between the surface and the air mass in contact with it (Gouda and Underwood 2000, Nielsen 2005). A RC network model of a solid surface is a set of linear differential equations whose order is equal to the number of capacitors. The heat and moisture exchange between a zone and the

outside due to the air supplied and extracted by the HVAC system can be modeled with ordinary differential equations.

4. Whole Building Energy Simulation Tools

4.1. Introduction

Building simulation as a discipline can be traced back to the 1960's when the US government was involved in projects to evaluate the thermal environment in fallout shelters (Kusuda 1999). Since then, building simulation as a discipline has evolved significantly. In the 80's, the building energy simulation tools aimed to help architects in the building's early design stages. It was until the 90's that this domain showed a major shift from not only focusing on peak loads and energy consumption but also examining other aspects in the building performance (Augenbroe 1992). This provoked the development of many simulation programs emerging from the research communities to professional practice and offering a variety of tools for different users.

4.2. Why do we need these tools?

Regulations concerning building thermal performance (energy consumption, thermal comfort, etc.) are becoming more and more restrictive (RT 2012). Designers need tools capable of providing an insight on the thermal behaviour of buildings especially during the early design stages. Through the aid of building energy simulation softwares (BES), designers can predict the energy consumption of dwellings, occupants' thermal comfort, sizes of the different HVAC systems, etc. prior to construction. BES tools can help engineers and architects decide on the optimal design of some features to be used in the building, such as windows size, solar shading devices, daylighting sensors, etc. These tools are used for both new construction and retrofit cases. They can perform an economic analysis to identify whether a proposed design or a proposed retrofitting solution is feasible or not.

Also, building simulation tools are used to demonstrate building energy code compliance. In many countries, there exist energy codes that must be met by new buildings or renovated ones. Another importance is to improve the understanding of how energy is used in buildings. This

improved understanding leads to better designs in which components are integrated into systems and subsystems so that the overall energy use is minimized.

4.3. Some Building Energy Simulation Softwares

4.3.1. EnergyPLus

EnergyPlus (EnergyPlus, http://apps1.eere.energy.gov/buildings/energyplus/) is a new generation whole building energy simulation tool based on the best features of two previous programs, BLAST and DOE-2. It was first released in 2001. EnergyPlus is an open-source simulation engine without having a user-friendly graphical interface. The building geometry can be imported from Google Sketchup using Open Studio plug-in for Google Sketchup (which are both free tools). Recently, SIMERGY, an open-source user-friendly graphical interface for EnergyPlus, is released (in May 2013). Otherwise, there are several commercial programs that provide this graphical interface (for e.g. DesignBuilder).

EnergyPlus models heating and cooling loads, levels of light, ventilation, and other energy flows and water use. It includes many innovative simulation capabilities, including, but not limited to, time-steps less than an hour, modular systems and plants with integrated heat balance-based zone simulation, multi-zone air flow, thermal comfort, water use, natural ventilation, and renewable energy systems.

4.3.2. TRNSYS

TRNSYS (Transient System Simulation, http://sel.me.wisc.edu/trnsys/) is a commercial program dating back to 1975. It is used to model the dynamic thermal behavior of energy systems. The components (TYPES) may range from simple heat pump to a multi-zone building model. These models are connected together using a graphical user interface, Simulation Studio. In building simulations, all HVAC components are solved simultaneously with the building envelope thermal balance and the air network. The software's library, in addition to a multi zone, allows the use of many commonly used components, including: solar panels, photovoltaic systems, HVAC systems, cogeneration systems, etc. The modular nature of this software tool facilitates the addition of mathematical models to it. TRNSYS allows the user to incorporate components developed in other software tools such as MATLAB.

4.3.3. IDA ICE

IDA Indoor Climate and Energy (IDA ICE, www.equa.se/ice) is a modular multi-zone energy simulation commercial software first released in 1998. It estimates the building energy consumption as well as assesses thermal comfort condition. The multi-domain physical systems are modeled using the symbolic equation format. Two levels are present: standard and expert. The standard is intended to target beginner to intermediate level users, while the expert is intended to target advanced level users. The expert level can be used to edit the mathematical model of the systems. The modular nature of IDA ICE makes it possible to write individual models extending its capabilities as needed by the individual user.

4.3.4. IES VE

IES VE (Integrated Environmental Solutions - Virtual Environment, www.iesve.com) is also commercial software dating back to the late 1990's. The building geometry modeling tool, ModelIT, enables the creation of a 3D model from scratch. Alternatively, CAD data can be imported into the system in 3D or 2D (e.g.. SketchUp, Revit, DXF…). Another tool, ApacheSim, performs the dynamic thermal simulation at sub-hourly timesteps for better computation of building components. ApacheSim can be linked to other components of IES-VE to include detailed results of shading devices and solar penetration (SunCast), airflow analysis (MacroFlow), component based HVAC systems (ApacheHVAC) and lighting (LightPro, RadianceIES). The results can also be exported for a more detailed computational fluid dynamics (CFD) simulation by Microflow.

4.3.5. ESP-r

ESP-r (www.esru.strath.ac.uk /Programs /ESP-r) is an integrated energy modeling tool for the simulation of the thermal, visual and acoustic performance of buildings and the energy use and gaseous emissions associated with environmental control systems. The system is equipped to model heat, air, moisture and electrical power flow. It was first developed in 1974. The geometry of the building can be constructed using CAD tools or other similar ones. ESP-r is based on a finite volume conservation approach in which a problem (specified in terms of geometry, construction, operation, etc.) is transformed into a set of conservation equations (for energy, mass, momentum, etc.) which are then integrated at successive time-steps in response to climate,

occupant and control system influences. ESP-r comprises a central Project Manager around which are arranged support databases, a simulator, various performance assessment tools, and a variety of third party applications for CAD, visualization, and report generation. One of the best features of ESP-r is the capability of performing CFD simulations as well as handling uncertainties (for e.g. uncertainty in thermophysical properties, climate data, convection correlations…).

4.4. Co-Simulation

4.4.1. Introduction

The analysis of the different building systems is too complex as it includes envelope, HVAC systems, controls, solar gains, renewable energy systems, etc. Since all these systems interact with each other, an integrated simulation solution approach is needed. However, in building simulation tools, all these subsystems are not equally modeled. For example, some tools are better in envelope modeling and simulation (for e.g. EnergyPlus, ESP-r). Others are more flexible in modeling HVAC systems (for e.g. TRNSYS, Modelica). Yet, other features may not be present in certain BES tools, such as CFD simulations or some innovative systems.

Here comes the importance of developing a flexible modeling environment that takes the advantage of the different features found in the different tools, as opposed to being restricted with the capabilities of one particular program, and also allows analyzing newly developed building systems that have not yet been implemented by the program developers. This is achieved by run-time interoperability. This latter is known as co-simulation (Wetter and Haves 2008, Trcka 2008), process model cooperation (Hensen et al. 2004), or external coupling (Djunaedy 2005). Co-simulation is defined as applications in which at least two simulators, each solving an initial-value differential or difference equation, are coupled to exchange data that depend on state variables.

4.4.2. Advantages of Co-simulation

According to Trcka et al. (2009), among the advantages of co-simulation are:

- There is no single tool that can be used to solve all simulation analysis problems encountered by designers.

- It allows combining heterogeneous solvers and modeling environments of specialized tools.
- Each tool can benefit from future simulation model developments of emerging technologies as soon as they become available.
- Rapid prototyping of new technologies.
- Multi-scale modeling and simulation can be done by combining various building and system models, developed by different parties, to simulate scenarios on the scale of a town or even regions.

4.4.3. Coupling Strategies

The two (or more) programs exchange data at each predefined time step. We have two strategies: loose coupling and strong coupling.

4.4.3.1. Loose Coupling

In the Loose Coupling (Trcka et al. 2007), also called quasi-dynamic synchronization (Zhai et al. 2002) or "ping pong" coupling (Trcka and Hensen 2006), the two programs exchange data only once at each time step. This is done in two ways: either the first program runs the next time step and returns its outputs to the second program as shown in Fig. 1.16, or the two programs run in parallel and they exchange data at the end of each time step. The received data are used for the next time step as shown Fig. 1.17.

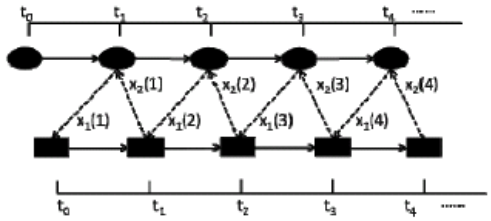

Fig. 1.16: Loose coupling - successive program runs (source: Tian and Zuo 2013)

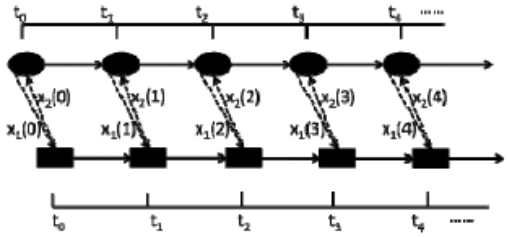

Fig. 1.17: Loose coupling - parallel program runs (source: Tian and Zuo 2013)

4.4.3.2. Strong Coupling

In the strong coupling (Trcka et al. 2009), also called fully dynamic synchronization strategy (Zhai et al. 2002) or onion coupling (Trcka and Hensen 2006), the two programs exchange data several times at each time step until convergence is reached for both of them (Fig. 1.18). The strong coupling is more accurate compared to the loose coupling; however, it is significantly slower, which can be a severe limitation for many applications (Zhai and Chen 2003).

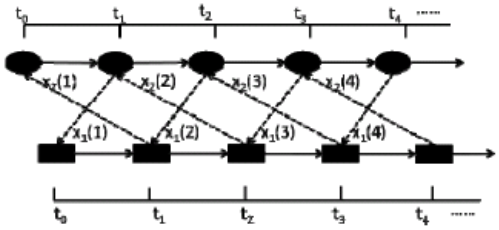

Fig. 1.18: Strong coupling (source: Tian and Zuo 2013)

4.4.4. Co-simulation Platforms

In 2010, MODELISAR (https://www.fmi-standard.org/) has launched the Functional Mock-up Interface for Model Exchange (FMI) to facilitate model exchange and co-simulation. Models are transformed into a Functional Mock-up Unit (FMU) which can then be integrated and used in other modeling and simulation environments. Also, it allows exchange of data through a co-simulation environment between different simulation tools. Another tool for co-simulation is the Building Controls Virtual Test Bed (BCVTB 2012). BCVTB is a middleware software environment that enables connecting different simulation softwares for co-simulation and also coupling simulation programs with actual hardware. The programs that can be linked together through BCVTB are EnergyPlus, Modelica/Dymola, MATLAB/Simulink, Radiance, ESP-r, BACnet stack (which allows exchanging data with BACnet compliant Building Automation System), and analog/digital interface USB-1208LS from Measurement Computing Corporation that can be connected to a USB port.

5. Résumé du Chapire en Français

Le premier chapitre de la thèse présente l'état de l'art sur l'analyse du comportement thermique du bâtiment. Un bâtiment peut être vu comme une boîte, il protège son contenu contre la variation des conditions climatiques. Son enveloppe agit comme un échangeur, qui permet l'absorption ou la libération d'énergie avec l'environnement extérieur. Il parait intéressant de bien concevoir cette enveloppe tout en examinant son effet sur la performance thermique du bâtiment afin d'améliorer le confort de ses occupants avec une consommation d'énergie optimisée.

De nombreux facteurs affectent la performance thermique du bâtiment. Parmi ceux-ci, on peut citer: l'isolation thermique, l'inertie thermique associée à une ventilation naturelle, et les gains solaires. Un mur bien isolé réduit les pertes de chaleur vers l'extérieur durant la saison froide et réduit la chaleur transmise à l'intérieur durant la saison chaude. L'isolation empêche également la condensation de vapeur dans la paroi. D'autre part, une enveloppe bien isolée peut entrainer des surchauffes durant les jours chauds d'été où le rayonnement solaire absorbé pendant la journée (entrée par les fenêtres) peut être piégé à l'intérieur. La position de l'isolant joue un rôle important sur le comportement thermique des murs extérieurs. Différents types de construction existent: isolation par l'extérieur, isolation par l'intérieur, isolation au milieu de la paroi, et isolation par l'intérieur et l'extérieur. Pendant la saison d'hiver, l'excès de la chaleur dû au rayonnement solaire est absorbé et stocké pendant la journée et libèré pendant la nuit quand il fait froid à l'extérieur (phénomène d'inertie thermique). Pendant les nuits d'été, lorsque la température à l'extérieur est inférieure à celle à l'intérieur du bâtiment, il est possible d'appliquer la ventilation naturelle.

Le rayonnement solaire pénètre les façades des bâtiments de deuxmanières différentes. La première est le rayonnement solaire absorbé par les surfaces opaques et puis transmis vers l'intérieur. La seconde est les gains solaires à travers les fenêtres qui sont absorbés à la surface des matériaux disposés à l'intérieur de la pièce.

L'un des aspects d'une bonne conception du bâtiment est le confort thermique des occupants. Le standard ISO 7730 (ISO 2005) définit le confort thermique comme l'état mental qui se déclare satisfait de l'ambiance thermique. Un grand nombre de facteurs affectent le confort thermique des habitants comme : la température ambiante, l'humidité, la vitesse d'air, etc. Des

recherches approfondies ont traité la modélisation du confort thermique. La plupart des ingénieurs utilisent des standards tels que la norme ASHRAE 55 (ASHRAE 2010) et la norme ISO 7730 (ISO 2005) pour estimer le confort thermique. Ces normes sont basées principalement sur des modèles mathématiques, mis au point par Fanger et ses collègues sur la base des études de laboratoire (Fanger 1970).

La nouvelle réglementation thermique vise à s'assurer que les nouveaux bâtiments auront un moindre recours aux ressources énergétiques. La priorité en France est la rénovation les bâtiments existants parce que ces bâtiments représentent une proportion élevée de consommation d'énergie et ils seront présents pour les décennies à venir. Plusieurs études ont montré que le moyen le plus efficace est de réduire la consommation d'énergie dans le secteur de la construction (nouvelle et existante). La réduction des pertes de chaleur est assurée en améliorant l'isolation de l'enveloppe du bâtiment (toit, sol, murs et fenêtres). Pour les bâtiments anciens et les nouveaux, l'épaisseur des couches d'isolation interne ou externe devient un enjeu majeur. Par conséquent, il y a un intérêt croissant pour les matériaux dits super-isolants, tels que les aérogels qui permettent de réduire l'épaisseur d'isolant à mettre en œuvre pour une même valeur de résistance thermique.

Les aérogels de silice sont issus de gels de silice séchés dans des conditions particulières. Ils sont légers et présentent d'exceptionnelles propriétés thermiques. Ils ont une porosité élevée (80-99,8 %), une faible densité (100 à 200 kg/m3) et une conductivité thermique faible (0.014 W/(m.K)). Les aérogels de silice constituent une alternative innovante à l'isolation traditionnelle en raison de leurs performances thermiques élevées, bien que les coûts du matériau restent élevés. Des recherches se poursuivent pour améliorer les performances de ce type d'isolation et pour diminuer les coûts de leur production. Leur faible conductivité thermique ainsi que leur transparence optique permettent aux aérogels d'être utilisé pour l'isolation des façades opaques et l'isolation des parties vitrées. Deux types différents de matériaux isolants basés sur l'aérogel de silice sont étudiés pour application dans le secteur du bâtiment. Le premier concerne des matériaux opaques à base d'aérogels de silice et le second concerne lui des matériaux d'isolation translucides.

Un enduit isolant innovant basé sur les aérogels de silice a été développé possédant une faible conductivité thermique. La technique employée repose sur l'application d'un tel enduit sur la surface extérieure du bâtiment pour réaliser un revêtement isolant thermiquement. Cet enduit

est formulé à sec à partir d'un liant hydraulique minéral avec éventuellement une fraction organique, une charge structurante si nécessaire et des adjuvants, auxquels est ajoutée une charge isolante comprenant une poudre ou un granulat de xérogel de silice hydrophobe Il est mis en œuvre par gachage avec de l'eau puis projeté sur le mur à isoler.

Pour examiner la performance énergétique des bâtiments, les concepteurs ont besoin d'outils capables de fournir le comportement thermique des bâtiments, surtout pendant les premières phases de la conception. Grâce à l'aide de logiciels de simulation énergétique des bâtiments, les concepteurs peuvent prédire la consommation énergétique, le confort thermique des habitants, etc. avant la construction. Ces Outils peuvent aider les ingénieurs et les architectes à définir la conception optimale de certaines fonctions du bâtiment. Ils servent aussi bien pour les études des nouvelles constructions que pour celles concernant la rénovation des bâtiments. En plus, ils aident à effectuer une analyse économique pour vérifier si une conception ou une solution proposée est faisable ou ne l'est pas. Aussi, les outils de simulation servent à démontrer la conformité à la réglementation thermique.

L'analyse des différents systèmes de bâtiment est trop complexe, puisqu'elle comprend les systèmes de chauffage et de climatisation, les systèmes de contrôle, les gains solaires, les systèmes d'énergie renouvelable, les enveloppes, etc. Une approche de solution intégrée est nécessaire. Toutefois, dans les outils de simulation, tous ces sous-systèmes ne sont pas également modélisés. Donc, il est nécessaire de développer un environnement de modélisation flexible qui prend l'avantage des différentes fonctionnalités présentes dans les différents outils et permet d'analyser les nouveaux systèmes qui n'ont pas encore été mis en œuvre par les développeurs de programme de simulation. Ceci est réalisé par ce qu'on appelle la « co-simulation ». La co-simulation est définie comme une technique dans laquelle au moins deux simulateurs sont couplés pour échanger des données qui dépendent des variables d'état.

CHAPTER 2

HEAT AND MASS TRANSFER THEORETICAL MODELING APPLIED TO WALLS COVERED WITH AEROGEL-BASED COATING

Chapter 2
Heat and Mass Transfer Theoretical Modeling Applied to Walls Covered with Aerogel-Based Coating

Chapter Contents

1. Introduction

As illustrated in Chapter 1, the objectives are to study the thermal behavior of buildings having the new Aerogel-Based insulating Coating (ABC) on their external facades and to propose a new assisting heating system. These objectives are summarized as following:

- Optimize the exterior walls' structure using the "ABC" under different operation modes of the heating system.
- Study the potential to limit thermal bridge heat losses using the "ABC" and propose a methodology to incorporate, dynamically, the thermal bridge effects into the whole building energy simulation program EnergyPlus.
- Assess the hygric performance of exterior walls covered with this coating
- Examine the effect of applying the "ABC" on energy consumption and thermal comfort for new and existing dwellings.
- Propose a new assisting heating system for the aim of decreasing the heating demand. Its concept is to capture the heat energy striking the south facade and transfer it to the north facade through the exterior envelope, particularly, through water pipes embedded in the coating.

In this chapter, we develop all the mathematical models needed to carry out all the simulations. We need: the one and two-dimensional conduction heat transfer models in a multi-layer wall, the one-dimensional heat and moisture (hygrothermal) transfer model, the whole building thermal model, and the proposed assisting heating system model. For each one of these, we start by an introduction to explain more the objectives behind developing this model. Then, all the mathematical equations and numerical solutions are presented. Some of these models are compared against analytical solutions or other solutions presented in international standards.

2. Multi-layer Wall One-Dimensional Heat Transfer Model

2.1. Introduction

The building's external fabric is in continuous interaction with the outside environment. As the outside air temperature and solar radiation vary throughout the day, the outside surface temperature of the walls is greatly affected leading to fluctuations in the heat flux passing through them to the inside. As a result, the indoor environment may be significantly changed. Thus, a great concern should be given to the design of external walls. Extensive research has been

carried out dealing with optimizing layers configuration in exterior walls. Some used energy consumption to maintain the indoor air temperature at a certain set-point value as the assessment parameter (Al-Sanea et al. 2011, Ozel 2012, Kossecka and Kosny 2002, Ibrahim et al. 2012, Balocco et al. 2008). The lower the energy consumption, the better is the wall. Others used time lag and decrement factor (Mavromatidis et al. 2012, Jin et al. 2012, Asan 2000, Kontoleon and Bikas 2007, Kontoleon and Eumorfopoulou 2008, Ulgen 2002). In general, walls are considered better when they have a low decrement factor and a high time lag.

Most of the studies dealing with optimizing exterior walls' structure have focused on continuous air-conditioning/heating where the indoor air temperature is kept fixed at a set-point value. Asan (2006) estimated the time lags and decrement factors for different building materials by solving the one-dimensional heat transfer equation numerically using the Crank-Nicholson scheme, and imposing a periodic boundary condition at the outside environment while keeping the room temperature fixed. Three groups of materials were used. The first had low thermal conductivity and low thermal capacitance, the second had high thermal conductivity and high thermal capacitance, and the third had moderate thermal conductivity and high thermal capacitance. Ulgen (2002) examined different wall compositions to obtain the best thermal performance from a time lag and decrement factor point of view. Time lag and decrement factor were estimated theoretically using an analytical solution and then compared to the results obtained from experimental measurements. Results showed that an increased density and heat capacity had good effects on the results. Kossecka et al. (2002) investigated the influence of insulation position within exterior walls on the heating and cooling loads in a continuously occupied building. The insulation position was varied within the wall and for each location the energy demand was calculated. Several studies have shown that placing the insulation layer at the outer wall surface provides better thermal performance than placing it at the inner surface (Ozel et al. 2007, Al-Sanea et al. 2003, Al-Sanea et al. 2012, Aste et al. 2009, Vijayalakshmi et al. 2006). Other studies found that placing insulation layers both at the inside and outside wall surfaces is the best configuration (Kossecka and Kosny 2002, Al-Sanea et al. 2011).

Fewer studies have dealt with optimizing the layer composition of exterior walls in non-air-conditioned spaces or in intermittently-air-conditioned (or heated) spaces. Tsilingiris (2006) investigated the best location of the insulation layer in exterior walls under the effect of

intermittent heating for a typical winter weather conditions representative of a mild Mediterranean climate. Results showed that locating the insulation at the inner wall surface reduces energy consumption by about 30%-40% compared to locating the insulation at the outer face of the walls. A similar study has been done by Bojic et al. (2001) but considering intermittent cooling in a hot, humid climate. They showed that, approximately, 11% energy savings were obtained when the insulation is placed at the inner surface of the walls compared to placing it at the outer surface. Barrios et al. (2012) studied the thermal performance of six wall/roof configurations in an intermittently air-conditioned room in a climate where the outdoor temperature swing crosses the thermal comfort zone. The results showed that when using one layer of insulation in a wall, the best thermal performance is achieved by placing it at the exterior side.

Our objectives are to optimize the exterior wall layer composition for: 1- continuously heated space (cH), 2- intermittently heated space (iH), and 3- not heated space (nH) using the aerogel-based insulating coating. For that, we need a numerical model for the one-dimensional heat transfer within a multi-layer wall structure. Several assessment parameters are considered for the different cases (cH, iH, and nH), such as time lag, decrement factor, energy load, and thermal comfort index.

2.2. Mathematical Equations

The transient one-dimensional (1D) heat conduction equation in a multi-layer wall of length L consisting of M parallel, isotropic, and homogeneous layers (Fig. 2.1) is given by equation (2.1):

$$\rho_l cp_l \frac{\partial T_l(x,t)}{\partial t} = k_l \frac{\partial^2 T_l(x,t)}{\partial x^2} \tag{2.1}$$

where: l represents the l^{th} layer within the wall. t and x are the time and spacial coordinates. T is the temperature. k, ρ, and cp are the thermal conductivity, density, and specific heat capacity, respectively.

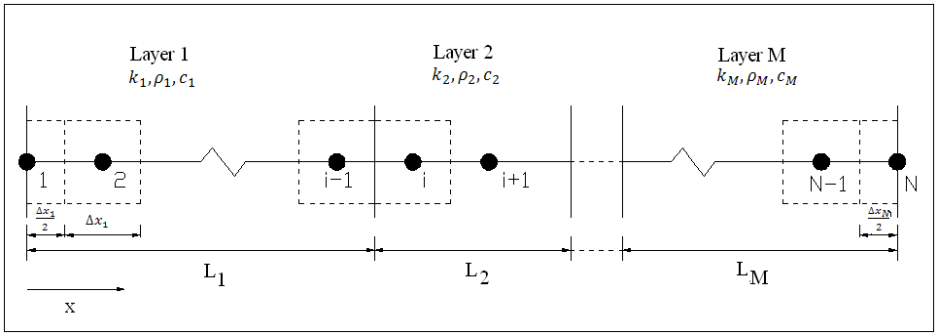

Fig. 2.1 : Wall layer discretization

The boundary conditions at the outdoor and indoor surfaces of the wall are given in equations (2.2-a) and (2.2-b), respectively.

$$h_{out}^{c}(T_{out} - T_{x=0}) + \alpha . I + \gamma . \Delta R = -k\frac{\partial T(0,t)}{\partial x} \qquad (2.2-\text{a})$$

$$h_{in}^{c}(T_{x=L} - T_{in}) + h_{in}^{r}(T_{x=L} - T_{MRT}) = -k\frac{\partial T(L,t)}{\partial x} \qquad (2.2-\text{b})$$

where $h_{out}^{c}, h_{in}^{c}, and h_{in}^{r}$ are the outside surface convective heat transfer coefficient, inside surface convective heat transfer coefficient, and radiative heat transfer coefficient with the other walls in the room, respectively. $T_{out}, T_{x=0}, T_{in}$, $and\ T_{x=L}$ are the outside air, outside wall surface, room air, inner wall surface temperatures, respectively. T_{MRT} is the mean radiant temperature of the other room surfaces. $\alpha, I,$ and ΔR are the exterior surface solar absorptivity, total incident solar radiation, and long-wave radiation heat exchange with the sky. γ is a correction (calibration) parameter to account for long-wave radiation heat exchange with the ground and other adjacent surfaces.

The long-wave radiation heat exchange with the sky is calculated using equation (2.3):

$$\Delta R = h_{sky}^{r}\left(T_{sky} - T_{x=0}\right) \qquad (2.3)$$

where T_{sky} is the effective sky temperature calculated using equations (2.4) and (2.5) (Clark and Allen 1978, Walton 1983) and h_{sky}^{r} is the radiative heat transfer coefficient calculated using equation (2.6).

$$T_{sky} = \left(\varepsilon_{sky}\right)^{0.25} T_{out} \qquad (2.4)$$

$$\varepsilon_{sky} = \left[0.787 + 0.764.Ln\left(\frac{T_{dp}}{273}\right)\right].(1 + 0.0224CC - 0.0035CC^2 + 0.00028CC^3) \qquad (2.5)$$

$$h_{sky}^{r} = \varepsilon.\sigma.F.(T_{sky}^2 + T_{x=0}^2)(T_{sky} + T_{x=0}) \qquad (2.6)$$

where $\varepsilon, \sigma,$ and F are the surface emissivity, Stephan-Boltzmann constant, and the view factor to the sky, respectively. T_{dp} and *CC* are the dewpoint temperature and cloudiness coefficient, respectively.

When the heating system is ON, the indoor air temperature is set to a constant value; however, when it is OFF, the indoor air temperature is considered to be only a function of the heat transfer through the wall, and is calculated using equation (2.7):

$$\rho_{air} cp_{air} V_{air} \frac{\partial T_{in}}{\partial t} = h_{in}^{c} A (T_{x=L} - T_{in}) \tag{2.7}$$

where ρ_{air}, cp_{air}, and V_{air} are air density, air specific heat, and air volume, respectively. *A* is the wall area.

For "cH" and "nH", the assessment parameters are time lag ($\emptyset$) and decrement factor (f). Also, we have two time lags, one for the minimums ($\emptyset_{min}$) and one for the maximums ($\emptyset_{max}$).

For "nH" case, in addition to time lag and decrement factor, another assessment parameter is used: thermal comfort index (*TCI*). This latter indicates how far the room air temperature is from the set-point value. In this study, our concern is thermal comfort during the occupied period assumed from 18:00 till 7:00; thus, TCI is calculated just for this period. The more TCI is lower, the more the discomfort hours are decreased. Its unit is degree.hour and is calculated as following:

$$TCI = \sum_{18h \to 7h} \left(T_{setpoint} - T_{in}\right) \Delta t \tag{2.8}$$

For the intermittent heating case (iH), several assumptions are made:

- the capacity of the heating system is always sufficient to meet the load (oversized)
- very rapid response of the heating system
- the room air reaches its set-point temperature in a very short time

For this case, the evaluation parameter is the heating load (*q*) when the heating system is ON. *q* is calculated using equation (2.9):

$$q = \sum_{18\text{h} \to 7\text{h}} h_{in}^{c} (T_{in} - T_{x=L}) \tag{2.9}$$

2.3. Numerical Solution

The 1D heat transfer equation (2.1) is discretized numerically using the implicit finite difference scheme. The code is developed using MATLAB®. The composite wall of *M* layers is

discretized into a number of control volumes. The result is a set of linear algebraic equations which can be written in a matrix form as,

$$A * T = b \tag{2.10}$$

where *A* is a tri-diagonal highly sparsed matrix.

The linear algebraic equation (2.10) is solved using built-in functions in MATLAB®. The latter uses different algorithms to solve the linear system of equations such as Gaussian elimination, Cholesky factorization, LU decomposition, etc. depending on the structure of the coefficient matrix *A*.

Starting from an arbitrary chosen initial values for the wall temperatures, the daily cycle of the outside environmental conditions is repeated on several consecutive days until a steady periodic solution is obtained during which quasi steady-state solutions are developed.

2.4. Comparison with Analytical Solutions

The 1D heat transfer model is compared to analytical solutions found in the literature. For a plane wall of length 2L initially at constant temperature T_i and subjected to convective heat transfer (of coefficient *h*) with the surrounding air of temperature *Ta*, the analytical solution can be derived and is given in equation (2.11) (Cengel 2005 Chapter 4, section 2).

$$\frac{T(x) - T_a}{T_i - T_a} = \sum_{n=1}^{\infty} A_n e^{-\gamma_n^2 F_o} cos(\gamma_n X) \tag{2.11}$$

where *X* is the dimensionless distance from the center (*X = x/L*) and F_o is the Fourrier number. F_o *and* A_n are calculated as following:

$$F_o = \frac{\alpha . t}{L^2} \tag{2.12 - a}$$

$$A_n = \frac{4sin(\gamma_n)}{2\gamma_n + sin(2\gamma_n)} \tag{2.12 - b}$$

where α and t are the thermal diffusivity and time, respectively. γ_n are the roots of equation (2.12-c).

$$\gamma_n \tan(\gamma_n) = B_i = \frac{h . L}{k} \tag{2.12 - c}$$

Figure 2.2 shows the temperature variation in the wall for the analytical solution and the numerical model for *X*=1, B_i= 5, and for different times. The figure shows the temperature profile only from half of the wall considering the model symmetry. From this figure, it is shown that the

numerical model is capable of reproducing, almost, the same temperatures calculated by the analytical solutions.

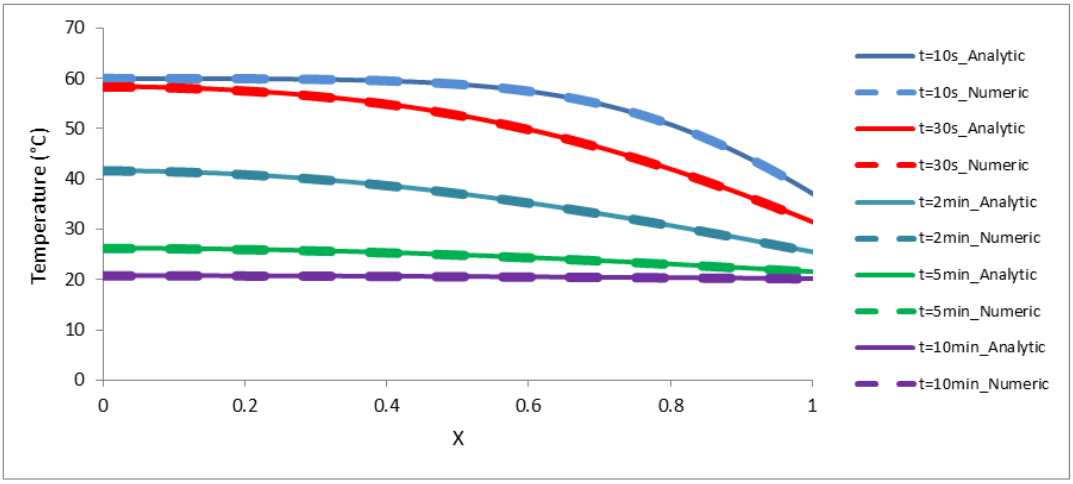

Fig. 2.2 : 1D heat transfer model comparison with analytical solution

3. Multi-layer Wall Two-Dimensional Heat Transfer Model

3.1. Introduction

Thermal bridges are weak areas of the building envelope, where heat can find its path through them penetrating the well-insulated walls. Moreover, the innovative technologies for modern buildings (for instance, silica aerogels based materials and vacuum insulation panels) induce thermal bridge effects that cannot be neglected (Alam et al. 2011). According to the French Scientific and Technical Center for Building Research (CSTB), thermal bridges can increase the thermal load of a house by 20% (CSTB, Réglementation thermique 2000). Furthermore, Kosny and Kossecka (2002) showed that the calculation of a thermal resistance of a wall, neglecting the thermal bridge effects and adopting the one-dimensional approach, could also lead to an overestimation greater than 44%.

A lot of research has been carried out concerning the effect of thermal bridges on energy consumption (Theodosiou and Papadopoulos 2008, Cappelletti et al. 2011), on thermal comfort (Campos et al. 2009), and on cost (Evola et al. 2011). Also, other studies have focused on conducting sensitivity analysis to identify the main important design variables affecting the heat losses through different types of thermal bridges (Capozzoli et al. 2013, Mechri et al. 2010).

Ascione et al. (2012) showed that approximate models of thermal bridges induce inaccurate interpretations and, consequently, inappropriate energy demands. They calculated the effect of the thermal bridges of a roof structure on the energy load of an office building using three different approaches for the thermal bridge representation; (a) a simplified scheme that considers an equivalent homogeneous structure, (b) a detailed subdivision in ‘‘series and ‘‘parallel’’ layers, and (c) the real structure modeled by means of CFD studies. Results showed that the thermal transmittance of the roof varied greatly between the three approaches. The energy demand also was quite variable depending on the modeling strategy. The accurate interpretation of the thermal behavior of the composite structures (approach 3) lead to a lower energy load for winter conditions, with respect to the simplified model (approach 1), by about 20% in the South of Italy and about 13.5% in the North. Al-Sanea and Zedan (2012) studied the effect of the two dimensional heat transfer of an insulated wall cut by mortar joints under steady periodic conditions for the climate of Riyadh. Transmission loads increased by 62% and 103% for mortar heights of 10 and 20 mm, respectively, compared to wall with no mortar joint effect.
Gao et al. (2008) developed a low-order three-dimensional heat transfer model to account for additional losses of thermal bridges. Then, they developed a new “TYPE” in TRNSYS in order to implement the thermal bridges effect into a whole building. This TYPE generates additional heat loss output with the reduced model. They showed that the additional thermal bridge heat losses in a room situated in the northern part of France for a 2 days simulation can reach 19%.

Most building energy simulation programs do not model the heat transfer in walls as two and three dimensional but rather consider it as merely one dimensional. This can lead to major deviations from the real load of the building especially for passive and low energy houses. To tackle this effect, we propose a methodology to incorporate the two-dimensional thermal bridge effects into the whole building energy simulation program EnergyPlus through co-simulation between this latter and a 2D heat transfer model developed in MATLAB®. As an application to this methodology, we tackle the effect of thermal bridges resulting from windows offset from exterior walls (window edges) on the total energy load of the space. We compute the heating load coming from the windows offset thermal bridges and show how much it constitutes of the total heating load of a typical French house before and after adding the insulating coating on the thermal bridges. In addition, we compare the time lag and decrement factor when the 2D heat

transfer effects of the thermal bridge are taken into consideration with those obtained for the 1D heat transfer case. In this section, we just present the 2D heat transfer mathematical equations and the numerical solution. In Chapter 4, we explain in details how the co-simulation is done with all the results.

3.2. Mathematical Equations

The two dimensional heat transfer equation within a multilayer wall structure, considering no heat generation, is given by equation (2.13):

$$\rho_l cp_l \frac{\partial T_l}{\partial t} = \frac{\partial}{\partial x}\left(k_l \frac{\partial T_l}{\partial x}\right) + \frac{\partial}{\partial y}\left(k_l \frac{\partial T_l}{\partial y}\right) \tag{2.13}$$

where $\rho, cp,$ and k are the density, specific heat, and thermal conductivity respectively. T stands for the temperature field. x and y are the spatial coordinates and t is the time. l represents each layer within the structure.

Boundary conditions

Consider a rectangular domain of length L and width W (Fig. 2.3).

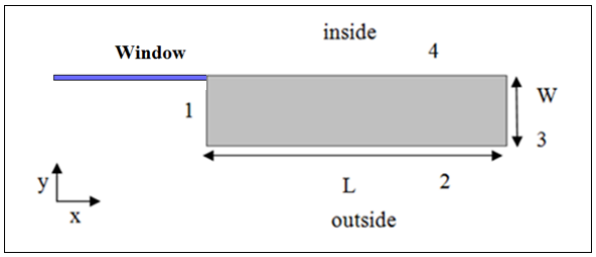

Fig. 2.3: Wall structure of length L and width W

At the inner wall surface "4":

$$-k\frac{\partial T}{\partial y}\Big|_{y=W} = h_{in}^{c}\left(T_{y=W} - T_{in}\right) + h_{in}^{r}\left(T_{y=W} - T_{MRT}\right) \tag{2.14-a}$$

At the outer wall surfaces "1 and 2":

$$-k\frac{\partial T}{\partial x}\Big|_{x=0} = h_{out}^{c}(T_{out} - T_{x=0}) + \alpha.I + \Delta R \tag{2.14-b}$$

$$-k\frac{\partial T}{\partial y}\Big|_{y=0} = h_{out}^{c}(T_{out} - T_{y=0}) + \alpha.I + \Delta R \tag{2.14-c}$$

At the adiabatic surfaces "3":

$$\left.\frac{\partial T}{\partial x}\right|_{x=L} = 0 \qquad (2.14-d)$$

An adiabatic boundary condition is assigned to the surface "3" where the two dimensional effects will no longer exist.

3.3. Numerical Solution

The implicit finite volume method is implemented to solve the above system of equations. The code is written in MATLAB®. The domain is divided into rectangular control volumes (see Fig. 2.4). The finite volume equations are derived by integrating equation (2.13) over a typical control volume and simultaneously averaging over a finite increment of time Δt as following:

$$\rho c \int_t^{t+\Delta t}\int_w^e\int_s^n \frac{\partial T}{\partial t}\,dxdydt = \int_t^{t+\Delta t}\int_w^e\int_s^n k\frac{\partial}{\partial x}\left(\frac{\partial T}{\partial x}\right)dxdydt + \int_t^{t+\Delta t}\int_w^e\int_s^n k\frac{\partial}{\partial y}\left(\frac{\partial T}{\partial y}\right)dxdydt \qquad (2.15)$$

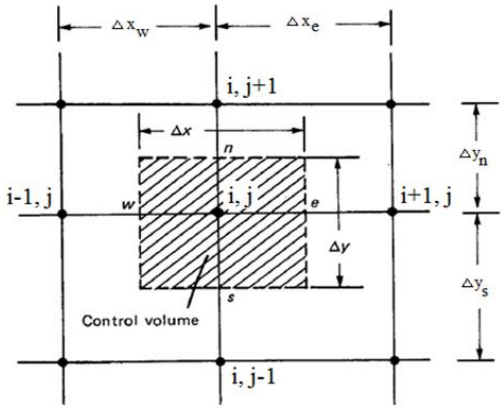

Fig. 2.4: Typical control volume

After integrating, we have the discretization equation as following:

$$a_{i,j}T_{i,j}^{t+\Delta t} = a_{i+1,j}T_{i+1,j}^{t+\Delta t} + a_{i-1,j}T_{i-1,j}^{t+\Delta t} + a_{i,j+1}T_{i,j+1}^{t+\Delta t} + a_{i,j-1}T_{i,j-1}^{t+\Delta t} + b \qquad (2.16)$$

where,

$$a_{i+1,j} = k_e\frac{\Delta y}{\Delta x_e} \qquad (2.17-a)$$

$$a_{i-1,j} = k_w \frac{\Delta y}{\Delta x_w} \qquad (2.17-b)$$

$$a_{i,j+1} = k_n \frac{\Delta x}{\Delta y_n} \qquad (2.17-c)$$

$$a_{i,j-1} = k_s \frac{\Delta x}{\Delta y_s} \qquad (2.17-d)$$

$$a_{i,j} = a_{i+1,j} + a_{i-1,j} + a_{i,j+1} + a_{i,j-1} + \rho cp \frac{\Delta x\, \Delta y}{\Delta t} \qquad (2.17-e)$$

$$b = \rho cp \frac{\Delta x\, \Delta y}{\Delta t} * T_{i,j}^{t} \qquad (2.17-f)$$

Note that for the boundary nodes, the boundary conditions will be absorbed in the vector b. Deriving the discretization equation for each control volume, we form a system of linear algebraic equations that is written in a matrix form as:

$$A * T = b \qquad (2.18)$$

3.4. Model Comparison with References

3.4.1. Comparison with the ISO 10211 Standard Test Cases

The simulation results of the 2D heat transfer model in a multi-layer domain are compared to the results of the EN ISO 10211 standard (ISO 10211 2007) test cases 1 and 2. Figure 2.5 shows the geometry and the surface temperatures (boundary temperatures) as well as the analytical solution at 28 points of an equidistant regular grid for test case 1. The model only includes the left half of the square considering symmetry boundary conditions.

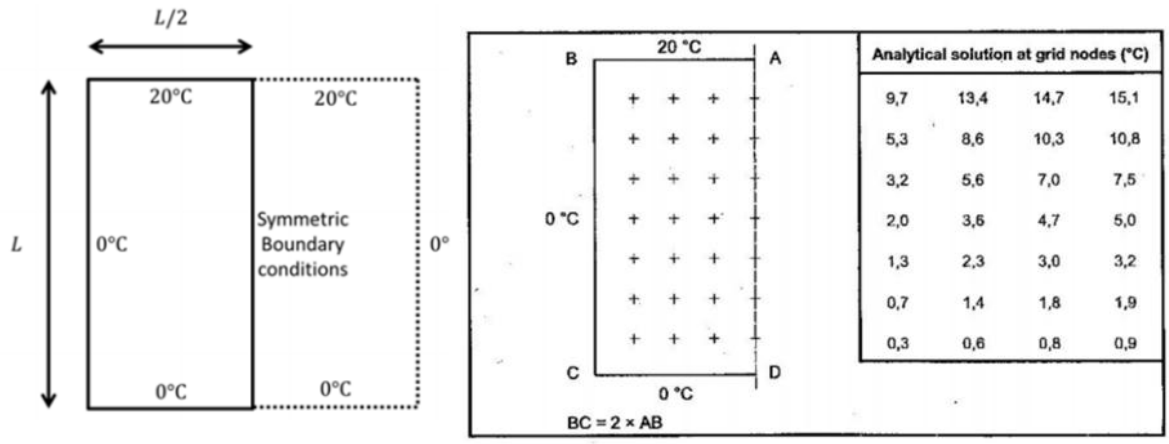

Fig. 2.5: Analytical solution at the grid points for ISO 10211 standard test case 1

Test case 2 studies the temperature distribution and heat flux through a multi-layer domain. Figure 2.6 shows the geometry, material distribution and characteristics, and the boundary conditions.

The difference between the temperatures (or heat flux) calculated by the method being validated and the temperatures (or heat flux) listed shall not exceed 0.1 °C (or 0.1 W/m).

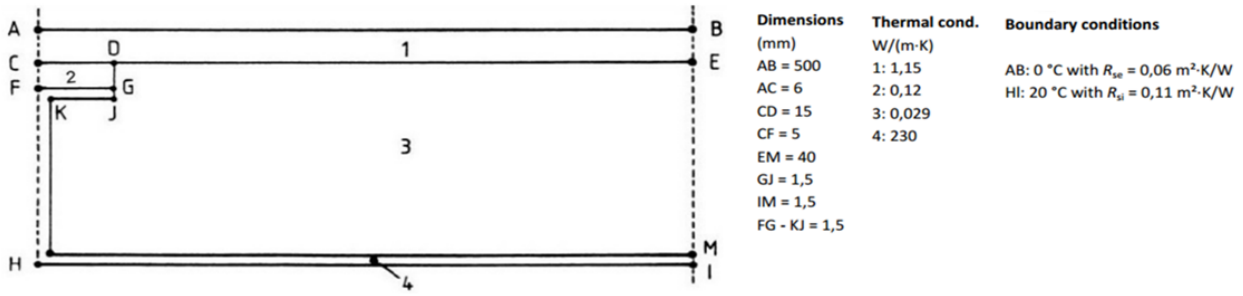

Fig. 2.6: Geometry and boundary conditions for ISO 10211 standard test case 2

Table 2.1 compares the temperatures calculated by the current developed code with those listed in the ISO Standard 10211 for test case 1. For our developed code, the meshing grid is a regular rectangular one, where the number of nodes in x and y directions are taken as 100 and 200, respectively. Further increase in the number of nodes did not affect the temperatures where the maximum relative error obtained was less than 0.5%. Table 2.2 compares the temperatures and the heat flux of the current developed code with those listed in the ISO Standard 10211 for test case 2. For both cases, a very good agreement is achieved where the difference between the temperatures/heat flux of the developed code and the reference ones do not exceed 0.1 as required by the standard.

Table 2.1: Model comparison with the ISO 10211:2007 standard test case 1

Analytical Solution Temperatures (°C) (ISO 10211)				Developed Code Temperatures (°C)			
9.7	13.4	14.7	15.1	9.690	13.421	14.758	15.132
5.3	8.6	10.3	10.8	5.261	8.658	10.342	10.841
3.20	5.6	7.0	7.5	3.184	5.650	7.050	7.537
2.0	3.6	4.7	5.0	2.004	3.650	4.690	5.042
1.3	2.3	3.0	3.2	1.256	2.316	3.005	3.234
0.7	1.4	1.8	1.9	0.734	1.362	1.776	1.914
0.3	0.6	0.8	0.9	0.339	0.630	0.823	0.891

Table 2.2: Model comparison with the ISO 10211:007 Standard Test Case 2

Temperature (°C)	A	B	C	D	E	F	G	H	I
ISO 10211	7.1	0.8	7.9	6.3	0.8	16.4	16.3	16.8	18.3
Developed Code	7.0599	0.7614	7.924	6.305	0.841	16.443	16.2801	16.789	18.336
Heat Flux (W/m)									
ISO 10211	9.5								
Developed Code	9.484								

3.4.2. Comparison with HEAT2

The 2D heat transfer model is also compared to the commercial software HEAT2© (HEAT2 v.5.02 2000). Figure 2.7 shows a block consisting of four arbitrary chosen materials whose characteristics are presented in this figure. We set the boundary outside air temperatures on the left, bottom, right, and top as shown on the same figure. The boundary temperature on the left side is allowed to vary as a sinusoidal function of time while all the other boundaries are constant. The convective heat transfer coefficient at all boundaries is taken as 25 W/(m^2.K). The time step is set to 10min.

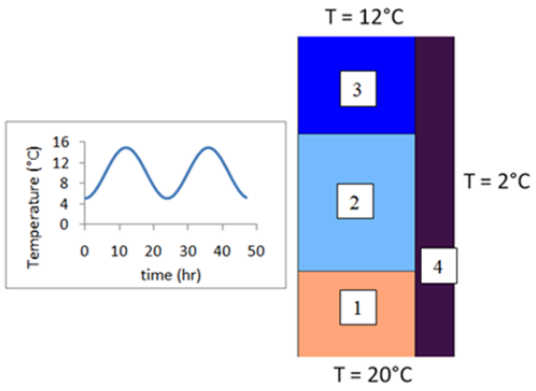

Material	Length (m)	Height (m)	Thermal conductivity (W/m.K)	Volumetric heat capacity ($\rho * cp$) (MJ/m^3.K)
1	0.03	0.03	0.45	1.49
2	0.03	0.04	2.5	0.45
3	0.03	0.03	0.044	0.01
4	0.01	0.1	2	1

Fig. 2.7 : Comparison with HEAT2, calculation domain and boundary conditions

Figure 2.8 shows the heat flux over one day passing through the left and bottom boundaries estimated by the MATLAB® code and by HEAT2. There is a very good agreement between the two. Also, the temperature variation over the day for three arbitrary chosen positions within the domain is plotted in Fig. 2.9.

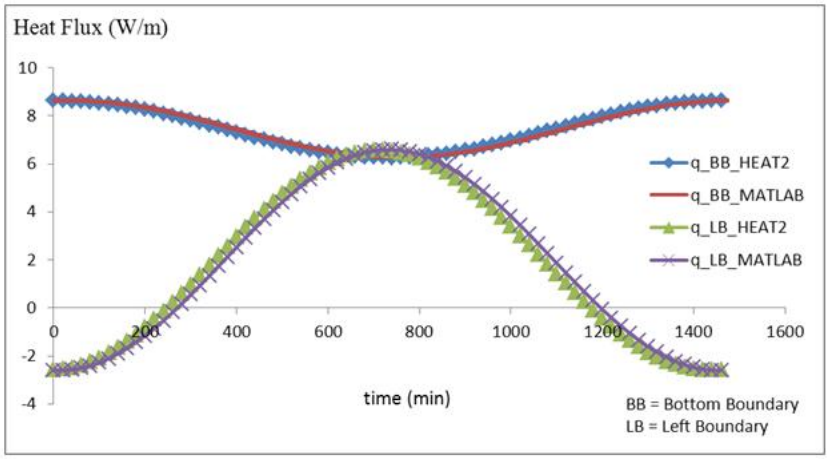

Fig. 2.8: Comparing the heat flux (q) across the bottom and left boundaries between HEAT2 and MATLAB code

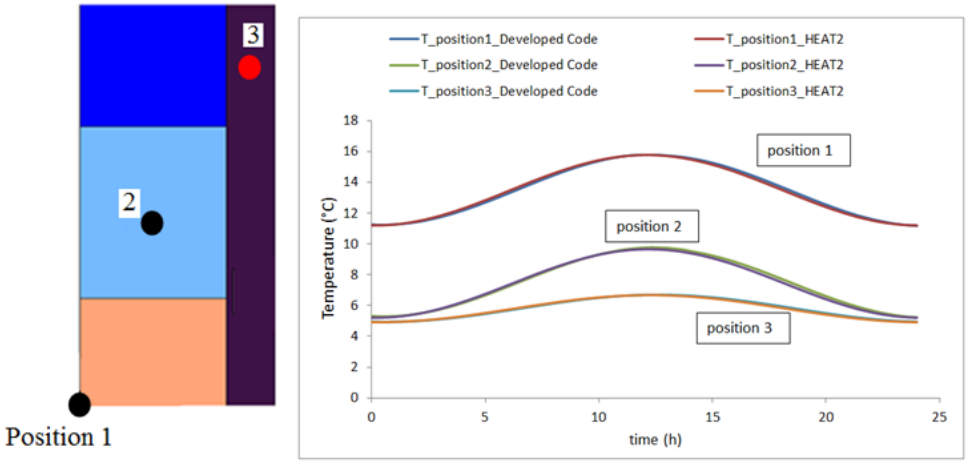

Fig. 2.9 : Comparing the temperature variation for 3 arbitrary chosen positions between HEAT2 and MATLAB code

4. Multi-layer Wall One-Dimensional Hygrothermal Model

4.1. Introduction

Other than energy efficiency, the hygric performance is a key consideration in the building envelope design. The occurrence of moisture problems resulting from poor design,

construction, or unexpected interactions of new building materials can lead to a host of undesirable consequences: wood decay, mold growth, poor indoor air quality, corrosion of metals, loss of thermal resistance in wet insulation, damage to materials and finishes from expansion or contraction, and loss of strength in building materials to the point of structural failure.

A lot of research was done examining the hygrothermal bahaviour of exterior walls. Kolaitis et al. (2013) conducted hygrothermal simulations to assess the behavior of exterior walls with interior or exterior insulation. Results revealed that external insulation outperforms internal insulation configuration by about 8% from a thermal energy point of view. From the hygric perspective, the installation of either external or internal thermal insulation in the warm Mediterranean climate regions results in negligible water vapour condensation potential. However, in the case of the temperate Oceanic climate region, which exhibits low temperature and high relative humidity values during the winter season, installing the thermal insulation at the inside surface might result in water vapour condensation incidents. Johansson (2011) studied the hygrothermal performance of an old Swedish building facade retrofitted with vacuum insulation panels. The energy efficiency and the risk for mold growth in the wall were examined. Experimental measurements as well as numerical simulations were carried out. Improved hygrothermal conditions were observed compared to the original wall where the moisture content of the wall decreased after retrofitting.

One of our objectives is to examine the hygrothermal performance of walls covered with the aerogel-based coating and to compare different thermal insulation configurations. Different exterior wall structures are examined: no insulation, exterior insulation using this coating, interior insulation using a traditional insulation, and interior and exterior insulation. Different assessment criteria are used such as assembly water content, drying rate, mold growth, condensation risk, and ASHRAE-160 criterion. In this section, we present all the mathematical and numerical equations for the coupled heat and moisture transfer in building envelopes.

4.2. WUFI® Presentation

The commercial software WUFI® (Kunzel 1995) is used to build the model and carry out all the simulations. WUFI® is widely used software which models and solves the transient coupled one-dimensional heat and moisture transport in multi-layer building components.

WUFI® was used in several studies to assess the hygrothermal performance of building facades (Kalamees and Vinha 2003, Mantha and Arena 2012, Delgado et al. 2010, Allinson and Hall 2010, Antretter et al. 2011). It was validated against analytical solutions and experimental measurements (Kunzel et al. 1995, Kunzel and Kießl 1996, Holm and Kunzel 1999). Kalamees and Vinha (2003) compared the results produced by several hygrothermal models including WUFI® with the results of laboratory tests to determine the heat and moisture performance of timber-framed external wall structures. They showed that these programs are useful tools in assessing the moisture behaviour of building components regarding moisture diffusion and heat conduction. A review conducted by Delgado et al. (2010) presented the coupled thermal and moisture transfer for 1D or multidimensional cases. Fourteen hygrothermal modeling tools were considered in the analysis. WUFI® was found to be more precise in quantitative computation of night-time cooling than any of the other softwares. Antretter et al. (2011) provided a validation study on the hygrothermal performance of WUFI® where the model was validated using existing standards and guidelines namely ASHRAE 140 (ANSI/ASHRAE 140 2007) and VDI 6020 (VDI Richtlinie 6020 2001).

4.3. Mathematical Equations

The governing equations for the heat and moisture transport are given in equations (2.19-a) and (2.19-b), respectively. More details on deriving these equations are found in the work of Kunzel (1995).

$$\frac{\partial H}{\partial T}\frac{\partial T}{\partial t} = \nabla(k\nabla T) + h_v\nabla\left(\delta_p\nabla(\varphi P_{sat})\right) \qquad (2.19-\text{a})$$

$$\frac{\partial w}{\partial \varphi}\frac{\partial \varphi}{\partial t} = \nabla\left(D_\varphi\nabla\varphi + \delta_p\nabla(\varphi P_{sat})\right) \qquad (2.19-\text{b})$$

where $H,\ T,\ w$ and φ are enthalpy, temperature, moisture content, and relative humidity, respectively. $Psat,\ k,\ h_v, \delta_p, and\ D_\varphi$ are the saturation pressure, thermal conductivity, evaporation enthalpy of water, water vapour permeability, and liquid conduction coefficient, respectively.

The water vapour saturation pressure is calculated using equation (2.20).

$$P_{sat} = 611e^{\frac{aT}{T_0+T}} \quad (2.20)$$

with $a = 22.44, T_0 = 272.144$ for $T < 0°C$ and $a = 17.08, T_0 = 234.18$ for $T \geq 0$

Boundary Conditions:

The boundary conditions for the heat transfer equation are presented in the previous sections. Thus, we just present the boundary conditions for the moisture transfer equation. Equation (2.21) shows the outside surface moisture flux due to rain and vapour convection. Equation (2.21) also applies for the inside surface but with no rain (R=0).

$$g = \beta(P_{out} - P_{x=0}) + \alpha_R R \quad (2.21)$$

where $\beta, P_{out}, P_{x=0}, \alpha_R$ and R are the water vapour transfer coefficient, outside air vapour pressure, outside surface vapour pressure, precipitation absorptivity, and rain load hitting the surface, respectively.

β can be derived from the convective heat transfer coefficient as confirmed from experimental results (Schwarz 1971). It is calculated using equation (2.22)

$$\beta = 7\text{x}10^{-9} * h^c \quad (2.22)$$

4.4. Numerical Solution

The equations (2.19-a) and (2.19-b) are discretized numerically using the implicit finite volume scheme (Fig. 2.10). These will convert to:

$$a_{T,i}T_i^{t+\Delta t} + a_{T,i+1}T_{i+1}^{t+\Delta t} + a_{T,i-1}T_{i-1}^{t+\Delta t} = \text{a}_{T,i}^0 \quad (2.23-\text{a})$$

$$a_{\varphi,i}\varphi_i^{t+\Delta t} + a_{\varphi,i+1}\varphi_{i+1}^{t+\Delta t} + a_{\varphi,i-1}\varphi_{i-1}^{t+\Delta t} = \text{a}_{\varphi,i}^0 \quad (2.23-\text{b})$$

where all the coefficients are given in Table 2.3 (Kunzel 1995).

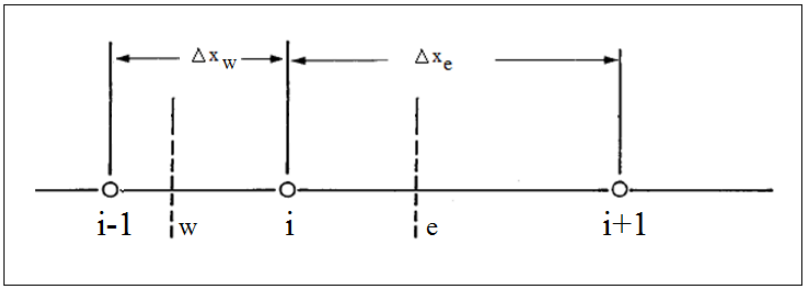

Fig. 2.10: Control volume with left and right neighbors

Table 2.3: Coefficients of the discretized heat and moisture transport equations (source: Kunzel 1995)

	Temperature coefficients	Moisture coefficients
$a_{T,i+1}$ / $a_{\varphi,i+1}$	$-k_e/\Delta x_e$	$-D\varphi_e/\Delta x_e - \left(P_{sat,i+1}\delta_{p,e}\right)/\Delta x_e$
$a_{T,i-1}$ / $a_{\varphi,i-1}$	$-k_w/\Delta x_w$	$-D\varphi_w/\Delta x_w - \left(P_{sat,i-1}\delta_{p,w}\right)/\Delta x_w$
$a_{T,i}$ / $a_{\varphi,i}$	$k_e/\Delta x_e + k_w/\Delta x_w + \frac{dH}{dT}\Delta x/\Delta t$	$D\varphi_e/\Delta x_e + \left(P_{sat,i}\delta_{p,e}\right)/\Delta x_e + D\varphi_w/\Delta x_w + \left(P_{sat,i}\delta_{p,w}\right)/\Delta x_w + \frac{dw}{d\varphi}\Delta x/\Delta t$
$a^0_{T,i}$ / $a^0_{\varphi,i}$	$\frac{dH}{dT}\Delta x/\Delta t\ T_i^t + \mathrm{S}.h_v.\Delta x$, *with* $S = \frac{P_{sat,i+1}\delta_{p,e}}{\Delta x_e}\varphi_{i+1}^{t+\Delta t} - \frac{P_{sat,i}\delta_{p,e}}{\Delta x_e}\varphi_i^{t+\Delta t} + \frac{P_{sat,i-1}\delta_{p,w}}{\Delta x_w}\varphi_{i-1}^{t+\Delta t} - \frac{P_{sat,i}\delta_{p,w}}{\Delta x_w}\varphi_i^{t+\Delta t}$	$\frac{dw}{d\varphi}\Delta x/\Delta t\ \varphi_i^t$

Since the heat and moisture equations are highly coupled, these equations are solved iteratively in each time step by adopting the following steps (See Fig. 2.11):

1- update all the moisture coefficients
2- calculate the moisture field using equation (2.23-b)
3- using these updated moisture values, update the temperature coefficients
4- solve for temperature field using equation (2.23-a)
5- using the new temperature values as better guesses, return to step 1
6- repeat these steps till a converged solution is reached for both the temperature and relative humidity
7- Go to a new time step and start again

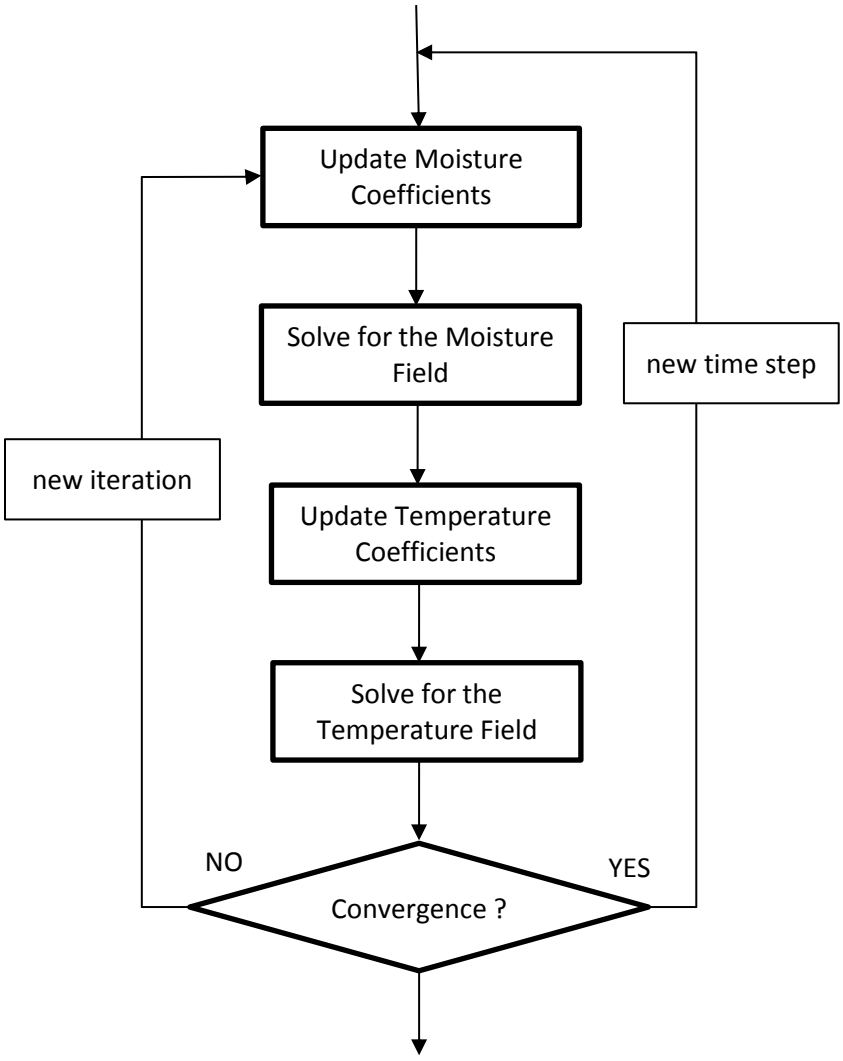

Fig. 2.11: Numerical solution algorithm for the coupled heat and moisture transport equations

5. Whole Building Energy Model

5.1. Introduction

In the previous sections, we are studying the thermal and hygrothermal performance of exterior walls having the aerogel-based coating on their exterior surfaces. Now, we want to examine the effect of adding the "ABC" on the energy consumption and thermal comfort of a typical French house. The objective is to develop a rapid assessment tool designated for architects, owners, engineers, and non-building-energy-simulation expert users to address the following:

- How much energy reduction (annual heating load) is achieved when adding the coating?

- What is the needed coating thickness if a certain heating demand is required?
- What is its effect on thermal comfort?

This tool is designed for new and existing dwellings (for retrofit purposes). Thus, all the building types for each of the different construction periods in France - described previously in Chapter 1, section 2 - are considered. Different wall structures, window-to-wall ratios, window's types, insulation thickness etc. are considered. Also, these all are examined under the different climates of France.

It is a simulation-based tool using the whole building energy simulation software EnergyPlus. In this section, we just speak about EnergyPlus and the model development. In Chapter 4, we describe in details the functionality and the capability of this tool and we present some of the results.

5.2. EnergyPlus Features

Energy Plus is a whole building thermal load and energy analysis simulation software. Some of its features include:

- Integrated, simultaneous solution where the building response and the primary and secondary systems are tightly coupled (iteration performed when necessary).
- Sub-hourly, user-definable time steps for the interaction between the thermal zones and the environment; variable time steps for interactions between the thermal zones and the HVAC systems (automatically varied to ensure solution stability).
- Advanced solar calculations where the amount of beam radiation falling on each surface in the zone, including floor, walls and windows, is calculated by projecting the sun's rays through the exterior windows, taking into account the effect of exterior shadowing surfaces and window shading devices.
- ASCII text based weather, input, and output files that include hourly or sub-hourly environmental conditions and standard and user definable reports.
- Heat balance based solution technique for building thermal loads that allows for simultaneous calculation of radiant and convective effects at both in the interior and exterior surface during each time step.
- Transient heat conduction through building elements such as walls, roofs, floors, etc. using conduction transfer functions or finite difference methods.

- Improved ground heat transfer modeling through links to three-dimensional finite difference ground models and simplified analytical techniques.
- Combined heat and mass transfer model that accounts for moisture transfer within envelopes.
- Different thermal comfort models such as Fanger PMV, ASHRAE Standard 55 adaptive model, etc.
- Advanced fenestration calculations including controllable window blinds, electrochromic glazings, layer-by-layer heat balances that allow proper assignment of solar energy absorbed by window panes, and a performance library for numerous commercially available windows.
- Daylighting controls including interior illuminance calculations and glare simulation and control.
- Atmospheric pollution calculations that predict CO_2, SO_x, NO_x, CO, particulate matter.

EnergyPlus has been widely used by a lot of researchers (Bojic et al. 2011, Hopkins et al. 2011, Boyano et al. 2013, Gamez Royuela 2011, Chuah et al. 2013, Ebrahimpour and Maerefat 2011, Wong et al. 2010, Chan et al. 2009, Wang et al. 2009). Each version of EnergyPlus is tested extensively before release (EnergyPlus Energy Simulation Software, Testing and Validation, http://apps1.eere.energy.gov/buildings/energyplus/energyplus_testing.cfm). The software has been tested using analytical solutions, empirical results, and the results of other softwares. Taking some examples, EnergyPlus has been tested using the IEA HVAC BESTEST series of tests (Henninger et al. 2004). The software has been verified by comparing the energy consumption simulation results to real measured data for a building located in Ravenna in Italy (Tronchin and Fabbri 2010). Also, the software gives results in good agreement with those of a series of experimental tests constructed in Duebendorf, Switzerland (Manz et al. 2006).

5.3. Full-scale House Implementation in EnergyPlus

A two-story house representative of a typical French house is modeled in EnergyPlus to serve as the case study for all the simulations. Since EnergyPlus is a simulation engine with no user-friendly graphical interface, the geometry of the building is modeled using the software Google Sketchup. Then it is imported to EnergyPlus using the interface Open Studio plug-in for Google Sketch. Figure 2.12 shows the geometry of the modeled house. It consists of four zones: crawl space, ground floor, first floor, and attic. The area of the living space for each floor is 50 m². Actually, this house's design represents a real experimental house (INCAS house) located in

the experimental field of the national solar energy institute (INES) in Chambery, France. This experimental house is described in details in Chapter 3 where the results of the EnergyPlus model are compared to on-site house measurements.

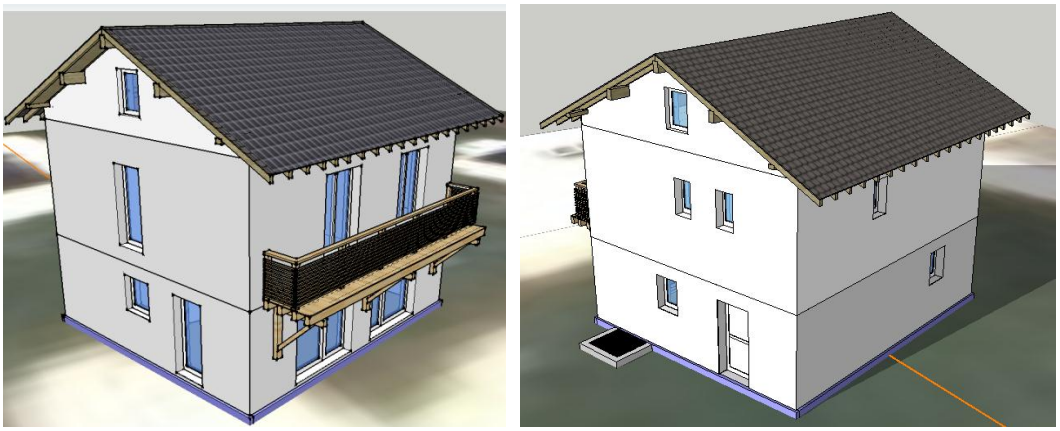

Fig. 2.12: Case study house's geometry

6. Multi-layer Wall with Active Loop System Model

6.1. Introduction

In the winter season, when the south wall is well insulated, a significant amount of energy falling on this facade is not transferred to the inside environment. Due to the high thermal resistance of the insulation, some of this energy is dissipated to the outside through convection with the cold outdoor air. The idea behind this system is to capture this wasted energy of the south facade available during non-cloudy winter days and transfer it to the (cooler) north facade through water pipes embedded in the outside aerogel-based rendering (Wurtz and Ibrahim 2013). This system is proposed for buildings adopting the exterior insulation technique. The coating's projection technique through spraying allows the ease of implementation of this system for retrofitting old buildings or for the application in new buildings as well. In this section, we present the mathematical equations and the numerical solution for this system.

6.2. System Description

The concept of this system is shown in Fig. 2.13. The exterior walls are composed of concrete with the "ABC" as exterior insulation. In the south wall, water pipes are placed at the exterior surface of the coating as a serpentine shape. In the north facade, they are placed in direct

contact with the concrete just at the interface between the coating and the concrete layer. By means of a pump, water flows through the south facade to recuperate some amount of the solar energy. It then passes through the east or west facade to reach the north one where it dissipates its heat through the concrete layer to the inside. Also, some of the energy is stored in the thermal inertia of the concrete layer to be used in a later time of day.

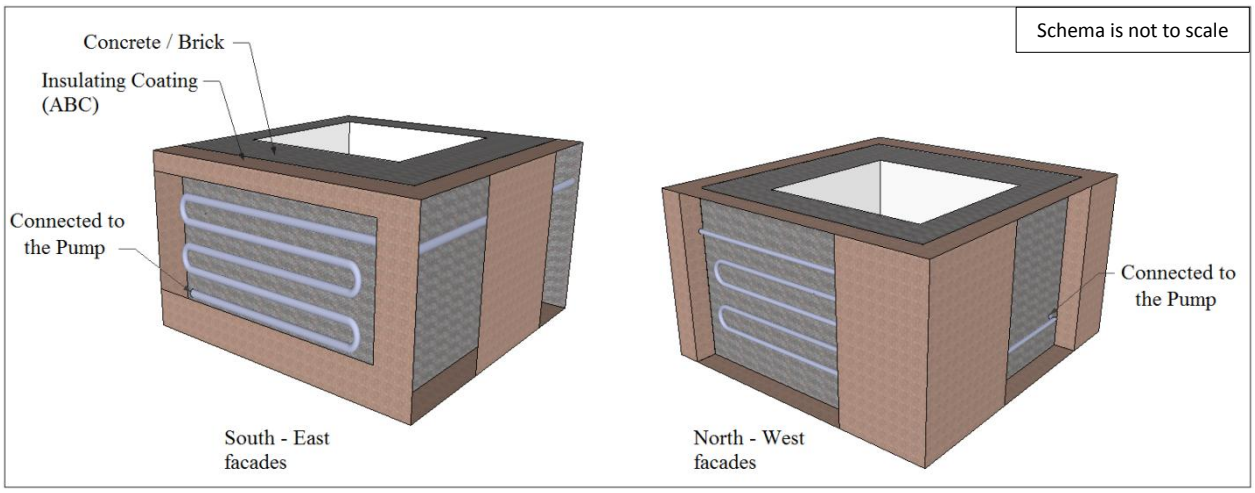

Fig. 2.13: Active embedded-pipe wall loop system

6.3. Mathematical Model

The heat transfer is a complex 3-dimensional problem. In our case, we simplified the heat transfer into 2-dimensional which is coupled to the moving fluid in the water pipes. Some assumptions are made:

- The serpentine water loop is modeled as a long horizontal pipe
- Symmetry boundary conditions are considered between the serpentine tubes
- No heat losses in the east (or west) wall for the water pipes passing from the south wall to the north wall
- The circular shape of the pipe is modeled as a square with the same area. Thus, the side of the square has a length of $\sqrt{\pi}r$, where r is the radius of the pipe
- Heat conduction in the longitudinal pipe direction is neglected since the conductive heat transfer is small compared to the fluid enthalpy flow

The pipe is divided into several segments. Figure 2.14 shows the face view of the south facade and the side view of one segment. For each segment, the 2D heat transfer equation is solved. The domain is discretized into rectangular control volumes. The outlet fluid temperature from the

previous segment is an inlet temperature for the current segment.

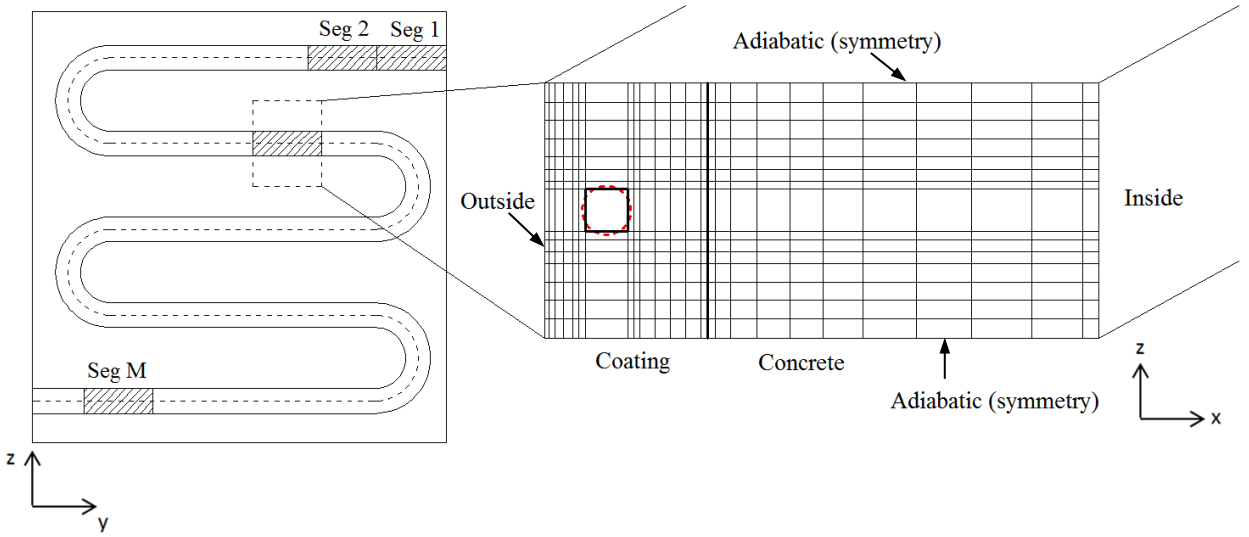

Fig. 2.14: South wall face view (left) and section view of one calculation domain segment (right)

For the wall's control volumes, the energy balance is written as:

$$\rho_{i,j} cp_{i,j} \frac{\partial T_{i,j}}{\partial t} dx_{i,j} dz_{i,j} = \sum_{adj} U_{adj} \left(T_{adj} - T_{i,j}\right) \tag{2.24}$$

where the subscript (i,j) represents a control volume. ρ , cp , dx , dz , T, and t are the density, specific heat, control volume width, control volume height, temperature, and time, respectively. U is the heat transfer coefficient between two adjacent control volumes and is calculated as following (taking the heat transfer coefficient with the west control volume, U_w ,as an illustration):

$$\begin{cases} U_w = \dfrac{dz_{i,j}}{\dfrac{dx_{i,j}}{2 * k_{i,j}} + \dfrac{dx_{i-1,j}}{2 * k_{i-1,j}}} & \text{, for nodes not adjacent to the water node} \quad (2.25-a) \\ U_w = \dfrac{dz_{i,j} * corr}{\dfrac{dx_{i,j}}{2 * k_{i,j}} + \dfrac{1}{h_{w,c}} + \dfrac{dx_{tube}}{k_{tube}}} & \text{, for nodes adjacent to the water node} \quad (2.25-b) \end{cases}$$

where k is the thermal conductivity, $h_{w,c}$ is the convective heat transfer coefficient between the fluid and the pipe wall. *corr* is a correction factor to account for the difference in the lateral area between the modeled square and the real circular shape of the pipe; it is given in equation (2.26). The energy balance for the fluid control volume is shown in equation (2.27):

$$corr = \frac{Lateral\ Area_{\ circle}}{Lateral\ Area_{\ square}} = \frac{2\pi r}{4\sqrt{\pi}\, r} = \frac{\sqrt{\pi}}{2} \tag{2.26}$$

$$\rho_f cp_f \frac{\partial T_f}{\partial t} dx_f dz_f = \sum_{adj} U_{adj}\left(T_{adj} - T_f\right) - \dot{m} cp_f \frac{dT_f}{dy} \tag{2.27}$$

where $\dot{m}$ is the fluid mass flow rate.

The last term in equation (2.27) corresponds to the enthalpy change due to fluid flow. The heat transfer at the outside and inside wall surfaces are given in equations (2.28-a) and (2.28-b), respectively.

$$h_{out}(T_{out} - T_{x=0}) + \alpha . I + hr_{sky}\left(T_{sky} - T_{x=0}\right) + hr_{gr}\left(T_{gr} - T_{x=0}\right) = -k\frac{\partial T(0,t)}{\partial x} \quad (2.28-\text{a})$$

$$h_{in}(T_{x=L} - T_{in}) + \sum_{s=1}^{S} hr_s(T_{x=L} - T_s) = -k\frac{\partial T(L,t)}{\partial x} \quad (2.28-\text{b})$$

where, h_{out} *and* h_{in} are the outside and inside convective heat transfer coefficients, respectively. hr_{sky} *and* hr_{gr} are the radiative heat transfer coefficient between the outer wall surface and the sky and the ground, respectively. hr_s is the radiative heat transfer coefficient between the inner wall surface and the room's other walls and windows inner surfaces. α and I are the surface solar absorptivity and solar irradiation, respectively. T_{out} , T_{in} , $T_{x=0}$, $T_{x=L}$, and T_s are the outside air temperature, the inside air temperature, the wall's outside surface temperature, the wall's inner surface temperature, and the inner surface temperature of the other walls/windows enclosing the room.

The heat transfer coefficient between the fluid and the pipe wall is given in equation (2.29) (Cengel 2005).

$$\begin{cases} h_{w,c} = 3.66 & \text{, for laminar flow} \\ h_{w,c} = 0.023 * Re^{0.8} * Pr^{\frac{1}{3}} & \text{, for turbulent flow} \end{cases} \tag{2.29}$$

where *Re* and *Pr* are the Reynold and Prandtl numbers, respectively. These are calculated using equations (2.30) and (2.31).

$$Re = \frac{V * D}{v} \tag{2.30}$$

$$Pr = \frac{v}{\alpha_d} \tag{2.31}$$

where V, D, v, and α_d are the fluid velocity, pipe's diameter, kinematic viscosity, and thermal diffusivity, respectively.

The radiative heat transfer coefficient between two surfaces is given by equation (2.32).

$$hr_{1\to2} = \frac{1}{\frac{1}{\varepsilon_1}+\frac{1}{\varepsilon_2}-1}\sigma F_{1\to2}(T_1^2 + T_2^2)(T_1 + T_2) \tag{2.32}$$

where $\varepsilon, \sigma,$ and F are the thermal emissivity, Stephan-Boltzmann constant, and the view factor, respectively.

For the numerical model, we used the finite difference technique for the spatial discretization of the energy equations, and the fully implicit scheme for the discretization in time. The simulation environment is MATLAB®.

6.4. Comparison with HEAT2

Consider a wall consisting of 5cm of "ABC" and 15cm of concrete. The indoor air temperature is fixed at 19°C whereas the outside air temperature varies as a sinusoidal function over a 24h period (Fig. 2.15). The indoor and outdoor heat transfer coefficients are 7 W/(m².K) and 25 W/(m².K), respectively. The top and bottom edges are adiabatic. The water pipe has a diameter of 1cm.

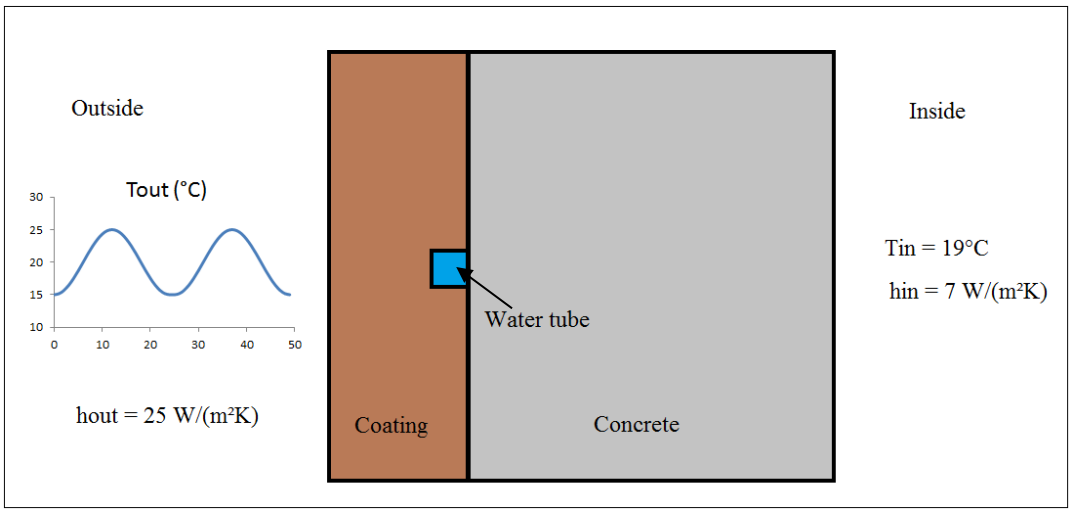

Fig. 2.15: Comparison of wall active loop system numerical model with HEAT2

Mesh refinement tests are performed for the numerical model to ensure that the results are independent of the numerical domain. Figure 2.16 shows the heat flux at the inside and outside surfaces of the wall. A very good agreement is achieved between the HEAT2 results and the current developed model. The water temperature in the pipe is compared in Fig. 2.17. Also, a very good agreement is obtained between the two.

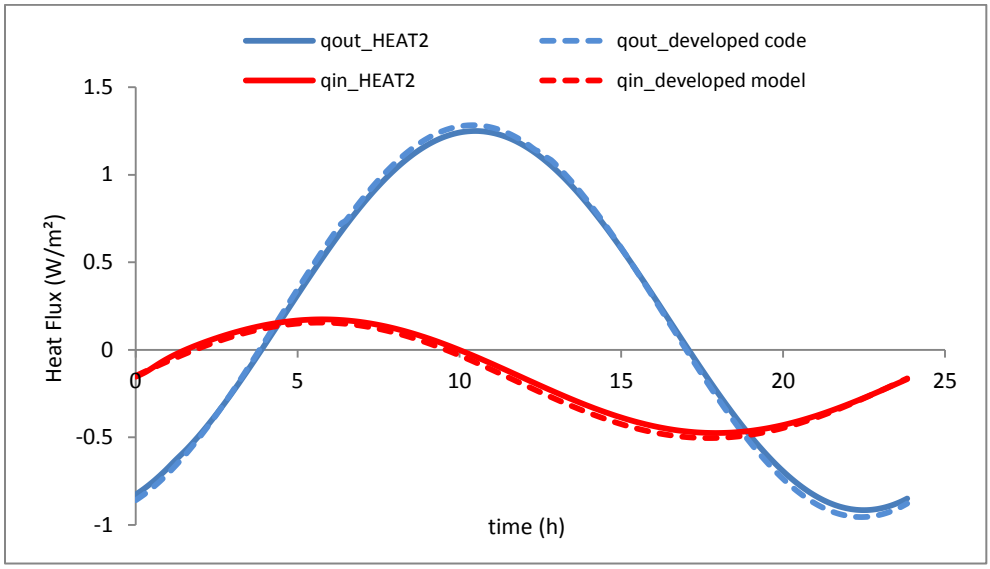

Fig. 2.16: Heat flux at the interior (qin) and exterior (qout) wall surfaces for the developed code and HEAT2

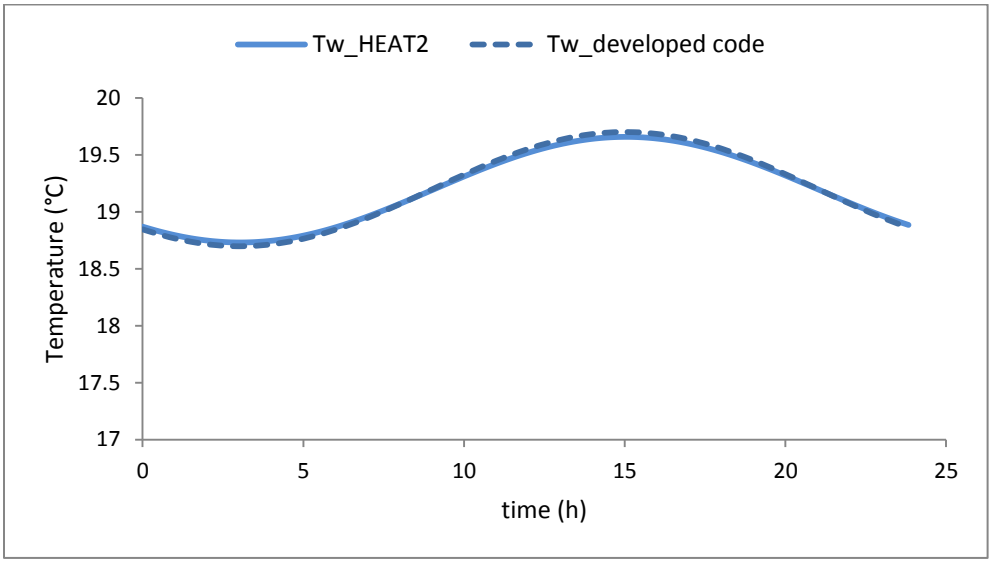

Fig. 2.17: Water temperature (Tw) comparison between the developed code and HEAT2

6.5. Room Thermal Model

The heat transfer in a room with no windows is modeled in MATLAB® to study the performance of the wall active loop system; we will call it, hereafter, "WALS". This model is a combination of the WALS model with the 1D heat transfer model presented previously in section 2. The east wall, west wall, roof, and ground are modeled as 1D heat transfer models; the south and north walls are modeled as 2D heat transfer active loop models. These are connected through the long-wave radiation heat exchange between the internal surfaces of the different facades. The algorithm is as following:

1- Solve for the south wall temperatures (2D WALS model)
2- Solve for the east wall, west wall, roof, and ground temperatures, successively (1D heat transfer model)
3- The exit water temperature from the south facade is an inlet water temperature for the first fluid pipe segment of the north facade
4- Solve for the north wall temperatures (2D WALS model)
5- The room air temperature is calculated if it is considered as free-floating; otherwise, it is maintained constant
6- Update the interior surface long-wave heat transfer coefficients using the updated internal surface temperatures
7- Go to step 2 until convergence is reached for all the temperatures
8- Go to a new time step

This latter will give us a first insight on the performance of this system; however, it is still not sufficient as we want to study its thermal performance on a full scale real house. To do so, the WALS MATLAB® code is coupled to the INCAS house EnergyPlus model through the co-simulation platform BCVTB. The co-simulation coupling is explained in details with all the results in chapter 4.

7. Conclusion

In this chapter, we developed all the mathematical models needed to carry out all the simulations. These are the one and two-dimensional conduction heat transfer models in a multi-layer wall, the one-dimensional heat and moisture (hygrothermal) transfer model, the whole

building thermal model, and the wall active embedded pipe water loop system. For each one of these, we explained the objectives behind developing the model. All the mathematical equations and numerical solutions were presented. These models were compared to analytical solutions, to the results of other softwares, or to some published data in the literature.

8. Résumé du Chapitre en Français

Dans ce chapitre, nous développons tous les modèles mathématiques nécessaires pour effectuer toutes les simulations. Pour cela, nous avons besoin des modèles suivants: un modèle de conduction thermique monodimensionnelle et bidimensionnelle dans un mur multicouche, un modèle de transfert hygrothermique, un modèle de thermique du bâtiment et un modèle de façade active.

Pour le modèle de transfert de chaleur unidimensionnel et bidimensionnel, nous présentons toutes les équations mathématiques avec les conditions aux limites nécessaires pour le transfert de chaleur au sein d'une structure d'un mur à multicouche. Ensuite, le modèle numérique est présenté. Ces modèles sont comparés d'abord avec les solutions analytiques de la littérature et après ils sont comparés avec les résultats obtenus des logiciels. Ensuite, pour le modèle hygrothermique, nous utiliserons le logiciel commercial WUFI pour développer le modèle numérique et effectuer toutes les simulations. WUFI est un logiciel dédié aux ingénieurs, chercheurs et à bien d'autres utilisateurs. Les équations mathématiques utilisées par WUFI et la solution numérique adoptée pour résoudre les équations couplées de transport de la chaleur et de l'humidité sont présentées. Passant à grande échelle, les processus de transfert de chaleur au sein d'un mur sont modélisés à l'aide du programme de simulation énergétique de bâtiment EnergyPlus. EnergyPlus est considéré comme l'un des outils puissants de simulation énergétique des bâtiments. Il est utilisé par de nombreux chercheurs et chaque version produite du logiciel est testée avant d'être distribuée. Actuellement, une maison à deux étages, typique des maisons françaises, est modélisé dans EnergyPlus avant d'être utilisé comme un cas d'étude pour toutes les simulations. Actuellement, cette conception est en cours d'étude expérimentale sur la plate-forme INCAS, un terrain d'étude localisée sur le terrain de l'Institut National de l'Energie Solaire de Chambéry (INES) en France. Enfin, un nouveau système de façade active est décrit. En hiver, quand le mur sud est bien isolé, une quantité importante d'énergie qui est disponible sur cette

façade n'est pas transférée à l'environnement interne. En raison de la résistance thermique élevée de l'isolation, la majorité de cette énergie est dissipée vers l'extérieur par le biais de convection avec l'air froid extérieur. L'idée de ce système est de capter cette énergie présente sur la façade sud pendant les jours d'hiver non nuageux et de la transferer à la façade nord à travers des conduites d'eau installées dans l'isolation externe à base d'aérogel. Ce système est proposé pour des bâtiments qui adopteraient la technique d'isolation par l'extérieur étudiée.

CHAPTER 3

ADVANCED BUILDING ENVELOPES EXPERIMENTAL STUDIES AND MODEL VALIDATION

Chapter 3
Advanced Building Envelopes Experimental Studies and Model Validation

Chapter contents

1. Introduction

In Chapter 2, we have developed all the mathematical models needed to carry out all the simulations. This chapter deals with all the experimental studies carried out to validate the mathematical models. It consists of three main parts: an experimental test-cell used to validate the 1D thermal and hygrothermal numerical models, a full-scale experimental house used to validate the whole building EnergyPlus energy simulation model, and a mock-up experiment for the validation of the active wall loop system numerical model.

2. PERSEE Test-Cell Wall Characterization

2.1. Introduction

An experimental test-unit was constructed in 1984 (Krauss 1985) at PERSEE research center in Sophia Antipolis (latitude 43.616 N, longitude 7.055 E) in the south-east Mediterranean region of France (See Fig. 3.1). It is composed of two adjacent cells orientated to the south which are identical in dimensions but differ in the composition of the south wall. The first one, we will call it hereafter the test-cell, has the south wall initially composed of heavy weight concrete with a layer of glass wool interior insulation. The second cell, the adjacent cell, has its south wall composed of a semi-transparent glazing system consisting of a composition of silica aerogel granules and phase change material (Berthou 2011, Johannes et al. 2011). A third cell (acquisition cell), adjacent to the other two, is also present and is oriented to the north

The south wall of the test-cell is our test wall to validate the one-dimensional heat transfer and the one-dimensional hygrothermal numerical models. It has an area of 17m². Initially, this wall is composed of a 25cm layer of concrete (exterior layer), a 16cm layer of glass wool, and a 1.3cm of plaster board. A 4cm layer of aerogel-based coating is then added at the exterior surface of this wall. Trying to isolate the south wall from the thermal effects of the other walls enclosing the test-cell, these elements - i.e. the east wall of the test cell, all the partition walls, the roof, and the ground - are very well insulated. Also, to avoid the effect of the direct solar gains, the test-cell has no windows. The geometry of the test-cell with the construction materials thermo-physical properties are presented in Annex A.

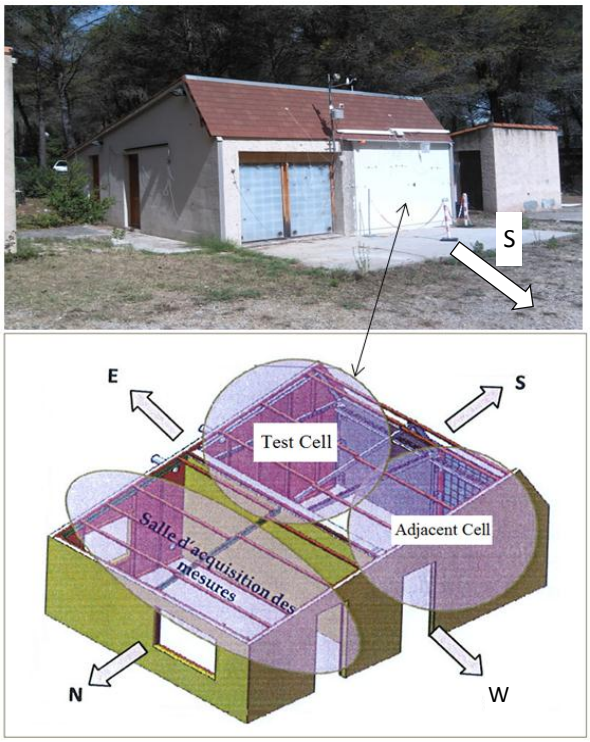

Fig. 3.1 : PERSEE experimental test-cell in Sophia Antipolis

2.2. Instrumentation

To compare the results of the experiment with those of the numerical models, we need to measure some variables to be inputs for the models and other variables to be outputs. As for the inputs, these are the outside and inside air temperature and relative humidity, the south wall solar radiation intensity, and the wind speed and direction. The outputs are the temperature and relative humidity at different positions within the wall. Now, we will present all the instrumentation used to measure all these variables.

2.2.1. Hygrothermal Sensor

Vaisala HUMICAP HMP110 hygrothermal sensors (Vaisala, http://www.vaisala.fr/fr/lifescience/products/probes/Pages/HMP110.aspx), mounted within a passive multi-plate solar shield, are used to measure the outside and inside air temperature and relative humidity, and also the relative humidity inside the wall. They have a temperature measurement range of -40°C-+80°C with an accuracy of ±0.2°C for temperature ranges between 0°C-40°C and an accuracy of ±0.4°C for temperature ranges between -40°C-0°C and +40°C-+80°C. The relative humidity (RH) measurement range is 0-100% with an accuracy of ±1.5% for RH between 0 and 90% and an accuracy of ±3% for RH greater than 90%.

2.2.2. Solar Radiation Sensor

Two HUKSEFLUX, Campbell Scientific pyranometers (HUKSEFLUX; https://www.campbellsci.fr/lp02) are installed: a horizontal one to measure the global solar radiation falling on a horizontal surface and a vertical one to measure the solar radiation falling on the south facade. They work in the range of 0-2000 W/m² with an accuracy of ±10%.

2.2.3. Temperature Sensor

Temperatures at the wall interior and exterior surfaces and within the wall are measured using K-type thermo-couples having a precision of ±0.5°C

2.2.4. Wind Speed and Direction Sensor

Wind speed and direction are measured using a Pulsonic Aliza 147 anemometer station (Pulsonic ; http://www.pulsonic.net/combo-vent/alizia-147-capteur-combine-vitesse-et-direction-du-vent/id menu-84.html) having a measuring range of 0-60m/s with a precision of ±0.5m/s for velocities in the range of 0-10m/s and a precision of 3% for velocities in the range of 10-60m/s.

2.3. Sensors Position

For the south wall, temperature sensors are placed at the exterior surface of the coating, at the interface between the coating and the concrete, at the interface between concrete and internal insulation (glass wool), and at the interior surface of the plaster layer. For each of these positions, three sensors are present: near the east edge, near the west edge, and at the middle of the wall. The hygrothermal sensors are placed at the interface between the coating and the concrete (See Fig. 3.2).

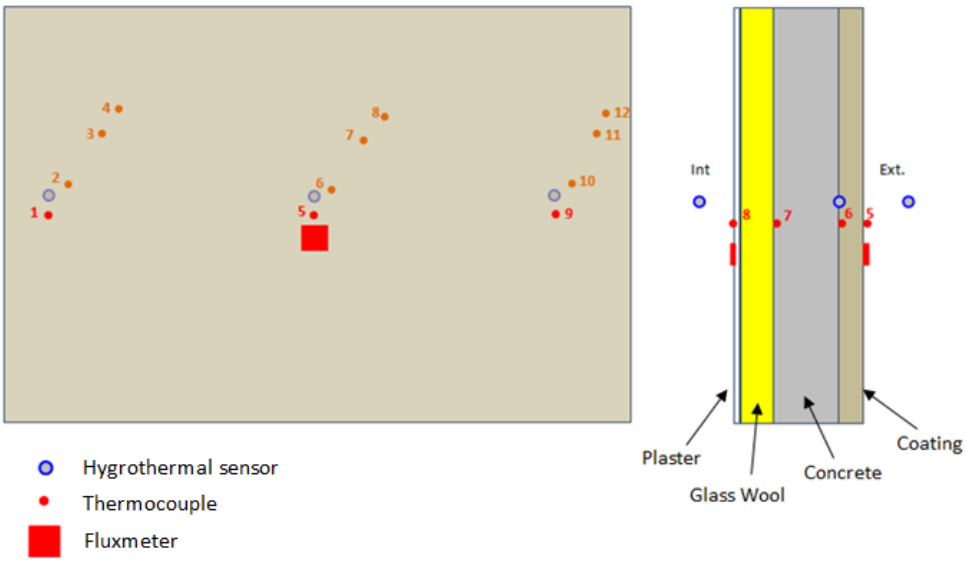

Fig. 3.2 : Measurement sensors within the south wall

The indoor air temperature of the test-cell is allowed to free-float (no heating or cooling system). Also, as we wanted to study the effect of the exterior envelope, no internal heat gains are present. Measurements are taken every 10 seconds and data are recorded every five minutes taking the average of the previous measurements.

2.4. Results

2.4.1. One-Dimensional Heat Transfer Model Validation

The simulation results of the 1D heat transfer wall model are compared to the measured data for a two weeks period in August. The measured outside and inside air temperature and solar irradiation falling on the south facade are shown in Fig. 3.3. During the first week, the interior insulation is present; however, during the second week, it is removed. The measured outside and inside climatic conditions serve as boundary conditions for the numerical model.

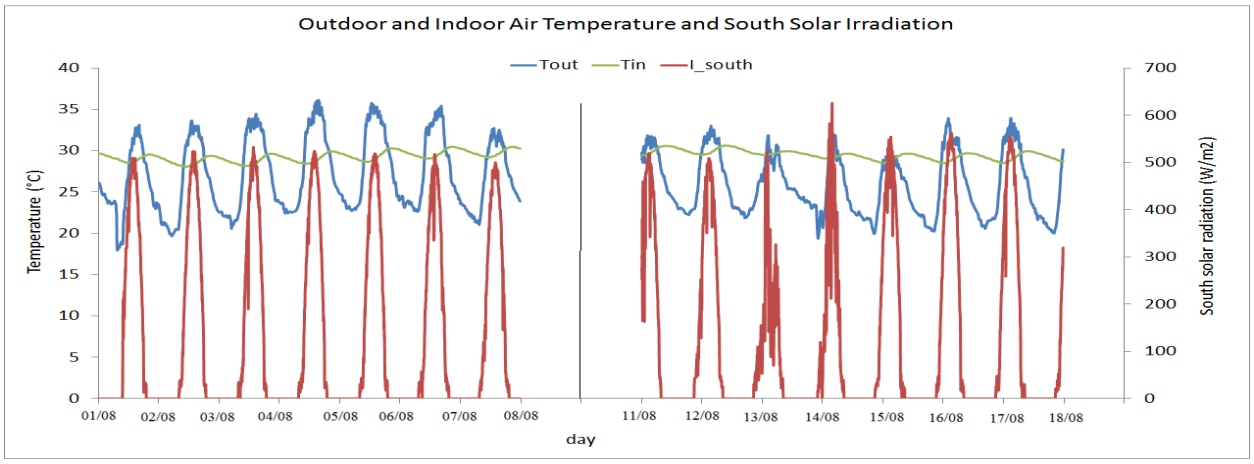

Fig. 3.3: Measured outside air temperature (Tout), inside air temperature (Tin) and south wall solar irradiation (I_south) for two weeks in August

The wall external surface temperature is shown in Fig. 3.4 for the cases with and without interior insulation. The blue curve represents the measured data and the green curve represents the simulated temperatures without taking into account the long-wave radiation heat exchange with the sky. We can see that during the nights the measured temperatures are cooler than those simulated due to the absence of the cooling effect of the sky in the simulation. Including this effect, we obtain the red curve temperatures which greatly approach the measured ones. The simulated temperatures fall down during nights to approach the measured temperatures.

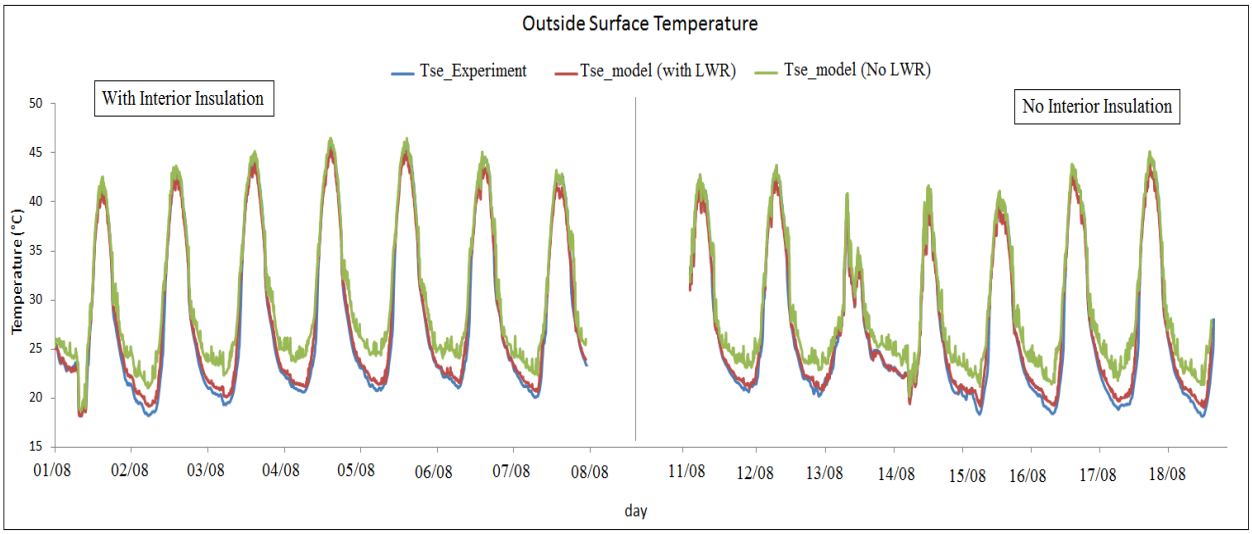

Fig. 3.4: Measured and simulated (with and without sky long-wave radiation "LWR") outside surface temperature (Tse)

The inner surface temperatures are presented in Fig. 3.5 for different values of the inside convective heat transfer coefficient (h_{in}). We can see that h_{in} has a great effect on the simulation results.

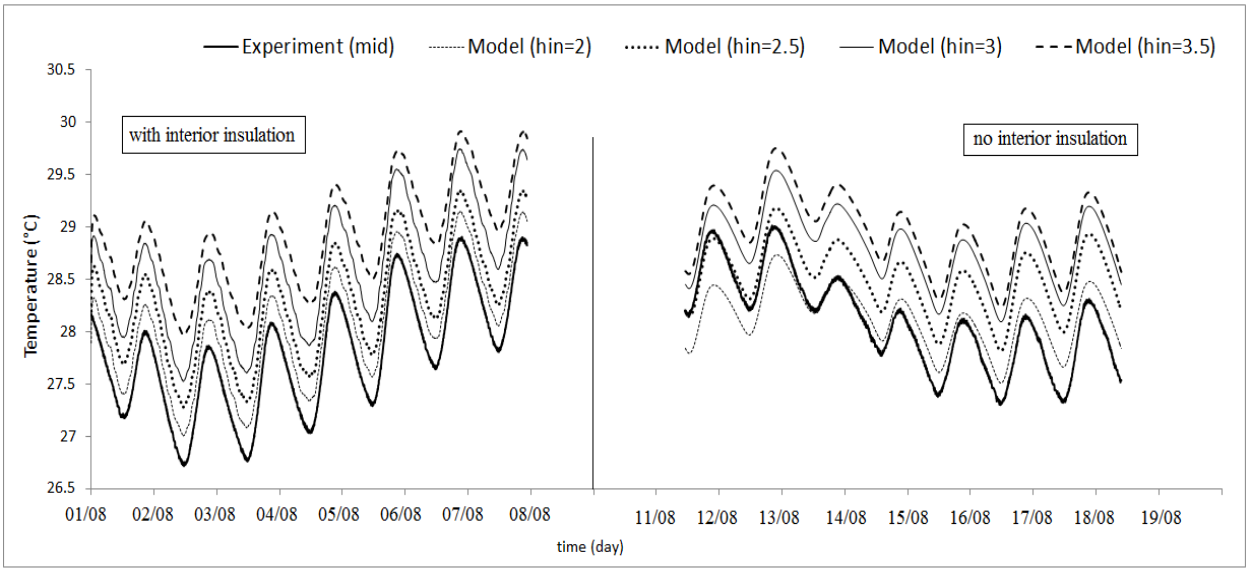

Fig. 3.5: Variation of the south inner wall surface temperature for different internal convection coefficients

Fig. 3.6 shows the temperatures at the interface between the coating and concrete for the two weeks at the east, west and middle positions. A very good agreement is obtained between the numerical simulation results and the experimental measurements at the middle (solid curve) and east (red curve) positions. However, there is a significant discrepancy when considering the west position. The reason for that is the presence of a thermal bridge near the west side of the wall which increases the heat transfer and as a result increases the wall temperature near this edge. We can see that the minimums and maximums obtained in simulation are in phase with those obtained from measurements; this is very important for determining the time lag for the different wall structures using our developed model. Also, the maximum difference between the two curves does not exceed 0.7°C.

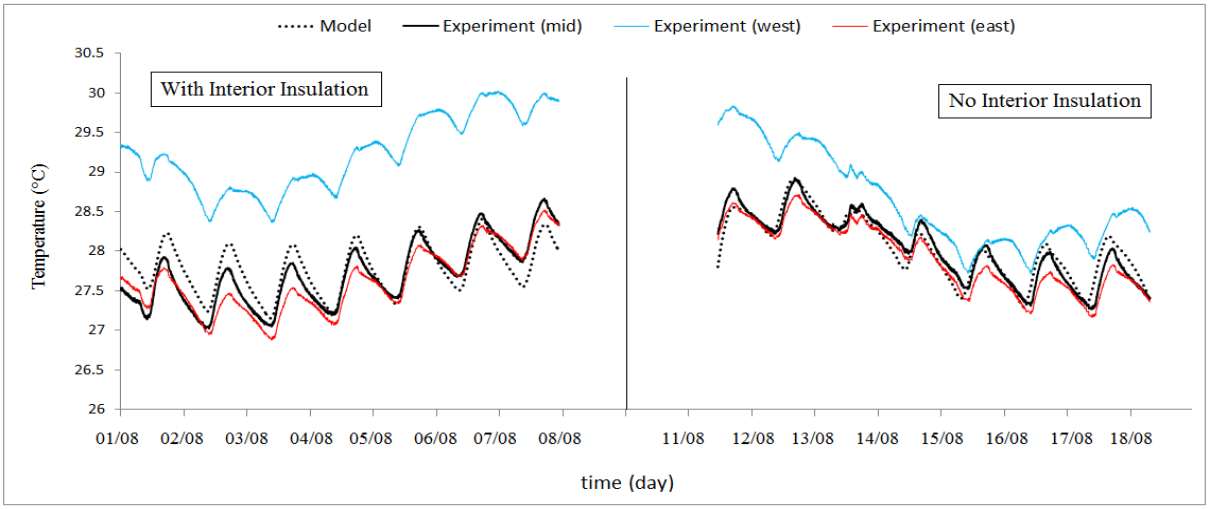

Fig. 3.6 : Measured and simulated temperatures at the interface aerogel-based coating/concrete

Fig. 3.7 shows the measured and simulated temperatures at the interface between the concrete layer and interior insulation (glass wool) for week 1. For week 2, we don't have this interface because the interior insulation is removed. The numerical model was able to generate a curve that behaves very similar to the data obtained through experimental measurements. The simulated temperatures are lower than those measured by about 0.4-0.5°C. Also here, the maximums and minimums between the two curves are in phase. Moreover, the decrement factor is very close between them.

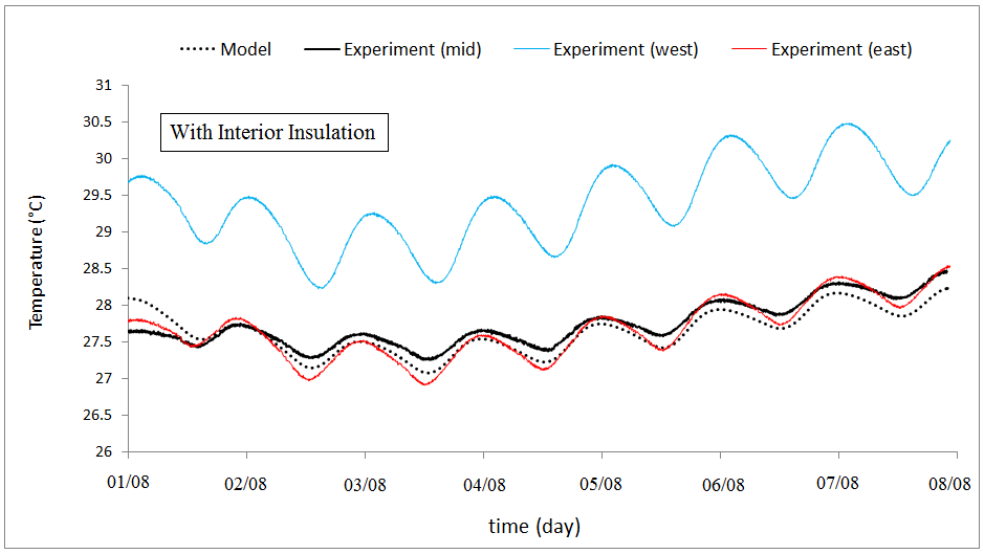

Fig. 3.7 : Measured and simulated temperatures at the interface concrete/interior insulation

A sensitivity analysis is carried out to determine the effect of some parameters on the thermal behavior of exterior walls. The parameters are:

- coating's thermal conductivity ($k_{coating}$)
- concrete's thermal conductivity ($k_{concrete}$)
- coating's volumetric heat capacitance ($\rho.cp_{coating}$)
- concrete's volumetric heat capacitance ($\rho.cp_{concrete}$)
- exterior surface solar absorptivity (α)

The value of each parameter is varied by ±20%. Two outputs are compared: the heat flux at the inner wall surface (q_{in}) and the decrement factor (f). Table 3.1 shows the sensitivity of these outputs to the input parameters. The negative sign means that there is a decrease in the value and the positive sign means there is an increase.

Table 3.1 : Sensitivity analysis of some parameters on the heat flux and decrement factor

		Parameter									
		$k_{coating}$		$k_{concrete}$		$\rho.cp_{coating}$		$\rho.cp_{concrete}$		α	
		-20%	+20%	-20%	+20%	-20%	+20%	-20%	+20%	-20%	+20%
relative difference from base case	q_{in} (%)	-17.48	+14.10	-1.47	+1.03	-	-	-	-	-12.14	+13.79
	f (%)	-18.9	+18.3	-6.6	+5.5	-	-	+26.77	-18.33	-6.6	+6.6

Form this table, it is shown that the thermal conductivity of the coating and the solar absorptivity has a great effect on the heat flux transmitted to the inside. A decrease in $k_{coating}$ by 20% decreases the heat flux by about 17.5%. A decrease in α by 20% decreases q_{in} by about 12%. All the other parameters do not have a significant influence on the heat flux. Concerning the decrement factor, the volumetric capacitance of the concrete layer as well as the thermal conductivity of the coating are the most influential parameters. An increase in $\rho.cp_{concrete}$ by 20% decreases f by about 18%; however, a decrease in $\rho.cp_{concrete}$ by 20% increases f by about 26%. The thermal conductivity of concrete and the solar absorptivity have a lower impact on the decrement factor.

2.4.2. One-Dimensional Hygrothermal Model Validation

As mentioned previously, the commercial software WUFI® Pro v.5 is used to perform the hygrothermal simulations. In this section, the experimental results are compared to those of the numerical model developed in WUFI®. As mentioned earlier, the hygrothermal and physical properties of the aerogel-based coating (rendering) are measured at the Scientific and Technical Center of Buildings (CSTB). Fig. 3.8 shows the sorption isotherm for this rendering (left) and the

dependence of its thermal conductivity on the relative humidity (right). The sorption isotherm is measured by weighing the samples in a conditioned climatic chamber according to the NF EN ISO 12571 standard. The thermal conductivity is measured by means of a guarded hot plate and heat flow meter according to the NF EN standard 12667. The rendering has a porosity of 98%, measured using a gas pycnometer (Micromeritics, model AccuPyc II) following the NF EN ISO 8130-2 standard. Its vapour diffusion resistance factor is shown in Table 3.2 and it is measured using the Cup method according the NF EN ISO 12572 standard.

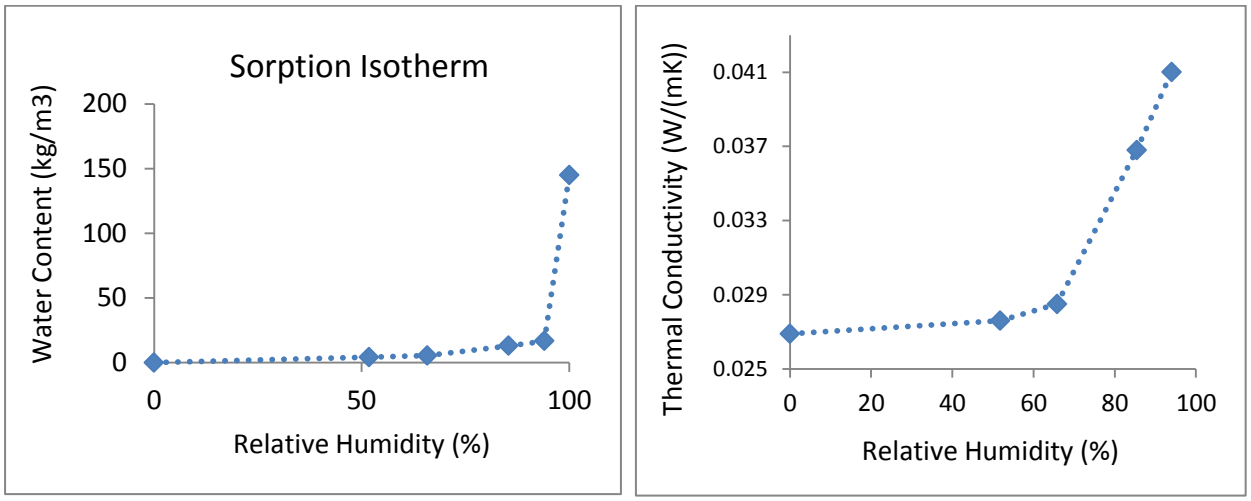

Fig. 3.8: Aerogel-based coating sorption curve and its thermal conductivity in dependence on relative humidity

Table 3.2: The aerogel-based coating vapour diffusion resistance factor

RH (%)	Vapour diffusion resistance factor (-)
0 – 50	5.3
50 – 75	3.3
75 – 95	3.2

Measurements are recorded for 2 weeks in summer. Fig. 3.9 shows the outside (a) and inside (b) air temperature and relative humidity. Customized climate files are created for the simulation using the weather data collected on site.

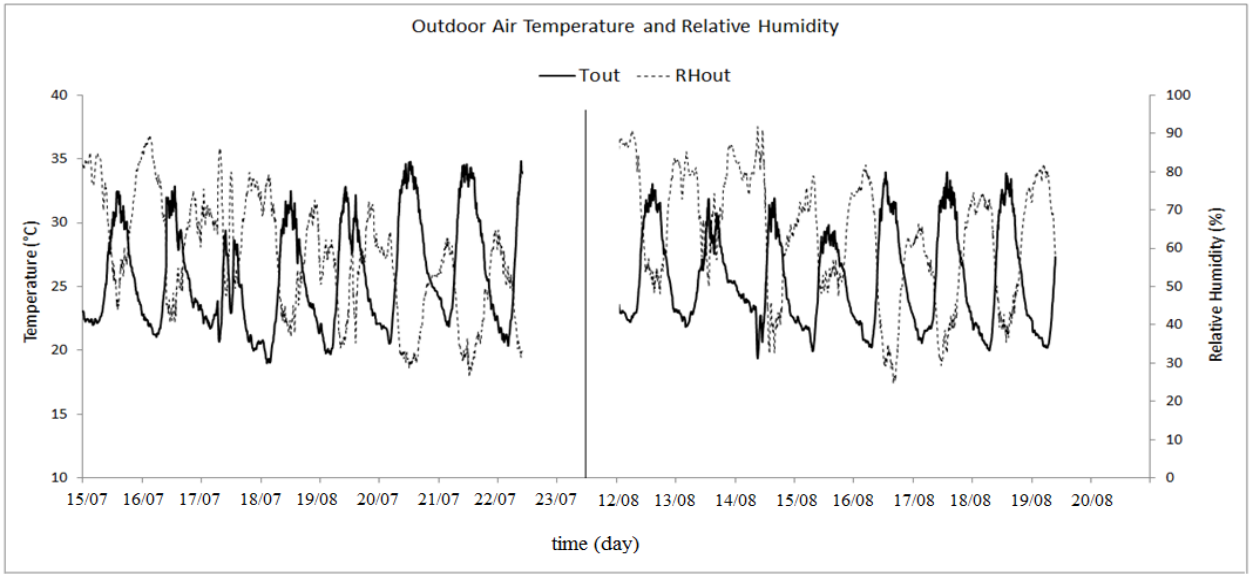

(a)

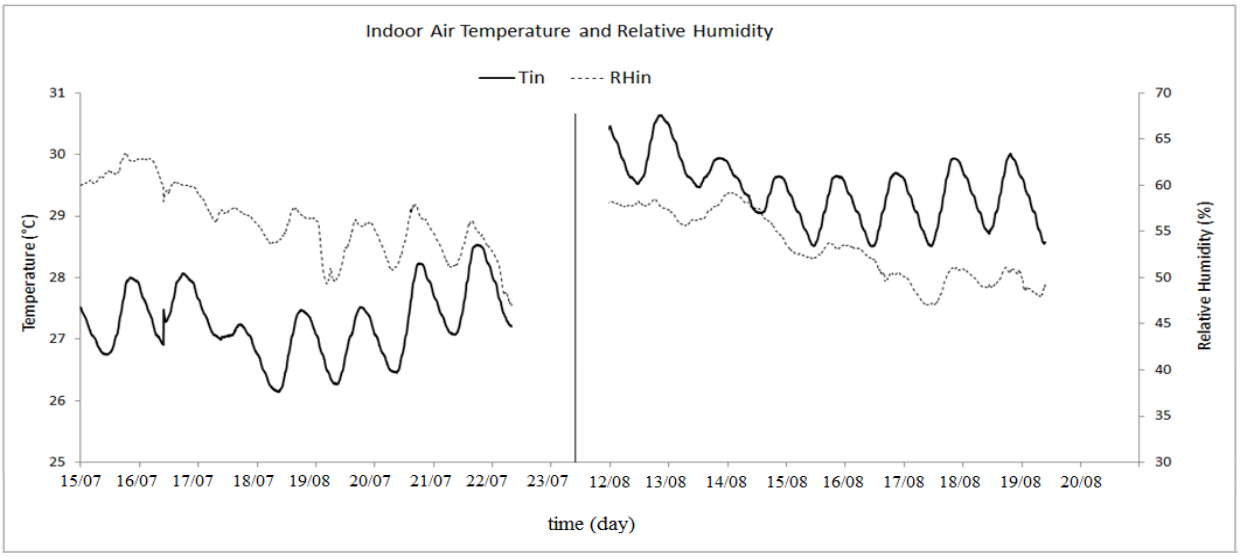

(b)

Fig. 3.9 : Measured outside (a) and inside (b) air temperature and relative humidity

The measured and simulated temperatures and relative humidity at the interface between the aerogel-based coating and concrete are plotted in Fig. 3.10. It can be seen from this figure that the numerical model is capable of generating temperatures and relative humidity close to those of measurements. The maximums and minimums of the simulated data are in phase with the measured ones. The temperatures are in good agreement between the two curves where the maximum discrepancy does not exceed 0.6°C. Concerning relative humidity, a satisfactory agreement is observed between the measurements and the simulation results; however, the maximums of the simulation results are lower than those measured where the discrepancy

between the two varies between 4% and 14%. A sensitivity analysis for different variables, especially the outside heat transfer coefficient and the initial conditions, is carried out to calibrate the model to approach the experimental results (See Annex B).

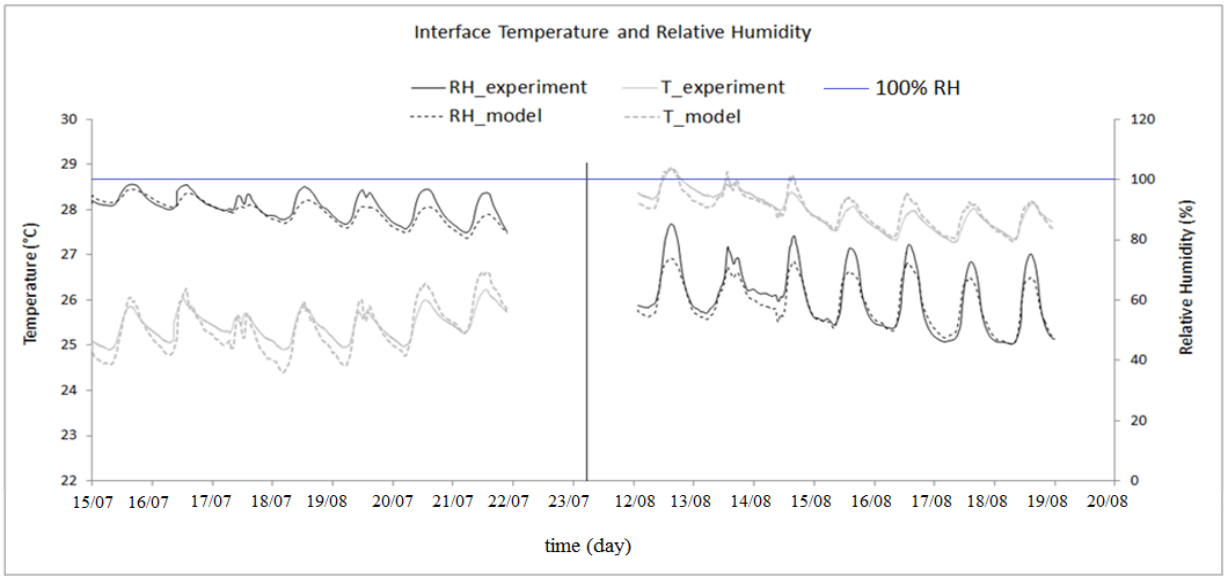

Fig. 3.10: Measured and simulated temperature and relative humidity at the interface coating/concrete

3. Full-Scale INCAS House Characterization

3.1. Introduction

This section presents the comparison of the results of a dynamic thermal simulation model developed in EnergyPlus with the experimental measurements carried out on an experimental full-scale house (INCAS house) recently built at the National Solar Energy Institute (INES) platform located in Bourget-du-Lac (Longitude 5.88°E , Latitude 45.65°N , Altitude 270 m) in the Rhone-Alpes region. The interest of this part is to show to what extent simulation tools are able to predict the thermal behaviour of buildings.

3.2. INCAS Experimental Houses Platform

The experimental field of INES (Fig. 3.11) is composed of several low energy houses, typical of a French residential house, having a similar geometry but having different construction techniques. These passive houses have been designed at INES and are intended for the study of new solar technologies as well as the validation of simulation tools to foster more energy efficient building designs. The interest of this platform is the ability to examine experimentally the

buildings' thermal behavior to improve design codes and make them capable to analyze, with a satisfactory accuracy level, the behavior of low and very low energy dwellings. Initially, the platform had three houses similar in shape but differ in the construction type of their exterior walls. Then, a fourth house (test house) was built in 2013, also with the same geometry but with different exterior walls' construction materials.

Fig. 3.11 : INES experimental platform and the experimental test house (in the red square)

The first house (back-right of Fig. 3.11) has concrete hollow block double walls with thermal insulation in the middle. The second house (back-left) has its exterior walls composed of heavy weight concrete with external insulation. The third one, (front-right) is designed with a wood frame wall structure. The fourth house (front-left) is the newly built one with its exterior walls composed of brick-monomur (Fig. 3.12) with the aerogel-based coating applied on its exterior surface.

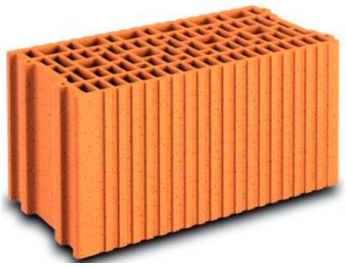

Fig. 3.12: Brick-monomur

3.3. Case Study House Description

The test-house is composed of four zones: crawl space, ground floor (GF), first floor (F1), and attic. The floor area of each zone is around 50 m². A relatively large glazing area is oriented to the south to maximize the heat gains due to solar radiation in winter. The glazing to floor area ratio is around 32% for the GF and 21% for the F1. To overcome the overheating problem in

summer, a balcony at the intermediate floor and a roof overhang are present. Also, all windows are equipped with automated roller shutters.

Fig. 3.13: The experimental test house while the aerogel-based coating being applied on its exterior facades

The exterior walls are composed of a 42cm layer of brick-monomur with a 4cm exterior layer of the aerogel-based coating (Fig. 3.13). The floor separating the attic from the first floor and that separating the ground floor from the crawl space are very well insulated. All the windows are doubled-glazed filled with argon except those oriented to the north which are triple-glazed. Fig. 3.14 shows the construction materials of each of the house's element. The house's floor plans and the construction materials' properties are presented in Annex C. The house is equipped with a double flux controlled mechanical ventilation system with a heat exchanger and a by-pass. The ventilation flow rate can be varied between 50m^3/h and 200m^3/h.

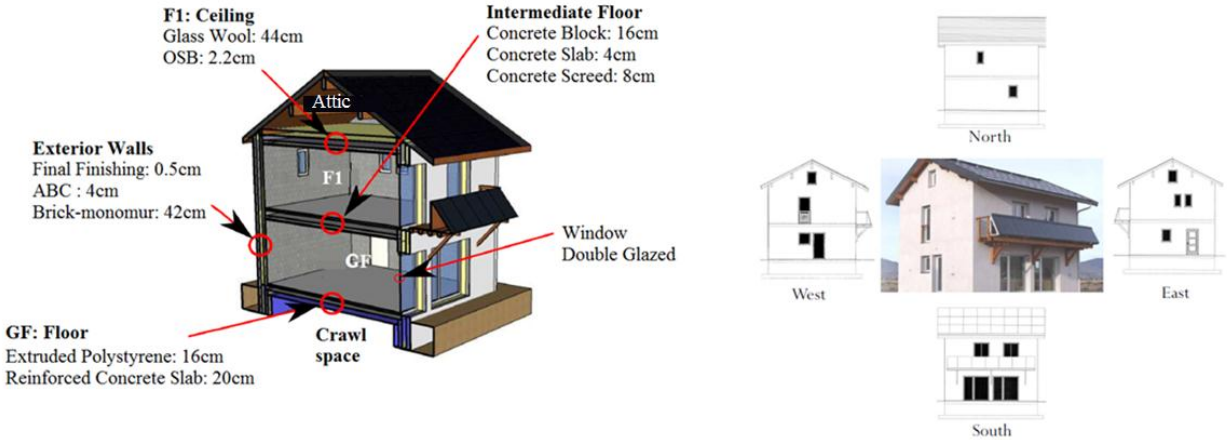

Fig. 3.14: The experimental test house construction materials

3.4. Instrumentation

3.4.1. Weather Station

A weather station is installed at the experimental field to measure all the environmental inputs needed for the dynamic thermal simulation. These include the solar radiation, air temperature and relative humidity, long-wave radiation intensity, and wind speed and direction. The measured climatic variables are the following:

- Global solar radiation on a horizontal plane measured via a pyranometer (Kipp and Zonen CMP22 Pyranometer; http://www.kippzonen.com/ProductGroup/3/ Pyranometers). The pyranometer works in the range of 0-4000 W/m² with an accuracy of ±10%.
- Direct normal solar radiation via a pyrheliometer mounted on a solar tracker (Kipp and Zonen CH1 pyrheliometer; http://www.kippzonen.com/Product/18/CHP-1-Pyrheliometer). The latter works in the range of 0-4000 W/m² with an accuracy of ±10%.
- Horizontal long-wave radiation intensity (Kipp and Zonen pyrgeometer CGR4; www.kippzonen.com/Product/17/CGR-4-Pyrgeometer).
- Wind direction and speed via an anemometer station (Windsonic WS1 anemometer; http://www.gillinstruments.com/products/anemometer/windsonic.htm) that has a measuring range of 0-60m/s with a precision of ±2m/s at 12m/s for the wind speed and a measuring range of 0-359°C with a precision of ±3° at 12m/s for the wind direction.
- Ambient air temperature and relative humidity using a hygrothermal sensor (Campbell scientific CS215; http://s.campbellsci.com/documents/au/manuals/cs215.pdf) placed in a multi-plate solar shield. The latter has a temperature measurement range of -40°C to +70°C with a precision of ±0.4°C for temperature ranges from +5°C to +40°C and a precision of ±0.9°C for temperature ranges from -40°C to 0°C and from +40°C to +70°C. For the relative humidity, it has a measurement range of 0-100% with an accuracy of ±2% for the range between 10-90%; otherwise, the accuracy is ±4%.

3.4.2. Inside Temperature Sensors

In order to identify a vertical air temperature gradient inside the rooms, houses are equipped with vertical poles on which three PT100 temperature sensors are installed at different heights. Each is inserted in a PVC tube to be protected from solar radiation. A black-globe thermometer is also installed on the pole to measure the radiant temperature. For the first floor,

three rooms are present; the air temperature of each of the rooms is measured. Other than measuring the rooms' air temperatures, the exterior walls' temperatures are also measured to examine the temperature gradient inside the walls. For each orientation for the ground and first floors, four PT100 sensors are placed: at the interior wall surface, at the middle of the brick-monomur layer inside the wall, at the interface between the brick-monomur and the coating, and at the exterior wall surface.

3.5. Measurements and simulation scenario

3.5.1. No aerogel-based coating

In this case, the comparison between the simulation results and the on-site field measurements is conducted for the INCAS house before applying the "ABC" on the exterior facades. The examined period is a one month period taken from the 20th of May 2013 till the 20th of Juin 2013. The following scenario is being adopted:

- The indoor air temperature is free-floating (no heating or cooling systems)
- A fixed volume flow rate mechanical ventilation is set to "ON" at all times (0.7ach)
- No internal heat gains are present
- The windows are kept closed at all times
- The roller shutters at the south windows are always open; however, all the others at the other orientations are always closed
- All internal doors (between the rooms) are opened

Measurements are recorded every one minute and the simulations are carried out with a 1 min timestep. Fig. 3.15 shows the outdoor air temperature (T_{out}) and the global horizontal solar irradiation (I_{Gh}) for the considered period.

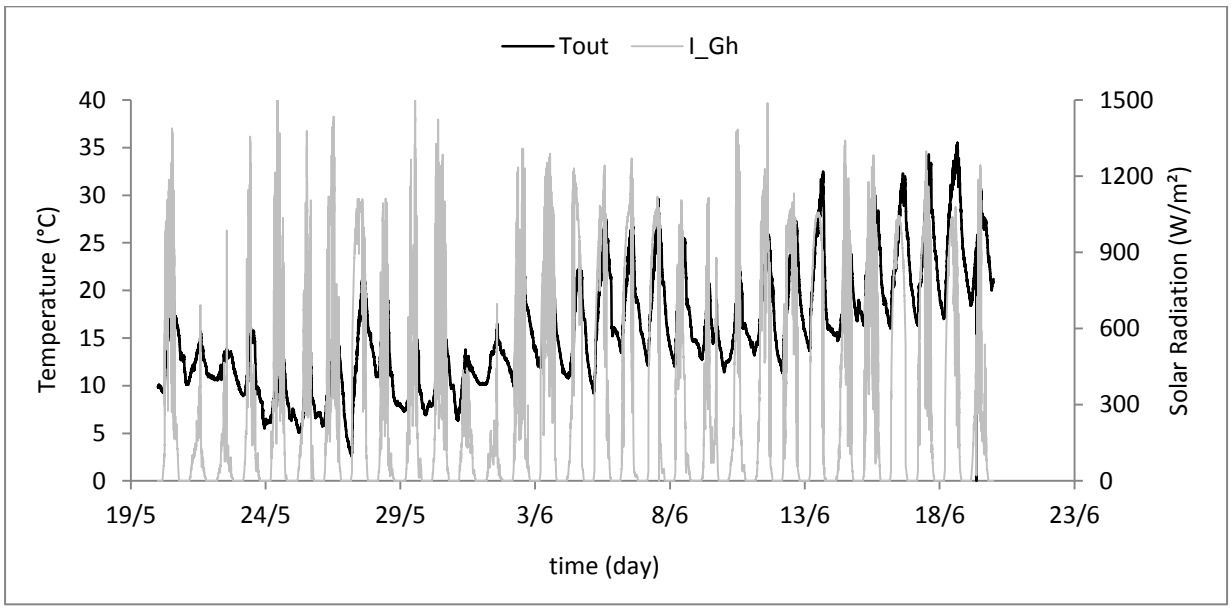

Fig. 3.15: Outside air temperature and solar radiation for the test period (case: no coating)

Fig. 3.16 shows the measured indoor air and operative temperatures at 1.7m height and the simulated ones for the ground and first floors. The black solid line represents the measured data while the dotted one represents the simulated results. The brown curve represents the absolute discrepancy between the measured and simulated temperatures.

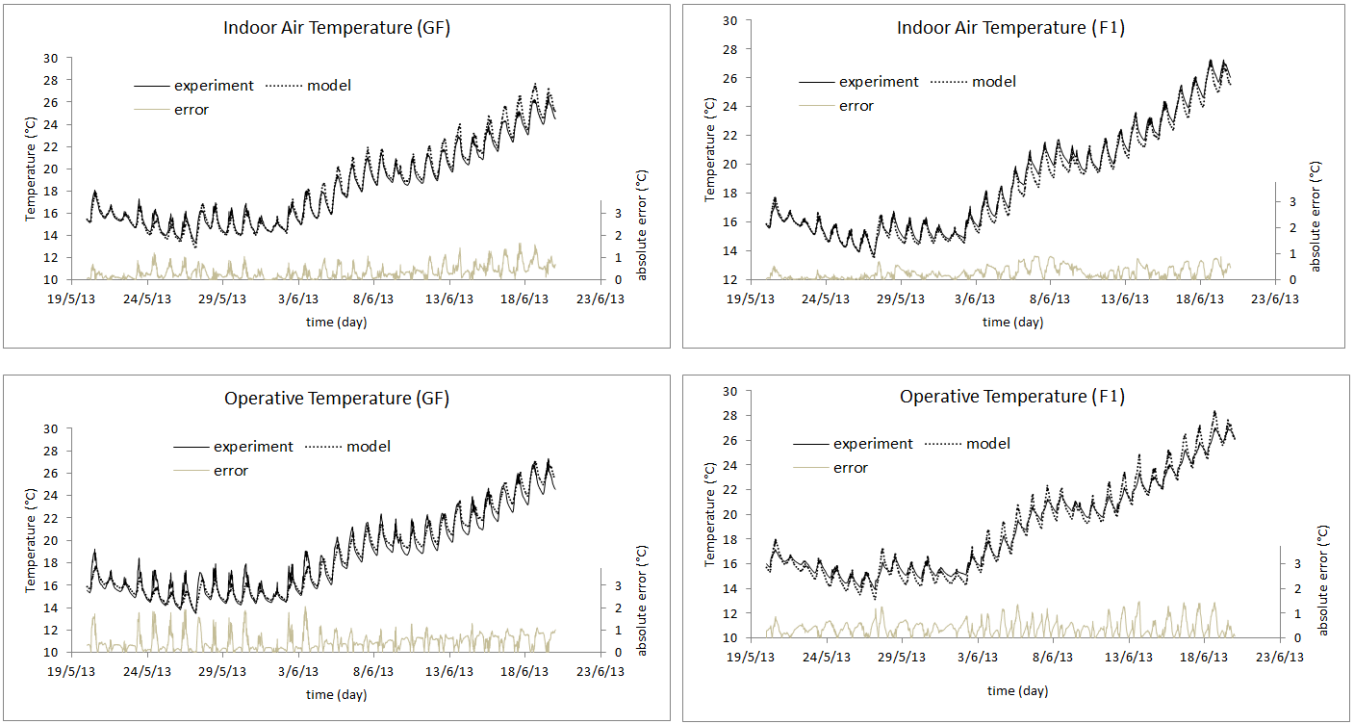

Fig. 3.16: Indoor air and operative temperatures for the GF and F1 (case: no coating)

From this figure, we can see that there is a good agreement between the simulated and the measured temperatures. However, for the air temperature of the GF, the peaks are more pronounced in the results of the numerical model at mid-day especially for days with, relatively, high solar radiation and outdoor air temperature (days after 11/06). The discrepancy between simulation and measurements for these peak hours can reach 1.6°C. The reason may be that the model is overestimating the amount of solar radiation entering the house and/or underestimating the thermal inertia of the house. For the days with low solar radiation (such as the days 21/05, 22/05, 31/05, 01/06), the simulated temperatures behave almost the same as the measured ones where the maximum discrepancy does not exceed 0.6°C. For the F1, as previously stated, we have three rooms; thus, the experimental measurements curve shown in the above figure represents the average of the temperatures of the three rooms. We can see that there is a very good agreement for the air temperature where the maximum discrepancy does not exceed 1°C.

For the operative temperatures, the simulation results of the GF are in a very good harmony with those measured for almost all the considered period. It is observed that for a few days (23/05 till 26/05), the simulated temperature peaks are lower than the measured ones by about 1.8°C. Also, it is seen that the measured temperatures get lower than those simulated during the nights. This can be explained by either an error in the calculation of the modeled radiative sky temperature or

by under-estimation in the building's thermal inertia. Concerning the operative temperature of the first floor, the model gives a more temperature range between day and night especially during the days with high solar radiation. During the first period where the mean temperature is decreasing over the days (20/05 – 02/06), the troughs of the model curve are lower than those of the experimental curve. However, for the second period where the mean temperature is increasing over the days (03/06 – 19/06), the simulated peaks are higher than the experimental ones. The maximum discrepancy between the peaks can reach 1.5°C and between the troughs can reach 1.3°C. The reason that can explain this difference may be the presence of the internal thermal inertia of the inner partition walls between the rooms which was not modeled in EnergyPlus. The first floor is modeled as one fully-mixed air zone. Thus, this thermal inertia may have the capability to absorb the excess heat during the day leading to lower peak temperatures (in the measured curve) and release it successively during the night leading to higher temperatures than those of the simulation at night time.

3.5.2. With aerogel-based coating

In this case, the comparison between the simulation results and the on-site field measurements is conducted for the INCAS house after applying the "ABC" on the exterior facades. The examined period is taken from the 30th of June 2014 till the 21th of July 2014. The outside air temperature and the global horizontal solar radiation are shown in Fig. 3.17

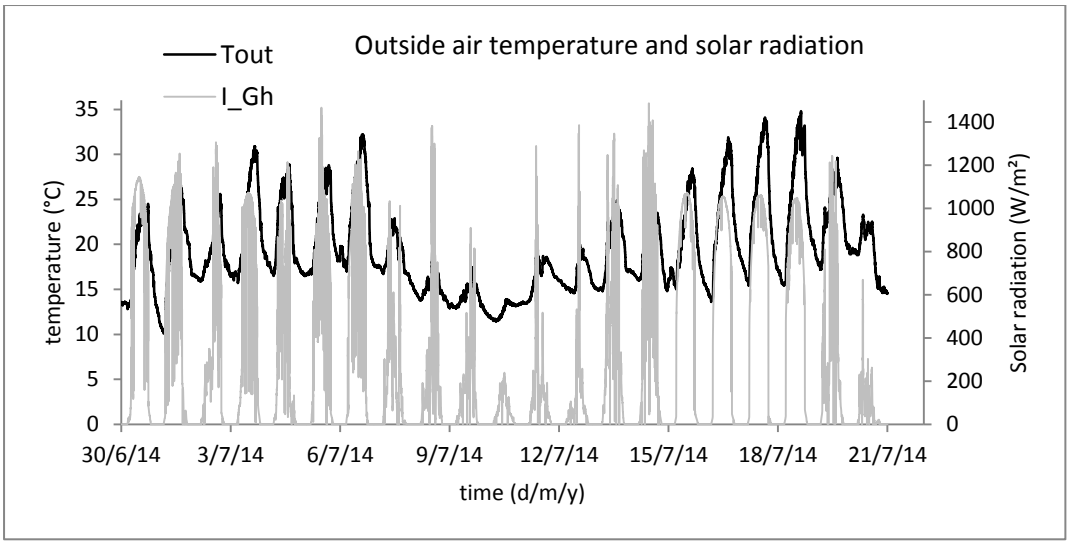

Fig. 3.17: Outside air temperature and global horizontal solar radiation for the test period (case: with coating)

The measured and simulated indoor air and operative temperatures for the ground and first floors are presented in Fig. 3.18. From this figure, we can see that there is a good agreement between the simulated and the measured temperatures.

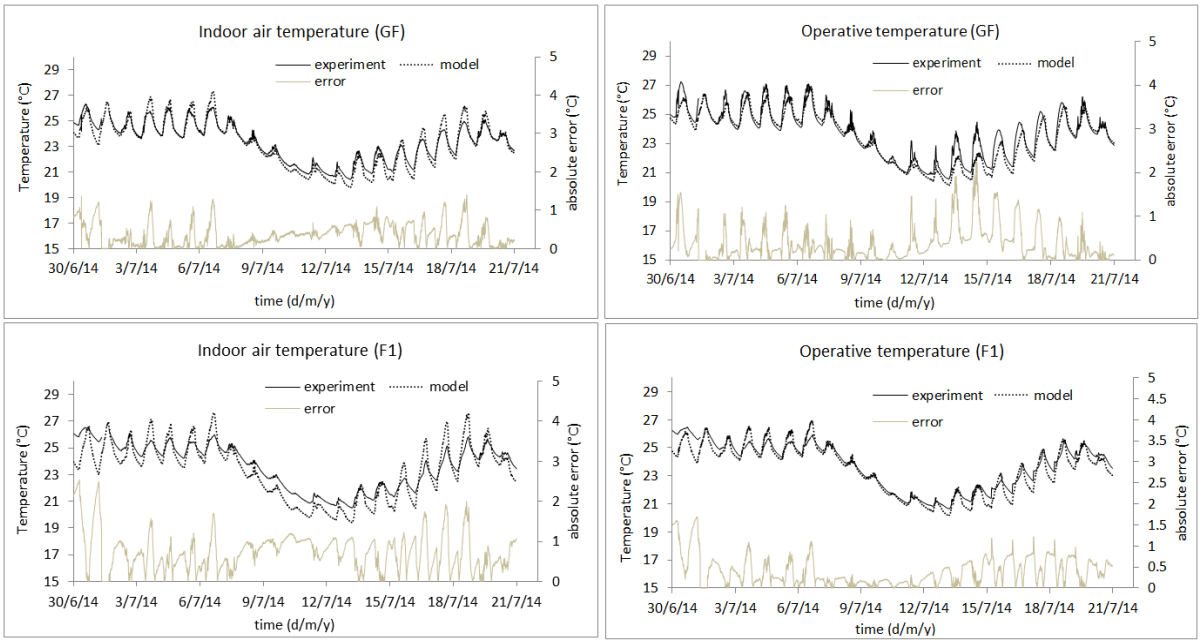

Fig. 3.18: Indoor air and operative temperatures for the GF and F1 (case: with coating)

However, for the GF, the air temperature peaks are more pronounced in the results of the numerical model at mid-day for days with, relatively, high solar radiation and outdoor air temperature (04/07 – 06/07 and 16/07-18/07). The discrepancy between simulation and measurements for these peak hours can reach 1.4°C. The reason may be that the model is overestimating the amount of solar radiation entering the house and/or underestimating the thermal inertia of the house. For the days with low solar radiation (07/07 - 12/07), the simulated temperatures behave almost the same as the measured ones where the maximum discrepancy does not exceed 0.5°C. Another thing observed is that the peaks and troughs are in phase between the two curves. For the operative temperatures of the GF, the simulation results agree well with those measured for almost all the considered period. It is observed that for the days 13/07 and 14/07, the simulated temperature peaks are lower than the measured ones by about 2°C. Also, the peaks of the simulation curve lag those of the measured one by about 1.2h.

Concerning the first floor, the thermal dynamics of the simulation results are in harmony with the measured ones; however, the EnergyPlus model gives a more temperature range between day and

night especially during the days with high solar radiation. The peaks of the model curve are higher and the troughs are lower than those of the experimental curve. The maximum discrepancy between the peaks can reach 2°C and between the troughs can reach 1.2°C. Also, the reason that can explain this difference may be the presence of the internal thermal inertia of the inner partition walls between the rooms which was not modeled in EnergyPlus. Similar to the air temperature, we can see a good agreement for the operative temperature.

Trying to examine the effect of solar radiation, air ventilation, and internal mass, Fig. 3.19 shows the indoor air temperature of the ground floor for different window's solar heat gain coefficients (SHGF), for different ground reflectivity values, and for different ventilation rates. Also, in the same figure, the effect of increasing the inner thermal inertia of the occupied space on the indoor air temperature is examined. From this figure, it is illustrated that increasing the window's SHGC and/or increasing the ground reflectivity increases significantly the indoor air temperatures. When these values are increased, the amount of solar radiation entering the house through the windows is increased leading to hotter indoor environment. Decreasing these values decreases the indoor air temperatures. Concerning thermal mass, compared to the base case model, increasing the thermal inertia inside the occupied space attenuates the fluctuations in the temperatures leading to lower peak values at daytime and higher values at nighttime, resulting in a temperature curve very close to the experimental one. However, when increasing the thermal inertia a small time lag is observed between the simulation results and the experimental data. Also, some instantaneous temperature fluctuations observed in measurements are flattened out and not observed in the results of the model with internal thermal mass. On the other hand, these instantaneous temperature fluctuations are observed in the results of the base case model with no increased thermal mass.

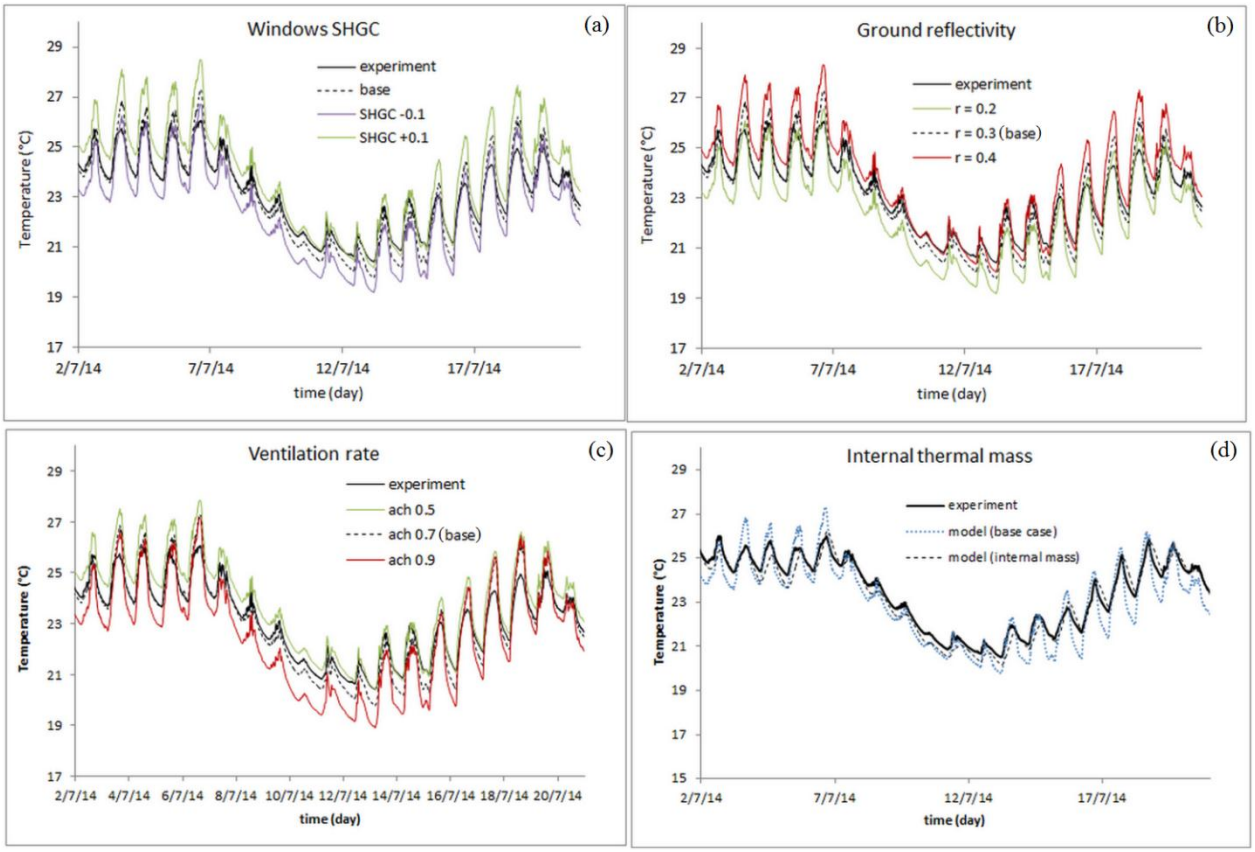

Fig. 3.19: Variation of the ground floor's indoor air temperature for different window's solar heat gain coefficients, (b) for different ground reflectivity values, (c) for different ventilation rates, and (d) with increased indoor thermal inertia

Other than the room temperatures, the wall temperatures are compared. Fig. 3.20 shows the temperature at the interface between the coating and the brick, the temperature at the middle of the brick layer, and the temperature at the inner surface temperature for the north facade of the first floor. As shown in this figure, the model is capable of generating temperatures very close to the experimental measurements with an absolute error that does not exceed 1.8°C.

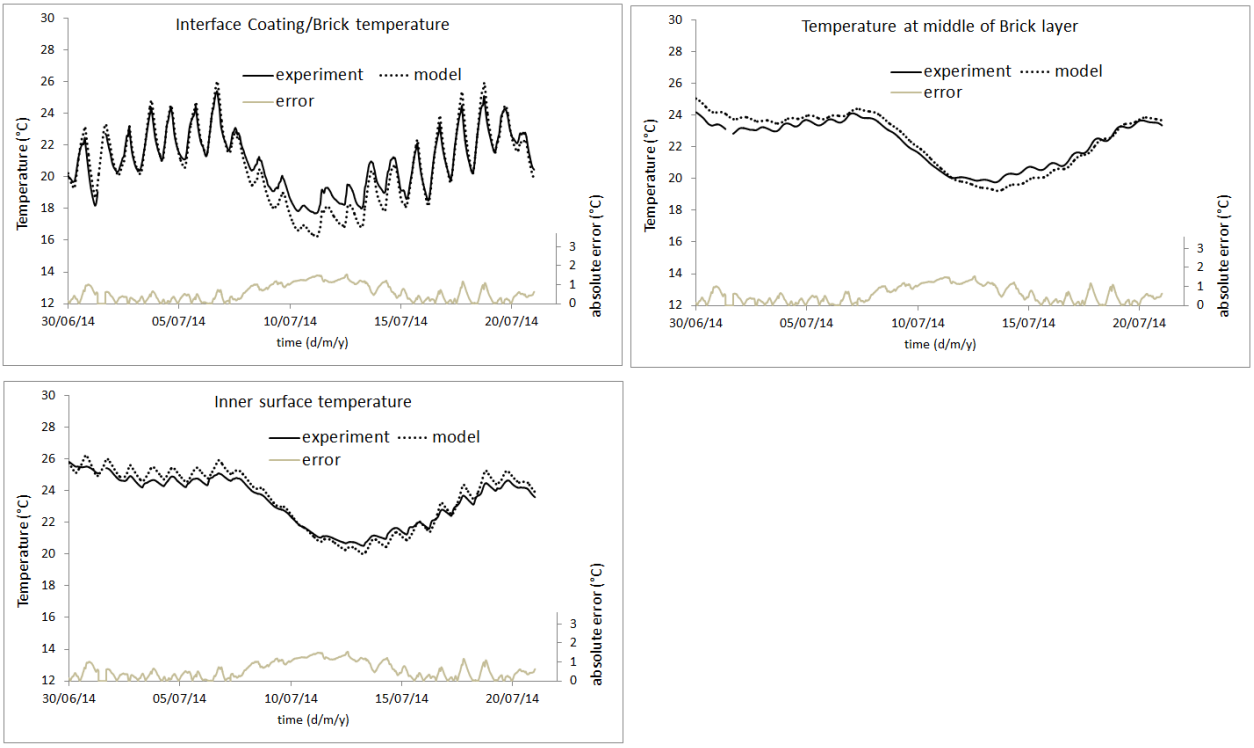

Fig. 3.20: North wall temperature comparison between model and experiment

3.5.3. Sensitivity Analysis

A sensitivity analysis is carried out to examine the impact of changing some variables on the results. The case of the house with the coating is considered. The examined parameters are:

- Ground reflectivity (r_{gr})
- Coating's thermal conductivity ($k_{coating}$)
- Brick's thermal conductivity (k_{brick})
- Coating's density ($\rho_{coating}$)
- Brick's density (ρ_{brick})
- Windows' solar heat gain coefficient ($SHGF$)
- Ventilation rate (ach)

For each parameter, its value is increased/decreased for a certain percentage and simulations are re-run. For each case, the absolute error (difference between measurement and simulation) for the ground floor's air temperature is calculated at each time-step, then, the mean error (α) is calculated taking the average of these. Also, the average of the standard deviations from the mean (β) is calculated. Table 3.3 shows the values selected for each variable and the corresponding α and β.

Table 3.3: Sensitivity of some input parameters on the indoor air temperature

		α	β
r_{gr} (-)	0.2	1.23	0.84
	0.3 (base)	0.79	0.87
	0.4	1.07	1.04
$k_{coating}$ (W/(m.K))	0.0268 (base)	0.79	0.87
	0.033	0.89	0.88
	0.039	0.92	0.88
$\rho_{coating}$ (kg/m3)	100	0.87	0.89
	150 (base)	0.79	0.87
	200	0.86	0.89
k_{brick} (W/(m.K))	0.08	0.84	0.93
	0.115 (base)	0.79	0.87
	0.3	1.11	0.87
ρ_{brick} (kg/m3)	500	0.93	0.89
	700 (base)	0.79	0.87
	900	0.81	0.9
SHGF (-)	-0.1	1.19	0.85
	base	0.79	0.87
	+ 0.1	1.2	1.05
ach	0.5	1.03	0.94
	0.7 (base)	0.79	0.87
	0.9	1.28	0.88

From Table 3.3, it is shown that a decrease or an increase in the ground solar reflectivity will increase the error between simulation results and measurements. Decreasing this value means the solar radiation entering the house is being underestimated; however, increasing it means the solar radiation is being overestimated. Same conclusions can be made for the window's solar heat gain coefficient. For the coating and brick thermal conductivities, an increase in this value increases the heat transfer through the envelope leading to an increase in the error. For the density, increasing or decreasing its value compared to the base case increases the error. The density has an effect on the thermal inertia of the building envelope. Concerning the ventilation rate, a lower value means lower cooling load during the day (than the base case) and lower cooling effect at night (outside air is cooler than inside air at night). Conversely, a higher value for the ventilation rate leads to higher cooling load at day time with a higher cooling effect at night time.

4. Wall Active Loop System Experimentation

4.1. Introduction

As reported in chapter 2, we introduced the wall active loop system (WALS) whose concept is to capture part of the solar energy of the south facade and transfer it to the north facade to act as an assisting heating system. We described the system with all the mathematical equations. In this section, an experimental mock-up is established for the aim of examining the performance of this system as well as validating the mathematical model.

4.2. Mock-up Experiment

Two experimental mock-ups having the same dimensions and construction materials have been established at INES experimental field. The first one serves as the test mock-up with the active embedded pipe loop system being implemented and the other serves as the reference one with no fluid pipes (see Fig. 3.21).Note that this figure was before applying the coating on all the exterior facades. Each mock-up unit has a length of 2.25m, a width of 1.6m and a height of 1.23m. The walls are composed of 10cm concrete with 4cm aerogel based coating. In the south facade, the fluid pipes are embedded in the aerogel coating and are placed near the exterior surface. These pipes are hold through a metallic bar with horizontal fixings as shown in Fig. 3.22 (upper part) which are fixed to the concrete layer through bolts. In the north facade, the pipes are in direct contact with the concrete layer. Since the coating is highly insulating, and to enhance the heat transfer from the fluid pipes in the north facade to the interior space, a layer of normal plastering is added between the concrete and the aerogel coating and covers the pipes (see Fig. 3.22 lower part). The ground and ceiling are composed of a layer of thermal insulation to minimize the heat transfer from these surfaces.

Fig. 3.21: The experimental mock-ups: the test-case with the fluid pipes and the reference case without the pipes (Note: this figure is before applying the coating on all the facades)

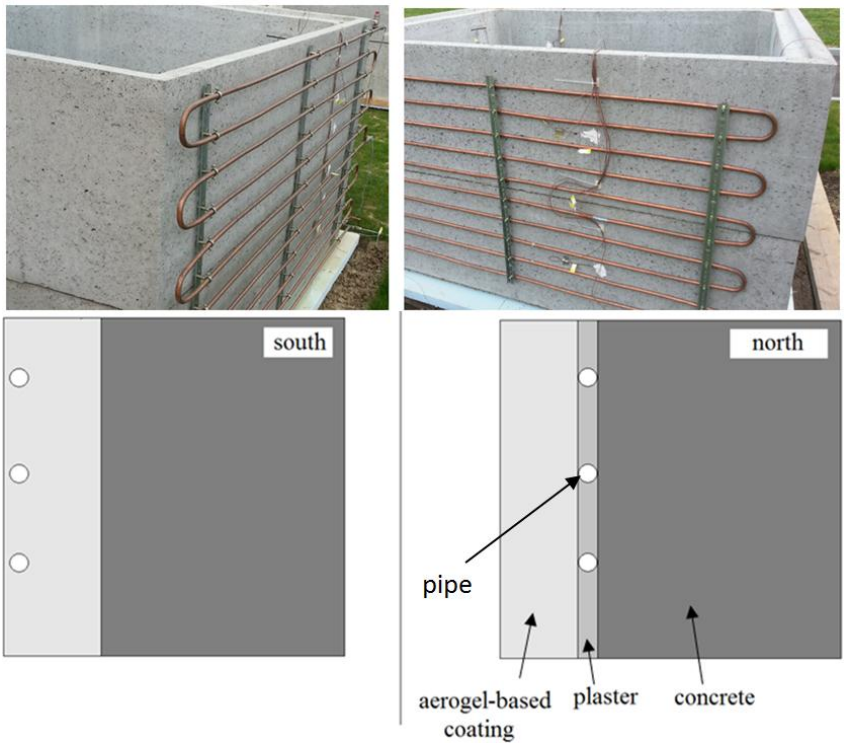

Fig. 3.22: Fluid pipes position in the south facade (left) and north facade (right)

A paint having a solar absorptivity of 0.6 is applied on the exterior surfaces of all the facades. The pipe's diameter is 1.5cm and the spacing is approximately 10cm. The system is equipped with a variable flow rate pump (see Fig. 3.23) connected to the pipes with an expansion tank for pressure regulation. The pump's flow rate could be varied from 5.53 to 116 l/h. Also, the pump is equipped with a control timer that sets the pump "ON" or "OFF" during pre-assigned scheduled hours of the day. The heat transfer fluid is a mixture of water/anti-freeze (60%/40%) to protect the system when exposed to low temperatures. Temperature sensors (Type T thermo-couples) are

placed at different positions to measure the wall and fluid temperatures. For each of the south and north walls, three sensors are placed at the exterior surface and other three sensors are placed at the interior surface at different heights: near the bottom (at 32cm from the bottom), at the middle, and near the top edge (at 92cm from the bottom). For each of the other walls and the roof, one sensor is placed at the middle of the exterior surface and another one at the middle of the interior surface. Also, a temperature sensor is placed at the inner surface of the ground. Other than the wall surface temperatures, the fluid temperature is measured. For each of the north and south facades of the test mock-up, the inlet and the outlet temperatures are measured as well as the temperature at a position near the middle of the serpentine loop.

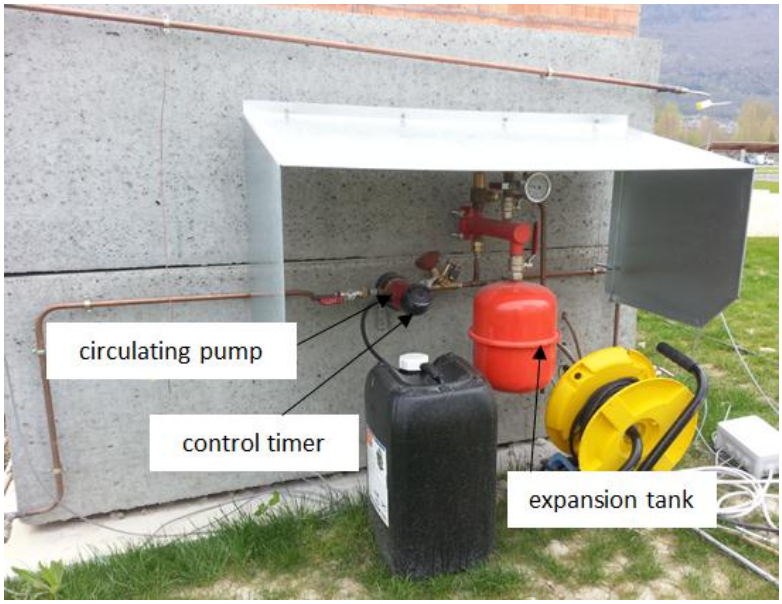

Fig. 3.23: The pumping system

4.3. Measurements and Performance Comparison

Since this mock-up is lately built, we could not test the system performance in different conditions. For that reason, we compare the system's test-case performance with that of the reference one for 15 days in October, 2014. Then, we compare the results of the test-case experiment with those of the numerical model. Measurements are recorded every 2 minutes. The pump is set to "ON" from 9 a.m. till 5 p.m. Fig. 3.24 shows the internal surface temperature at the middle of the north facade for both mock-ups as well as the exterior air temperature and the vertical south solar radiation. It is shown that the north inner surface temperatures of the test case (with the WALS) are higher than those of the reference case. The difference between the two can reach more than 4°C for the days with relatively high solar irradiation (08/10 – 09/10, 17/10 –

20/10). For the days from 10/10 till 12/10, the surface temperature decreases compared to the previous day due to the relatively lower solar radiation but it remains higher than the temperature of the reference case. For the days (13/10 and 16/10), the north inner surface temperatures of the test and reference cases are almost the same due to the very low solar radiation available during this day. Then in the last four days, the temperature of the test case shows a significant increase compared to the reference temperatures. During a specific day, and due to the effect of thermal storage in the concrete structure, the north wall inner surface temperature reaches its maximum value at approximately 5p.m. then starts to decrease gradually where the wall dissipates its energy to the inside space. Due to this storage, we can see that the temperature decreases slowly at night providing heat to the space. Also, a significant time shift is observed between the inner surface temperature and the outside air temperature.

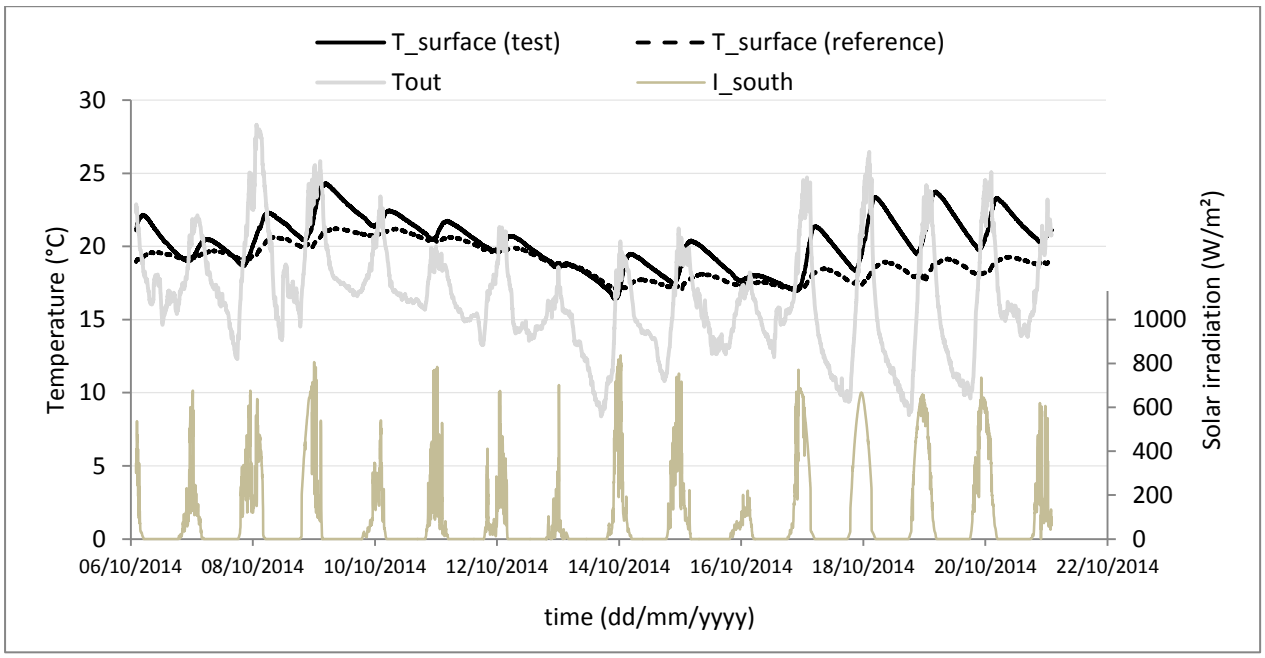

Fig. 3.24: North wall inner surface temperature for the test and reference cases, outdoor air temperature, and south wall solar irradiation

Fig. 3.25 shows the south wall outside surface temperatures for both the test and reference mock-ups. It is shown that during day time, the temperatures of the reference case are higher than those of the test case especially during the days with high solar irradiation. The difference between the two during these days can reach 10°C. The reason that explains this is the presence of the fluid

pipes near the outside surface of the south facade (in the test mock-up) which receives part of the solar energy and transfers it to the north facade.

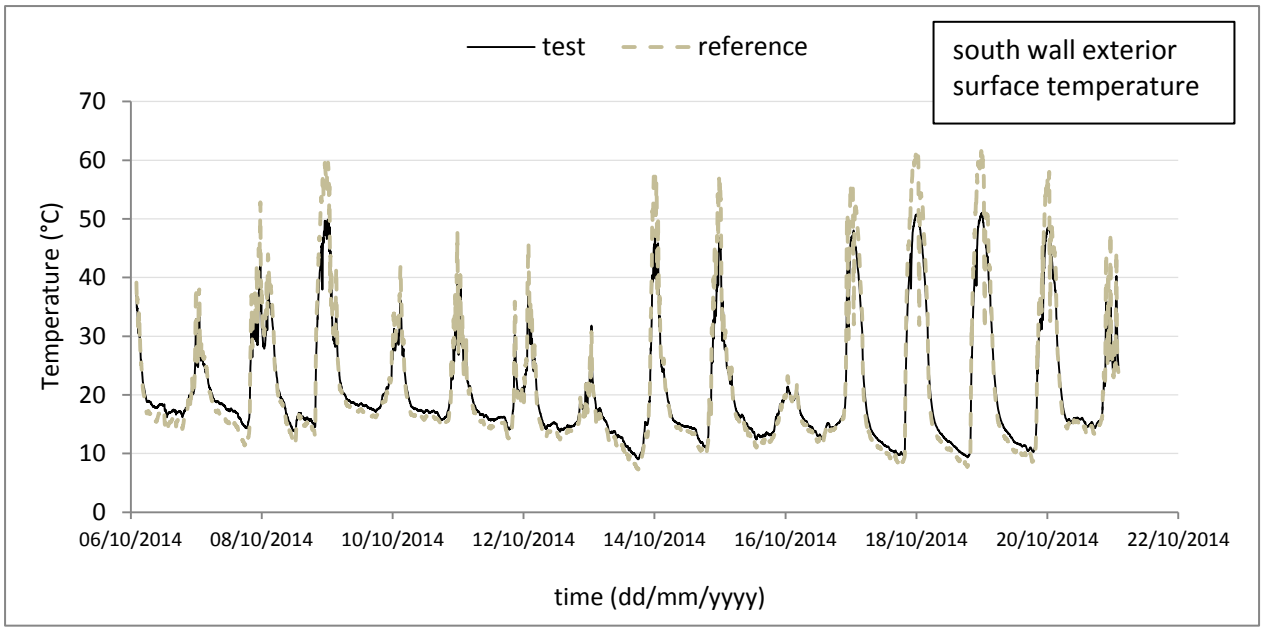

Fig. 3.25: South wall exterior surface temperature for the test and reference cases

The temperature of the air inside the mock-up units are shown in Fig. 3.26. We can see that the air temperature of the test case (with the WALS) is always higher than that of the reference case. The difference is much higher during the days with high solar irradiation where it can reach 2°C.

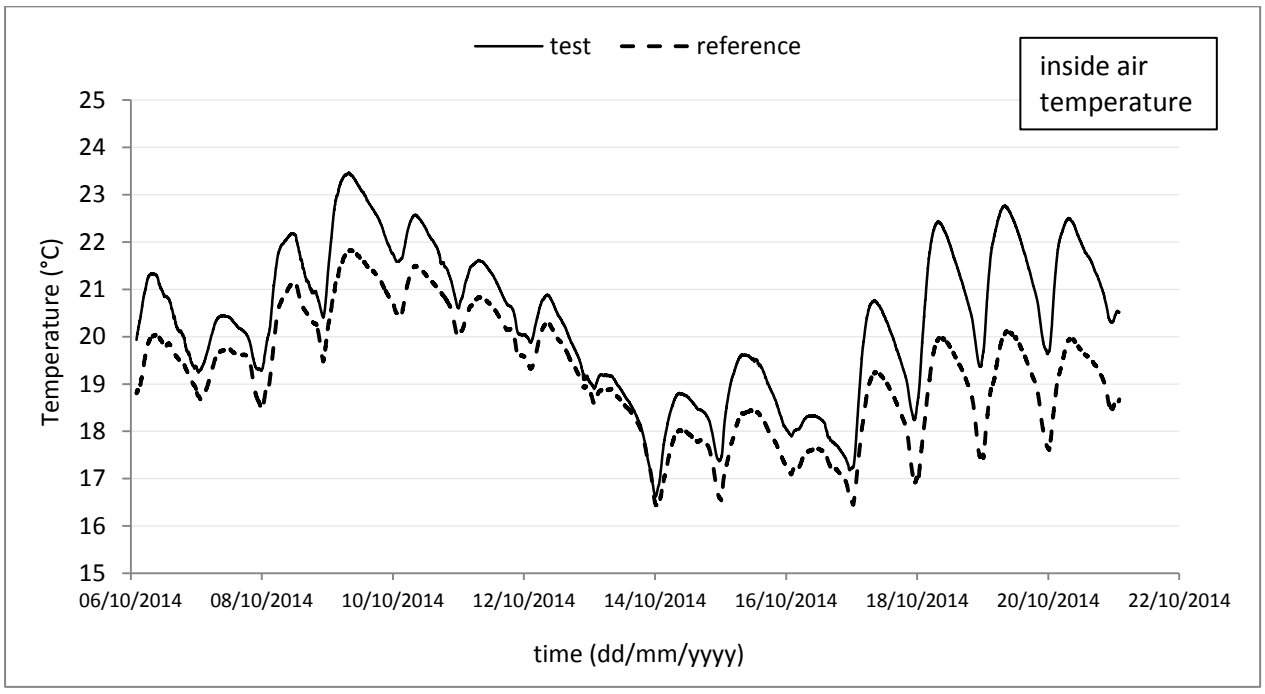

Fig. 3.26: Inside air temperature for the test and reference cases

Fig. 3.27 shows the inlet and outlet fluid temperatures of the south facade, the time when the circulating pump is ON or OFF, and the collected heat flux. The collected heat flux is the heat received by the fluid during its flow through the serpentine pipes of the south wall and is calculated using equation (3.1).

$$q_c = \frac{\dot{m}_f cp_f \Delta T_f}{A_w} \tag{3.1}$$

where $q_c, \dot{m}_f, cp_f, \Delta T_f$, and A_w are the collected heat flux per unit area of the wall, the fluid mass flow rate, the fluid specific heat, the difference between outlet and inlet fluid temperatures, and the area of the south wall, respectively.

For the days with high solar radiation, the exit fluid temperature from the south wall reaches values more than 35°C at mid-day. With this temperature, the fluid passes to the north wall and returns with temperatures in the range of 24°C to 28°C. For the days with lower solar radiation, the south wall outlet fluid temperature can reach 30°C at mid-day. For the days with poor solar radiation, the fluid's outlet temperature (from the south wall) remains close to the inlet temperature.

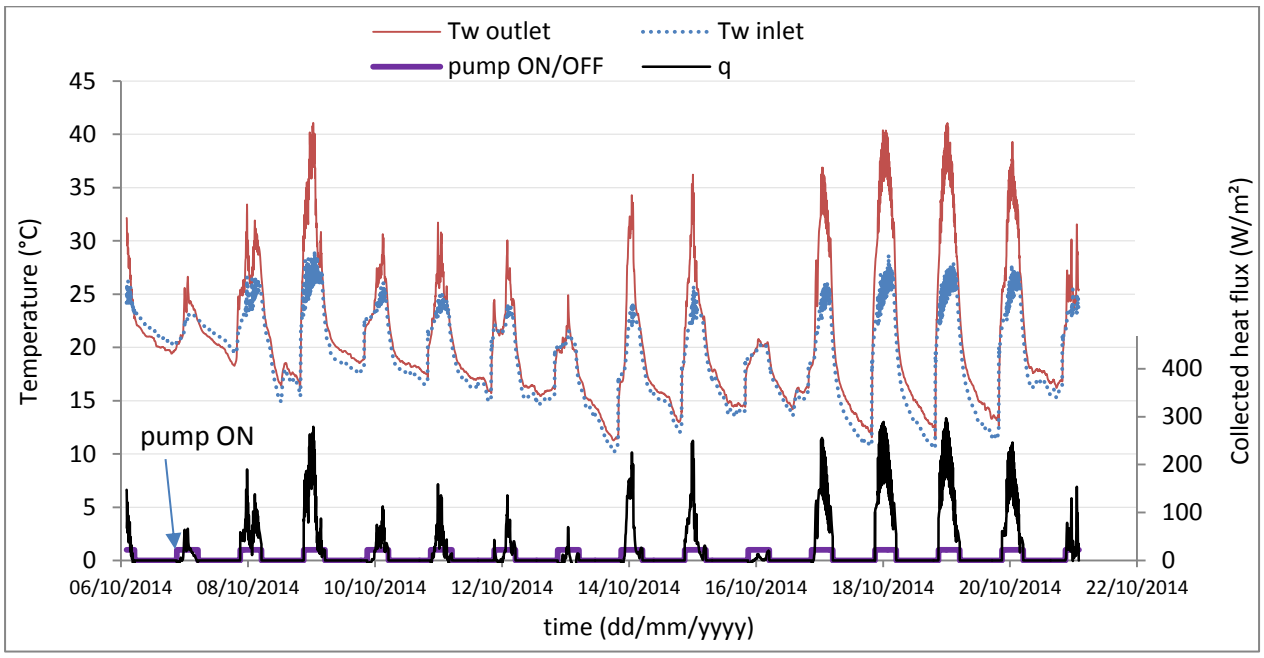

Fig. 3.27: Inlet and outlet fluid temperature of the south facade and the collected heat flux

As highlighted by several authors (Srivastava et al. 1982, Nayak et al. 1989, Bopshetty et al. 1992, D'Antoni and Saro 2012), the notion of the instantaneous energy efficiency becomes meaningless in the case of massive solar thermal collectors, because inertial effects delay the energy response at time instants where no availability of solar radiation is present. This leads to the conclusion that under certain circumstances (e.g. cloud passing) the energy efficiency would be very close to 100%. Thus, some authors refer to medium (week) or long-term (season) energy efficiency. The latter is the ratio of the collected heat energy during a certain period of time to the available solar energy during the same period, and is calculated using equation (3.2-a) (Srivastava et al. 1982, Nayak et al. 1989) or equation (3.2-b) (D'Antoni and Saro 2012). The difference between these two equations is the presence of the solar absorptivity in the denominator.

$$\bar{\eta}_1 = \frac{\int q_c \, dt}{\int I_s \, dt} \qquad (3.2-a)$$

$$\bar{\eta}_2 = \frac{\int q_c \, dt}{\alpha \int I_s \, dt} \qquad (3.2-b)$$

where $\bar{\eta}$, α, and I_s are the system's efficiency (over a period of time), the solar absorptivity, and the instantaneous solar irradiation, respectively.

In our case, we calculate the system's efficiency for the 15 days testing period. It is found that the efficiency $\bar{\eta}_1$ is around 27% and $\bar{\eta}_2$ is around 45%. However, it is essential to calculate the

efficiency for different periods of the year, especially in winter. It is important to note that the efficiency $\bar{\eta}$ may not be a real indicator of the system's performance because it depends greatly on the outlet fluid temperature of the serpentine loop of the north facade which becomes an inlet to the south loop. As reported by D'Antoni and Saro (2013), for massive solar thermal collectors, the inlet fluid temperature is the major operation parameter influencing greatly the energy output and efficiency. This is true in our case because the numerator of equation (3.2) depends on the difference between the inlet and outlet temperatures; thus, lower inlet temperatures increase the efficiency. The latter depends greatly on the system's working conditions, the system's size, and the indoor and outdoor boundary temperatures.

Fig. 3.28 shows the inner surface temperature of the south wall for the test and reference cases. It is shown that the temperatures of the test case are higher than those of the reference case except for the days with no solar radiation. This is due to the convection heat transfer with the inside hotter (compared to the reference) air and the long-wave radiative heat transfer with the hotter north facade. Similar trends are observed for the other walls.

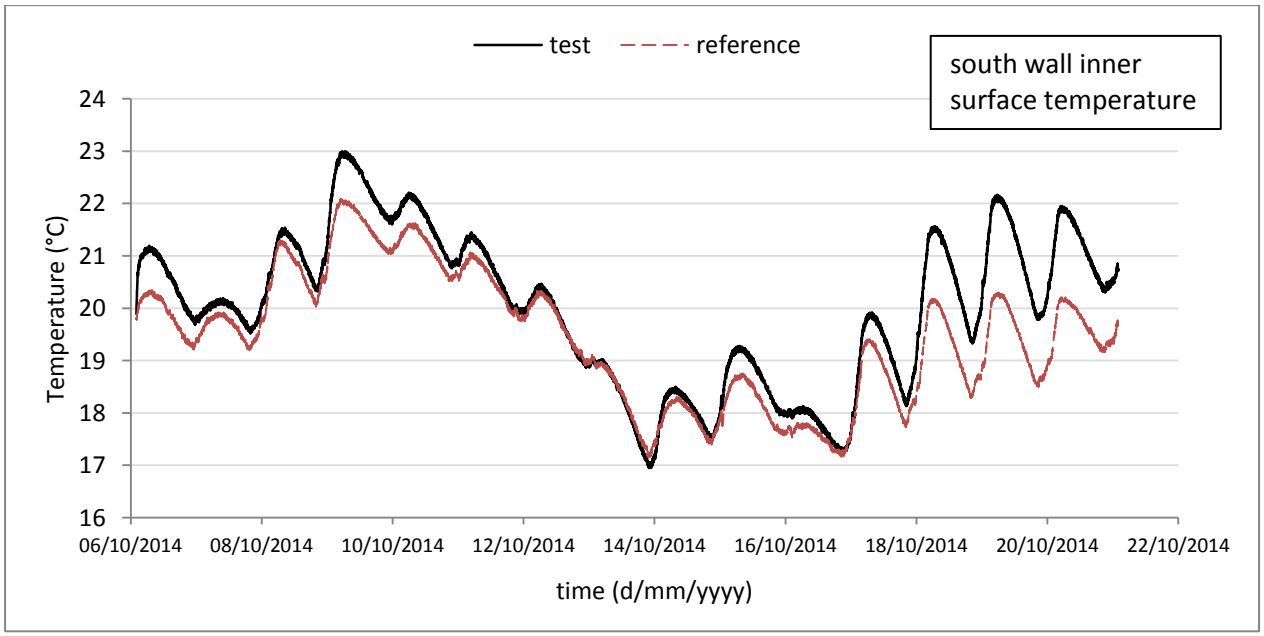

Fig. 3.28: South wall inner surface temperature for the test and reference cases

4.4. Numerical Model Validation

The results of the experimental measurements are compared to the simulation results of the numerical model already presented in chapter 2 (section 6). The simulation time-step is taken as

2min. After doing a mesh refinement test, the calculation domain is divided into a total of 450 control volumes.

The inlet and outlet water temperatures of the south facade are shown in Fig. 3.29 for both the experiment and the model. The south inlet fluid temperatures (outlet temperature from the north facade) resulting from the numerical model are generally higher than the measured temperatures. At peak hours, the discrepancy is in the range of 1.5-3°C. At night, the discrepancy is around 1.5-2°C. One reason for this difference may be the presence of the plaster layer between the aerogel coating and the concrete which cover the fluid pipes. This plaster layer was not taken in consideration in the numerical model. Therefore, due to this layer in the experiment, the heat transfer is enhanced between the fluid and the surrounding making its temperature to remain lower than those of the numerical model. A satisfactory agreement between the simulation and the experimental results is obtained for the south fluid outlet temperature.

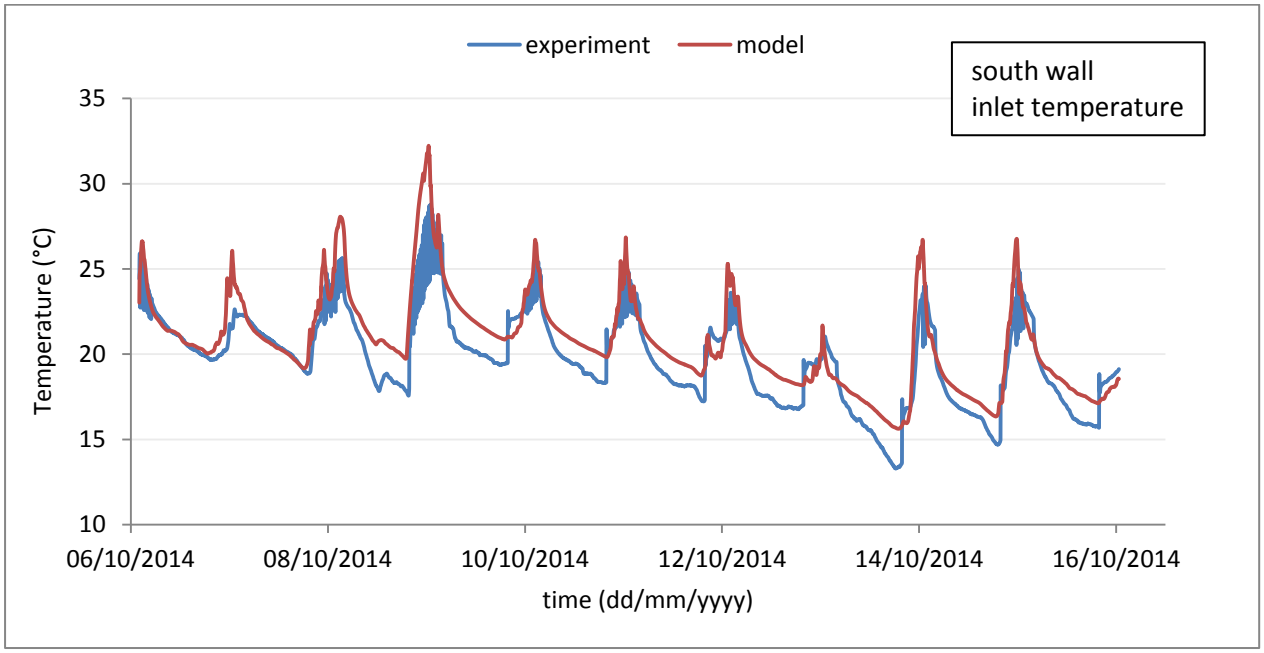

(a)

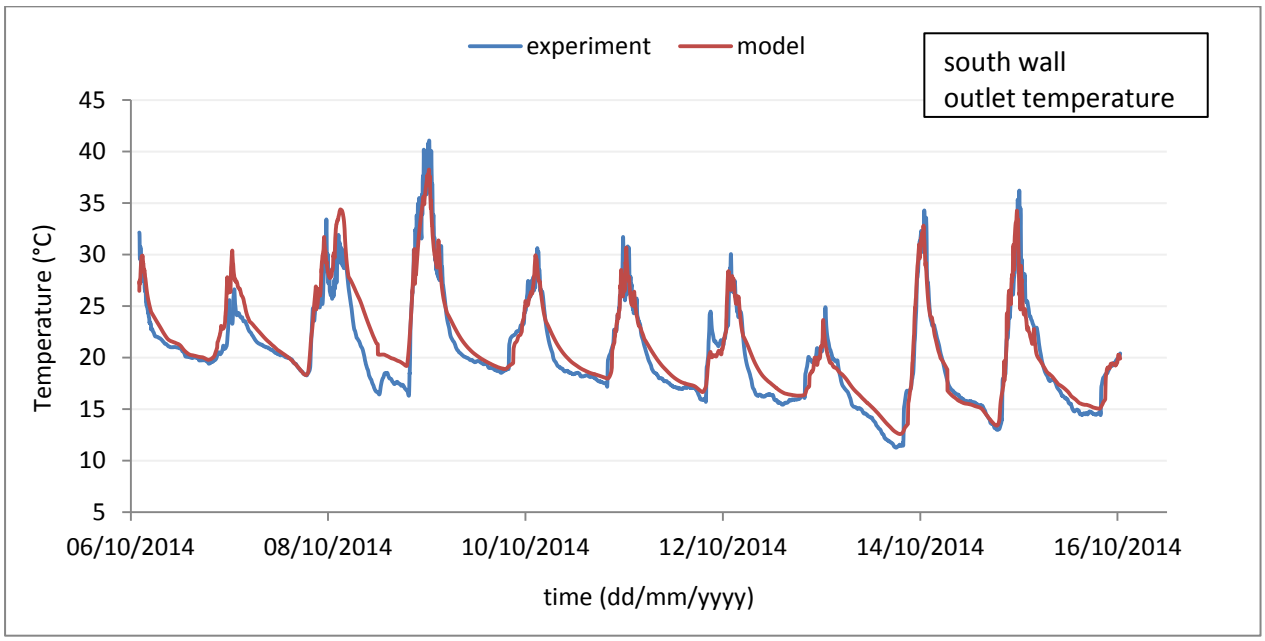

(b)

Fig. 3.29: South wall fluid inlet (a) and outlet (b) temperatures

Fig. 3.30 shows (a) the south and (b) the north inner surface temperatures at the middle position of the wall surface. It is illustrated from these figures that the model is capable of generating temperatures in good agreement with the experimental data. Also, the two curves are almost in phase and have close decrement factors. This is important in such systems because the thermal storage and the time delay of the heat transferred to the space are major factors affecting the system's performance. The average discrepancy between the simulation and the measured data is around 0.5°C with a maximum value that does not exceed 1.2°C and 1.4°C for the south and north wall, respectively.

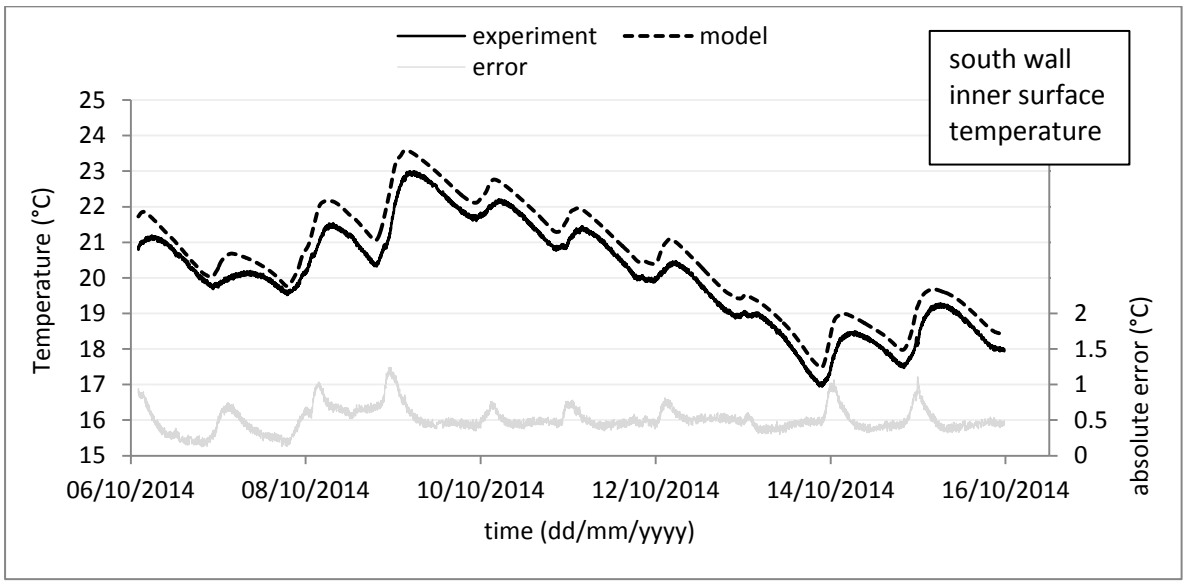

(a)

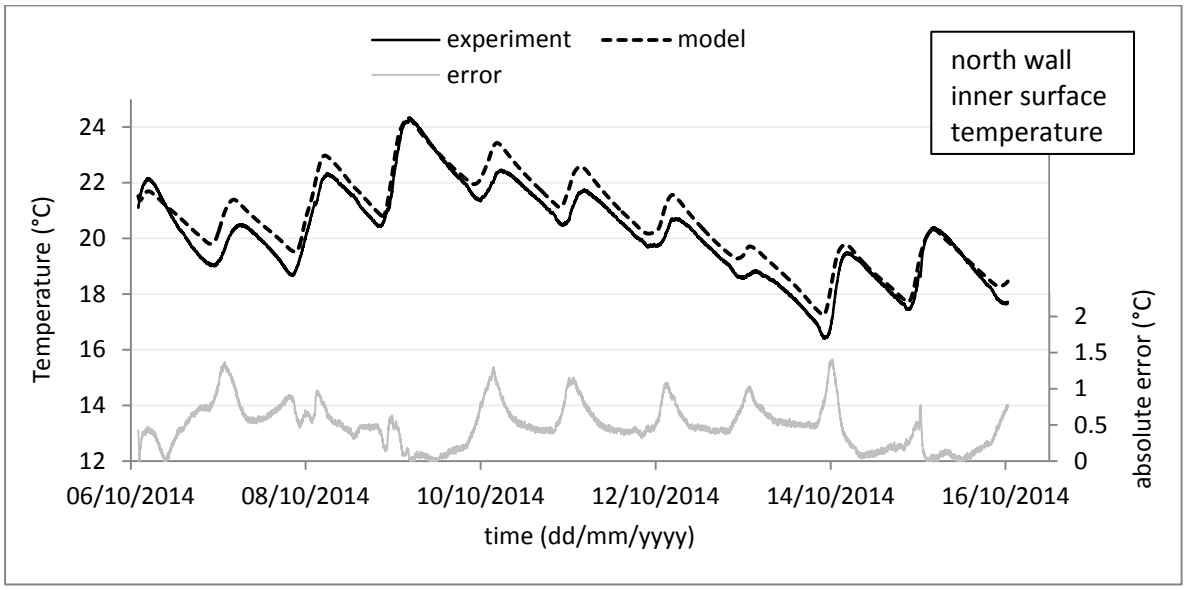

(b)

Fig. 3.30: South and north inner surface temperature of the experimental and simulation results and the corresponding error

The inside air temperature within the mock-up test unit is shown in Fig 3.31. Also, there is a good agreement between the model and the experiment except that there is a short time lag between the two curves.

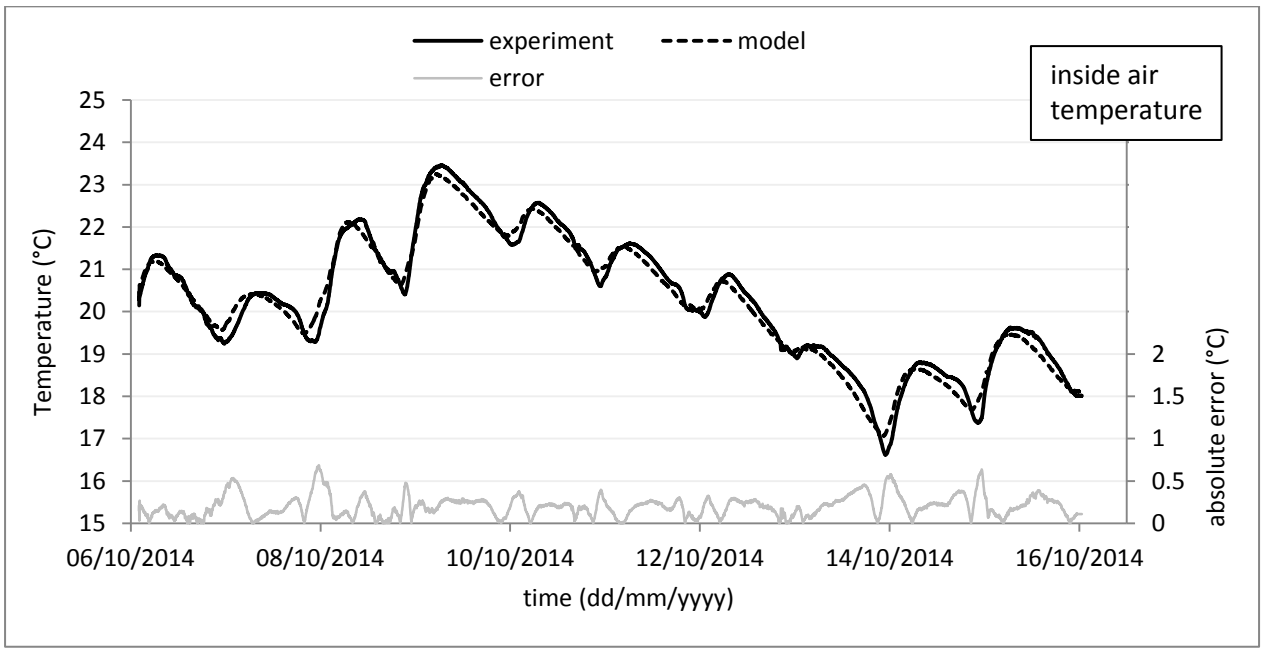

Fig. 3.31: Inside air temperature comparison between the experiment and the numerical model

5. Conclusion

In this chapter, all the experimental studies are presented. Firstly, an experimental test-cell located in the PERSEE research center at Sophia Antipolis is demonstrated. A layer of aerogel-based coating is added on the exterior surface of the south wall of the test-cell. The experimental measurements are compared to the simulation results of the one-dimensional thermal and hygrothermal numerical models. Secondly, a full-scale experimental house, recently built at INES in Chambery, with the coating being applied on its exterior facades is described. The thermal behavior of the house is modeled using the whole building energy simulation program EnergyPlus. Also, the simulation results of the EnergyPlus numerical model are compared to the on-site measurements. Finally, a mock-up experiment is recently built in the experimental field of INES to test the performance of the active wall loop system. It is composed of two mock-up units, the test unit having the active loop system and a reference unit without this system. The thermal behavior of the two mock-up units are compared under real weather conditions. In addition, the experimental data of the test unit are compared to the developed numerical model's simulation results.

6. Résumé du Chapitre en Français

Le chapitre suivant présente les différentes expérimentations effectuées afin de valider les modèles numériques. Il est constitué de trois parties principales correspondant chacune à une expérimentation : une cellule-test expérimentale ayant pour objectif de valider le modèle numérique thermique et hygrothermique en 1D, une maison expérimentale à pleine échelle pour valider le modèle thermique du bâtiment entier développé avec EnergyPlus et la troisième partie concerne une maquette pour valider le modèle numérique du système de façade active.

La cellule-test a été construite en 1984. Elle est située sur le terrain expérimental du centre PERSEE de Mines-ParisTech à Sophia Antipolis (latitude 43,616 N, longitude 7.055 E) dans la région méditerranéenne du sud de la France. Le mur sud de la cellule d'essai est notre mur d'essai pour valider les modèles numériques thermique et hygrothermique unidimensionnel. Il a une superficie de 17 m². Initialement, ce mur était composé d'une couche de 25 cm de béton (couche extérieure), une couche de 16 cm de laine de verre, et une plaque de plâtre de 1,3 cm. Une couche de 4cm d'enduit isolant à base d'aérogel a été ensuite ajoutée à la surface extérieure de ce mur.

Afin d'isoler le mur sud des effets thermiques des autres murs d'enceinte de la cellule d'essai, tous les autres murs de la cellule d'essai, le toit et le sol sont très bien isolés. En outre, la cellule-test n'a pas de fenêtres pour éviter l'effet des gains solaires directs. Des capteurs de température et d'humidité sont placés sur différents endroits du mur. Une station météorologique permet de mesurer les conditions climatiques. Les résultats de la simulation des modèles numériques sont comparés aux données expérimentales. La comparaison montre une bonne concordance dans les résultats.

Ensuite, une comparaison a été effectuée entre les résultats d'un modèle de simulation thermique dynamique développé dans « EnergyPlus » avec les mesures expérimentales effectuées sur une maison expérimentale à pleine échelle (maison INCAS) construite à cette fin à l'Institut National de l'Energie Solaire (INES) sur une plateforme située au Bourget-du-Lac (Longitude 5,88 ° E, Latitude 45.65 ° N, Altitude 270 m) dans la région Rhône-Alpes. L'intérêt de cette partie est de montrer quels outils étendus de simulation sont capables de prédire le comportement thermique des bâtiments. Le champ expérimental de l'INES est composé de plusieurs maisons basse énergie, représentant une maison d'habitation française typique, ayant une géométrie similaire, mais avec différentes techniques de construction. Ces maisons passives ont été conçues à l'INES et sont destinées à l'étude de nouvelles technologies solaires ainsi qu'à la validation des

outils de simulation pour favoriser une plus grande efficacité énergétique dans la conception des bâtiments. Initialement, la plate-forme avait trois maisons identiques dans leur forme mais diffèrentes par le type de construction de leurs murs extérieurs. Ensuite, une quatrième maison (maison-test) a été construite en 2014, également avec la même géométrie mais des matériaux de construction de murs extérieurs différents. La maison se compose de quatre zones: l'espace sanitaire, un rez-de-chaussée, un premier étage et un comble. La superficie de chaque zone est d'environ 50 m². Une proportion relativement importante de surfaces vitrées est orientée vers le sud afin de maximiser les gains de chaleur dus au rayonnement solaire en hiver.. Pour surmonter le problème de surchauffe en été, un balcon à l'étage intermédiaire et une projection de l'avant-toit sont construits. Aussi, toutes les fenêtres sont équipées de volets roulants automatisés. Les parois extérieures sont composées d'une couche de 42 cm de brique mono-mur avec une couche extérieure de 4 cm de revêtement à base d'aérogel. La maison est équipée d'un grand nombre de capteurs et d'une station météorologique à l'extérieur. Les résultats du modèle numérique « EnergyPlus » sont comparés aux mesures expérimentales pour une période d'environ 2 mois. Un très bon accord est obtenu entre la simulation et les résultats expérimentaux.

Enfin, deux maquettes expérimentales ayant les mêmes dimensions et matériaux de construction ont été mise en place sur la plate-forme expérimentale de l'INES. Le premier sert de maquette de test avec les tuyaux intégrés dans l'enduit isolant et l'autre sert de référence. Les murs sont composés de 10 cm de béton avec 4 cm de revêtement à base d'aérogel. Dans la façade sud, des conduites de fluide sont incorporées dans le revêtement à base d' aérogel et placées près de la surface extérieure. Ces tuyaux sont maintenus en attente avec des fixations horizontales qui sont fixées à la couche de béton au moyen de boulons. Sur la façade nord, les tuyaux sont en contact direct avec la couche de béton. Le sol et le plafond sont composés d'une couche d'isolation thermique pour minimiser le transfert de chaleur. Une peinture ayant une absorptivité solaire de 0,6 est appliquée sur les surfaces extérieures de toutes les façades. Le diamètre de la canalisation est de 1,5 cm et l'espacement est d'environ 10 cm. Le système est équipé d'une pompe à débit variable. En outre, la pompe est équipée d'une minuterie de commande qui met la pompe en position "ON" ou "OFF" pendant des heures régulières pré-affectées de la journée. Des capteurs de température sont placés à des positions différentes pour mesurer la température de la paroi et celle du fluide. Tout d'abord, les performances des deux cellules maquettes sont comparées. Les résultats ont montré que la cellule-test équipée du système de façade active

montre une performance plus élevée lorsque la température de surface interne des murs et la température de l'air à l'intérieur sont supérieures à celles de la cellule de référence. Par ailleurs, les données expérimentales sont comparées à des résultats de simulation du modèle numérique développé.

CHAPTER 4

ADVANCED BUILDING ENVELOPES SIMULATION RESULTS AND DISCUSSION

Chapter 4
Advanced Building Envelopes Simulation Results and Discussion

Chapter contents

1. Introduction

After developing and validating the numerical models in chapters 2 and 3, this chapter presents all the simulation results. We start by examining the thermal and hygro-thermal performance of exterior walls covered with the aerogel-based coating. Then, we examine the impact of the "ABC" to limit thermal bridge heat losses. After that, we move to study the energy and thermal comfort behavior of houses adopting the coating as external insulation. Finally, the potential to decrease the heating load by adopting the wall active water loop system is scrutinized.

2. Exterior Walls' Thermal Performance

2.1. Introduction

The objectives here are to optimize the exterior walls' layer composition for: 1- continuously heated space (cH), 2- intermittently heated space (iH), and 3- non heated space (nH). Several assessment parameters are considered for the different cases: time lag, decrement factor, energy load, and thermal comfort index. Six wall configurations are scrutinized: 1- insulation is placed at the exterior wall surface (ext), 2- at the interior wall surface (int), 3- at the interior and exterior surfaces (int/ext), 4- in the middle of the wall (mid), 5- in the middle and exterior surface (mid/ext), and 6- in the middle and interior surface (int/mid). We have chosen 3 base wall materials: heavy weight concrete (C), concrete hollow blocks (HB), and brick-monomur (B). As for the insulating materials, we have also chosen 3 materials: expanded polystyrene (EPS), glass wool (GW), and the aerogel-based coating (ABC). The thickness of the base wall materials is 15cm while that of insulation is 5cm. The thermo-physical properties of all the materials are given in Table 4.1. The setpoint temperature for "cH" and "iH" is 20°C. For "iH", the heating system is set to "ON" during occupied hours taken from 6p.m. till 7a.m.

Table 4.1: Thermo-physical properties of all materials used in the walls under investigation

Material	Thickness (cm)	Thermal Conductivity (W/(m.K))	Specific Heat (J/(kg.K))	Density (kg/m^3)
Concrete	15	2	1000	2000
Hollow Blocks	15	0.9	800	650
Brick-Monomur	15	0.115	986	700
Aerogel-Based Coating	5	0.0267	990	150
Expanded Polystyrene	5	0.033	1200	30
Glass Wool	5	0.041	840	12

2.2. Simulation Results

From the measured climate data for the months December and January in Nice-Sophia Antipolis, we have derived 3 typical days: days with high solar radiation, days with medium solar radiation, and days with almost no solar radiation. The results presented here are for the medium solar radiation typical day. The outside air temperature and south wall radiation are shown in Fig. 4.1. For the days with no solar radiation and high solar radiation, the results are qualitatively the same; so we do not show them here. For all simulations, we start by choosing arbitrary initial values for the wall temperatures, then the daily cycle of the outside environmental conditions is repeated on several consecutive days until a steady periodic solution is obtained during which quasi steady-state solutions are developed.

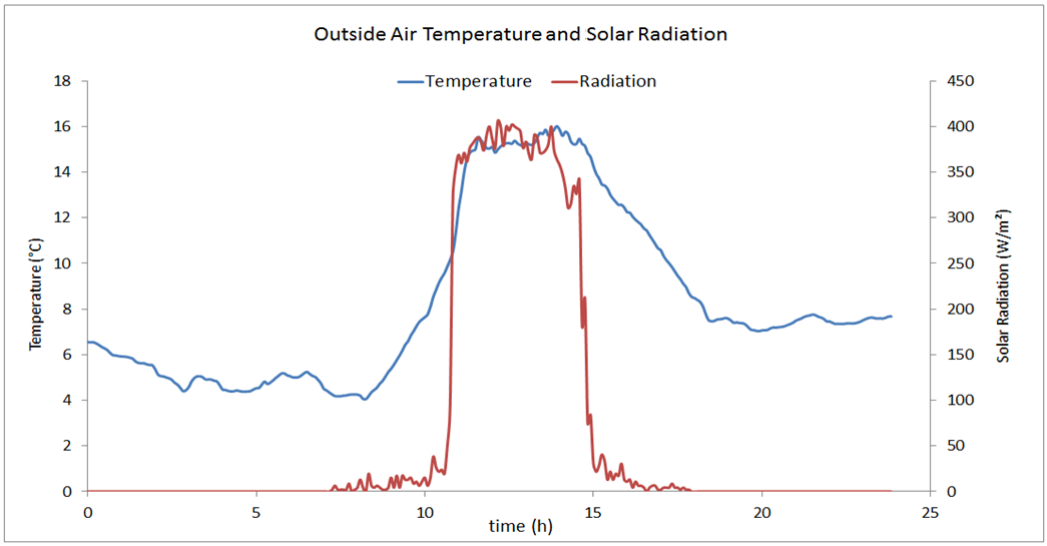

Fig. 4.1: Outside air temperature and solar radiation used in the simulation

2.2.1. Continuous Heating (cH)

In this case, time lag and decrement factor are considered as the assessment parameters. The best wall is the one having a high time lag and a low decrement factor. Figure 4.2 shows the time lag of the maximums ($\emptyset_{max}$) in blue curve, time lag of minimums ($\emptyset_{min}$) in red curve, and decrement factor (f) in green curve for the different positions of insulation layers. This figure shows the case of concrete as base wall structure with the three different insulating materials. First of all, let us compare $\emptyset$ and f for the different insulation positions. For all the three insulating materials, it is shown that the case where insulation is placed at the middle and exterior wall surface (mid/ext) is the best case from maximum time lag and minimum decrement factor. Though $f_{mid/ext}$ is slightly more than $f_{int/ext}$; however, $\emptyset_{mid/ext}$ is much more higher. The worst case is when insulation is placed as one layer at the interior wall surface (int). Comparing this case with exterior insulation (ext), when the coating is used, f_{ext} is approximately 40% lower than f_{int} and $\emptyset max_{ext}$ ($\emptyset min_{ext}$) is higher than $\emptyset max_{int}$ ($\emptyset min_{int}$) by about 13% (10%). Placing insulation at the middle (mid) shows better time lags than the exterior case ($\emptyset max_{mid}$ = 1.28 $\emptyset max_{ext}$); however, the decrement factor is higher (f_{mid} = 1.4 f_{ext}).

Now, comparing the different insulating materials, the coating shows the best performance due to having a lower thermal conductivity and higher volumetric thermal capacitance as well. The decrement factors for "Glass Wool" cases are the highest, then come "Expanded Polystyrene, then the "Aerogel-Based Coating". This is expected because the decrement factor is greatly affected by the thermal diffusivity of the material used. As k decreases, f decreases. As for the time lag, the cases of "GW" and "EPS" are approximately the same. Taking the "mid/ext" case, $\emptyset_{coating\text{-}C}$ is about 20% more than $\emptyset_{GW\text{-}C}$ and $\emptyset_{EPS\text{-}C}$.

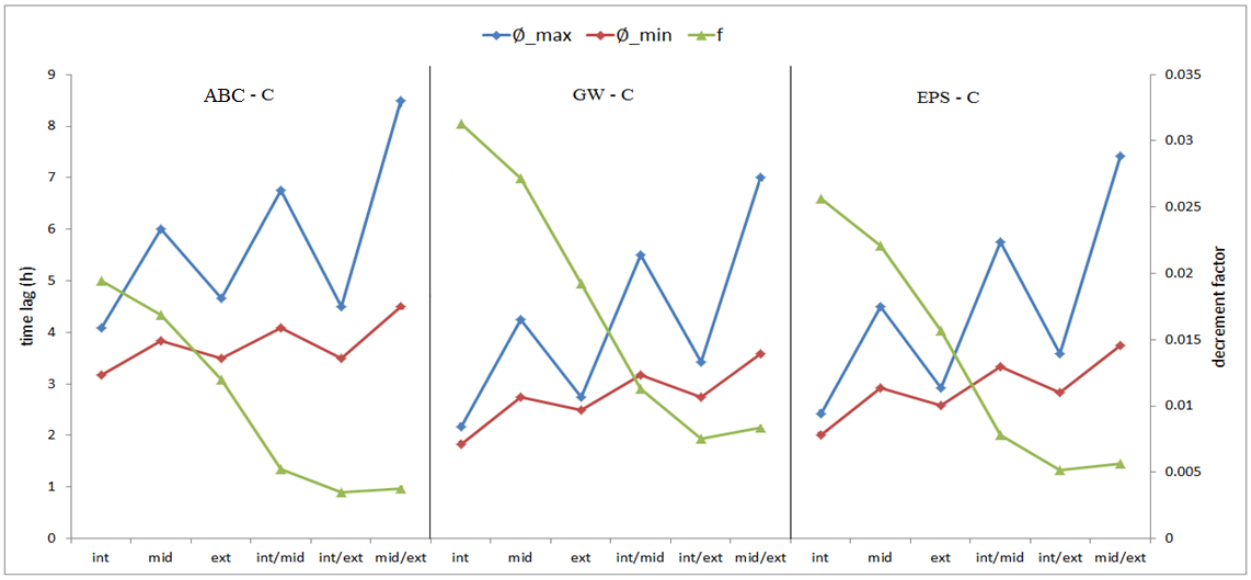

Fig. 4.2: Time lag and decrement factor for different insulation types and configurations for concrete walls (cH)

Now, we want to compare $\emptyset$ and f between concrete (C), hollow blocks (HB), and brick-monomur (B) (See Fig. 4.3). The insulation material is taken to be "ABC". The wall with concrete hollow blocks shows the highest decrement factors and lowest time lags. Its low thermal capacity doesn't allow this wall to store a large amount of heat to be released at a later time. Comparing concrete and brick-monomur, the time lags for brick walls are higher than those of concrete for all insulation positions and the decrement factors are lower for insulation positions: int, mid, and ext. For the other insulation configurations (int/mid, int/ext, mid/ext), f is almost the same between concrete and brick-monomur walls. The reason for the better performance of brick-monomur is the lower thermal conductivity of this material (0.115 W/(m.K)) than that of concrete. Even though the thermal capacitance of concrete is much higher than that of brick-monomur; however, its thermal conductivity is also higher; that makes the thermal diffusivity (α) of brick-monomur lower than that of concrete ($\alpha_{brick-monomur} = 0.17\text{x}10^{-6}\ \text{m}^2s^{-1}$, $\alpha_{concrete} = 1\text{x}10^{-6}\text{m}^2s^{-1}$).

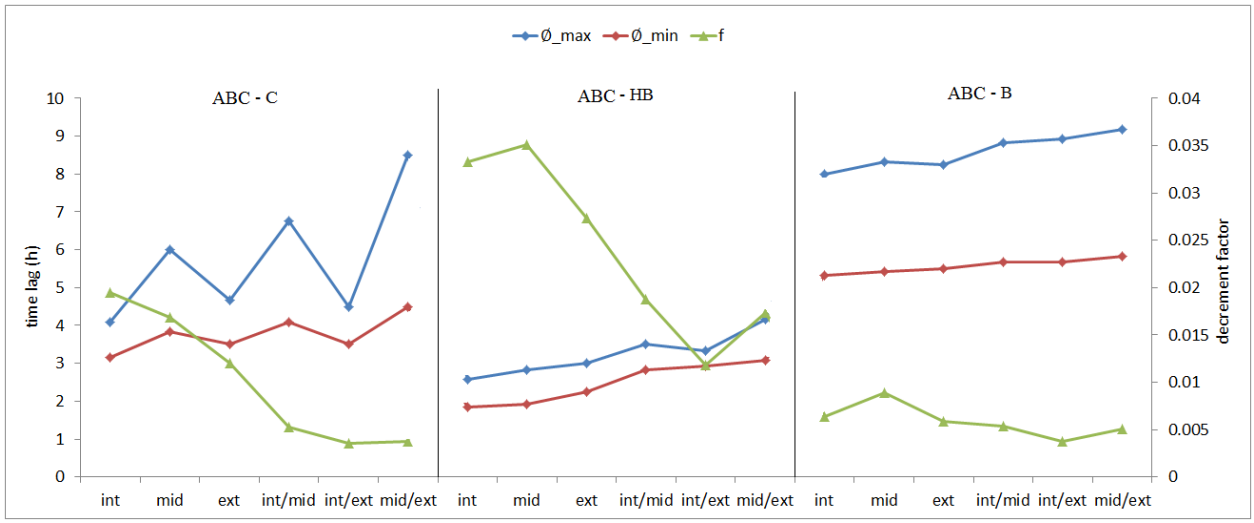

Fig. 4.3: Time lag and decrement factor for the different configurations for concrete, hollow blocks, and brick-monomur when using the coating as the insulation material (cH)

Conclusion "cH":

For continuous heating, we conclude:

- the coating has shown a better performance than other traditional insulating materials due to possessing both lower thermal conductivity and higher thermal mass
- the position and number of insulation layers within the wall are very important
- dividing the insulation into two parts; placing one at the middle of the wall and one at the exterior surface provides the best performance
- the lightweight structure shows the least thermal performance from maximum time lag and minimum decrement factor perspective
- for the base wall materials, brick-monomur shows the best performance due to its low thermal conductivity relative to the other used materials.

2.2.2. Intermittent Heating (iH)

In the intermittent heating, the assessment parameter is the heat losses through the wall during the occupied period considered from 6p.m. till 7a.m. (when the heating system is set to ON). The daily heat losses for different base wall materials as well as different insulation positions are plotted in Fig. 4.4. It is illustrated that for all cases, placing the insulation at the interior surface of the wall results in the least energy consumption. Then it comes the case int/mid and int/ext. All the cases where thermal mass is placed near the interior have shown high

heat losses. Compared to the case “insulation outside”, “insulation inside” provides 38%, 23%, and 21% energy load reductions for “ABC-C”, “ABC-HB”, and “ABC-B” wall structures, respectively.

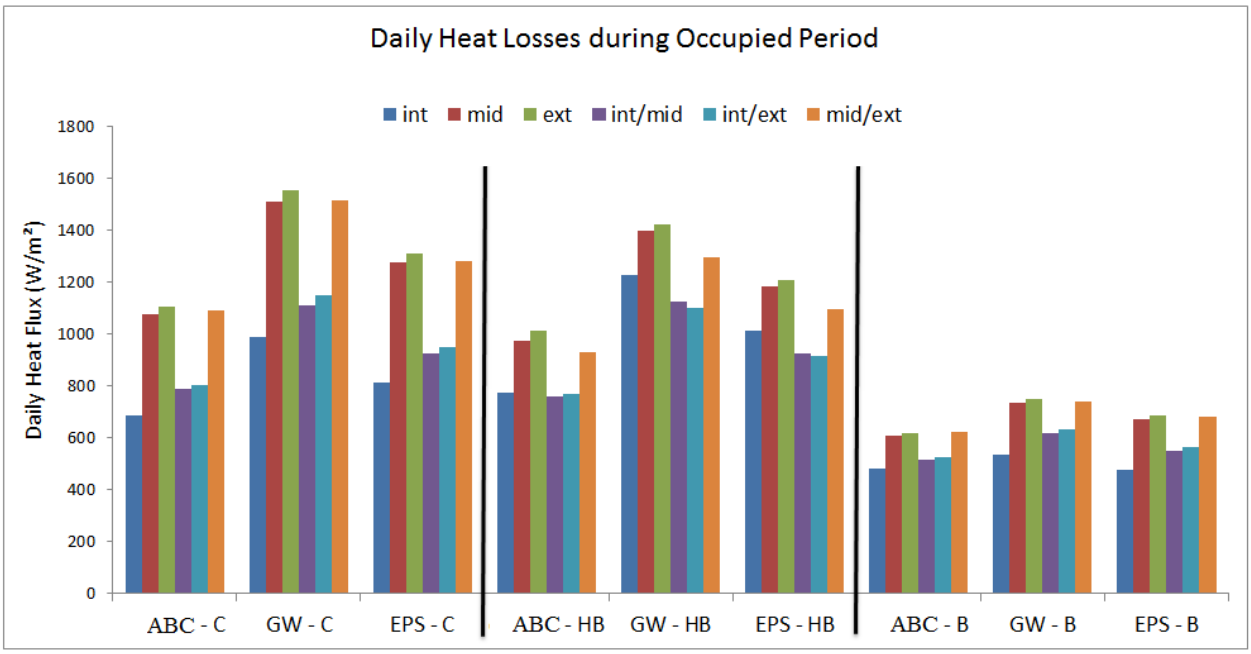

Fig. 4.4: Daily heat losses in W/m² for the different wall configurations (iH)

To illustrate this more, the inner wall surface temperatures for some insulation configurations for “ABC-C” wall structure are shown in Fig. 4.5. When the heating system is OFF, the temperatures for the case where insulation is inside fall down significantly; however, at the onset of the heating period, these temperatures increase rapidly to approach the set-point level. This is due to the low thermal mass placed inside leading to rapid response to the imposed thermal stresses. On the other side, since we have high heat storage layers placed at the inside in the cases “ext” and “mid”, we see this slow response to reach the set-point temperature resulting in higher heat losses through the wall.

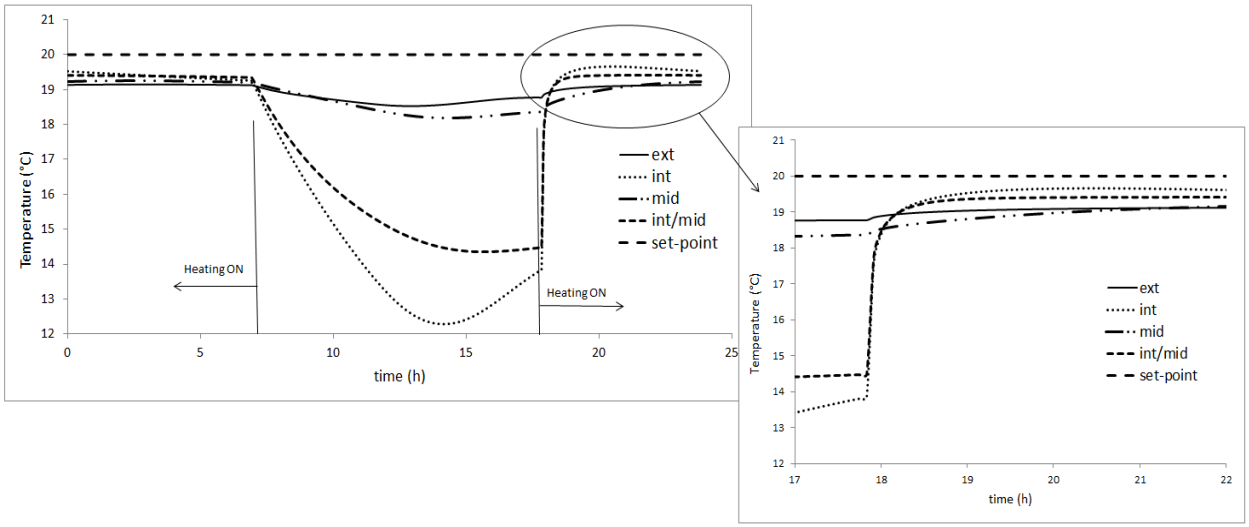

Fig. 4.5: Inside wall surface temperature during the whole day for some insulation configurations (iH)

Conclusion "iH":

For intermittent heating, we conclude:

- placing the insulation at the interior wall surface is the best case from an energy consumption point of view
- the coating shows better performances due to its lower thermal conductivity
- Brick-monomur wall structure has the lowest energy consumption due to its low thermal conductivity compared to concrete and hollow blocks

2.2.3. No Heating (nH)

In this case, the evaluation parameters are time lag, decrement factor, and thermal comfort index during occupied hours (degree.hours). Figure 4.6 shows the time lag and decrement factor for the different insulation positions and materials for concrete walls. Similar to the case "cH", placing insulation material at the middle and outer surface of the wall shows the best performance from maximum time lag and minimum decrement factor point of view. Then comes the "int/ext" and "int/mid" cases. Again, the coating performs better than glass wool and polystyrene insulation. The results for hollow block and brick wall structures are qualitatively the same.

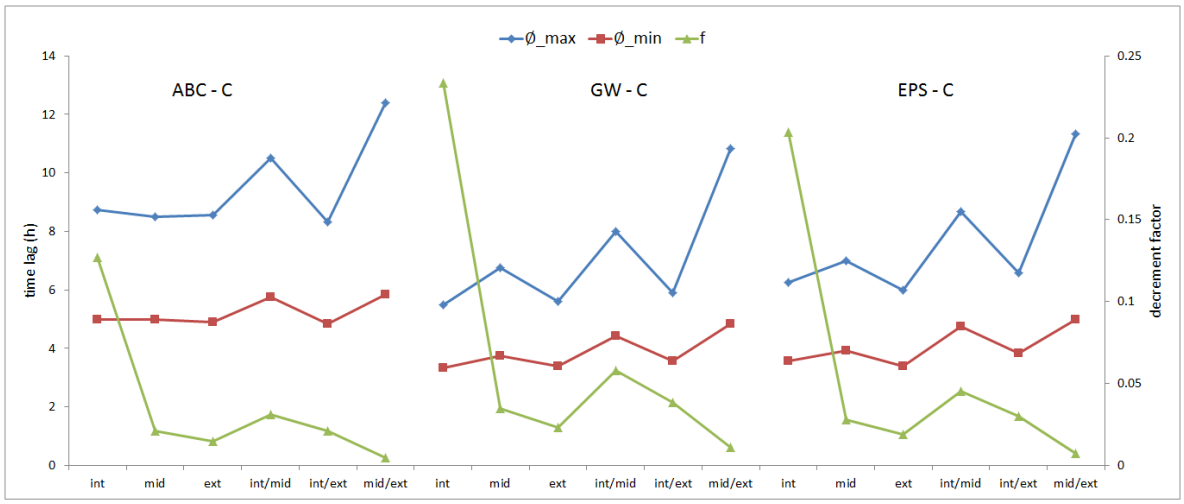

Fig. 4.6: time lag and decrement factor for different insulation types and configurations for concrete walls (nH)

Figure 4.7 shows the thermal comfort index (TCI) during occupied hours till for all cases. The interior insulation configuration shows the best performance for all cases except for hollow blocks structure with glass wool or polystyrene, where the best case is interior and middle insulation followed by interior insulation. For concrete walls, TCI for "int" insulation is lower than that of the other insulation configurations by about 12%. For brick walls, the difference is not significant between the different cases.

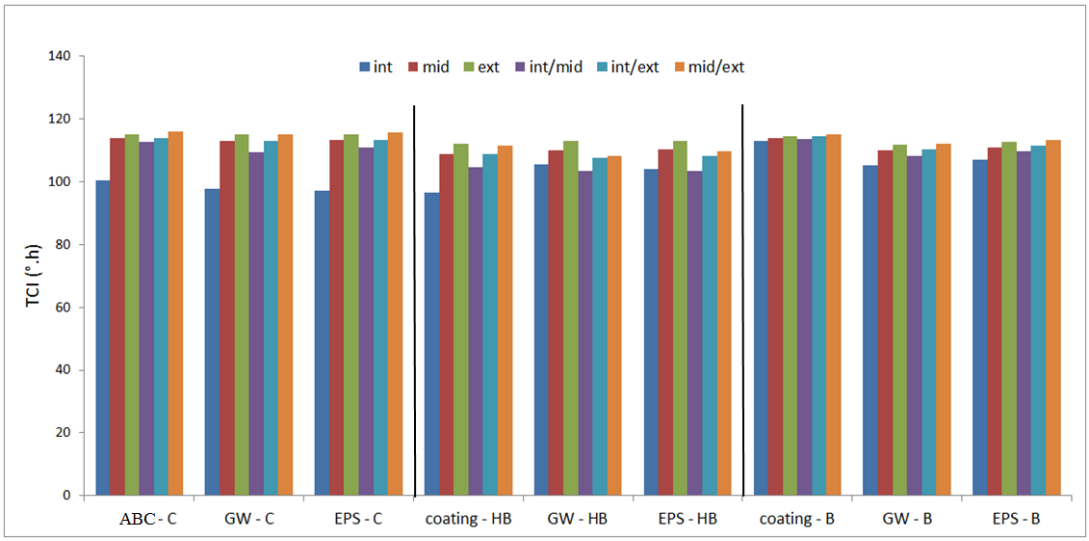

Fig. 4.7: Thermal comfort index for all the wall structures (nH)

Conclusion "nH":

For non-heated spaces, we conclude:

- placing insulation at the middle of the wall and at the exterior surface provides the best performance from maximum time lag and minimum decrement value point of view
- placing the insulation at the interior wall surface is the best solution when considering the discomfort hours during the occupied period as the assessment parameter

3. Exterior Wall's Hygro-Thermal Performance

3.1. Introduction

The objectives of this section are to examine the hygrothermal performance of walls covered with the coating and to compare different thermal insulation configurations. The software WUFI® is used to conduct all the simulations. Different exterior wall structures are examined: no insulation, exterior insulation using the coating, interior insulation using a traditional insulating material, and interior and exterior insulation. Different assessment criteria are used: assembly water content, drying rate, mold growth, condensation risk, ASHRAE-160 criterion, and heat losses.

3.2. Wall Assemblies

Different wall assemblies are considered. We examine 3 base wall structures: concrete (20cm), stone (50cm), and hollow bricks (20cm). For each one of these walls, 9 configurations are considered: no insulation, insulation inside (5/10cm of expanded polystyrene), insulation outside (5/10cm of aerogel-based coating), and insulation inside and outside. All the cases are shown in Table 4.2 for the concrete wall structure. No vapour retarder is considered in all the simulation cases. The hygrothermal properties of the all the materials used are presented in Annex D.

Table 4.2: Wall assembly insulation configurations

case	Configuration	Outside layer	Layer 2	Layer 3	Layer 4	Layer 5
W-1	No Insulation	stucco	Concrete 20cm	Plaster		
W-2	Interior Insulation	stucco	Concrete 20cm	Polystyrene 5cm	Plaster	
W-3		stucco	Concrete 20cm	Polystyrene 10cm	Plaster	
W-4	Exterior Insulation	stucco	Aerogel Coating 5cm	Concrete 20cm	Plaster	
W-5		stucco	Aerogel Coating 10cm	Concrete 20cm	Plaster	
W-6	Interior + Exterior Insulation	stucco	Aerogel Coating 5cm	Concrete 20cm	Polystyrene 5cm	Plaster
W-7		stucco	Aerogel Coating 5cm	Concrete 20cm	Polystyrene 10cm	Plaster
W-8		stucco	Aerogel Coating 10cm	Concrete 20cm	Polystyrene 5cm	Plaster
W-9		stucco	Aerogel Coating 10cm	Concrete 20cm	Polystyrene 10cm	Plaster

The simulations are carried out for Grenoble climate representative of a semi-continental French climate. The city of Grenoble was chosen as a simulation case because of its very specific climate: rain is more abundant, winter is colder and summer is generally warmer than most other cities in France. Due to the mountainous environment that slows the winds and decreases their thermal regulation effect, the daily temperature range is much higher than any other place in France. The nights are generally cooler (except during heat wave periods) and the afternoon is warmer than those in other main cities. The surrounding Alps Mountain forms a barrier preventing rain-filled clouds to move out while rainy westerly winds are trapped.

The interior conditions were generated using the EN 15026 standard (DIN EN 15026, 2007) with a high moisture generation load. According to this standard, the indoor conditions are determined in relation to the exterior climate which provides an algorithm that determines the indoor climate taking outdoor conditions as a reference (see Fig. 4.8). The outdoor and indoor air temperatures and relative humidity over one year are shown in Fig. 4.9.

For each of the studied cases, two extreme orientations for the wall are taken: "North" orientation (N) due to the lack of solar radiation which makes the wall cooler, and the "Driving Rain" orientation (R) which increases the moisture load due to rain absorption. This latter can be derived from WUFI's "outdoor climate analysis" which shows the directions from which the rain loads are mainly to be expected. For Grenoble, the "R" orientation is the south-west (SW) one. The simulation duration is 4 years to examine the drying effect of the walls over the years. The rain absorptivity is taken as 0.7 and the initial relative humidity in the wall assembly is taken as 80%.

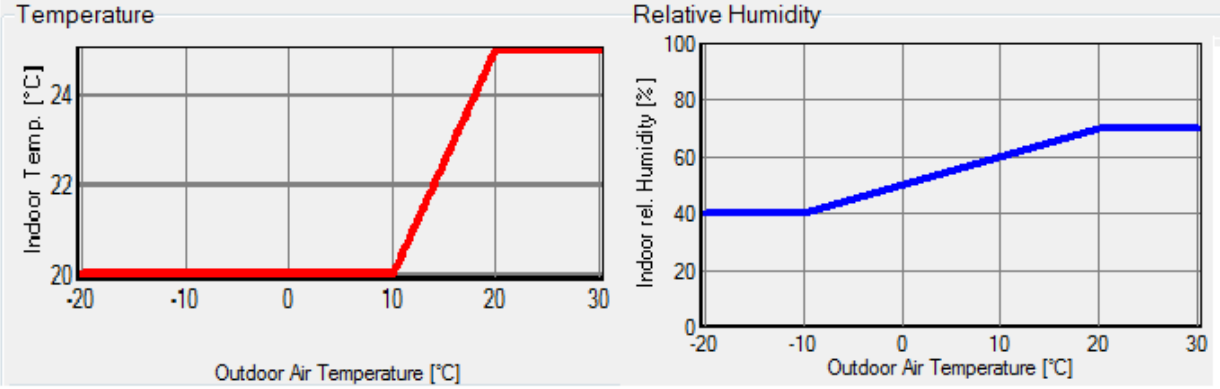

Fig. 4.8: Indoor air temperature and relative humidity calculated according to EN 15026 standard

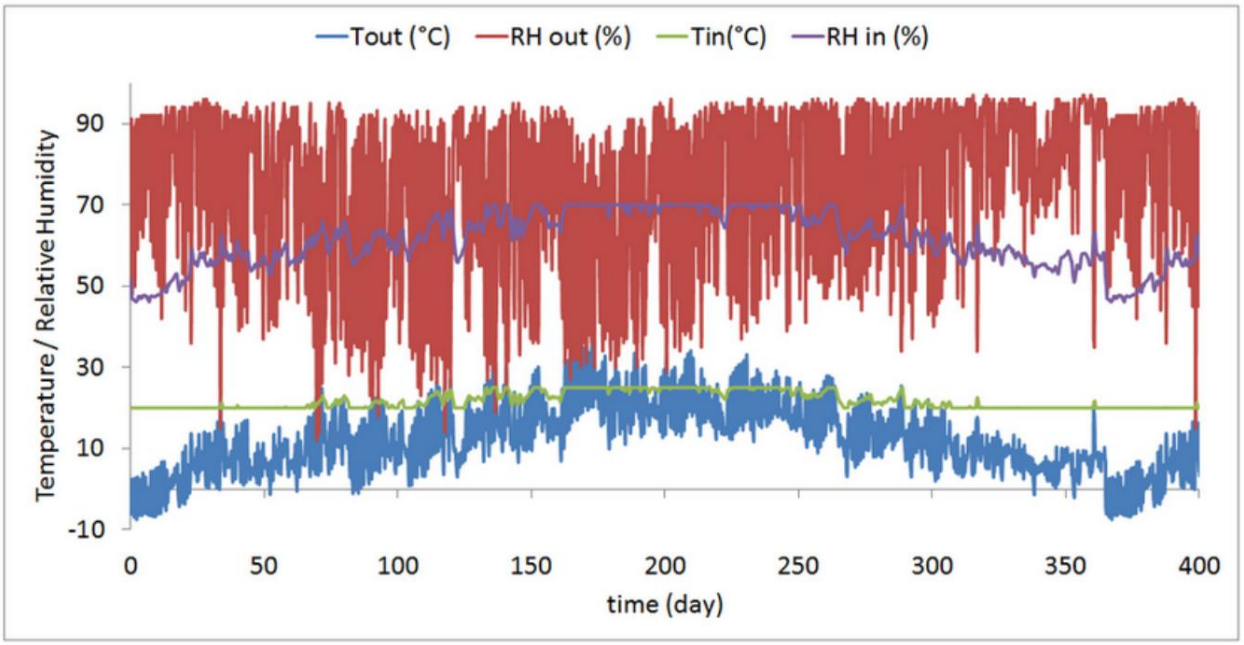

Fig. 4.9: Exterior air temperature and relative humidity over one year for the city of Grenoble

3.3. Failure Criteria

3.3.1. Total Water Content (TWC)

This criterion indicates the ability of the wall assembly to dry out over time. The initial and final moisture content for the entire assembly are evaluated for each wall over a 4-year period. If the final value at the end of the modeling period is less than the initial value, this means that the wall has the potential to dry out; hence, it passes this criterion.

3.3.2. Dryness Rate (DR)

If the wall passes the first criterion, we calculate the dryness percentage over the 4 years period. This indicates the difference between the final water content from the initial water content as a percentage. The higher the "DR" is, the more is the wall's capability to dry out faster over time.

3.3.3. Condensation Risk (CR)

Condensation potential within the wall is evaluated by comparing the interior air dew point temperature to the interior surface temperature as well as the temperature at the interface surfaces between concrete and interior/exterior insulation. The interface surfaces are also considered

assuming there is a risk of air flow within the plaster due to cracks. If the surface temperature of the material is lower than the dew point temperature of the indoor air, condensation is likely to occur (Straube and Smegal 2009). The longer the period during which the surface temperature falls below the air dew point temperature, the greater is the risk for damage. The percentage of time that the surface temperature falls below the dew point is calculated for each wall.

3.3.4. Mold Growth (MG)

WUFI® generates graphs called "Isopleths" which identify potential mold growth on the interior surface of the wall assembly. An isopleth graph represents the growth rates of mold based on humidity and temperature of the surface. WUFI® assigns two limits: LIM BI for the bio-utilizable substrates such as wall papers and plaster boards, and LIM BII for the substrates with porous structure, such as plasters and mineral building materials. If the conditions lie above the limiting isopleths, mold growth could be possible.

3.3.5. ASHRAE Criterion (ASH)

In 2009, ASHRAE published the ASHRAE Standard 160: Criteria for Moisture-Control Design Analysis in Buildings (ASHRAE Standard 160, 2009). This standard sets the performance criteria to minimize problems associated with moisture in building envelope assemblies. The standard specifies that the following conditions be met: A 30-day running average surface relative humidity should be less than 80% when the 30-day running average surface temperature is between 5°C and 41°C. This threshold applies to all materials and surfaces in the building envelope except the exterior surface.

3.3.6. Heat Loss (q)

The previous criteria represent the hygric performance of the wall assemblies. In this criterion, we focus on the thermal performance where the heat losses (q) through the interior surface of the walls during the winter season are computed for all the different cases. The set-point for the indoor air temperature during winter is taken 20°C.

3.4. Simulation Results and Discussion

Since the results for the three base wall structures, concrete, hollow blocks and bricks, are qualitatively the same, the results for only the concrete wall base structure are shown.

3.4.1. Total Water Content (TWC)

Table 4.3 shows which of the wall assemblies pass this criterion. "P" means that the wall has passed, and "F" means it has failed. For the north orientation, the walls with interior insulation "W-2" and "W-3" do not pass this criterion; meaning that the average water content within the wall increases over time without being able to dry out. For this orientation, Fig. 4.10 shows the assembly water content for two cases: 5cm "Polystyrene" interior insulation (W-2), 5cm "Coating" exterior insulation (W-4), and 5cm "Polystyrene" interior insulation with 5cm "Coating" exterior insulation (W-6). By placing interior insulation, the temperatures in the wall go low reducing the drying capacity of the wall leading to higher average moisture contents. To overcome this problem, a vapour retarder is usually added for interior insulated walls. However, for the driving rain orientation which is the south-west, all walls pass this criterion even those with interior insulation. The presence of solar radiation on this facade increases the drying potential of the walls.

Table 4.3: Total water content criterion

North Orientation (N) P = Pass F = Fail								
W-1	W-2	W-3	W-4	W-5	W-6	W-7	W-8	W-9
P	F	F	P	P	P	P	P	P
Driving Rain (SW)								
W-1	W-2	W-3	W-4	W-5	W-6	W-7	W-8	W-9
P	P	P	P	P	P	P	P	P

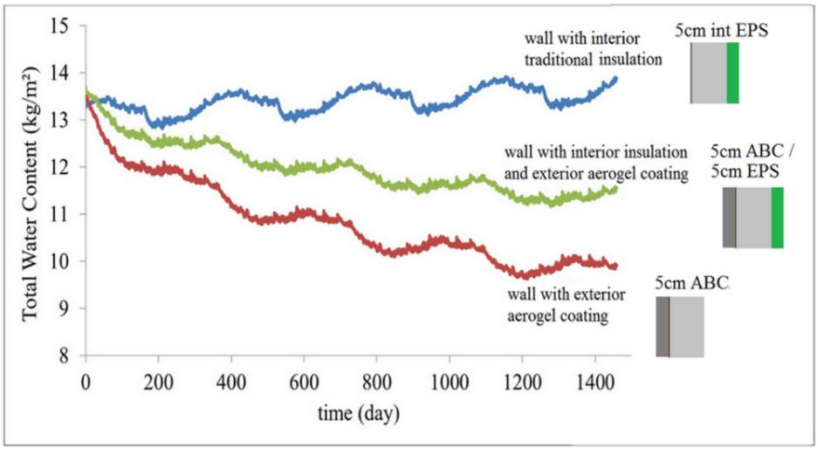

Fig. 4.10: Evolution of the total water content over the 4 years for W-2, W-4, and W-6 for the north orientation

3.4.2. Dryness Rate (DR)

As mentioned earlier, this criterion evaluates the dryness percentage over the 4 year period. It is the difference between the initial water content (WC_i) and the final water content at the end of the simulation period (WC_f). Figure 4.11 shows the "DR" for the different walls. DR for "W-4" and "W-5" configurations (5cm and 10cm exterior insulation) is about 23% more than DR for the un-insulated wall "W-1". This means that adding the aerogel-based coating to exterior facades increases the drying potential of the wall assembly. Moreover, the DR for exterior insulation is the highest of all configurations. Adding the thickness of aerogel-based coating (exterior insulation) increases the wall drying potential. For walls with interior insulation, adding aerogel-based coating at the exterior surface (W-6, W-7, W-8, W-9) also improves the dryness rate compared to the un-insulated wall. Comparing "W-6" with "W-7" and "W-8" with "W-9", we can conclude that applying more thickness of interior insulation leads to lower performance.

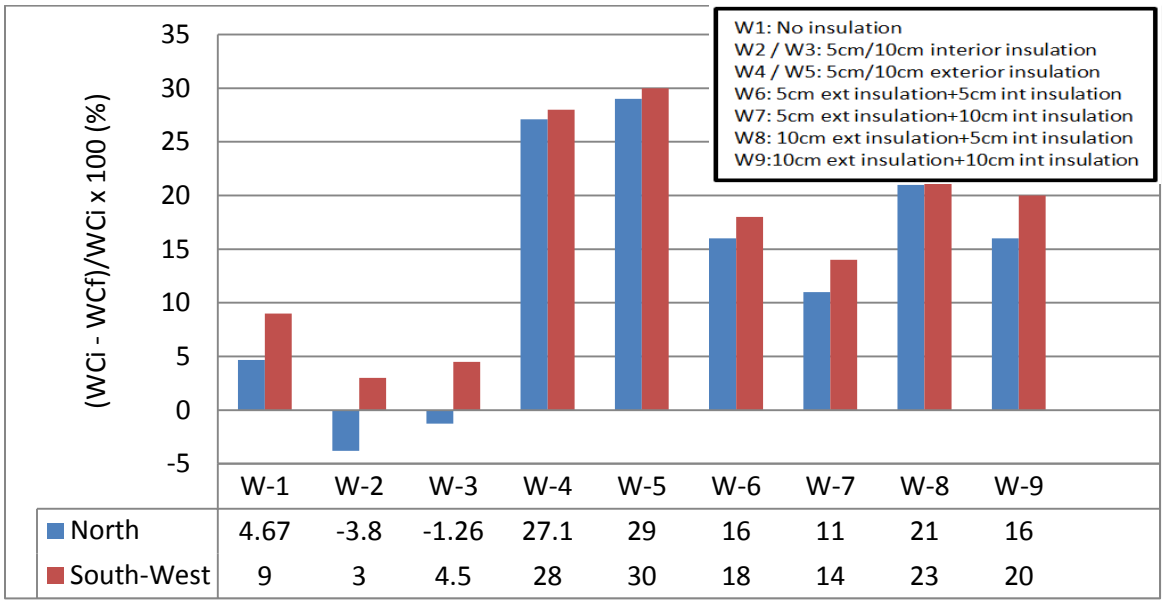

	W-1	W-2	W-3	W-4	W-5	W-6	W-7	W-8	W-9
North	4.67	-3.8	-1.26	27.1	29	16	11	21	16
South-West	9	3	4.5	28	30	18	14	23	20

Fig. 4.11: Dryness rate (DR) for the different walls

3.4.3. Condensation Risk (CR)

Table 4.4 shows which of the wall configurations passes this criterion. The internally insulated walls (W-2 and W-3) show a high risk of condensation where the percentage of simulation time when condensation might occur reaches 40% and 50% for "N" and "R" wall orientations, respectively. This is because with interior insulation, the wall becomes in contact with the outside cold environment that causes its temperatures to go down. Also, a risk of

condensation of about 9-12% is observed for "W-7" (5cm coating + 10cm polystyrene). This is due to the high relative humidity observed at the interface between concrete and polystyrene as will be illustrated in a later section.

Table 4.4: Condensation risk for the different wall configurations

	North Orientation (N) P = Pass F = Fail							
	W-2	W-3	W-4	W-5	W-6	W-7	W-8	W-9
% of time Condensation might occur	F	F	P	P	P	F	P	P
	49%	52%	-	-	-	12%	-	-
	Driving Rain (SW)							
	W-2	W-3	W-4	W-5	W-6	W-7	W-8	W-9
% of time Condensation might occur	F	F	P	P	P	F	P	P
	42%	45%	-	-	-	9%	-	-

We can conclude that if existing buildings, which already have interior insulation, are to be rehabilitated (from thermal point of view) by adding more insulation, it is not suitable to apply more insulation at the inside; however, applying the coating on the exterior facade surfaces reduces or eliminates the risk of condensation within the wall structure.

3.4.4. Mold Growth (MG)

From the Isopleths generated by WUFI®, we can examine the possibility for mold growth. All wall configurations pass this criterion for the two orientations (N and SW) except the un-insulated wall (W-1). Figure 4.12 shows the Isopleths for "W-1" and "W-5" (taken as illustration cases) for the two orientations. Each point in the graphs represents the hygrothermal condition. For "W-1", there is a risk for mold growth as there are a lot of points lying above the limit lines. For "W-5", no risk is observed.

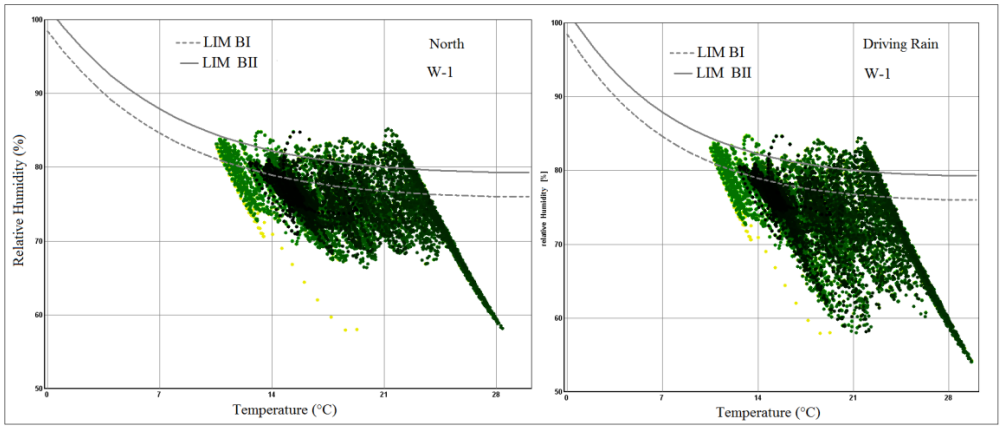

(a)

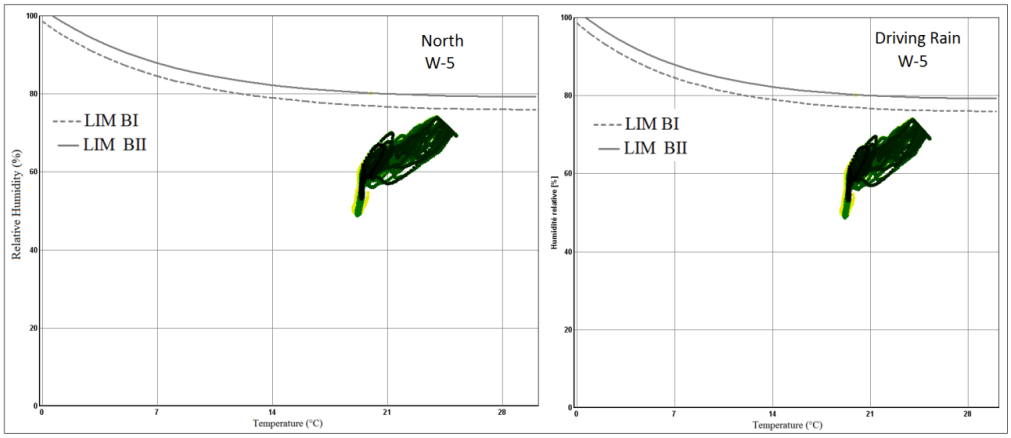

(b)

Fig. 4.12: Isopleths for (a) the un-insulated wall "W-1" and (b) 10cm exterior coating for the north and driving rain orientations

3.4.5. ASHRAE-160 Criterion (ASH)

Figure 4.13 shows which of the walls fail the ASHRAE-160 criterion and to what extent. It is shown that the worst cases are the interior insulation cases “W-2” and “W-3” where 90%, this criterion is not met for the north facade and between 64 and 77% for the south-west facade. This means the accumulation of high vapour contents ($\varphi > 80\%$) for a long period of time. The most critical place where this happens is at the interface between concrete layer and interior insulation. The un-insulated wall has not met this criterion by about 66% for the north facade and 40% for the south-west facade. All the other cases where aerogel-based coating is present show very good performance where the percentage remains below 10%, except for the wall having 10cm interior insulation “W-7”. To illustrate this more, the relative humidity and the temperature at the inner concrete/polystyrene interface for the north orientation are plotted in Fig. 4.14 for W-2, W-6, and

W-8. The relative humidity of "W-2" configuration is high and is increasing over time. For the other wall configurations, most of the simulation time the RH is lower than 80% and its annual average decreases over time. The wall which has the best performance is "W-8".It is shown that placing the insulation at the inner side of the wall makes the wall in contact with the outside cold air which lowers its temperature, decreasing its ability to dry out and accumulating high moisture contents. On the other side, placing the aerogel-based coating (rendering) on the outer side of the wall ensures, relatively, higher temperatures leading to a higher potential to dry out to the outside - due to the low vapour diffusion resistance of the coating (rendering) - or to the inside when the boundary conditions allow.

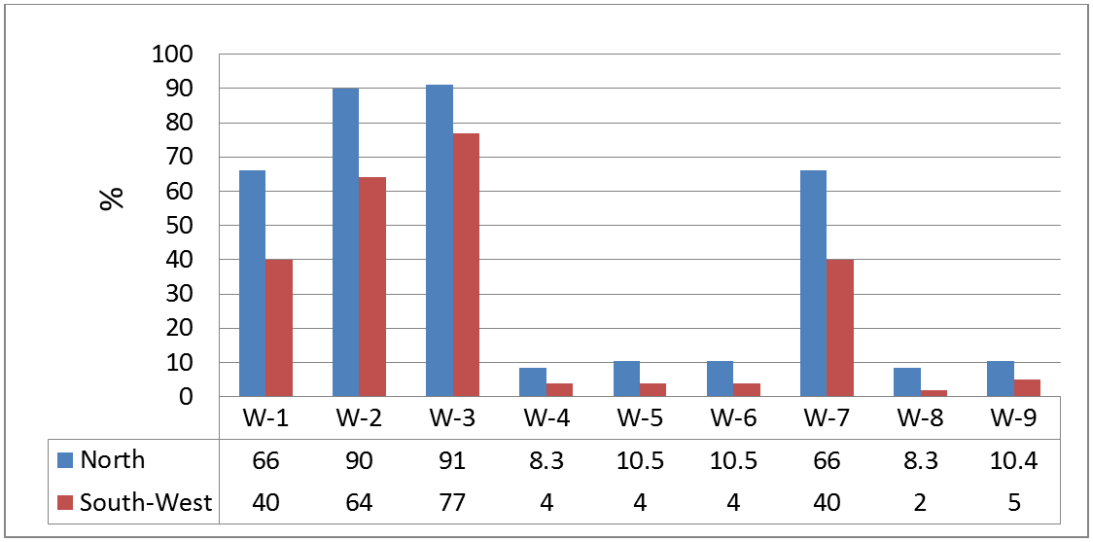

	W-1	W-2	W-3	W-4	W-5	W-6	W-7	W-8	W-9
North	66	90	91	8.3	10.5	10.5	66	8.3	10.4
South-West	40	64	77	4	4	4	40	2	5

Fig. 4.13: Percentage of the total number of averages that each wall failed the ASHRAE-160 criterion

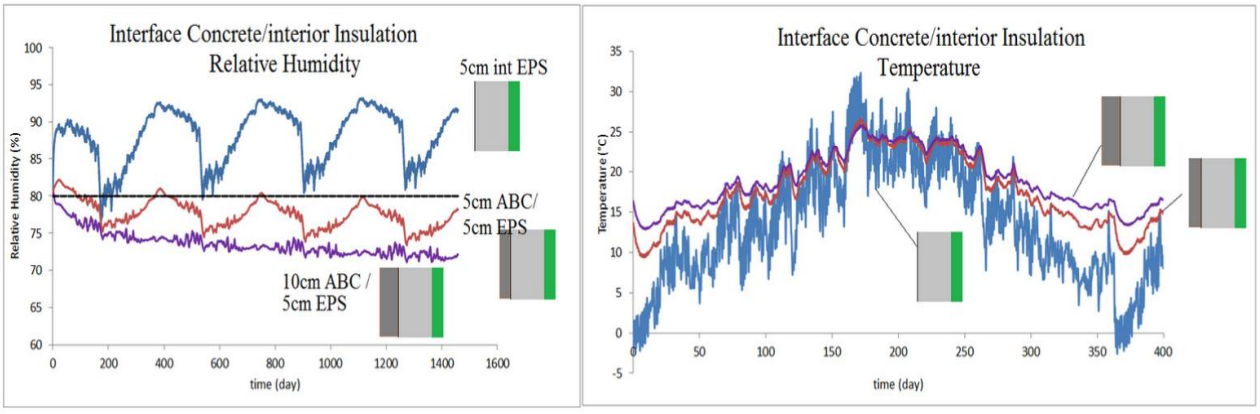

Fig. 4.14: Relative humidity (over 4 years) and temperature (over 1 year) at the interface concrete/internal insulation for W-2, W-6, and W-8

3.4.6. Heat Loss (q)

Figure 4.15 shows the heat losses through the different insulation configurations. Compared to the un-insulated walls, all other walls achieve between 80% and 90% reductions in heat losses. Walls with the aerogel-based coating have lower heat losses than walls with polystyrene. Comparing "W-2" and "W-4", q_{W-4} is lower than q_{W-2} by about 24%.

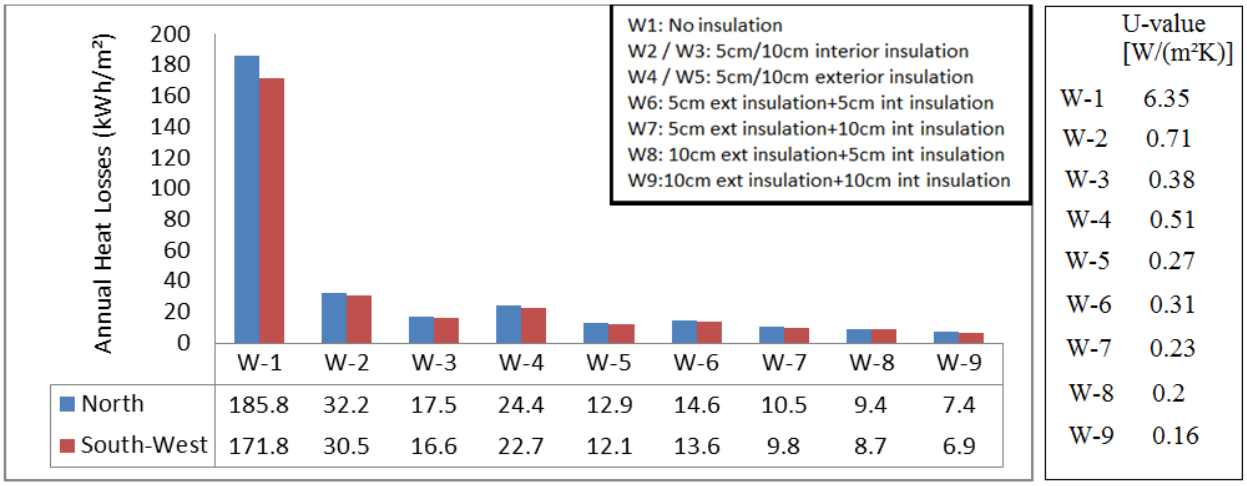

Fig. 4.15: Heat Losses at the internal wall surface for the different configurations

3.5. Conclusion

The results show that interior thermal insulation systems can cause several moisture problems: no capability to dry out over the years, condensation risk, etc. Adding the aerogel-based coating on the exterior surface of the un-insulated or the already internally insulated walls reduces significantly or removes the moisture risks. It also reduces significantly the wall heat losses.

4. Thermal Bridge Heat Losses Treatment

4.1. Introduction

In this section, we propose a methodology to incorporate the 2D heat transfer thermal bridges' effects into EnergyPlus. As an application, we compute the heating load coming from the windows offset (window edges) thermal bridges and show how much it constitutes of the total house load before and after adding the insulating coating on the thermal bridges. The

methodology is to couple the 2D heat transfer code developed in MATLAB® to EnergyPlus through co-simulation. Additionally, we compare the time lag and decrement factor when the 2D heat transfer effects of the thermal bridge are taken into consideration with those obtained for the 1D heat transfer case.

4.2. Thermal Bridge Representation

Windows offset from exterior walls leads to the generation of four thermal bridges (at the left, right, top, and bottom edges). Due to symmetrical conditions and because these four are, with a rough approximation, subjected to the same boundary conditions, we assume that the energy load of the four is identical; thus, only one of them in each facade orientation is considered where the heat transfer phenomenon is represented by two dimensional heat conduction. Considering the left side of the window, the top view of the thermal bridge viewed from inside is shown in Fig. 4.16. We have at sides 1 and 2, the outside environment as boundary condition; at boundary 4, the indoor environment and at boundary 3, an adiabatic surface considering a long wall where the two dimensional effects will no longer exist. As shown in Fig. 4.16, the window is placed in line with the inner surface of the wall. This case is the worst for the window's frame thermal bridge; however, this construction technique is widely spread in France.

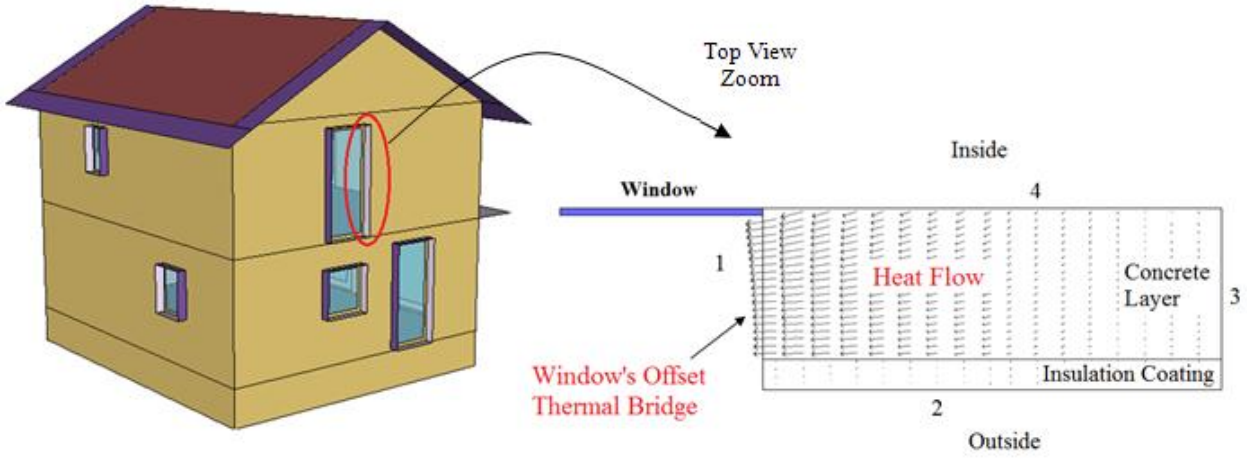

Fig. 4.16: Top view of the thermal bridge

4.3. Coupling EnergyPlus with MATLAB using BCVTB

Figure 4.17 shows how to link EnergyPlus to MATLAB using BCVTB. The outputs of EnergyPlus are inputs to MATLAB and vice versa. At each time step taken as 1 hour, for a simulation period of 1 year, for each of the 4 facades of the building, EnergyPlus updates the internal and external heat transfer coefficients (h_{in} and h_o), the external wall surface temperature (T_{surf_out}), and the room air temperature (T_{in}). The weather file updates the outdoor air temperature (T_{out}). Then, these are sent to the 2D heat transfer MATLAB code to serve as boundary conditions as shown in Fig. 4.18. For the thermal bridge boundary (boundary 1 of Fig. 4.16), we didn't include the effect of solar radiation because, first, all windows are modeled with fins and overhangs (at all window edges), and second, due to the assumption of the presence of self-shading of the windows offset. Since the diffused solar radiation is not taken into account for the boundary condition near the thermal bridge in the y-axis, the heat losses through the thermal bridge are slightly increased. Using these boundary conditions, the MATLAB code calculates the temperature field within the domain and computes the resulting heat flux (denoted hereafter by q2D) at the inner wall surface. In addition, EnergyPlus sends to MATLAB at each time step, the inside wall surface heat flux (in W/m²). This heat flux is then multiplied by the wall length L to have the one-dimensional heat flux already incorporated in the total house load (denoted hereafter by q1D). The net value which is 'q2D - q1D' multiplied by the height of the thermal bridge is the net heat flux which is sent back to EnergyPlus to be an added load to the total energy load.

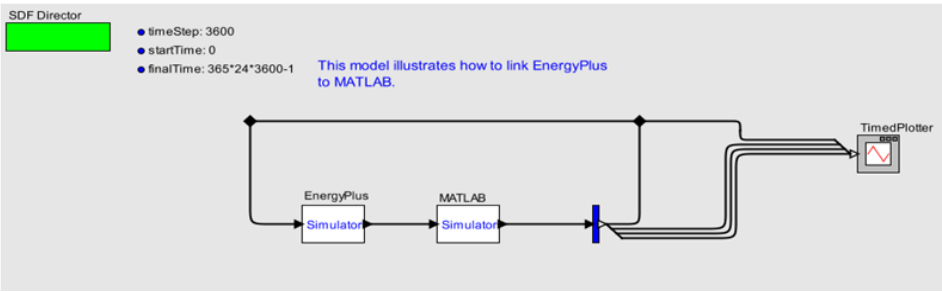

Fig. 4.17: Coupling EnergyPlus to MATLAB through BCVTB

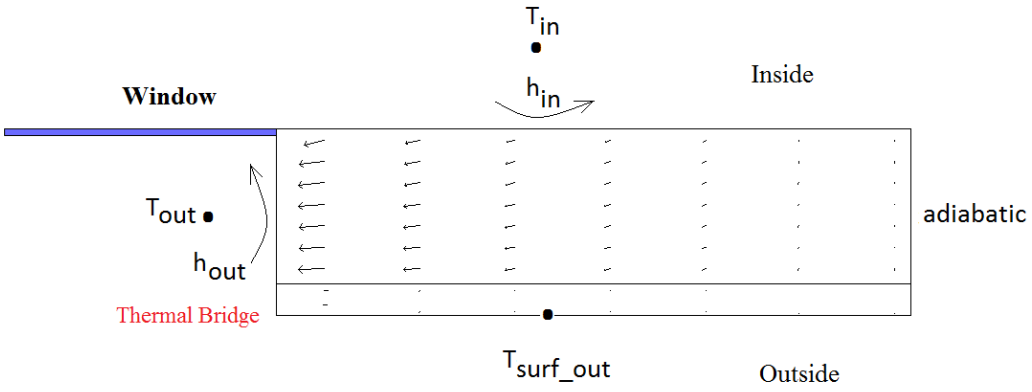

Fig. 4.18: Boundary conditions for MATLAB model

The annual simulation (4 simultaneous simulations; 1 for each facade orientation) with an hourly time step took around 2 hours on a "core i5-2500 CPU 3.3GHz" computer. In our case here, we were not concerned with running times; thus, we did not try to seek the minimum number of control volumes that makes the program's execution fast but still ensures accuracy. We just used a relatively big number of control volumes that will ensure accuracy of the simulation results. Thus, from computational effort point of view, if the number of control volumes is decreased (not exceeding a certain accuracy limit), it is possible to simulate more types of thermal bridges at the same time with relatively short simulation times.

4.4. Results

4.4.1. Thermal Bridge Energy Load

4.4.1.1. Case 1: No interior insulation

As a case study, the considered house is the INCAS house previously described in chapter 3. As a first case, no interior wall insulation is present. The exterior walls consist of 15 cm concrete with 3.5 or 7 cm coating as exterior layer. The case with 3.5cm external coating is denoted by "case1-a" and that with 7cm by "case1-b". Simulations are carried out for the city of Bordeaux (Oceanic region). Fig. 4.19 shows the windows offset thermal bridges energy load percentage of the total load of the house for 3 different cases: (a) no coating on the thermal bridges, (b) 1cm coating is added, and (c) 2cm coating is added. For case 1-a, we can see that these thermal bridges contribute to about 6% of the total load. When 1 and 2cm coating are applied on the edges of the thermal bridges, the percentage decreases to 3% and 2.4%

respectively. These percentages increase when exterior walls are more insulated with 7cm external insulation to become 8.5, 4.4, and 3.5% for no coating, 1cm coating, and 2cm coating, respectively.

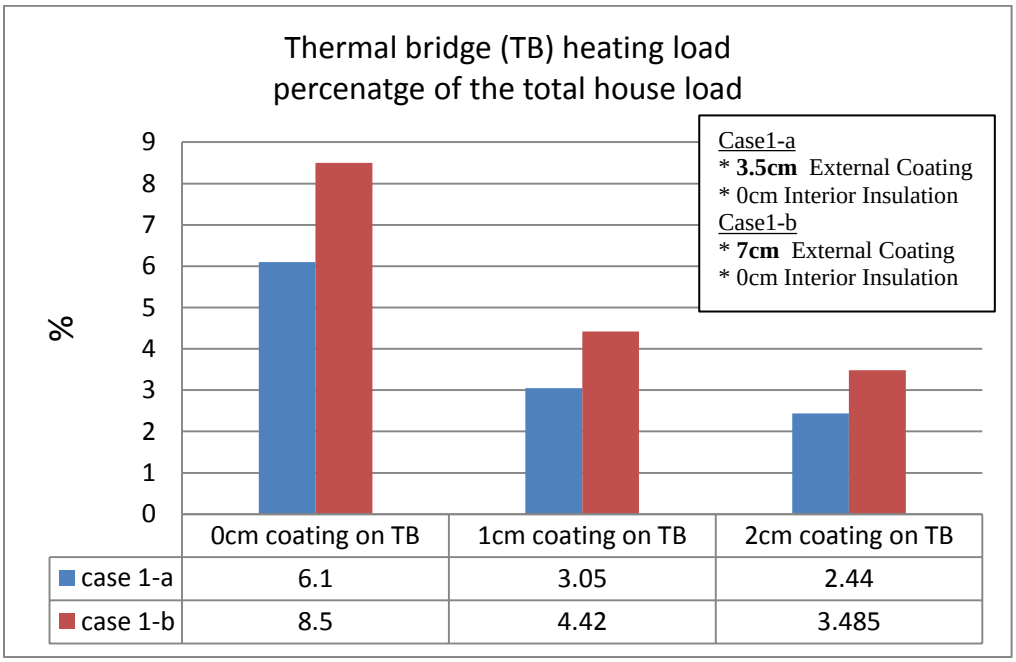

Fig. 4.19: Windows offset thermal bridge load percentage of the total heating load of the house (case1)

We can conclude that the effect of this type of thermal bridge is significant and can't be neglected especially for very well insulated envelopes. Also, as the thermal resistance of the walls increases, the thermal bridge energy load percentage increases.

Figure 4.20 compares the annual thermal bridge energy load when applying 1 and 2cm of the coating on the thermal bridges to that when no coating exists for "case1-a". reductions of around 50% and 63% are obtained, respectively. For "case1-b", approximately the same percentages are obtained.

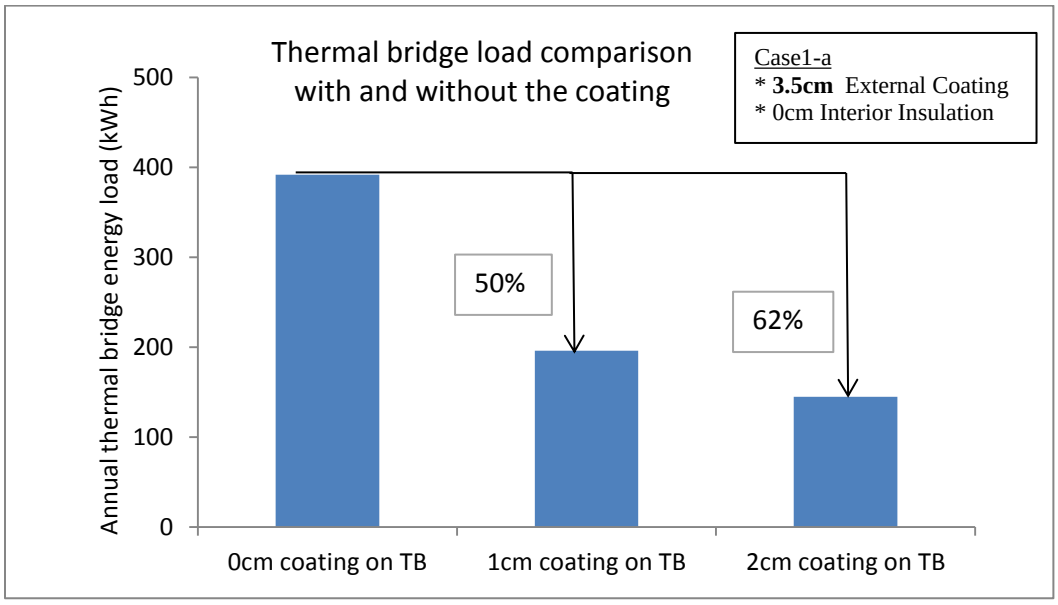

Fig. 4.20: Comparing the annual thermal bridge heating load with and without the coating (case1)

4.4.1.2. Case 2: With interior insulation

In this case, we added 5cm insulation to the interior surface of the walls. Figure 4.21 shows the thermal bridges energy load percentage of the total heating load of the house when there is no coating and when 1 and 2cm coating are added on the thermal bridge. From this figure and the previous figures (case 1), we realize that adding interior insulation decreases the percentage contribution of the thermal bridges on the total house energy load where it becomes (for case "a": 3.5cm external coating) 3.4% instead of 6% for no coating on the thermal bridges, 2.3% instead of 3% for 1cm coating, and 2% instead of 2.5% for 2cm coating. Also, for case "b" (7cm external coating) these percentages become 5.4% instead of 8%, 3.67% instead of 4.4%, and 3.24% instead of 3.5% for no coating, 1cm coating, and 2cm, respectively.

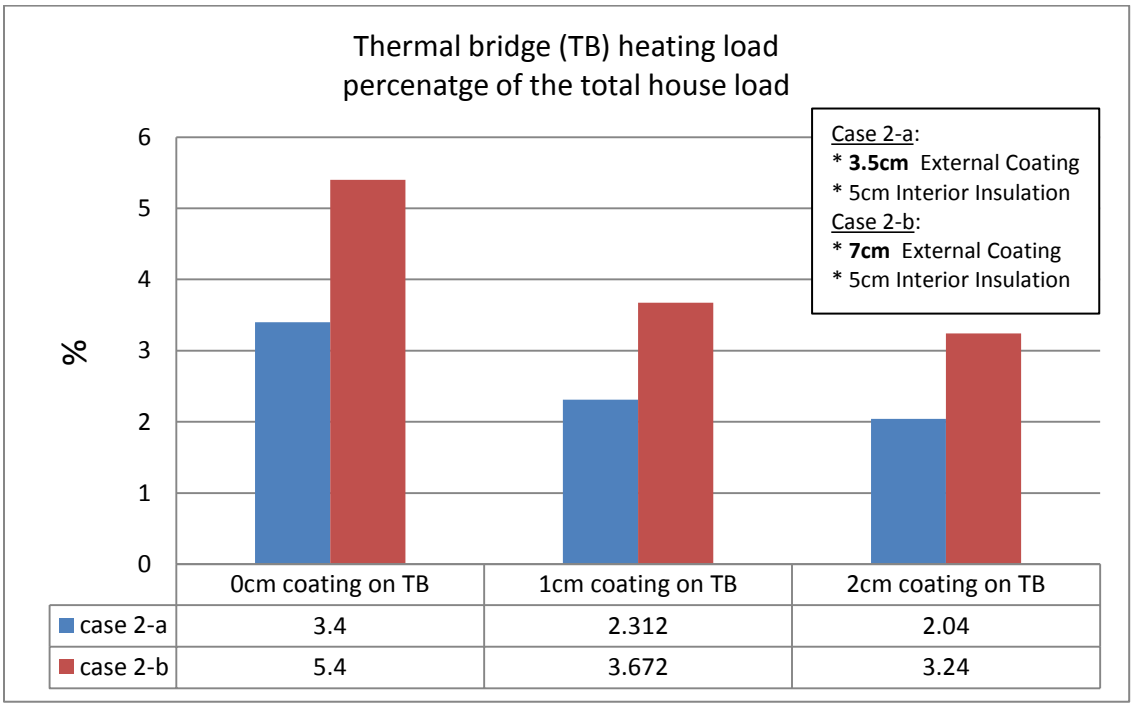

Fig. 4.21: Windows offset thermal bridge load percentage of the total heating load of the house (case2)

We can conclude that as the exterior insulation thickness increases, the fraction of the thermal bridges energy load on the total load increases. On the other hand, when interior insulation is added, this fraction decreases because internal insulation acts as a thermal resistance that suppresses the heat flow of the thermal bridge. When 1 or 2cm coating are added on the thermal bridge, the annual thermal bridge energy load decreases significantly (50 to 65%) when no interior insulation is present, while it shows a less decrease when interior insulation is present (30 to 40%).

4.4.2. Thermal Bridge Time Lag and Decrement Factor

4.4.2.1. Case 1: No interior insulation

Time lag and decrement factor are calculated for different wall positions as shown in Fig. 4.22 to show the effect of the thermal bridge.

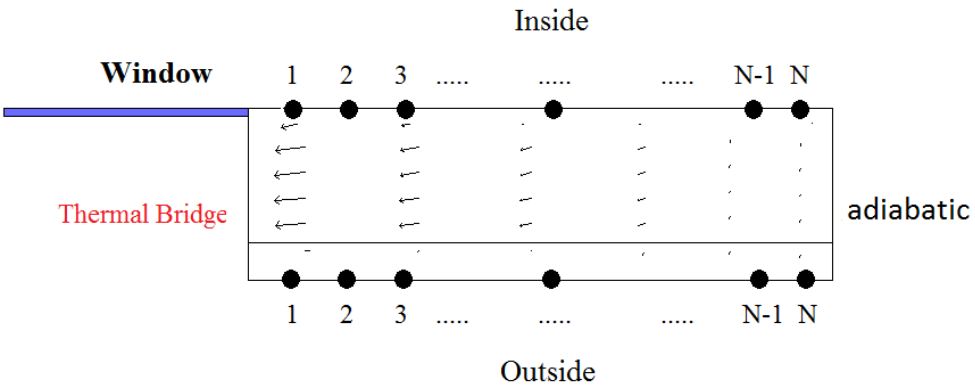

Fig. 4.22: Different positions in the wall to calculate the time lag and decrement factor

In all what follows, the calculations are done after reaching a steady periodic solution for a typical day in winter. Fig. 4.23 plots $\emptyset$ and f for "case1-a": 3.5cm external coating and "case1-b": 7cm external coating. As we go far from the thermal bridge, the decrement factor decreases till reaching a constant value (this value is the same obtained for the 1D heat transfer case) while the time lag increases till reaching a constant value. Comparing positions 0cm (very close to the thermal bridge) and 80cm (1D heat transfer) for case 1-a, there is a very large difference where $\emptyset_{80cm}$ is approximately 4 times greater than $\emptyset_{0cm}$, and f_{80cm} is lower by about 90% compared to f_{0cm}.

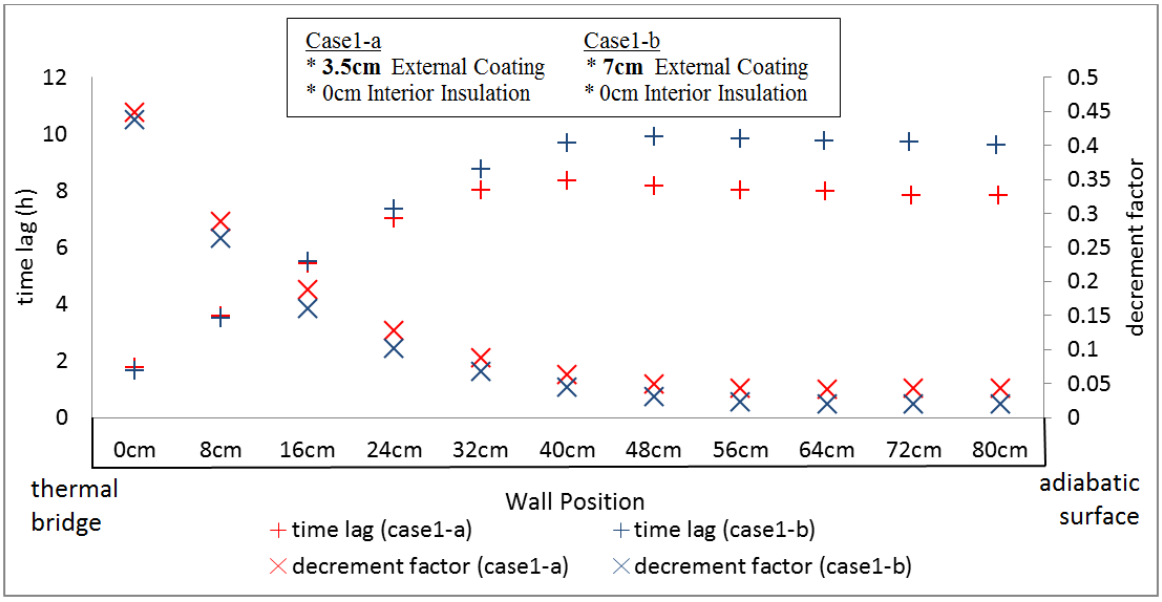

Fig. 4.23: Time lag and decrement factor for case-1 with no coating on thermal bridge

From the above figure, we conclude that, due to the presence of the thermal bridge, time lag and decrement factor differ greatly for the different positions in the wall, where the worst are those that are close to the thermal bridge. Case 1-b shows a better performance from maximum time lag and minimum decrement factor point of view due to the presence of more insulation on the exterior wall surface. Fig. 4.24 plots $\emptyset$ and f when 1 and 2cm coating are added on the thermal bridge for case 1-a. The "x" mark represents the decrement factor and the "+" represents the time lag. The 3 different colors represent 3 different cases: 1- No coating on the thermal bridge, 2- 1cm coating added on the thermal bridge, and 3- 2cm coating is added. By examining the "x" points, f is decreased significantly when adding 1 or 2cm coating for wall positions up to 30cm away from the TB. After 30cm, the decrement factor becomes approximately the same for all the 3 cases (this is due to the large decrease in the 2D heat transfer effects). Taking position 8cm, as an illustration, f decreased by 50% and 65% when adding 1 and 2cm coating, respectively. Concerning the time lag, for the first 30cm, adding the coating increases $\emptyset$ by about 0.5-2 hours, then $\emptyset$ becomes approximately the same. The same performance for $\emptyset$ and f is obtained for case 1-b.

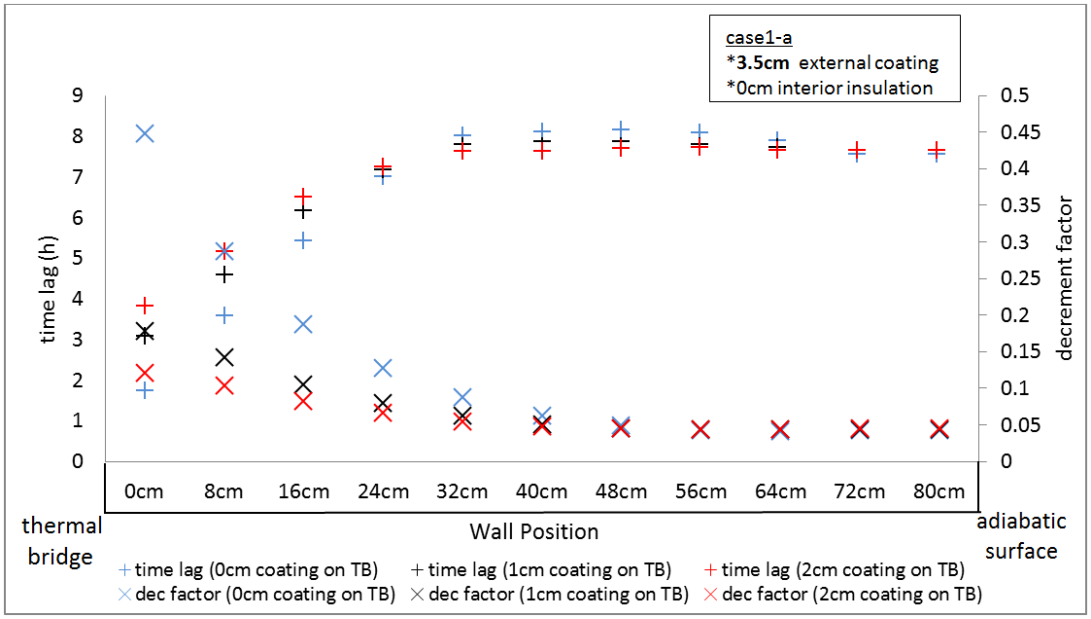

Fig. 4.24: Time lag and decrement factor for case1-a with and without the coating on thermal bridge

4.4.2.2. Case 2: With interior insulation

Time lag and decrement factor are calculated for the different wall positions but in this case, we add 5cm thermal insulation at the inner wall surface. The decrement factor and time lag follow the same trend similar to case 1 (no interior insulation). Comparing positions 8cm and 80cm, $\emptyset_{8cm}$ is smaller than $\emptyset_{80cm}$ by a factor of 2.4 and 2.9 for cases 2-a (3.5cm external coating) and 2-b (7cm external coating) ,respectively, and f_{8cm} is greater than f_{80cm} by about 87% than 94% for cases 2-a and 2-b, respectively. When 1 and 2cm coating are added on the thermal bridge, the performance is the same compared to case 1.

4.5. Conclusion

We calculated the annual energy load of the windows offset thermal bridges for a typical French house with and without the coating. Co-simulation was used to incorporate the two dimensional heat transfer effects to EnergyPlus. Results showed that:

- The percentage of the windows' offset thermal bridges energy load of the total house load is approximately 4-8% for the case of exterior walls having no interior insulation and approximately 2-5% for the case of exterior walls having 5cm interior insulation. Furthermore, when using more exterior insulation, the relative effect of the thermal bridge is higher.
- Applying 1 and 2cm of the coating on the window edges reduces the windows offset energy load by about 50 and 64%, respectively, for the case of exterior walls having no interior insulation, and by about 30 and 40% for the case of exterior walls having interior insulation.

We also calculated the time lag and decrement factor for a wall structure near the thermal bridge. We can conclude the following:

- for wall positions near the thermal bridge (2D heat transfer effects), we obtain high values for the decrement factor and low values for the time lag compared to those for wall positions far from the thermal bridge (no effects of the 2D heat transfer)
- Adding 1 and 2cm coating on the thermal bridge showed a reduction in the decrement factor values for positions near the thermal bridge up to 70% and an increase in time tag up to 2 hours.

5. Energy Load and Thermal Comfort Analysis

5.1. Introduction

In this section, we present a simulation-based rapid assessment tool designated for architects, building engineers, and non-energy-expert users to examine the effect of adding this coating on the energy consumption and thermal comfort. Depending on the construction period, different window-to-wall ratios, interior insulation thicknesses, wall structures, etc. are considered. Also, all these are examined under the different climates of France. The output of this tool is the house heating demand with and without the coating. As an inverse problem, the user can enter the required heating demand and the output will be the coating thickness. Moreover, the tool provides a thermal comfort assessment based on different thermal comfort models. In what follows, we describe the features of the tool then we present and discuss some of the simulation results.

5.2. Rapid Assessment Tool

5.2.1. The Tool's Features

The tool addresses the following:

Direct: How much energy reduction (annual heating load) is achieved when adding the coating?

Inverse: What is the needed coating thickness if a certain heating load is required?

Comfort: What is its effect on thermal comfort?

Simulations are carried out for the different construction periods and under the different climates of France: Mediterranean, Oceanic, and Semi-Continental. A two-story house with an attic and crawl space is modeled using the whole building energy simulation program EnergyPlus. Depending on the construction period, different window-to-wall ratios, wall, roof, and ground insulation thicknesses, air change rates, wall structures, etc. are considered. The tool is based on EnergyPlus simulation results and is developed using the MATLAB's graphical user interface (GUI). More than 10,000 simulation runs are carried out.

Firstly, you choose the construction period: before 1948, 1948-1967, 1968-1974, 1975-1990, or after 1990.

Secondly, you choose between the Direct and the Inverse calculation. The Direct calculation gives the annual heating load for a given coating's thickness while the Inverse calculation gives the coating's thickness for a given annual heating load.

Thirdly, you select the construction inputs (note that these change with the different construction periods).

Fourthly, you enter the coating thickness (Direct) or the annual heating load (Inverse). Finally, you run the case and obtain the outputs. The tool will estimate the heating load with and without the coating. Also, it will generate a curve showing the variation of the annual heating load as a function of the coating thickness. In addition to the energy calculations, a thermal comfort assessment is performed when choosing the "Thermal Comfort Analysis". This latter includes different assessment criteria. These are:

- ASHRAE standard 55 (2004) simple comfort diagrams: the output is the percentage of occupied time where comfort is met for winter and summer
- Percentage of occupied time heating is not needed (for winter). In addition to this output the degree.hour is also calculated to show how far the room temperature is from the set-point value.
- Fanger's PMV index: the output is the percentage of occupied time where comfort is met ($-0.5 \leq PMV \leq 0.5$)
- ASHRAE standard 55 adaptive thermal comfort model (for summer): it shows the percentage of occupied time where overheating is probably to occur for different satisfaction levels 90% and 80%, and also its degree.hour.
- EN 15251 adaptive thermal comfort model (for summer): it shows the percentage of occupied time where overheating is probably to occur for the different satisfaction levels 90%, 80%, and 65%, and also its degree.hour.

In addition to these, some options can be chosen such as to increase the heating set-point in winter or to increase the night ventilation rate in summer.

Screen shots for the Rapid Assessment Tool are provided in Annex E.

5.2.2. Building Model

5.2.2.1. Geometrical Description

The INCAS house's geometry is taken as a reference case. The considered house consists of two air-conditioned zones, ground (GF) and first (1F) floors of 50m^2 floor area each with a height of 2.7m, and two unconditioned zones (Attic and crawl space).

5.2.2.2. Internal Loads

A scenario for people occupancy and equipment usage simulating a real case has been modeled. Four inhabitants are considered. The load of each person is taken as 70W when sleeping, 100W when seated at rest, and 140W when doing a light activity. The occupancy schedule is different between weekdays and weekends and it also differs between the ground and first floors. Fig. 4.25 shows the occupancy schedule for both floors for week days and for weekends. Fig. 4.26 shows the equipment schedule for both floors for week days and for weekends.

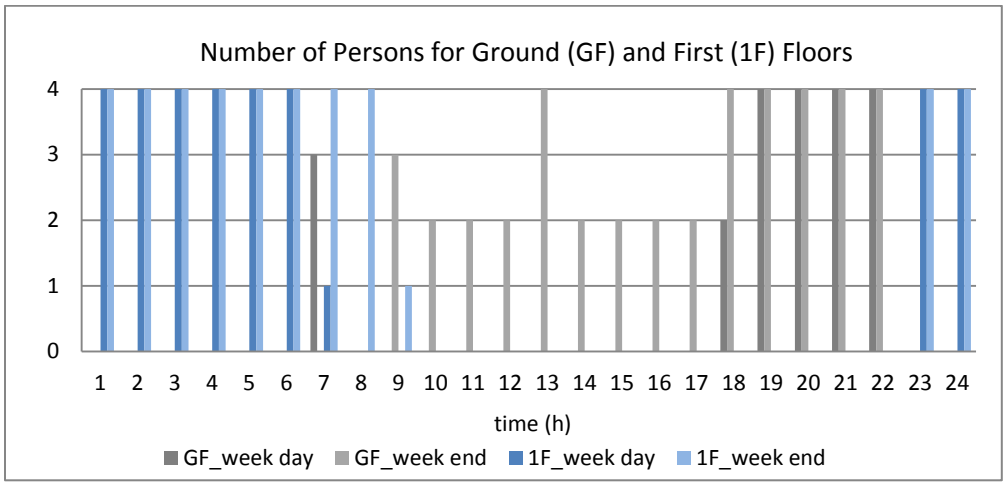

Fig. 4.25: Occupancy schedule for ground and first floors for week days and weekends

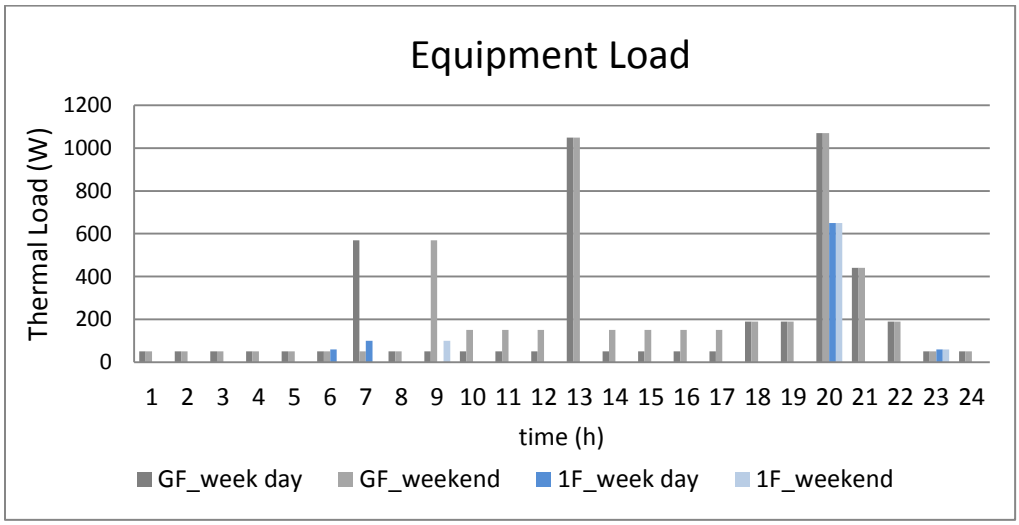

Fig. 4.26: Equipment load schedule for ground and first floors for week days and weekends

5.2.2.3. HVAC System

An Ideal HVAC system is chosen in EnergyPlus which maintains the interior air temperature of the conditioned spaces constant and equals to 19°C during the heating season. The air change rate (ACR) differs for the different construction periods and it is kept "ON" during all time.

5.3. Curve Fitting and Inverse Modeling

It is very difficult and time consuming to simulate all cases; i.e. to vary the coating's thickness from 0cm to 15cm and to simulate all these cases. So what we did is taking some values of the coating thickness which are 0, 0.5, 1.5, 3, 7, 10, and 15cm, simulating the different cases, and then performing a curve fitting for the heating load as a function of the "ABC" thickness. Fig. 4.27 shows an illustration of this for a randomly chosen case. The variation of the energy load against the coating thickness can be fitted by a power curve function having an equation of the form:

$$y = a * x^b \quad (4.1)$$

where x is the coating thickness and y is the annual heating demand. a and b are the coefficients of the curve fit.

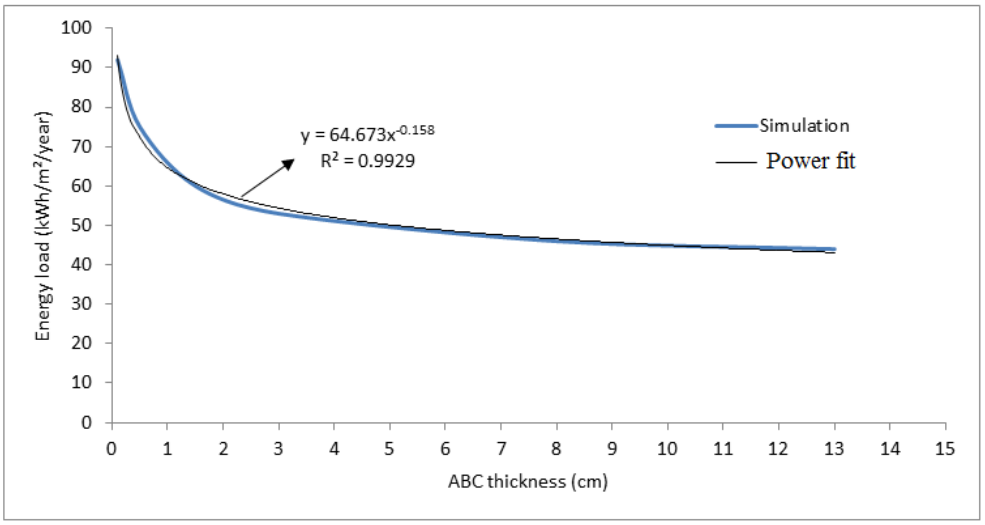

Fig. 4.27: Energy load versus ABC thickness power curve fit

Thus, for each of the different cases, a curve fitting is done, and the coefficients "a" and "b" are determined. The above equation serves as a direct method to determine the energy load having been given the "ABC" thickness. For the inverse calculation, we want to know the "ABC" thickness when a certain value of the energy load is required; equation (4.2) is used. This latter is obtained through linearizing and inverting equation (4.1).

$$x = e^{\frac{(\ln(y)-\ln(a))}{b}} \tag{4.2}$$

5.4. Results and Discussion

5.4.1. Energy Load

Fig. 4.28 shows the house's energy load without the ABC and with 5cm ABC on the exterior facades for the different construction periods and for the different climates. For the period 1968-1974, we modeled two different houses: the first one "1968-1974(1)" has simple glazed windows with no insulation in the roof; the second one "1968-1974(2)" has double glazed windows with 6cm thermal insulation in the roof. Also, for the period after 1990, we distinguish two cases: the first one, >1990(1), has the exterior walls composed of concrete structure with 10cm internal thermal insulation and the second one, >1990(2), has the exterior walls composed of 42cm of brick-monomur with no internal insulation.

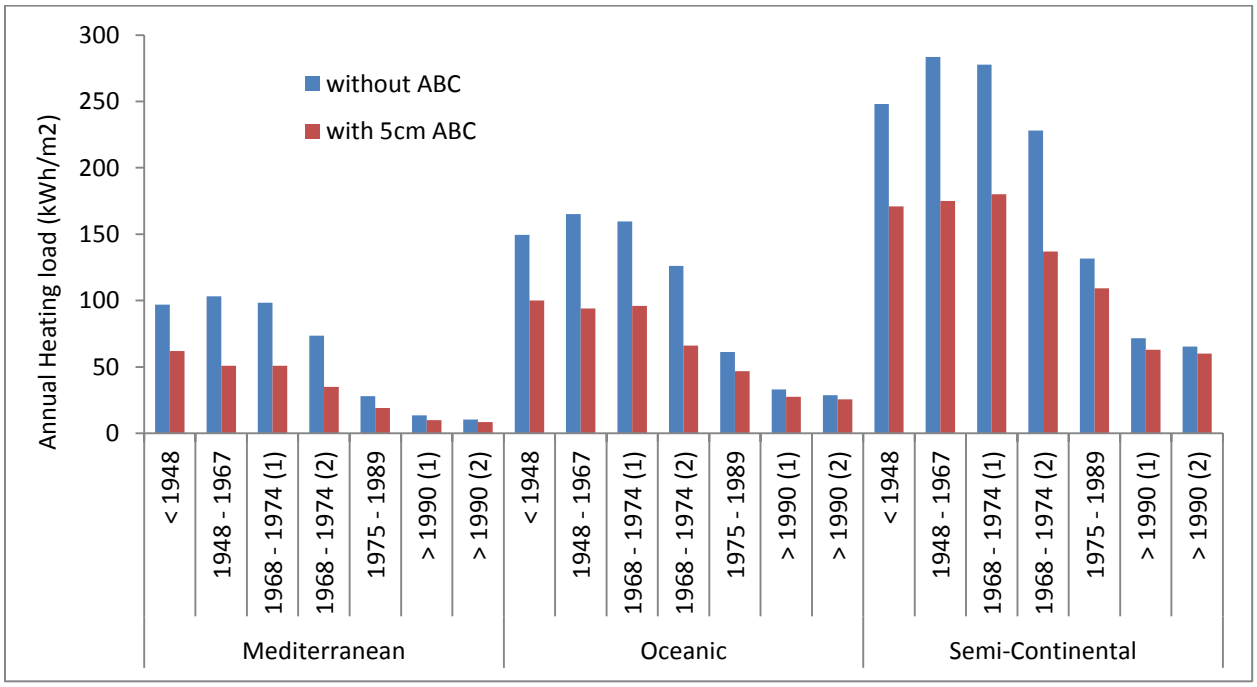

Fig. 4.28: Annual heating load for the different climates and the different construction periods with and without the coating [(1) and (2) represent different construction techniques within the same period]

From this figure, it is shown that for the old houses built before 1974, the percentages of energy reductions are between 40 – 53% for the Mediterranean climate, 37 – 48% for the oceanic climate, and 33 – 40% for the Semi-Continental climate. For the houses built in the period 1975-1989, the reductions are about 32%, 23%, and 17% for the Mediterranean, Oceanic, and Semi-Continental climates. Lower reductions are achieved in the new houses, 23%, 14%, and 10% for the three climates, respectively. Since the new houses have already thermal insulation in the exterior envelope, adding the ABC will not decrease a lot the annual load. To examine this more, the variation of the energy load with respect to the coating thickness for 3 cases: without interior insulation, with 5cm interior insulation, and with 10cm interior insulation is shown in Fig. 4.29.

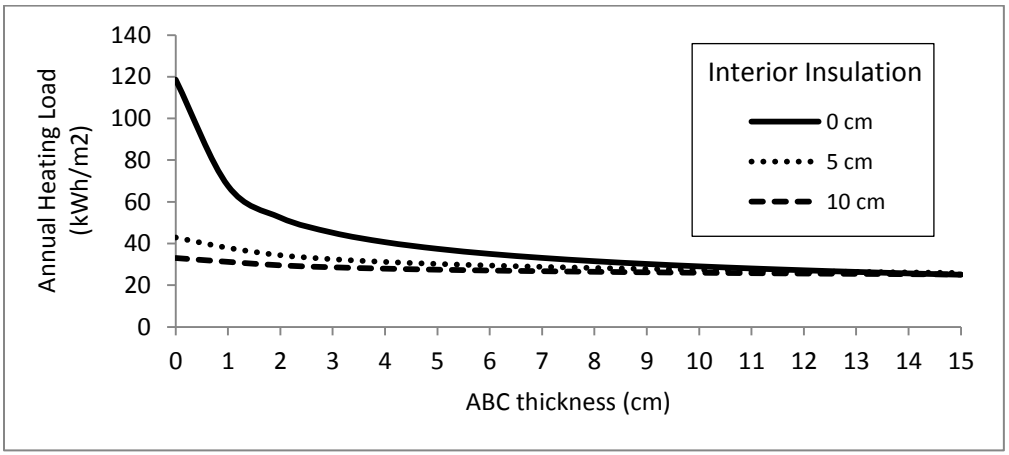

Fig. 4.29: Heating load as a function of the coating thickness for different interior insulation thicknesses

From this figure, we can conclude that this coating is very interesting and beneficial for buildings under rehabilitation, especially the uninsulated houses, where a small thickness can reduce extensively the energy load, which also means conservation of the house's livable area. For a medium level insulated house, adding the coating also has a good advantage. For very well insulated houses, adding the coating will still reduce the energy load, but certainly its importance lies in achieving more and more energy efficient houses to reach or even passes the new thermal regulations (RT 2012) levels of the low energy buildings.

5.4.2. Thermal Comfort

In summer, the building is considered as uncomfortable when the operative temperature falls out of the comfort range in condition that the house is being occupied. This comfort range is based on the adaptive thermal comfort temperatures according to ASHRAE 55 and EN 15251 standards.

In winter and inter-seasons (October till April), the assessment factor is the percentage of occupied time where heating is not needed. The implementation of the coating contributes in increasing this percentage.

5.4.2.1. Winter and Inter-seasons

The percentage of occupied time where heating is not needed for different coating thicknesses for the old house is shown in Fig. 4.30. As the coating thickness increases, the number of hours where heating is not needed increases. Taking the 5cm as an illustration, the

percentage increases by 10%, 6%, and 3% for the Mediterranean, Oceanic, and Semi-Continental climates, respectively, compared to the house with no coating.

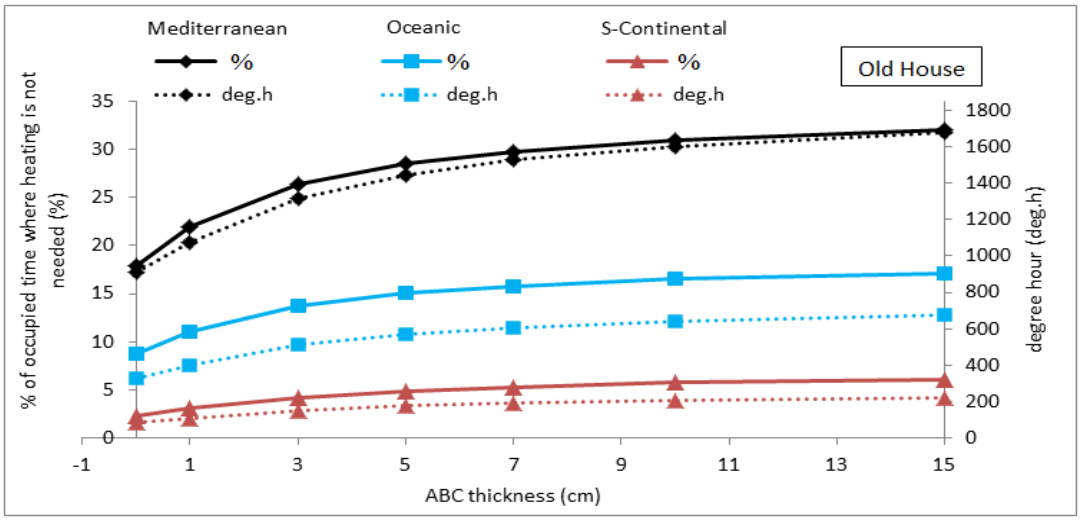

Fig. 4.30: Percentage of occupied time where heating is not needed and its degree.hour for different coating thickness and different climates (old house)

Fig. 4.31 shows the percentage of occupied time where heating is not needed for the new house for 0, 5, and 10cm interior insulation. The black curves are for the Mediterranean climate, the blue ones are for the Oceanic climate, and the red ones are for the Semi-Continental climate. For the cases with no interior insulation, applying 5cm of the coating increases the percentage by 28%, 17%, and 10% for the Mediterranean, Oceanic, and Semi-Continental climates. For the houses with 5cm interior insulation, adding 5cm coating on the exterior facades increases the percentage by 12%, 6%, and 4% for the three climates, respectively. For the houses with 10cm interior insulation, the increase is about 6%, 3.5%, and 2.5%, respectively.

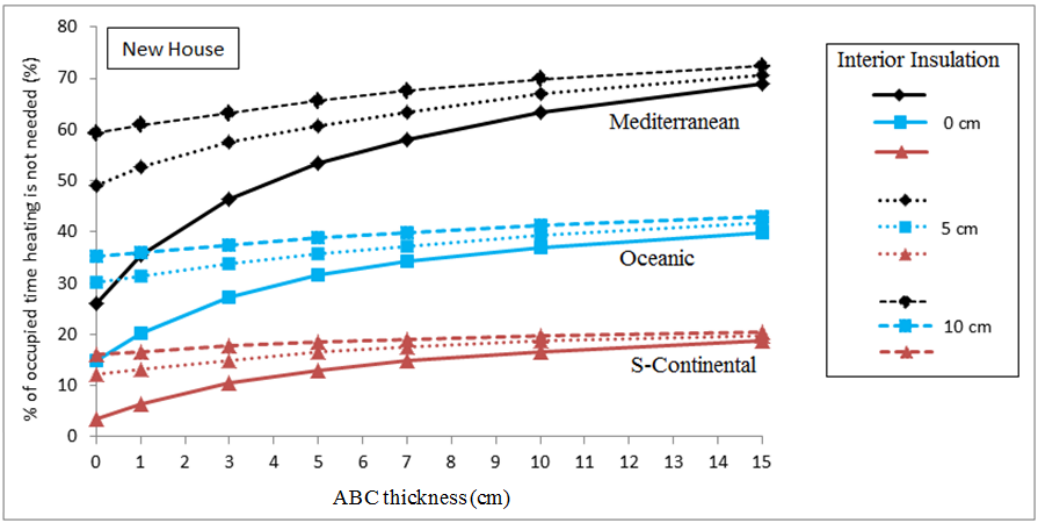

Fig. 4.31: Percentage of occupied time where heating is not needed its degree.hour for different coating thicknesses and different climates (new house)

5.4.2.2. Summer

Old House

Fig. 4.32 shows the percentage of occupied time where overheating will probably occur according to (a) EN 15251 adaptive comfort model and (b) ASHRAE 55 adaptive comfort model for different levels of satisfaction. According to the EN standard, it is shown that the house with no coating has a discomfort time percentage of 15%, 9%, and 4% for the Mediterranean, Oceanic, and Semi-Continental climates for 90% of occupants satisfied. For 80% and 65% satisfaction, the overheating percentage decreases to less than 3% for all the climates. For Mediterranean climate, adding the coating increases the discomfort hours with respect to the uninsulated house from 15% to approximately 17% (90% satisfaction level). However, for oceanic and semi-continental climates, adding the coating decreases the discomfort hours from 9% and 4% to about 3.5% and 1.5%, respectively. The same conclusions are derived when using the ASHRAE 55 standard. However, in this latter, the discomfort hours are more than those calculated using the EN standard because the thermal comfort requirements of ASHRAE 55 are more strict; thus, occupants can tolerate higher operative temperatures according to EN 15251 standard.

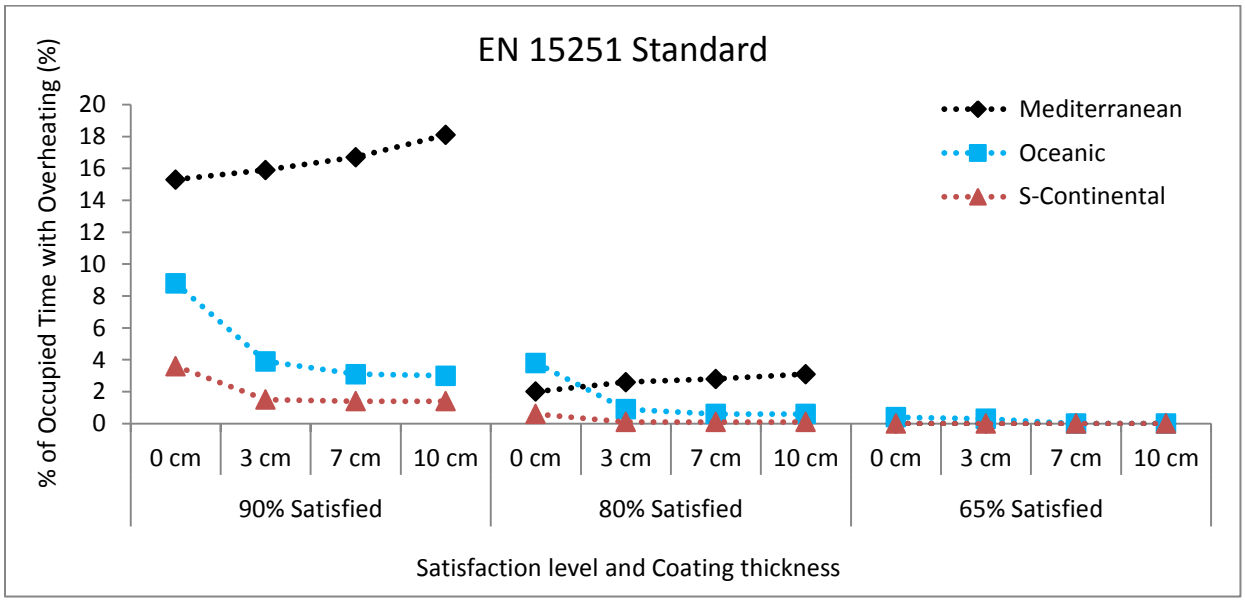

(a)

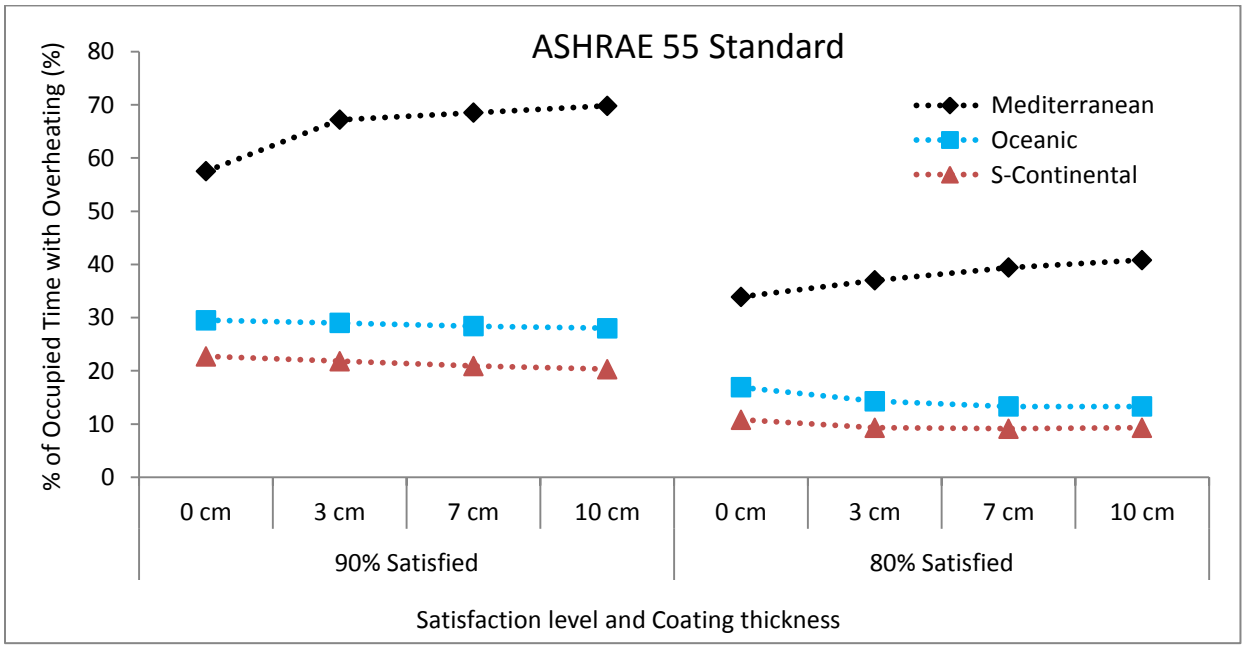

(b)

Fig. 4.32: The percentage of occupied time where overheating will probably occur according to (a) EN 15251 adaptive comfort model and (b) ASHRAE 55 adaptive comfort model for different levels of satisfaction (old house)

Conclusion 1 (old house):

The conclusions are based on the EN 15251 adaptive thermal comfort standard.

- In the Mediterranean climate, for an old house initially with no coating, there is not so much risk of overheating where the percentage of occupied time thermal comfort is not met does not exceed 2% and 16% for 80% and 90% of occupants satisfied, respectively. Applying the coating does not have a significant effect on this percentage. This latter increases by about 2% when a 7cm layer of the coating is added on the exterior facades.
- For the Oceanic climate, the discomfort time is about 4% and 9% for 80% and 90% of occupants are satisfied, respectively. Adding a 7cm layer of the coating decreases the percentage of discomfort time to less than 1%
- For the Semi-Continental region, no overheating is observed during the occupied hours in the summer period.

New House

Fig. 4.33 shows the percentage of occupied time where overheating occurs for a new house having (a) no interior insulation, (b) 5cm interior insulation, and (c) 10cm interior insulation. Let us take the case where 80% of occupants are satisfied for a house situated in the Mediterranean region. Initially, when no coating is applied, the percentage of discomfort time is about 30%, 53%, and 72% for 0, 5, and 10cm interior wall insulation, respectively. When a 3cm layer of the coating is applied on the exterior facades, the discomfort time percentage is increased to 47%, 70%, and 80% for the three interior insulation thicknesses, respectively. When a 7cm layer of the coating is added, the percentage increases to 73%, 81%, and 85%, respectively.

To overcome this risk of overheating, night ventilation can be adopted as the outside air temperature drops at night time. This is illustrated in Fig. 4.34, where it shows the percentage of discomfort time for a house situated in the Mediterranean region for no increased ventilation at night (0.7ach at all time, no increase at night) and for increased night ventilation to 2ach and 5ach. Note that as mentioned earlier, the rapid assessment tool has options to increase the ventilation rates during summer nights.

For the oceanic climate, the percentage of discomfort time during occupied period is approximately 12%, 16% and 20% for 0, 5, and 10cm interior insulation, respectively. These percentages increase by about 4% when a 7cm coating layer is added. For the Semi-Continental climate, the discomfort time stays below 10% for all the cases. Also, adding the coating doesn't have a significant effect on the discomfort time percentage.

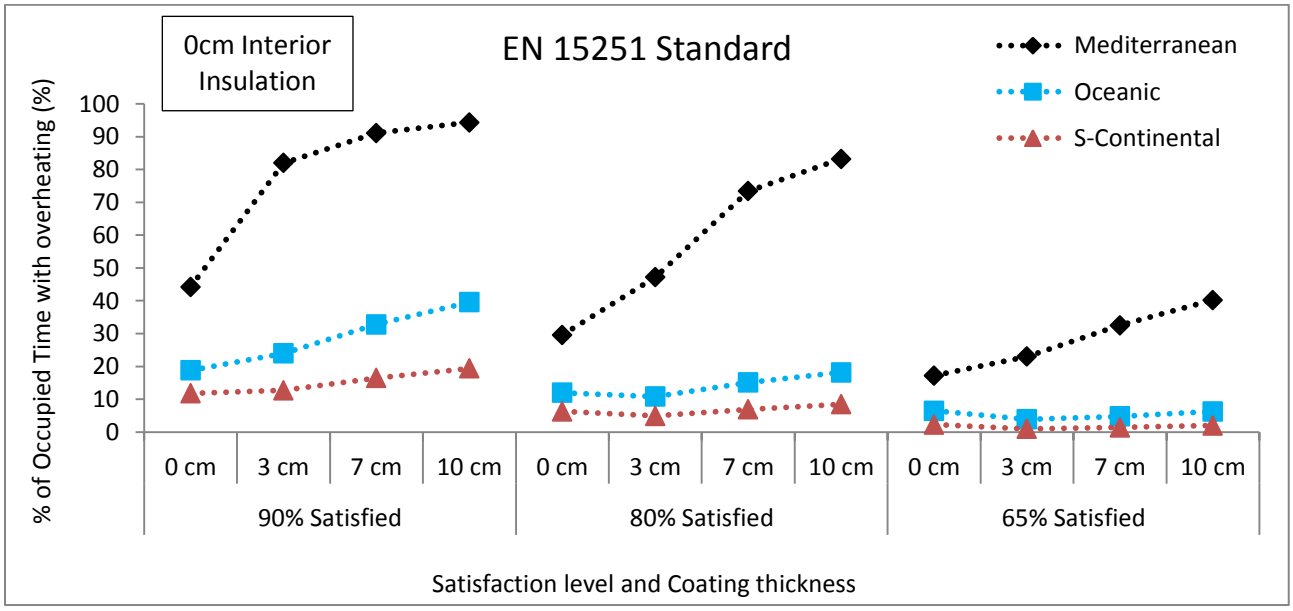

(a)

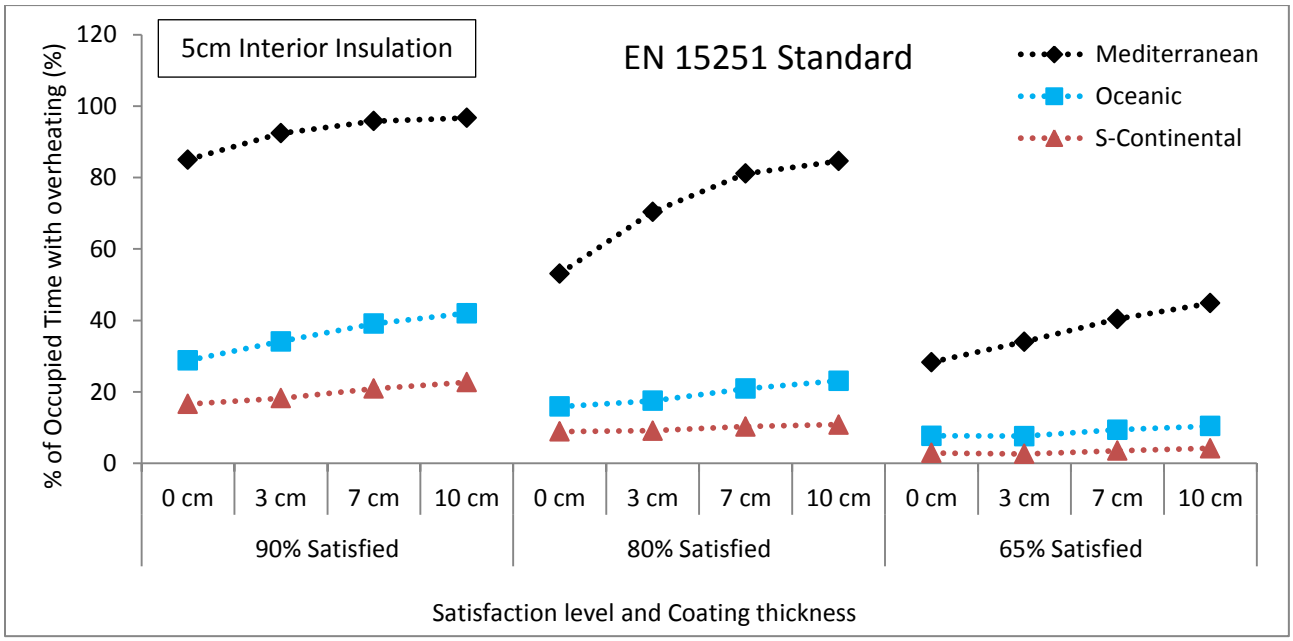

(b)

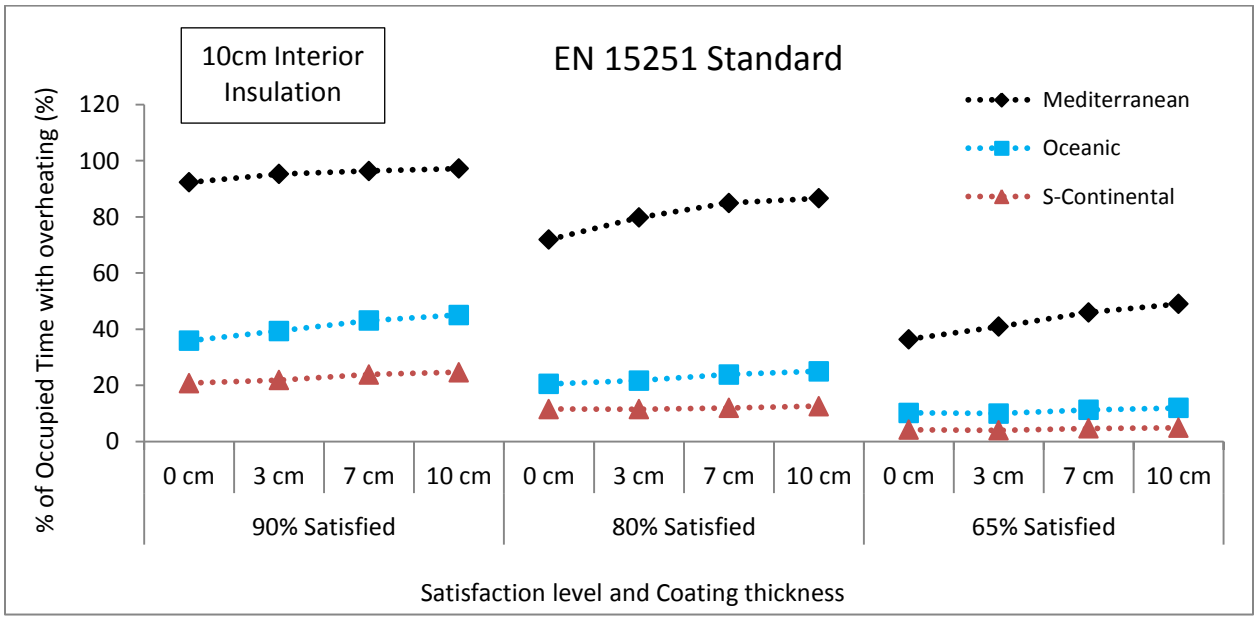

(c)

Fig. 4.33: The percentage of occupied time where overheating occurs for a new house having (a) no interior insulation, (b) 5cm interior insulation, and (c) 10cm interior insulation

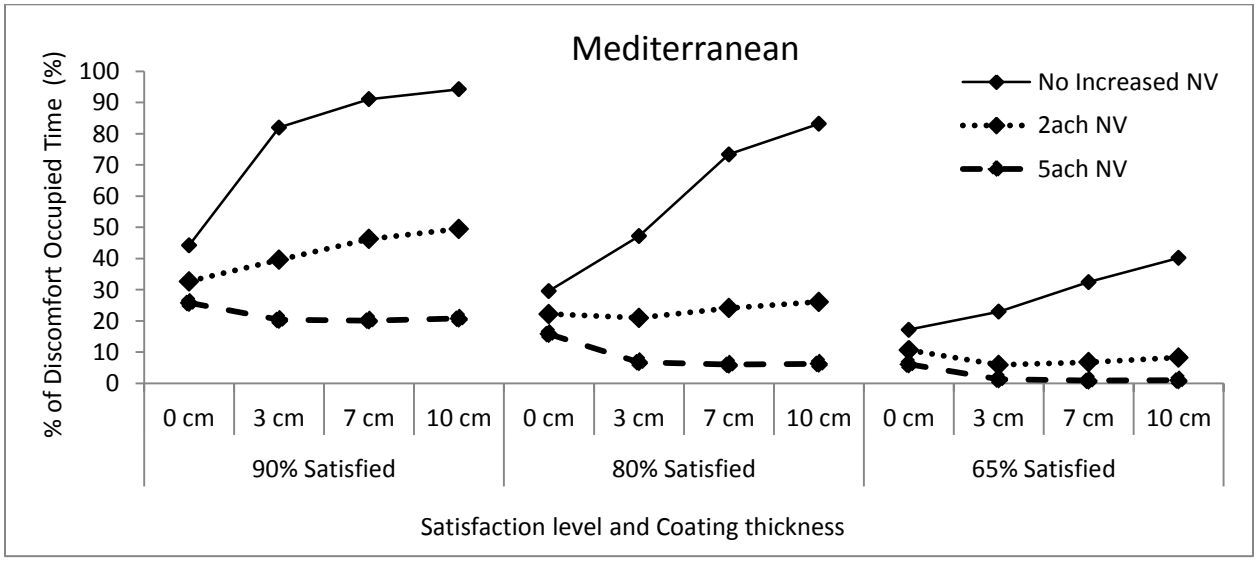

Fig. 4.34: Percentage of discomfort time for different night ventilation rates for a new house in a Mediterranean climate

Conclusion 2 (New house):

The conclusions are based on the EN 15251 adaptive thermal comfort standard.

- In the Mediterranean climate, for a new house initially with no coating, there is a risk of overheating especially for very well insulated envelopes. The percentage of occupied time when thermal comfort is not met can reach 30% for the case of 0cm wall's interior insulation

and 70% for 10cm wall's interior insulation. This is due to the fact that the dissipation of the heat inside the house to the outside environment becomes more difficult when the envelope is more insulated.

Applying the coating increases significantly the risk of overheating for the house having un-insulated or medium-insulated (5cm) walls.

To overcome this high risk of overheating, night ventilation should be adopted.

- For the Oceanic and Semi-Continental climates, the discomfort time remains below 20% and 10%, respectively, for the different interior insulation thicknesses. Also, the addition of the coating slightly increases these percentages.

5.5. Cost analysis and thickness optimization

Selection and determination of the optimum thickness of insulation has been of prime interest for many researchers in recent years. The concept of optimum thermal insulation thickness considers both the initial cost of the insulation and the energy savings over the life cycle of the insulation material. The optimum insulation thickness corresponds to the value that provides minimum total life cycle cost. The optimum insulation thickness based on heating requirement depends mainly on the yearly heating load, the costs of electricity and insulation material, the building lifetime, and the interest and inflation rates. The total cost is given in equation (4.3).

$$C_t = C_h + C_c \tag{4.3}$$

where C_h is the heating cost over the lifetime of the building. The total heating cost over a lifetime of *N* years is evaluated in present value using the present worth factor *PWF* and is given in equation (4.4). C_c is the insulating coating initial investment cost calculated using equation (4.5).

$$C_h = \frac{Q_h}{\eta_h} * C_e * PWF \tag{4.4}$$

$$C_c = V_{ABC} * C_{\frac{€}{m^3}} \tag{4.5}$$

where Q_h, η_h, C_e, and PWF are the annual heating load, heating system efficiency, cost of electricity, and the present worth factor, respectively. V_{ABC} and $C_{€/m^3}$ are the coating's volume and coating's cost in euro/m^3.

The present worth factor represents the amount of cash today that is equivalent in value to a payment, or to a stream of payments, in the future. It depends on the inflation rate "*g"*, on the interest rate "*i"*, and on the lifetime of the building "*N*". It is calculated using equation (4.6) (Bolattürk 2008, Cuce et al. 2014).

$$\begin{cases} PWF = \dfrac{(1+r)^N - 1}{r(1+r)^N}\ , & if \begin{cases} i > g\ , & r = \dfrac{i-g}{1+g} \\ i < g\ , & r = \dfrac{g-i}{1+i} \end{cases} \\ PWF = \dfrac{N}{1+i}\ , & if \quad i = g \end{cases} \tag{4.6}$$

The coating's thickness optimization is carried out for different climates. Three cities of France are chosen representing different climates: Nice (Mediterranean climate; latitude 43.7° N, longitude 7.266° E), Bordeaux (Oceanic climate; 44.84° N, 0.58° W), and Strasbourg (Semi-Continental; 48.58° N, 7.748° E). Other than France, we have also chosen three cold Nordic cities: Moscow (Russia; 55.75° N, 37.616° E), Stockholm (Sweden; 59.329° N, 18.068° E), and Montreal (Canada; 45.50° N, 73.566° W). The analyses are carried out for a typical house built before 1974. The majority of these houses have no thermal insulation in their envelope. As a base case, the building life time, the interest rate, and the inflation rate are taken as 40 years, 2.5% and 2%, respectively. The heating system is electric with an efficiency of 0.9. The heating set-point is taken as 19°C. The cost of electricity is 0.13€/kWh. The cost of aerogels is very erratic in the current market. However, it has a decreasing trend with time. According to Koebel et al. (2012), this cost could drop below 1500 US$/m^3 (≅1100 €/m^3) by the year 2020. Cuce et al. (2014) in their study assumed a value of 600 €/m^3 for the cost of aerogel insulation based on future predictions. In our study here, 800 €/m^3 (including labor cost) is considered as a base case, then this value as well as the values of the other parameters are changed to examine the sensitivity of the optimum thickness to these inputs. Note that for the cities out of France, the simulations are carried out with the same electricity tariff just for comparison purposes.

According to Comakli and Yuksel (2003), excessive insulation as well as low insulation is not desired from an economic perspective. Excessive insulation means high initial investments while low insulation means high energy consumption costs. Here comes the necessity to find the

optimum insulation levels that represents a compromise between the two. Fig. 4.35 shows the coating's cost, the heating consumption cost, and the total cost for the different climates. From these figures, we can deduce that the heating cost decreases exponentially as the coating's thickness increases. The cost of insulation always varies linearly with the thickness. The total cost decreases to a certain minimum then starts to increase. The optimum coating's thickness is the one that ensures this minimum of the total cost. For each climate, the optimum thickness is presented in Table 4.5. We can conclude that as the climate gets colder, the optimum thickness increases. This is due to the increasing heating loads and, as a result, the increasing electricity costs. So, in the cold climates, there is larger potential to reduce energy consumption through applying the insulating rendering. As illustration, applying 2cm layer of the coating saves around 4000€ for Nice while 9000€ for Strasbourg; however, the initial investment cost remains the same.

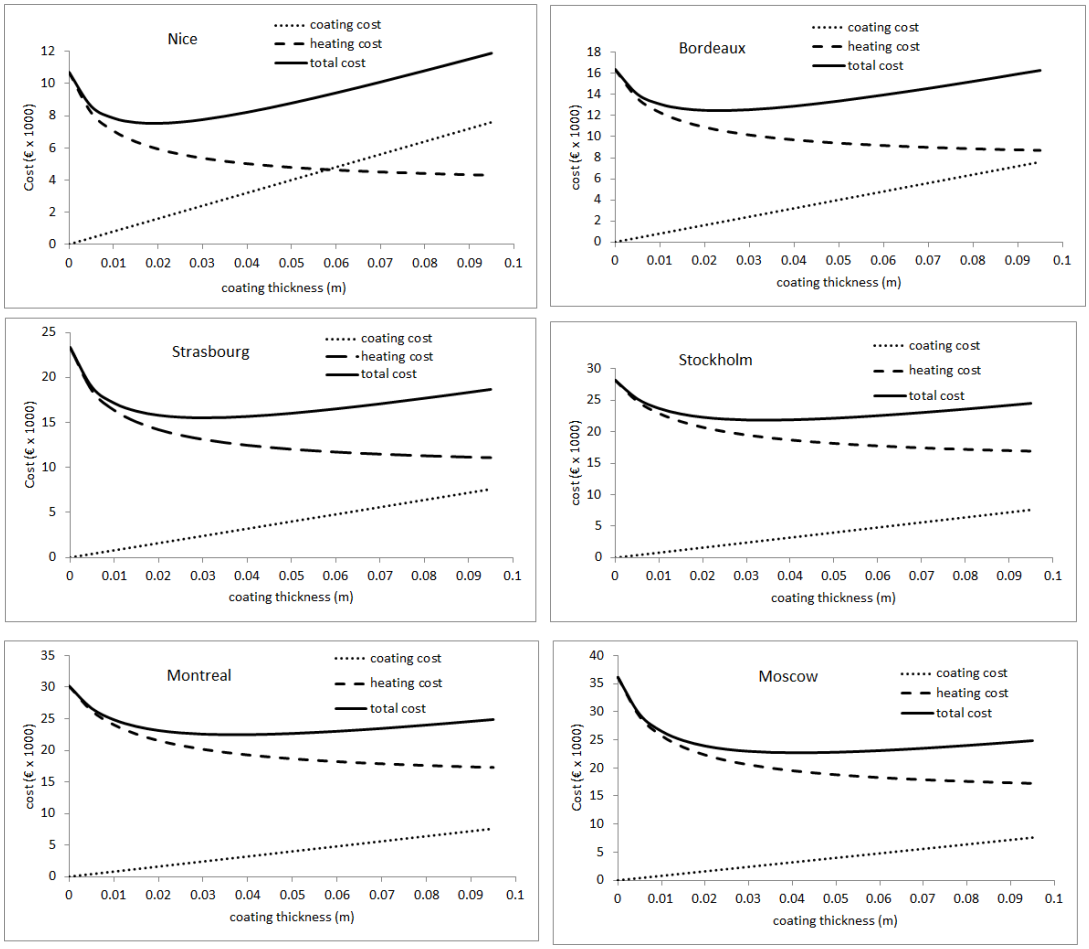

Fig. 4.35: Aerogel-based coating, heating, and total costs for the different climates

Table 4.5: optimum coating thickness for the different climates

City	Optimum thickness (cm)
Nice	1.71
Bordeaux	2.10
Strasbourg	2.93
Stockholm	3.26
Montreal	3.61
Moscow	4.37

After determining the optimum coating thickness, the payback period (*PP*) is calculated. It is defined as the time required to recover the initial investment cost. Long payback periods are not desired especially in the building sector. The *PP* is calculated using equation (4.7) (Sisman et al. 2007).

$$PP = \frac{C_C}{CS_E} * PWF \tag{4.7}$$

where CS_E is the annual cost savings due to energy consumption reduction. It is defined as the difference between the energy cost when the wall is not insulated and the energy cost when it is insulated with optimum thickness (Sisman et al. 2007, Ozel 2011, Cuce et al. 2014).

Table 4.6 presents the payback period for the different cities when the optimum coating thickness is applied.

Table 4.6: Payback period

City	Payback period (year)
Nice	2.7
Bordeaux	2.21
Strasbourg	1.64
Stockholm	2.1
Montreal	1.96
Moscow	1.47

From this table, it is understood that the payback period ranges between 1.4 – 2.7 years. These results are in harmony with those of Cuce et al. (2014) where they determined the optimum thickness of aerogel insulation for some climates. Due to the relatively low payback periods, it is concluded that applying the coating could be seen as a good investment from economical point

of view. As stated previously, several parameters affect the optimum thickness. Among these are the present worth factor, heating set-point, and the cost of aerogels. Starting with the *PWF*, Fig. 4.36 shows the dependency of the optimum coating thickness on the *PWF*. It is shown that it increases almost linearly as the *PWF* increases. Also, here it is noted that as the *PWF* increases, this will allow us to invest in thicker insulation in the cold climates due to the increase in the energy consumption savings which will compensate the initial investment costs.

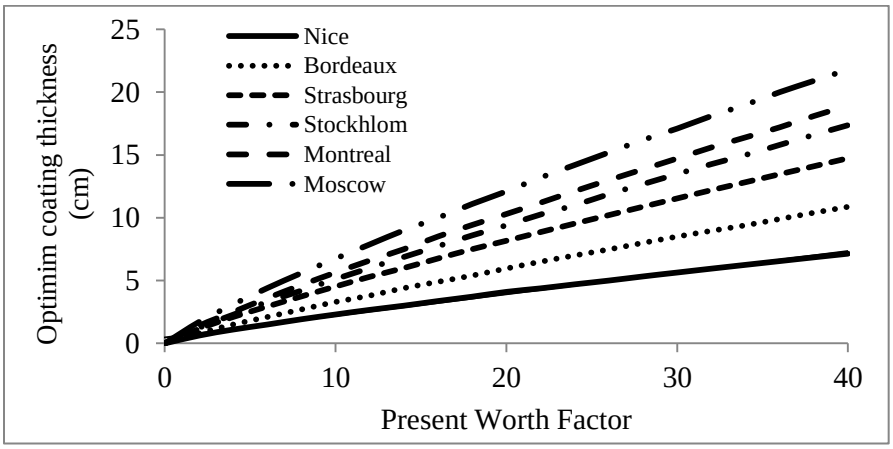

Fig. 4.36: Effect of present worth factor on the optimum coating thickness

Moving to the second influencing parameter, Fig. 4.37 shows the optimum coating thickness for different aerogel's costs: 600, 800, 1000, 1500, and 2000 €/m^3. It is expected that as the cost increases, the optimum value decreases. This is due to the higher initial cost associated with the application of the coating making it difficult to recover this cost from the energy savings.

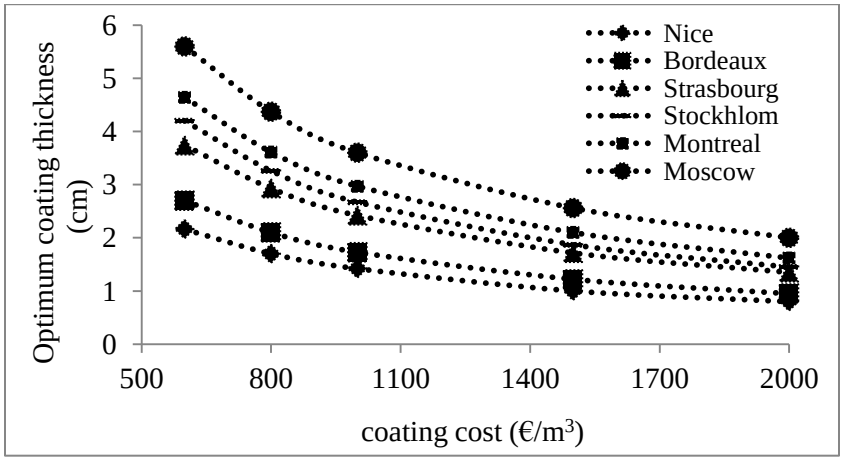

Fig. 4.37: Effect of the coating cost on the optimum thickness

The third parameter is the heating set-point. The variation of the optimum thickness as a function of the heating set-point is shown in Fig. 4.38. It is illustrated that the optimum thickness varies linearly with the heating set-point. As the heating set-point increases, meaning that the annual heating consumption increases, the optimum thickness increases.

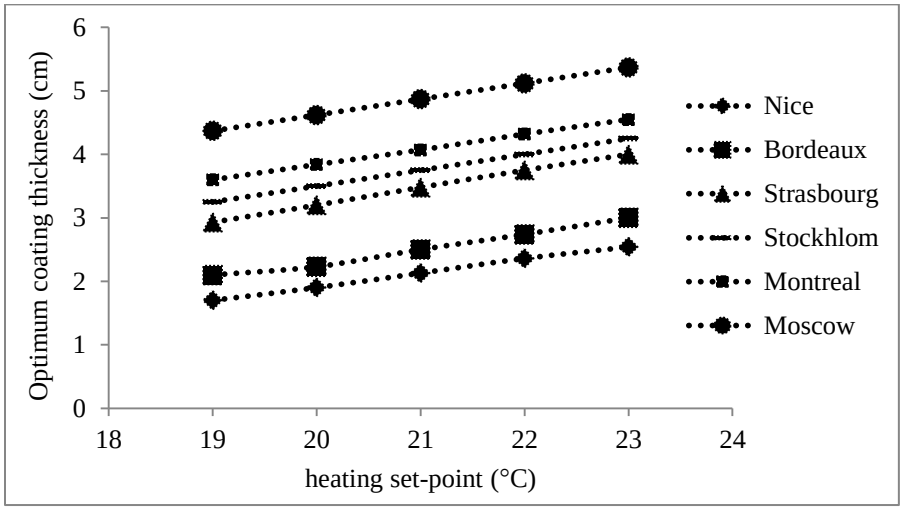

Fig. 4.38: Effect of the heating set-point on the optimum coating thickness

6. Wall Active Loop System Performance

6.1. Introduction

As previously stated, the concept of the active wall loop system (WALS) is to capture the wasted solar energy falling on the south facade available during non-cloudy winter days and transfer it to the north facade through water pipes embedded in the outside aerogel-based coating. The coating's projection technique manually or through spraying using a plastering machine allows the easy implementation of this system for retrofitting old buildings or for the application in new buildings as well. After presenting the mathematical model (developed in MATLAB®) in chapter 2, we present here the methodology to examine the performance of this system on a full-scale house through co-simulation. Then, a case study is considered and simulation results under different climates are presented and discussed.

6.2. Coupling Strategy

Fig. 4.39 shows how to link EnergyPlus to MATLAB® using BCVTB. The outputs of

EnergyPlus are inputs to MATLAB® and vice versa. At each time step taken as 15min, for a simulation period of 1 year, the two programs exchange information as following:

1- EnergyPlus sends to MATLAB® through BCVTB the following:
   - indoor and outdoor air temperatures
   - external wall surface total incident solar radiation for the north and south facades
   - sky temperature
   - internal surface temperatures of all the room's other walls and windows (except the south and north walls embedding the pipes)
2- Using these inputs as boundary conditions, the MATLAB® code calculates the temperature field within the wall embedding the pipes in the south facade.
3- The exit water temperature from the south water loop is an inlet water temperature for the north facade.
4- The MATLAB® code calculates the temperature field within the wall embedding the pipes in the north facade water loop.
5- The resulting internal surface temperatures for the south and north wall areas, where the water pipes are present, are sent back to EnergyPlus.
6- For these wall parts, EnergyPlus is forced to set the inner surface temperatures to the values received from MATLAB®.

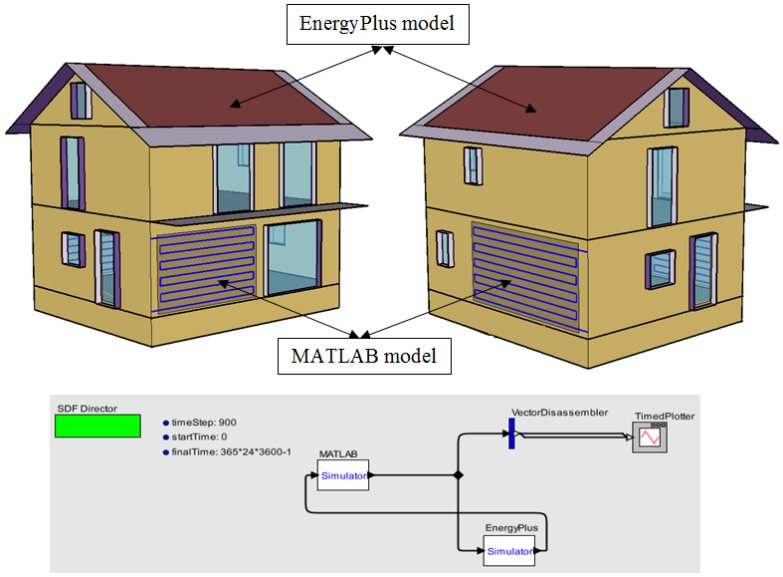

Fig. 4.39: EnergyPlus and MATLAB Co-simulation through BCVTB

6.3. Coupling Validation

To validate the coupling methodology, a one-dimensional heat transfer wall model is coupled to the EnergyPlus model. The south wall is chosen to be the examined wall. If the coupling strategy functions well, it should approximately generate the same values for the south wall interior surface temperature compared to the values calculated by EnergyPlus alone.

Fig. 4.40 shows the internal wall surface temperatures resulting from EnergyPlus (standalone) and from the coupling through BCVTB. A very good agreement is obtained between the two where the maximum absolute error doesn't exceed 0.3°C.

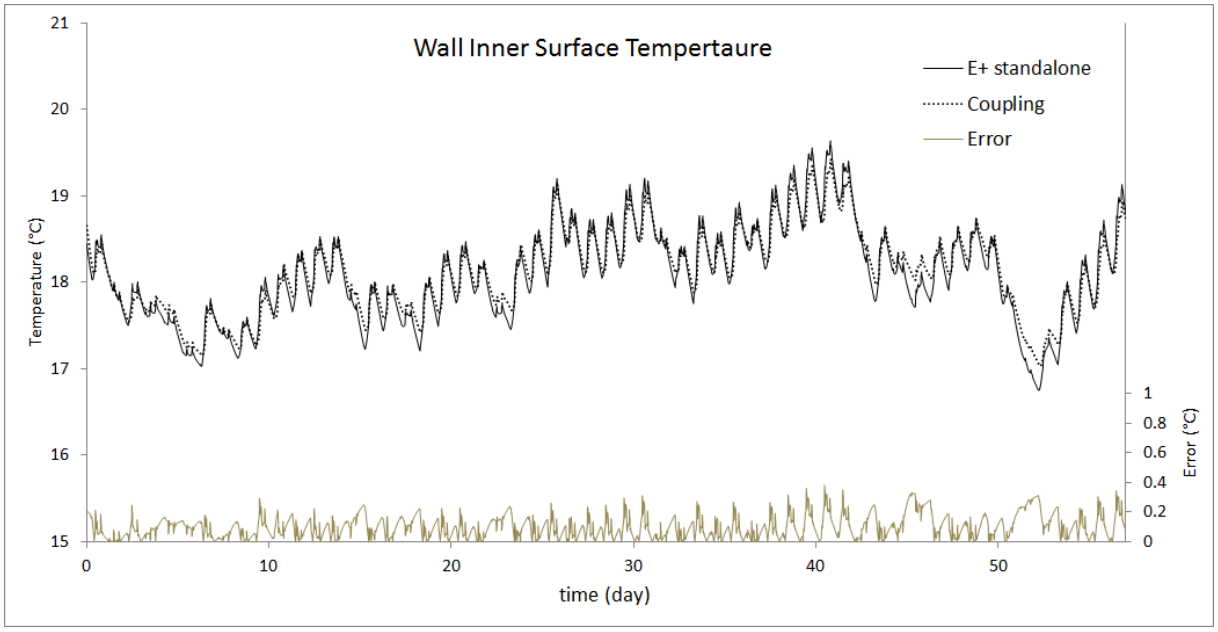

Fig. 4.40: Inner wall surface temperature resulting from EnergyPlus (E+) standalone and from the coupling strategy.

6.4. Simulation Results

The simulations are carried out using the design parameters presented in Table 4.7. Five cities are chosen: Nice (latitude 43.7° N, longitude 7.266° E) at the Mediterranean coast, Bordeaux (44.84° N, 0.58° W) and Nantes (47.22° N, 1.553° W) in the lower and upper Oceanic region, and Clermont Ferrand (45.78° N, 3.082° E) and Strasbourg (48.58° N, 7.748° E) in the lower and upper Semi-Continental region. All the simulations are carried out for the climates of these five cities. The source of the weather files is the International Weather for Energy Calculations (IWEC) (ASHRAE IWEC 2001). The IWEC data files are typical weather files

suitable for use with building energy simulation programs. These are derived from up to 18 years of archived hourly weather data.

Table 4.7: Case study design parameters

South wall area having the WALS	10 m²
North wall area having the WALS	10 m²
Pipe diameter	1.5 cm
Pipe spacing	10 cm
Pipe Material	Polyethylene
Pipe thermal conductivity	0.4 W/(m.K)
Water mass flow rate	0.01 kg/s
Exterior Walls Construction • Coating thickness • Concrete Thickness • Solar absorptivity	 5 cm 15 cm 0.6

A simple ON/OFF control strategy for the pump is adopted based on the intensity of solar radiation. If the south wall solar radiation is greater than a threshold value ($I_{control}$), then the pump is set to "ON". Otherwise, it is set to "OFF". To choose $I_{control}$, simulations are carried out for the month of January (for Nice) using different values of $I_{control}$, and for each case the heating load is computed as shown in Fig. 4.41. From this figure, the control solar radiation is taken as 150 W/m². The solar absorptivity of the south facade has a great influence on the system's performance. Increasing this value will increase the amount of captured solar radiation; thus, increasing the heating energy transferred to the space.

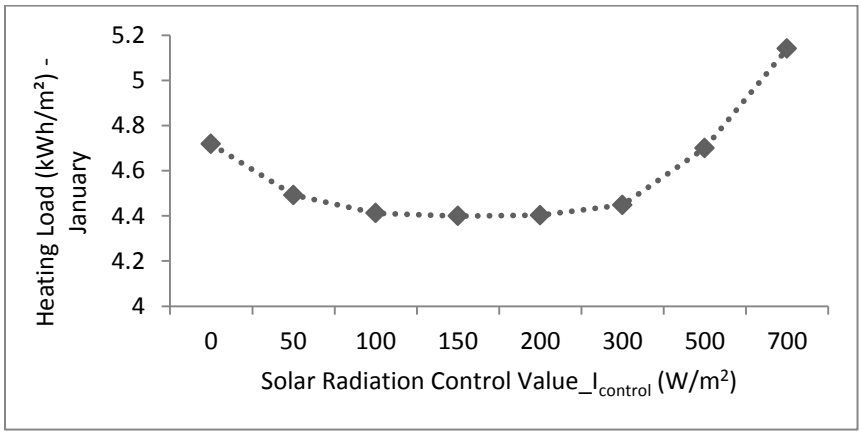

Fig. 4.41: Heating load (January - Nice) for different solar radiation control values (Icontrol)

Fig. 4.42 shows the annual heating load for the old and the new house with and without the WALS for the different climates of France. Also, it shows the effective heating energy added to the space. This is calculated as the difference between the energy load with the WALS and the energy load without this system. For both the new and old house, the insulating coating is present on the exterior facades, so the difference lies in the presence of the water pipes. The reference case does not have water pipes embedded in the coating.

The air change rate for the old house is taken as 0.4ach (due to infiltration) and for the new houses 0.8ach (due to both infiltration and ventilation). Note that these air change rates are taken as a base case; later, these values are varied.

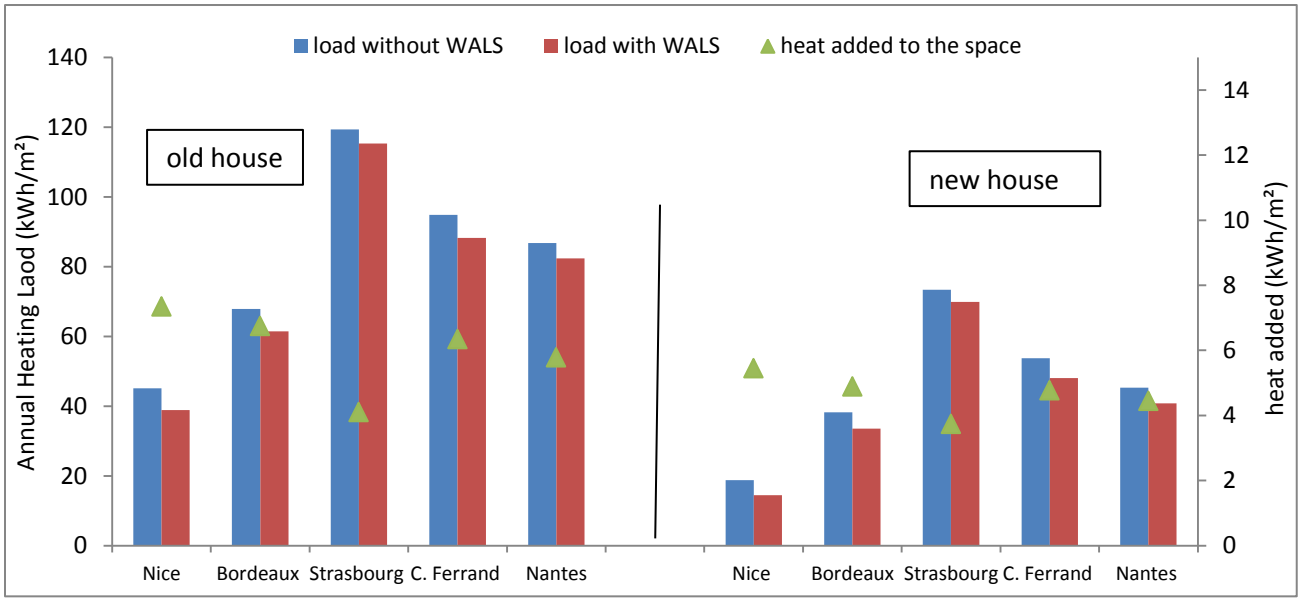

Fig. 4.42: Annual heating load for the old and new houses with and without the WALS

For the Mediterranean climate (Nice), WALS decreases the annual heating load by about 22% and 13% for the new and old houses, respectively. The percentage reduction is lower for the old house because of the poor thermal performance of its windows, ceiling, and floor. For the new house, the heating load coming from the walls represents a higher percentage of the total load than that of the old house. Lower reductions are obtained for the Oceanic climate (Bordeaux and Nantes) and the lower Semi-Continental climate (Clermont Ferrand) where the WALS decreases the annual heating load by about 10-13% for the new house and about 6-9% for the old house, respectively. For the upper Semi-Continental region (Strasbourg), the reductions are 3% and 4%

for the new and old houses. This is due to the fact that the solar radiation is more present and the outside air temperatures are higher in the Mediterranean climate than those in the other climates. To illustrate this more, the energy of the total incident solar radiation on the south facade during the winter and inter-seasons (fall and spring), taken from October till April, is plotted in Fig. 4.43 for the different cities. As we go higher in the latitude, the amount of solar radiation decreases. For example, for the city of Nice (latitude 43.7° N), the total solar irradiation incident on the south wall is around 663 kWh/m²; however, for the city of Strasbourg (latitude 48.58° N), it is around 360 kWh/m². Note that for the cold climates such as Strasbourg, the use of a glycol/water mixture is necessary. Although this might affect the system's efficiency, simulations are not carried out with this mixture because, even with just water, the system has not shown to be so effective in such climates.

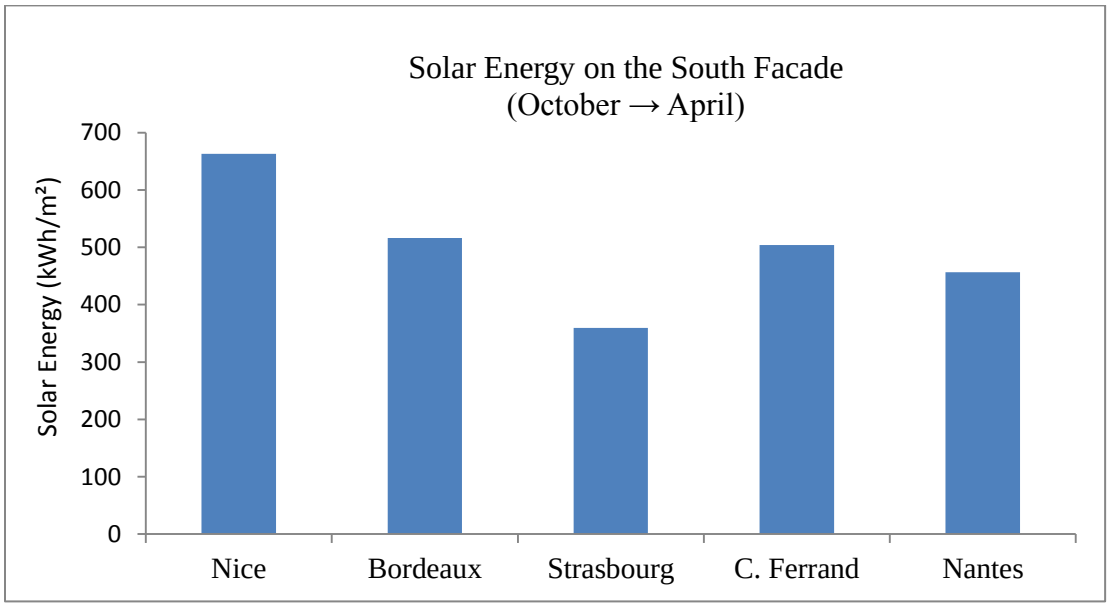

Fig. 4.43: Available south wall solar radiation during the period from October to April

Fig. 4.44 shows the percentage reduction in the annual heating load for the old and new houses adopting the WALS with respect to the houses without this system for different air change rates. For the old house, the air change rate (ACR) is varied from 0.2ach to 0.6ach, while for the new house, it is varied from 0.4ach to 0.8ach. From these figures, it is shown that as the ACR decreases, the relative (percentage) reductions in the heating load increases. As an illustration, the percentage reduction increases from 11% to 15% when the air change rate is decreased from

0.6ach to 0.2ach for an old house located in Nice, and it increases from 22% to 33% when the ACR is decreased from 0.8ach to 0.4ach for a new house located in Nice.

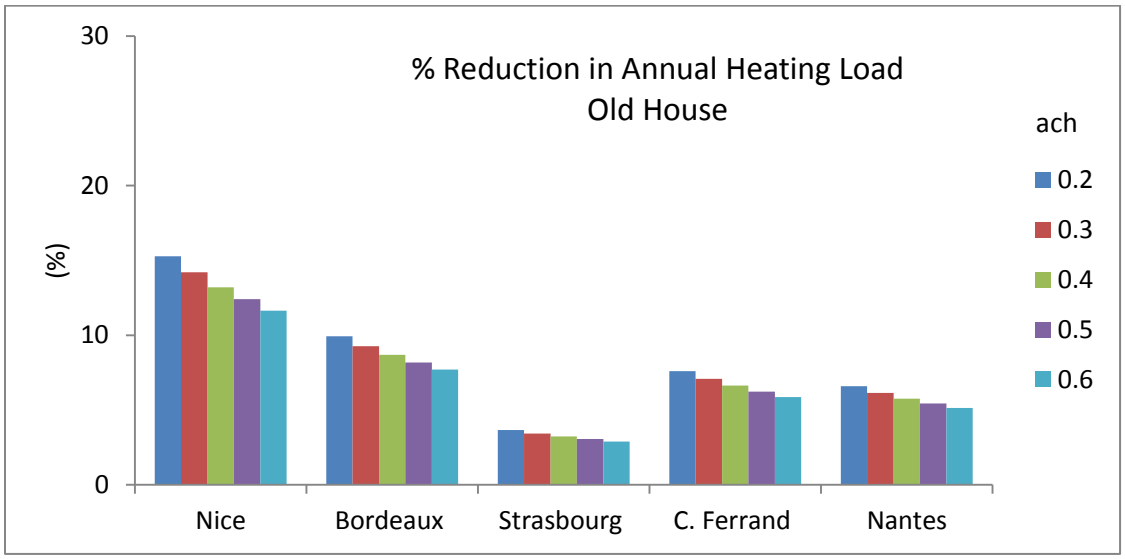

(a)

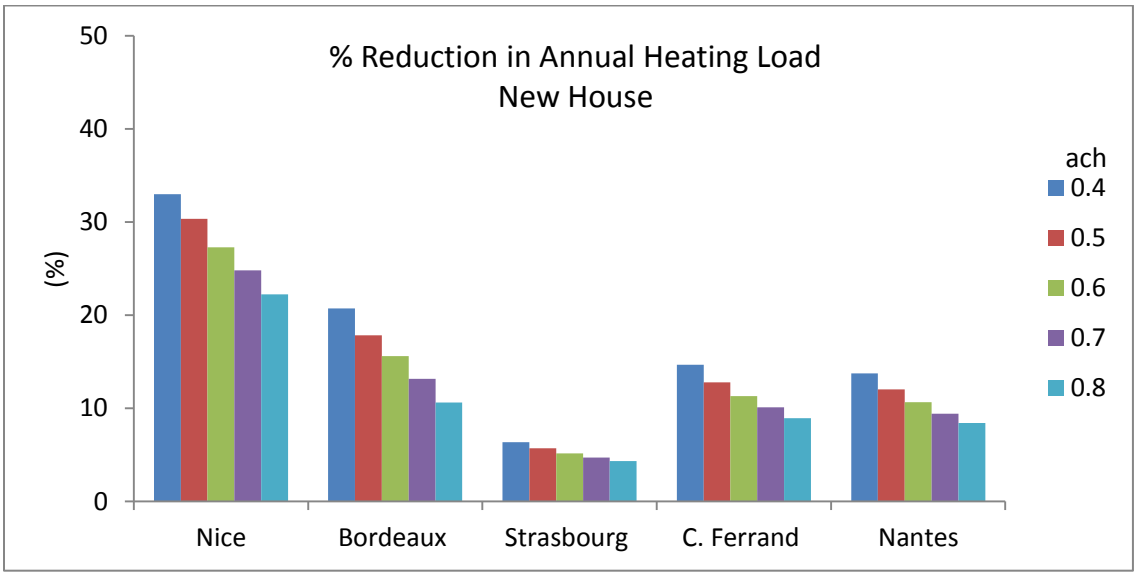

(b)

Fig. 4.44: Percentage reduction in the annual heating load compared to the houses without WALS for (a) old houses and (b) new houses

Now, we examine the impact of applying the WALS on the heat losses through the north facade. Fig. 4.45 shows the sum of the heat losses through the north facade. For the new houses, the heat losses are almost eliminated through this facade for the city of Nice where the heat loss reductions can reach 80%. For Bordeaux, C. Ferrand, and Nantes, the reductions are between

37% and 48%. For Strasbourg, it is 20%. For the old houses, the percentage reductions are lower. These are 60%, 41%, 32%, 28%, and 16% for Nice, Bordeaux, C. Ferrand, Nantes, and Strasbourg, respectively.

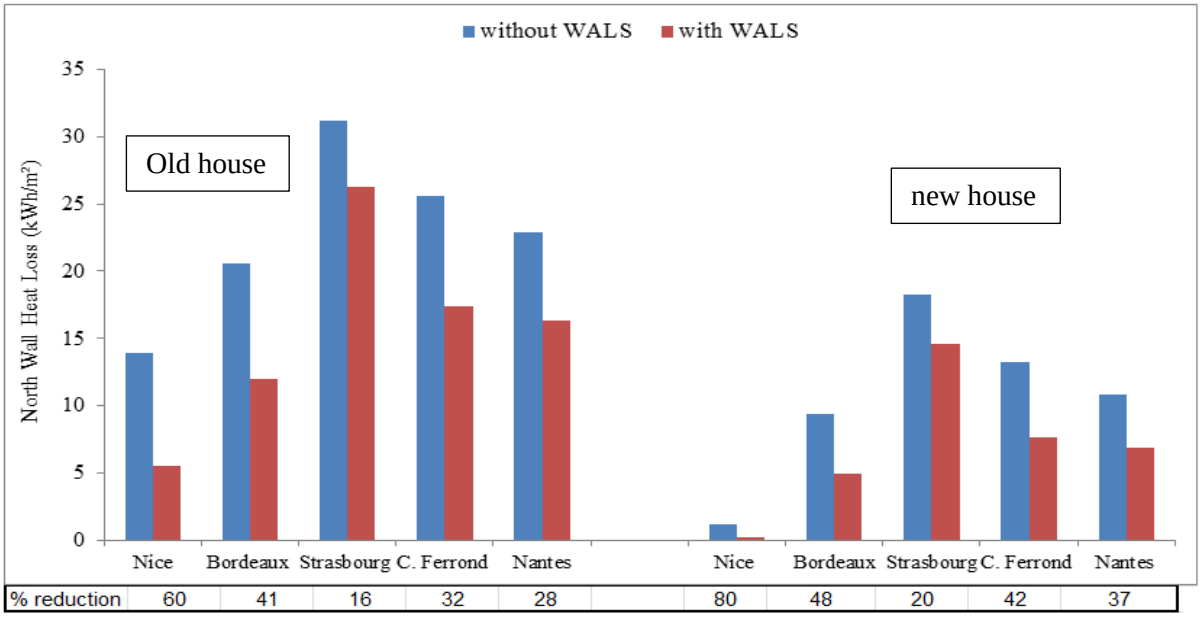

Fig. 4.45: North wall heat losses for houses with and without the WALS, and their corresponding percentage reductions

Fig. 4.46 shows the outside air temperature, the south wall total incident solar radiation, and the north wall inner surface temperatures with and without the WALS for the new house case for three weeks in January for Nice and Bordeaux. For the other cities, the temperatures show similar trends; thus, we are not showing them here. For sunny days, the north wall temperature starts to increase at the afternoon (at 1p.m.) due to the heat received from the heated water passing from the south to the north facades. It reaches its maximum value at approximately 6p.m. then starts to decrease where the wall dissipates its energy to the inside space. Due to the energy storage in the north wall's thermal mass, we can see that the temperature decreases slowly at night providing heat to the space. This is very important in residential buildings where you need to supply heat to the space at night when it gets cold outside. The north inner surface temperatures can reach 3°C more for the house with the WALS than those for the house without this system for Nice and Bordeaux climates. The inlet and outlet water temperatures of the south loop are shown in Fig. 4.47. For sunny days, the water temperature out of the south facade can reach more than 30°C. The energy consumption of the circulating pump is calculated and the

obtained results show that this energy could be neglected compared to the heating energy transferred to the house.

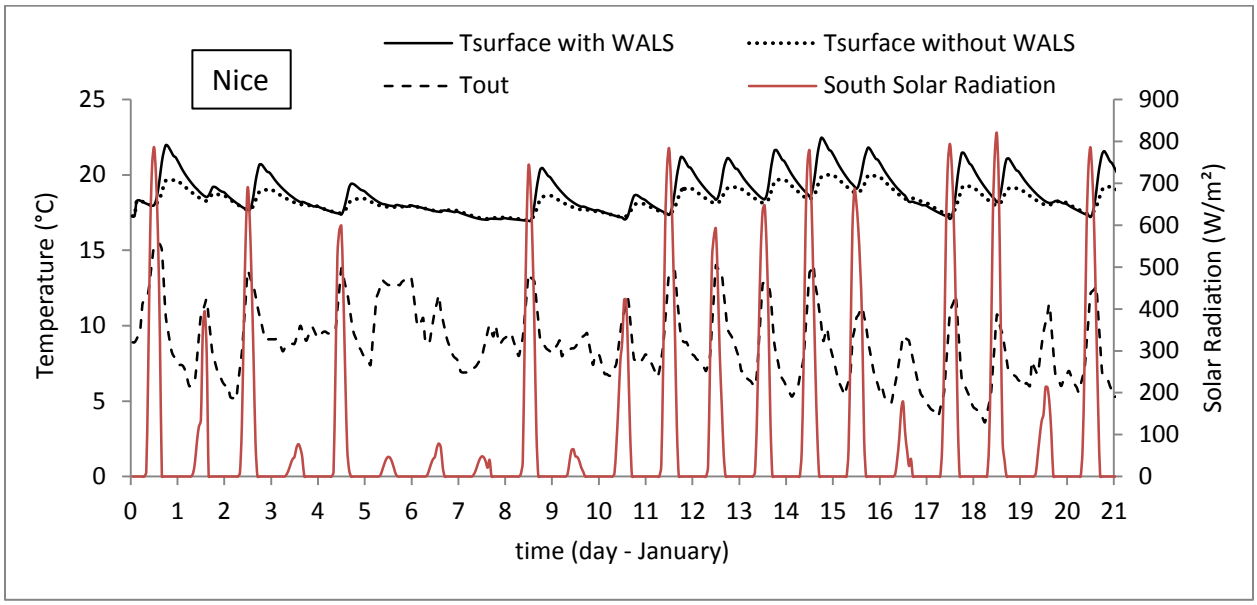

(a)

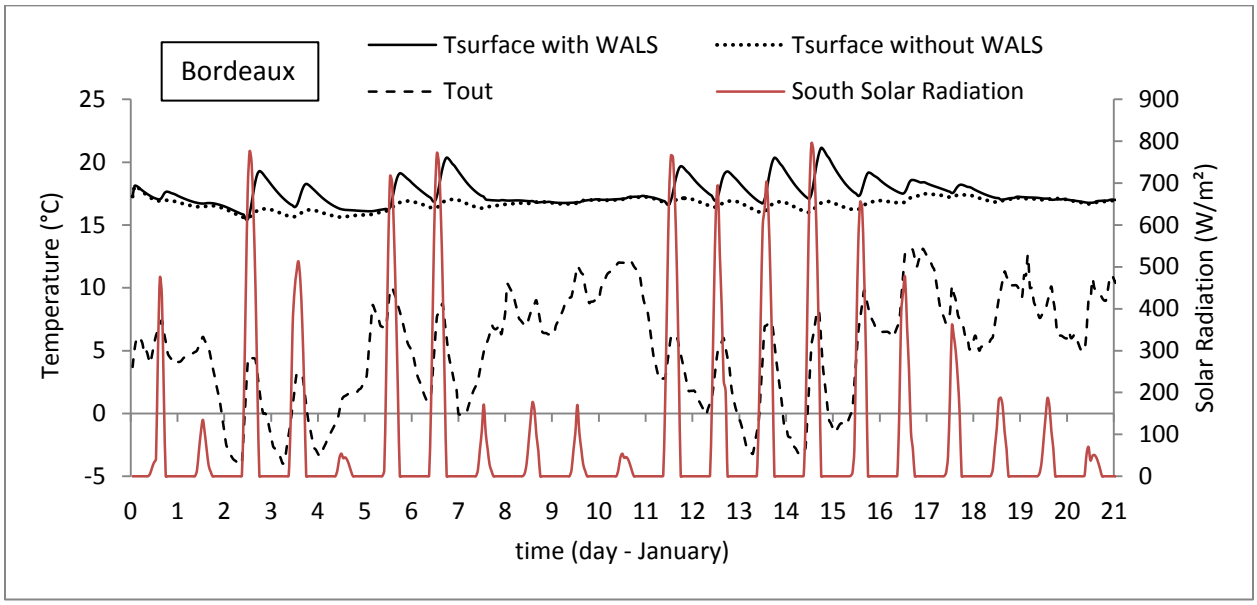

(b)

Fig. 4.46: North wall inner surface temperature with and without the WALS, outdoor air temperature, and south wall solar radiation intensity

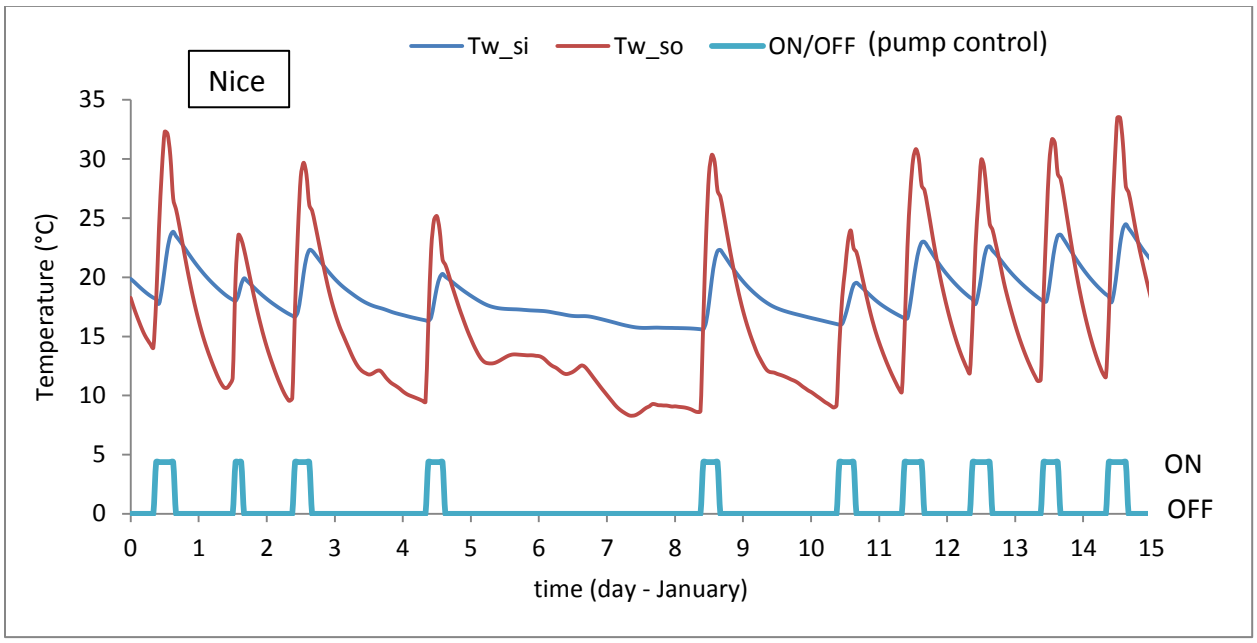

Fig. 4.47: South wall outlet (Tw_so) and inlet (Tw_si) water temperatures, and the pump operation strategy

6.5. System Optimization

The objective here is to optimize the system's performance by optimizing the water mass flow rate ($\dot{m}$) for different pipe's inner diameters (D). The inner diameter is varied from 1cm to 2.5cm and for each diameter the mass flow rate is varied from 0.003 kg/s to 0.05 kg/s. All these cases are simulated during the months of December and January for the weather of Nice. The optimum design is the one that ensures the lowest heating load during the simulation period.

Fig. 4.48 shows the heating load as a function of the water mass flow rates for different pipe's diameters. As shown in this figure, for a certain water mass flow rate, increasing the pipe's diameter decreases the space heating load. This is because increasing the diameter will increase the heat transfer area between the water pipes and the wall's structure.

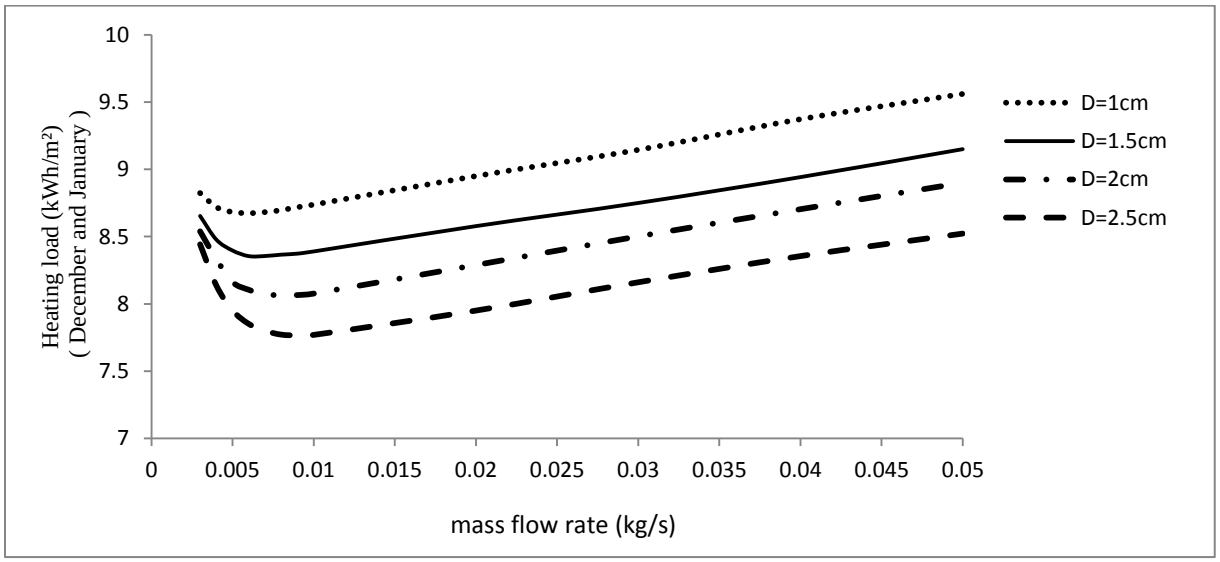

Fig. 4.48: Heating load as a function of the water mass flow rate for different pipe's diameter

As $\dot{m}$ increases, the heating load decreases to a certain minimum then starts to increase. It is noted that as D increases, this minimum shifts to the right meaning a bigger $\dot{m}$. The appropriate pipe diameter should be chosen depending on the available wall thickness. This optimization results depend on the case study; i.e. the capture and the sink wall surface areas, here taken as $10m^2$.

6.6. Summary

A case study is taken: $10m^2$ capturing area (south area embedding the water pipes) and $10m^2$ sink area (north facade). Annual simulations are carried out for five cities representing the different climatic regions of France for an old and a new house. Results show that reductions in the annual heating load for the house adopting the WALS relative to the one without this system are between 22-33% for new houses and 12-15% for the old houses for the Mediterranean climate. For the Oceanic and the lower Semi-Continental climates, the reductions are around 11-22% for new houses and 7-10% for the old ones. Lower reductions, 3-7%, are obtained for the upper Semi-Continental climate. Examining the heat losses through the north facade, these are reduced by about 60% and 80% for the old and new house, respectively, for the Mediterranean climate. For the Oceanic and lower semi-continental climates, the reductions are about 30-50%, and for the upper semi-continental one, these are between 16-20%.

7. Conclusion

In this chapter, simulations are carried out. Firstly, we compared different wall structure configurations under different operation modes of the heating system. It is shown that the aerogel coating has a good performance due to possessing low thermal conductivity and moderate thermal mass. Secondly, a hygrothermal assessment is done for different thermal insulation configurations. The results show that adding the aerogel-based coating on the exterior surface of the un-insulated or the already internally insulated walls reduces significantly or removes the moisture risks. Thirdly, the effect of adding the coating on the exterior surfaces of houses is examined. It is concluded that the coating has a maximum impact on the old houses which are poorly insulated. The heating load can be reduced up to 50%. Also, it increases the thermal comfort during the winter season by decreasing the cold wall effects. For moderately insulated buildings, such as those built in the 80's and 90's with their exterior walls made of brick-monomur (20cm) or made of concrete with a 5 to 7cm layer of interior thermal insulation, the reductions in the heating load can reach up to 25% when adding the coating. This is important for these houses to pass the newly imposed strict thermal regulations for buildings and be classified as energy efficient. For new buildings, lower reductions are achieved (7-12%) when adding the coating. This is due to the fact that the exterior envelope is already highly insulated. Thus, we can conclude that the coating has a significant effect when considering existing building rehabilitation. For new buildings, the coating has a lower effect on the energy consumption; however, these buildings will be considered as highly energy efficient ones. From another aspect, the coating can lead to overheating in the summer period which can be overcome by adopting night ventilation. Finally, the wall active loop system has shown a good performance in climates where there is a potential of solar radiation in the winter season.

8. Résumé du Chapitre en Français

Après l'élaboration et la validation des modèles mathématiques et numériques dans les chapitres 2 et 3, ce chapitre présente tous les résultats de simulation. D'abord, nous commençons par l'examen de la performance thermique et hygrothermique des murs extérieurs recouverts par l'enduit à base d'aérogel. Ensuite, nous examinons l'impact de l'enduit pour limiter les pertes de chaleur par les ponts thermiques. Après cela, nous étudions le comportement de confort thermique et énergétique des maisons adoptant le revêtement étudié comme isolation extérieure. Enfin, le potentiel de réduction du besoin de chauffage en adoptant le système de façade active dans les murs est analysé.

Concernant la performance thermique, l'objectif est d'optimiser la composition des couches des murs extérieurs pour les cas suivants: (1)- chauffage continu (2) chauffage intermittent et (3) pas de chauffage. Plusieurs paramètres d'évaluation sont considérés pour les différents cas: l'indice de confort, le facteur d'amortissement, le déphasage et la besoin de chauffage. Six configurations de mur sont examinées: 1- isolation par l'extérieur, 2- isolation par l'intérieur, 3- isolation par l'intérieur et l'extérieur, 4- isolation au milieu du mur, 5- isolation au milieu et à l'extérieur et 6- isolation au milieu et à l'intérieur. Nous avons choisi comme matériaux isolants: le polystyrène expansé, la laine de verre et l'enduit à base d'aérogel de silice. Pour le chauffage continu, nous avons déduit que l'enduit a une meilleure performance en le comparant avec les isolants traditionnels. Puisqu'il possède la plus faible conductivité thermique et la capacité thermique la plus élevée. De plus, le fait de placer l'isolant au milieu du mur et à la surface extérieure permet d'améliorer la performance. En cas d'un chauffage intermittent, l'isolation interne est la meilleure solution si la consommation d'énergie est le paramètre d'évaluation. Le revêtement présente de meilleures performances en raison de sa basse conductivité thermique. Pour les espaces non chauffés, la meilleur performance sera assurée en plaçant l'isolant au milieu du mur et à la surface extérieure, si on considère le facteur d'amortissement et le décalage comme paramètres d'évaluation. Concernant la performance hygrothermique, les objectifs sont d'examiner celle des murs couverts par l'enduit et de comparer avec celle des différentes configurations d'isolant thermique. Différents assemblages de murs sont considérés: aucune isolation, isolation par l'intérieur, isolation par l'extérieur et isolation par l'intérieur et l'extérieur. Plusieurs critères d'évaluation sont utilisés tels que la teneur en eau, le taux de

séchage, le risque de condensation, et les pertes de chaleur. Les résultats montrent que les systèmes d'isolation thermique par l'intérieur peuvent causer plusieurs problèmes d'humidité. L'ajout de l'enduit d'aérogel sur la surface extérieure des murs non isolés ou déjà isolés par l'intérieur réduit d'une manière significative ou même supprime les risques dus à sl'humidité. Il réduit aussi considérablement les pertes de chaleur du mur.

Concernant les ponts thermiques, nous proposons une méthodologie pour intégrer les effets du transfert thermique 2D dus aux ponts thermiques à EnergyPlus. Comme application, nous calculons la charge de chauffage des ponts thermiques du tableau des fenêtre savant et après l'ajout de l'enduit isolant sur les ponts thermiques. La méthodologie consiste à coupler le code de transfert de chaleur 2D développé dans MATLAB® à EnergyPlus, par co-simulation.

Ensuite, nous présentons un outil d'évaluation rapide basé sur des simulations destinées aux architectes, ingénieurs du bâtiment et les utilisateurs non experts pour qu'ils puissent examiner l'effet de revêtement sur le confort thermique et la consommation de l'énergie du bâtiment. Selon la période de construction, différents ratios de fenêtre-mur, épaisseurs d'isolation intérieure, type de construction des murs, etc. sont étudiés. En outre, tous sont examinés sous les différents climats de la France. La sortie de cet outil est la consommation d'énergie avec et sans le revêtement. Comme problème inverse, l'utilisateur peut entrer la consommation d'énergie et la sortie sera l'épaisseur du revêtement à mettre en oeuvre; Aussi, l'outil fournit une évaluation du confort thermique, basée sur des différents modèles de confort thermique.

Concernant le système de façade active, et comme indiqué précédemment, le concept de ce système est de capter l'énergie solaire de la façade sud disponible pendant les journées d'hiver non nuageuses et de transférer l'énergie captée à la façade nord par l'intermédiaire de canalisations d'eau incorporées dans l'enduit extérieur en aérogel. La technique de projection du revêtement par pulvérisation en utilisant une machine à projeter permet la mise en œuvre simple de ce système pour la rénovation de bâtiments anciens ou pour l'application dans les nouveaux immeubles. Nous présentons ici la méthodologie pour évaluer la performance de ce système sur une maison à grande échelle par co-simulation. Ensuite, une étude de cas est examinée. Les simulations annuelles sont effectuées pour cinq villes représentant les différentes régions climatiques de France pour une maison ancienne et une nouvelle. Les résultats montrent que les réductions de la charge annuelle de chauffage pour la maison en adoptant ce système par rapport

à celle qui n'en est pas équipée sont entre 22 et 33 % pour les maisons neuves et entre 11 et 15 % pour les maisons anciennes pour le climat méditerranéen. Pour le climat Océanique, les réductions sont d'environ 11 à 22 % pour les maisons neuves et 7 à 11 % pour les maisons anciennes. Pour le climat semi-continental, on obtient des réductions entre 4 et 8 %.

GENERAL CONCLUSION AND PERSPECTIVES

The objectives of this study are to examine the thermal behavior and to foster energy efficiency of buildings through the use of a newly developed aerogel-based insulating coating as well as the use of renewable energy sources, specifically solar energy.

In the first part, we present a literature review concerning heat transfer and thermal behavior of buildings as well as thermal comfort. We also present the progress in the building construction of the houses in France since before the World War 2 till the current time. Furthermore, some of the building thermal and energy modeling methods and energy simulation tools are examined.

In the second part, all the mathematical and numerical models needed to carry out all the simulations are developed after explaining the objectives behind developing them. These are the one and two-dimensional conduction heat transfer models, the one-dimensional heat and moisture (hygrothermal) transfer model, the whole building thermal model, and the active embedded pipe wall loop system model. The results of these models are compared to the results of analytical solutions, the results of commercial softwares, or to those of some published data in the literature.

In the third part, we present all the experimental set-ups carried out to validate the mathematical models. It consists of three main parts: an experimental test-cell used to validate the one-dimensional thermal and hygrothermal numerical models, a full-scale experimental house to validate the whole building EnergyPlus energy model, and a mock-up experiment for the validation of the active wall loop system numerical model.

Finally, the fourth part deals with all the simulation results. We start by examining the thermal and hygrothermal performance of exterior walls covered with the aerogel-based coating. Different wall construction techniques under different operation modes of the heating system are studied. Then, we examine the impact of the coating on limiting thermal bridge heat losses. We proposed a methodology to incorporate the 2D thermal bridge effects into a whole building energy simulation software. As an application, the heat losses through the windows edges of an external insulated envelope are examined with and without the coating on these edges. After that we move to study the energy and thermal comfort behavior of houses adopting the coating as external insulation. The heating energy demand as well as the risk of summer overheating is estimated for different houses' construction periods. Finally, the potential to decrease the heating

load by adopting the wall active water pipe as assisting heating system is scrutinized. This system is tested for old and new houses under different climates.

The results have shown that when retrofitting old houses, this coating reduces significantly the energy consumption. For new buildings, lower reductions are achieved but this may be necessary to pass the strict thermal regulations (RT 2012). On an envelope scale, the position and number of insulation layers within the wall are very important and this should be optimized by linking the thermal behavior of exterior walls to the real operation of the heating system. Also, interior thermal insulation systems can cause several moisture problems. Adding the aerogel-based coating on the exterior surface of the un-insulated or the already internally insulated walls reduces significantly or removes the moisture risks. Concerning the assisting heating systems, the active embedded pipe wall loop system has shown a good performance in climates where solar radiation is available during the winter season.

Some of the results of the current work are published in peer-reviewed journals. One *French Patent* application has been submitted concerning the "Active Wall Loop System" (Wurtz and Ibrahim 2013). Four journal papers were published or accepted for publication. The first paper, entitled "Limiting windows offset thermal bridge losses using a new insulating coating", is published in *"Applied Energy"* (Ibrahim et al. 2014). The second one, entitled "A study on the thermal performance of exterior walls covered with a recently patented silica-aerogel-based insulating coating", is published in *"Building and Environment"* (Ibrahim et al. 2014). The third one, entitled "Hygrothermal performance of exterior walls covered with aerogel-based insulating rendering", is published in *"Energy and Buildings"* (Ibrahim et al. 2014). The fourth one, entitled "Transferring the South Solar Energy to the North Facade through Embedded Water Pipes", is accepted for publication in *"Energy"* journal (Ibrahim et al. 2014). Other than these, one journal paper, entitled "Building envelope with a new aerogel-based insulating coating: experimental and numerical study, cost analysis, and thickness optimization", is sent to *"Applied Energy"* journal. Its current status is "under review".

Yet, a lot of work is still needed to be done. It is a very interesting challenge to examine the suitability of applying the coating to limit different types of thermal bridges (due to chimneys for example) and also singular points such as acroterions (vertical wall termination at flat roof junction). Also, the feasibility of using the aerogel-based coating should be compared to other

insulating plasters or insulating materials based on current and future cost and performance predictions. This should be done for different types of house constructions (not-insulated, medium-insulated and high-insulated houses) under different climates.

In our study here, the thermal behavior of buildings adopting the aerogel-based coating as external thermal insulation is studied mainly for European cold climates. An interesting thing is to examine this behavior under hot and very hot climates such as the Saharan ones and try to optimize the envelope as a whole: glazing type and size, insulation thickness, orientation, etc. Furthermore, a detailed life-cycle analysis is important to show the efficiency of such insulating materials through the whole life time of the building. When considering a life-cycle assessment, it is necessary to evaluate the evolution of the coating's characteristics over time (especially the thermal conductivity) to examine the effect of aging on the coating's performance. From another aspect, research should continue to focus on improving the aerogel manufacturing techniques for the aim of reducing the cost of aerogel-based materials. Concerning the wall active loop system, the testing of these systems on a full-scale house and in different climates is essential. In addition, a methodology should be proposed for sizing and optimizing the performance of these systems depending on different variables and constraints. Also, a more robust control strategy should be adopted to improve its performance. Furthermore, we should try to improve the system's design or to find alternative solutions in order to improve the performance, especially in the cold climates.

*Résumé de la Conclusion en Fran*çais

L'objectif de ce travail est d'étudier l'amélioration du comportement thermique et l'économie d'énergie possible pour des bâtiments par l'utilisation de nouveaux enduits isolants à base d'aérogel et aussi d'énergies renouvelables, notamment l'énergie solaire.

Le premier chapitre de la thèse présente l'état de l'art sur l'analyse du comportement thermique du bâtiment. En outre, certaines méthodes de modélisation thermique et des outils de simulation énergétique sont examinés.

Le deuxième chapitre décrit les modèles mathématiques et numériques utilisés pour cette étude; Les résultats de ces modèles sont comparés aux résultats de solutions analytiques, à des résultats de logiciels commerciaux, ou aux données publiées dans la littérature. Le troisième chapitre explique toutes les expériences qui ont été faites pour valider les modèles numériques. Il est constitué de trois parties principales correspondant chacune à une expérimentation: une cellule-test expérimentale ayant pour objectif de valider le modèle numérique thermique et hygrothermique en 1D, une maison expérimentale à pleine échelle pour valider le modèle thermique du bâtiment entier développé avec EnergyPlus et la troisième partie concerne une maquette pour valider le modèle numérique du système de façade active.

Après l'élaboration et la validation des modèles mathématiques et numériques dans les chapitres 2 et 3, le quatrième chapitre présente tous les résultats de simulation. D'abord, nous commençons par l'examen de la performance thermique et hygrothermique des murs extérieurs recouverts par l'enduit à base d'aérogel. Ensuite, nous examinons l'impact de l'enduit pour limiter les pertes de chaleur par les ponts thermiques. Après cela, nous étudions le confort thermique et le comportement énergétique des maisons adoptant le revêtement étudié comme isolation extérieure. Enfin, le potentiel de réduction du besoin de chauffage en adoptant le système de façade active dans les murs est analysé.

Les résultats ont montré que, pour la réhabilitation de maisons anciennes, ce revêtement réduit considérablement la consommation d'énergie. Il devrait donc trouver dans ce secteur applicatif de larges débouchés. Dans les murs extérieurs, la position et le nombre de couches d'isolation sont très importants et cela devrait être optimisé en reliant le comportement thermique de ces murs avec le fonctionnement réel du chauffage. En outre, les systèmes d'isolation thermique par

l’intérieur peuvent augmenter le niveau d’'humidité dans le bâtiment. L’ajout de l’enduit à base d'aérogel sur la surface extérieure des murs non isolés ou des murs isolés par l’intérieur permet de réduire de manière significative les risques dus à l'humidité. Concernant le système de façade active, une bonne performance a été démontrée pour des murs orientés au sud dans les climats où le rayonnement solaire est disponible en hiver.

En perspectives, beaucoup de travail reste à faire. Dans toutes nos études, le comportement thermique des enveloppes de bâtiment, adoptant l’enduit à base d'aérogel comme isolation par l’extérieur, est étudié principalement pour les climats froids en Europe. Il serait intéressant d'examiner la performance de ce revêtement dans des climats chauds ou très chauds. En outre, il serait très important de mener une analyse détaillée du cycle de vie afin de montrer l'efficacité de tels matériaux isolants à travers la durée de vie entière des bâtiments. Il serait également très intéressant d'examiner de manière approfondie la pertinence de l'application de l'enduit sur les différents types de ponts thermiques. Concernant le système de façade active, il est essentiel de tester ce type de système sur une maison à grande échelle et dans des climats différents. De plus, une méthodologie doit être proposée pour dimensionner et optimiser la performance de ce type de système.

REFERENCES

Achard P., Rigacci A., Echantillac T., Bellet A., Aulagnier M., Daubresse A. Enduit isolant à base de xerogel de silice. WIPO Patent WO/083174, 2011.

ADEME (French Environment and Energy Management Agency), 2014. Buildings. Retrieved from http://www2.ademe.fr/servlet/KBaseShow?sort=-1&cid=96&m=3&catid=12846 on May 2014.

ADEME (French Environment and Energy Management Agency). Chiffres clés du batiment, 2009.

Alam M., Singh H, Limbachiya M.C., Vacuum insulation panels (VIPs) for building construction industry - a review of the contemporary developments and future directions. Applied Energy 2011; 88(11):3592–602.

Allinson D., Hall M. Hygrothermal analysis of a stabilized rammed earth test building in the UK. Energy and Buildings, 42 (2010), pp. 845–852

Al-Sanea S.A., Zedan M.F. Improving thermal performance of building walls by optimizing insulation layer distribution and thickness for same thermal mass. Applied Energy, 88 (2011), pp. 3113–3124

Al-Sanea S., Zedan M.F. Effect of thermal bridges on transmission loads and thermal resistance of building walls under dynamic conditions. Applied Energy 98 (2012) 584–593

Al-Sanea SA, Zedan MF, Al-Ajlan SA, Hadi ASA. Heat transfer characteristics and optimum insulation thickness for cavity walls. J Build Phys 2003;26(3):285–307.

Al-Sanea SA, Zedan MF, Al-Hussain SN. Effect of thermal mass on performance of insulated building walls and the concept of energy savings potential. Applied Energy 2012;89:430–42.

Analyse Détaillée du Parc Résidentiel Existant, Report 2009, www.reglesdelart-grenelle-environnement-2012.fr.

ANSI/ASHRAE 140. Standard Method of Test for the Evaluation of Building Energy Analysis Computer Programs, 2007

ANSI/ASHRAE 55. Thermal environmental conditions for human occupancy. American Society of Heating, Refrigerating and Air-conditioning Engineers Inc., Atlanta, USA, 2004.

ANSI/ASHRAE 55. Thermal environmental conditions for human occupancy. American Society of Heating, Refrigerating and Air-conditioning Engineers Inc., Atlanta, USA, 2004.

Antretter F., Sauer F., Schopfer T., Holm A.. Validation of a hygrothermal whole building simulation software Proc. of Building Simulation 2011, 12th Conference of International Building Performance Simulation Association, Sydney, (2011) 1694–1701

Asan H. Investigation of wall's optimum insulation position from maximum time lag and minimum decrement factor point of view. Energy and Buildings 32 (2000) 197–203.

Asan H. Numerical computation of time lags and decrement factors for different building materials. Building and Environment 41 (2006) 615–620

Asan H., Sancaktar Y.S. Effects of wall's thermophysical properties on time lag and decrement factor, Energy and Buildings 28 (1998) 159–166.

Ascione F., Bianco N., de'Rossi F., Turni G., Vanoli G. P. Different methods for the modeling of thermal bridges into energy simulation programs: Comparisons of accuracy for flat heterogeneous roofs in Italian climates. Applied Energy 97 (2012) 405–418

ASHRAE Standard 160. Criteria for Moisture-Control Design Analysis in Buildings; 2009

ASHRAE 2001. International Weather for Energy Calculations (IWEC Weather Files) Users Manual, Atlanta: ASHRAE

Aste N, Angelotti A, Buzzetti M. The influence of the external walls thermal inertia on the energy performance of well insulated buildings. Energy and Buildings 2009; 41:1181–7.

Augenbroe G.Integrated building performance evaluation in the early design stages. Building and Environment 27(2): 149-161, 1992.

Azer, N.Z., Hsu, S. The prediction of Thermal Sensation from Simple model of Human Physiological Regulatory Response. ASHRAE Trans., Vol.83, 1977.

Baetens R., Jelle B.P., Gustavsen A. Aerogel insulation for building applications: a state-of-the-art review. Energy and Buildings, 43(2011) 761-769.

Balocco C., Grazzini G., Cavalera A. Transient analysis of an external building cladding. Energy and Buildings, 40 (2008), pp. 1273–1277

Barbero S., Marco D., Ferrua C., and Pereno A. Analysis on existent thermal insulating plasters towards innovative applications: Evaluation methodology for a real cost-performance comparison. Energy and Buildings 77 (2014), 40-47.

Barrios G., Huelsz G., Rojas J. Thermal performance of envelope wall/roofs of intermittent air-conditioned rooms. Applied Thermal Engineering 40 (2012) 1-7

BCVTB v. 1.1.0. Lawrence Berkeley National Laboratory. Building Technologies Department, 2012. http://simulationresearch.lbl.gov/bcvtb.

Berglund L. Mathematical Models for Predicting the Thermal Comfort Response of Building Occupants. ASHRAE Trans., Vol.84. 1978

Berthou Y. Etude de parois de batiments passifs associant un materiau à changement de phase et une super isolation transparents. PhD thesis, Mines ParisTech, Sophia Antipolis, 2011.

Bisson A., Rigacci A., Lecomte D., Achard P. Effective thermal conductivity of divided silica xerogel beds. Journal of Non-Crystalline Solids, 350 (2004) 379-384.

Bisson A., Rodier E., Rigacci A., Lecomte D., Achard P. Study of evaporative drying of treated silica gels. Journal of Non-Crystalline Solids, 350, (2004) 230-237.

Bojic, M., Nikolic, N., Nikolic, D., Skerlic, J., Miletic, I. (2011). Toward a Positive-Net-Energy Residential Building in Serbian Conditions. Applied Energy; (88:7); pp. 2407-2419.

Bojic M., Yik F., and Sat P. The influence of thermal insulation position in building envelope on the space cooling of high rise residential buildings in Hong Kong, Energy and Buildings 33 (2001) 569-581.

Bolattürk A. Optimum insulation thicknesses for building walls with respect to cooling and heating degree-hours in the warmest zone of Turkey. Build Environ, 43 (2008), pp. 1055–1064

Bopshetty S.V., Nayak J.K., Sukhatme S.P. Performance analysis of a solar concrete collector Energy Conversion and Management, 33 (11) (1992)1007–1016

Boyano, A., Hernandez, P., Wolf, O. (2013). Energy demands and potential savings in European office buildings: Case studies based on EnergyPlus simulations. Energy and Buildings, 65, 19-28.

Cadiergues R. Consommation de chauffage : la récupération des apports gratuits. Promoclim E., 1986.

Campbell scientific hygrothermal sensor CS215; retrieved from http://s.campbellsci.com/documents/au/manuals/cs215.pdf on May 2014.

Campos A., Martín K., Mvuama C., Garcia C., Odriozola M., Sala J.M. The effect of thermal bridges on the thermal comfort of buildings, in: 4th International Building Physics Conference, Istanbul, Turkey, 2009.

Capozzoli A., Gorrino A., Corrado V. A building thermal bridges sensitivity analysis. Applied Energy 107 (2013) 229–243

Cappelletti F., Gasparella A., Romagnoni P., Baggio P. Analysis of the influence of installation thermal bridges on windows performance: the case of clay block walls, Energy and Buildings 43 (6) (2011) 1435–1442.

Case Study: Aerogel Insulation Converts Old Mill House Into Modern Energy-Saving Passive House , Retrieved from http://www.aerogel.com/markets/Case_Study_House_Renovation_ web.pdf

Case Study: Aerogel Interior Wall Insulation Reduces U-Values by 44%, Lowers Energy Use and Carbon Emissions, retrieved from http://www.aerogel.com/markets/Case_Study_Interior_ Wall_web.pdf

Case Study: Wood Framing Insulated with Aerogel Improves Energy Efficiency by 15%, retrieved from, http://www.aerogel.com/markets/Case_Study_Framing_web.pdf

Cengel Y.A. Heat Transfer: A Practical Approach, 2nd edition, McGraw-Hill, 2005.

Centre Scientifique et Technique du Bâtiment. Réglementation thermique, Paris, France; 2000.

Chan, A.L.S., Chow, T.T., Fong, K.F., Lin, Z. (2009). Investigation on Energy Performance of Double Skin Facade in Hong Kong. Energy and Buildings; (41:11); pp. 1135-1142.

Chuah, J. W., Raghunathan, A., & Jha, N. K. (2013). ROBESim: A retrofit-oriented building energy simulator based on EnergyPlus. Energy and Buildings, 66, 88-103.

Chiffres clés du batiment, Agence de l'Environnement et de la Maîtrise de l'Energie (ADEME) 2009.

Clark, G. and Allen C. The Estimation of Atmospheric Radiation for Clear and Cloudy Skies. Proceedings 2nd National Passive Solar Conference (AS/ISES), 1978, pp. 675-678.

Comakli K., Yuksel B. Optimum insulation thickness of external walls for energy saving, Applied Thermal Engineering 23 (2003) 473–479.

Cuce E., Cuce P.M., Wood C.J., Riffat S.B. Toward aerogel based thermal super insulation in buildings: A comprehensive review. Renewable and Sustainable Energy Reviews 34(2014) 273–299

Cuce E., Cuce P.M., Wood C.J., Riffat S.B. Optimizing insulation thickness and analysing environmental impacts of aerogel-based thermal superinsulation in buildings. Energy and Buildings 77, (2014) 28–39

D'Antoni M., Saro O. Massive Solar-Thermal Collectors: A critical literature review Renewable and Sustainable Energy Reviews 16 (2012) 3666–3679.

D'Antoni M., Saro O. Energy potential of a Massive Solar-Thermal Collector design in European climates. Solar Energy 93 (2013) 195–208

Dautin S. Réduction de modèles thermiques de bâtiments : amélioration des techniques par modélisation des sollicitations météorologiques. Thèse de doctorat, Université de POITIERS, 1997.

Delgado J., Ramos N., Barreira E., de Freitas V. A critical review of hygrothermal models used in porous building materials. Journal of Porous Media, 13 (2010), pp. 221–234

Dexter M.E., Bickle L.W. 1978. Dexter building shell elements as passive solar collectors; Proceedings of conference on systems simulation and economic analysis for solar heating and cooling. San Diego, CA (162-164)

DIN EN 15026. Hygrothermal performance of building components and building elements -Assessment of moisture transfer by numerical simulation; 2007

Djunaedy, E., 2005. External coupling between building energy simulation and computational fluid dynamics. Thesis (PhD). Technische Universiteit Eindhoven.

Dowson M., Grogan M., Birks T., Harrison D., and Craig S. Streamlined life cycle assessment of transparent silica aerogel made by supercritical drying. Journal of Applied Energy 2012, Pages 396–404

Duffie J.A., Beckman W.A., Solar engineering of thermal processes, 3rd edition. Solar Energy Laboratory University of Wisconsin-Madison (2006)

Ebrahimpour A., Maerefat M. (2011). Application of Advanced Glazing and Overhangs in Residential Buildings. Energy Conversion and Management; (52:1); pp. 212-219.

EEW (Energy Efficiency Watch), Final Report, 2013. Improving and implementing national energy efficiency strategies in the EU framework.

EMPA material science and technology. www.empa.ch/

Enerdata, 2012. Energy Efficiency Trends in Buildings in the EU: Lessons from the ODYSSEE MURE project.

Energy Efficiency Watch, Final Report, 2013. Improving and implementing national energy efficiency strategies in the EU framework.

EnergyPlus v. 7.0.0. US Department of Energy. Energy Efficiency and Renewable Energy Office, Building Technology Program, 2011. http://apps1.eere.energy.gov/buildings/energyplus/.

EnergyPlus Energy Simulation Software, Testing and Validation, http://apps1.eere.energy.gov/ buildings/energyplus/energyplus_testing.cfm

Energy Use in the New Millennium - Trends in IEA Countries, International Energy Agency (IEA) 2007

EN ISO 10211. Thermal bridges in building construction - Heat flows and surface temperatures - Detailed calculations, 2007.

Enkvist P.A., Naucler T., Rosander J. A cost curve for greenhouse gas reduction, The Mc Kinsey Quaterly, 2007

EN Standard 15251. Indoor environmental input parameters for design and assessment of energy performance of buildings addressing indoor air quality, thermal environment, lighting and acoustics, 2007.

EN standard 15026 (2007). Hygrothermal performance of building components and building elements. Assessment of moisture transfer by numerical simulation

ESP-r, Energy Systems Research Unit University of Strathclyde. www.esru.strath.ac.uk /Programs /ESP-r

Etude socio-technico-économique du gisement de travaux de rénovation énergétique dans le secteur immobilier résidentiel – Outil de modélisation énergétique territoriale ENERTER. Direction de l'habitat, de l'urbanisme et des paysages (DHUP) 2011

Evola G., Margani G., Marletta L. Energy and cost evaluation of thermal bridge correction in Mediterranean climate, Energy and Buildings 43 (9) (2011) 2385–2393.

Fanger P. Thermal comfort: analysis and applications in environmental Engineering. United States: McGraw-Hill Book Company, 1970.

Gagge, A.P., Fobelets, A.P., Berglund, L. G. A Standard Predictive Index of Human Response to the Thermal Environment. ASHRAE Trans., Vol.92, 1986.

Gagge, A.P., Stolwijk, J. A. J., Nishi, Y. An Effective Temperature Scale Based on a Simple Model of Human Physiological Regulatory Response. ASHRAE Trans., Vol.70, 1970.

Gamez Royuela, I. (2011). Comparison of Energy Performance Rating of Dwellings in Malta Software (Eprdm) with Designbuilder: EnergyPlus Simulation Programme. Thesis: Bachelor of Industrial Engineering. University of Valladolid, Spain.

Gao Y., Roux J.J., Zhao L.H., Jiang Y.. Dynamical building simulation: A low order model for thermal bridges losses. Energy and Buildings 40 (2008) 2236–2243

Givoni B. Passive and Low Energy Cooling of Buildings. Van nostrand Reinhold, USA, 1994.

Gouda M., Underwood S.DC. Low-order model for the simulation of a building and its heating Building Services Energy Research Technology, 2000.

Groupement International d'expert sur l'Evolution du Climat. http://www.ipcc.ch/ home_languages_main_french.shtml

Guizzardi, M. Hygrothermal Performance Assessment of Novel Interior Insulation Solutions. PhD thesis. ETH-Zürich (2014). http://dx.doi.org/10.3929/ethz-a-010277871

HEAT2 version 5.02. Department of building physics, http://www.buildingphysics.com

Henninger R., Witte M., Crawley D. Analytical and comparative testing of EnergyPlus using IEA HVAC BESTEST E100–E200 test suite. Energy and Buildings, 36 (2004), pp. 855–863

Hensen, J.L.M., Djunaedy, E., Radoevi¢, M., and Yahiaoui, A., 2004. Building performance simulation for better design: Some issues and solutions. In: Proceedings of 21st Conference on Passive and Low Energy Architecture, Technische Universiteit Eindhoven, The Netherlands.

Hollands, K G. T., T. E. Unny, G. D. Raithby, and L. Konicek, Free Convection Heat Transfer Across Inclined Air Layers. Trans. ASME J. Heat Transfer, 98, 189 (1976).

Holm A., Künzel H.M. 1999. Combined effect of tem-perature and humidity on the deterioration process of insulation materials in ETICS. Proceedings of the 5th Symposium on Building Physics in the Nordic Countries, Göteborg, Vol. 2, pp. 677-684

Hopkins, A.S.; Lekov, A.; Lutz, J.; Rosenquist, G.; Gu, L. (2011). Simulating a Nationally Representative Housing Sample Using EnergyPlus. LBNL-4420E. Berkeley, CA (US): Ernest Orlando Lawrence Berkeley National Laboratory. 55 pp.

Huang L. Feasibility study of using silica aerogel as insulation for buildings. Master of Science Thesis, KTH School of Industrial Engineering and Management, Stockholm, Sweden, 2012.

HUKSEFLUX Pyranometer; retrieved from https://www.campbellsci.fr/lp02 on May 2014.

Humphreys M, Nicol J. The validity of ISO-PMV for predicting comfort votes for every-day thermal environments. Energy and Buildings, 2002.

Ibrahim M., Biwole P.H., Wurtz E., Achard P. A Study on the Thermal Performance of Exterior Walls Covered with a Recently Patented Silica-Aerogel-Based Insulating Coating. Building and Environment 81 (2014) 112-122.

Ibrahim M., Biwole P.H., Wurtz E., Achard P. Limiting windows offset thermal bridge losses using a new insulating coating. Applied Energy, 123 (2014) 220-231.

Ibrahim M., Ghaddar N., Ghali, K. Optimal location and thickness of insulation layers for minimizing building energy consumption. Journal of Building Performance Simulation, (2012) 5(6), 384-398.

Ibrahim M., Wurtz E., Biwole P.H., Achard P., Sallee H. Hygrothermal performance of exterior walls covered with aerogel-based insulating rendering. Energy and Buildings 84 (2014) 241-251

Ibrahim M., Wurtz E., Biwole P.H., Achard P. Transferring the south solar energy to the north facade through embedded water pipes. Accepted for publication. Energy (2014).

IES-VE, Integrated Environmental Solutions - Virtual Environment. www.iesve.com

IDA ICE, IDA Indoor Climate and Energy. www.equa.se/ice.

ISO 7730. Ergonomics of the thermal environment – Analytical determination and interpretation of thermal comfort using the PMV and PPD indices and local thermal comfort criteria. International Organisation for Standardization, Switzerland; 2005.

Jensen K.I., Schultz J.M., Kristiansen F.H. Development of windows based on highly insulating aerogel glazings. Journal of Non-Crystalline Solids 350 (2004) 351–357.

Jin X., Zhang X., Cao Y.,Wang G. Thermal performance evaluation of the wall using heat flux time lag and decrement factor. Energy and Buildings 47 (2012) 369–374

Johansson, P. (2011). Assessment of the Risk for Mold Growth in a Wall Retrofitted with Vacuum Insulation Panels. In Proceedings of the 9th Nordic Symposium on Building Physics, Tampere, Finland, 29 May-2 June, 2011.

Johansson, P. (2011). In situ Measurements of Facade Retrofitted with Vacuum Insulation Panels. In Proceedings of the 10th International Vacuum Insulation Symposium, Ottawa, Canada, 15-16 September, 2011.

Johannes K., Kuznik F., Jay F., Roquette P., Achard P, Berthou Y. Université Claude Bernard & ARMINES. Elément d'enveloppe d'un bâtiment et ensemble comprenant un tel élément. French Patent application, n°11 581 9414, submitted on 14 September 2011.

Jokl M, Kabele K. The substitution of comfort PMV values by a new experimental operative temperature. Electronic proceedings of Clima, WellBeing Indoors, Helsinki, Finland, 2007.

Kalamees T., Vinha J. Hygrothermal calculations and laboratory tests on timber-framed wall structures. Building and Environment 38 (2003) 689–697

Kaska Ö., Yumrutas R. Comparison of experimental and theoretical results for the transient heat flow through multilayer walls and flat roofs, Energy 33 (2008) 1816–1823.

Kaska Ö., Yumrutas R. Experimental investigation for total equivalent temperature difference (TETD) values of building walls and flat roofs. Energy Conversion and Management 50 (2009) 2818–2825.

Kipp and Zonen CMP22 and CMP11 Pyranometer. Retrieved from www.http://www.kippzonen.com/ProductGroup/3/Pyranometers on May 2014.

Kipp and Zonen CH1 pyrheliometer ; retrieved from http://www.kippzonen.com/Product/ 18/CHP-1-Pyrheliometer on May 2014

Kipp and Zonen CGR4 pyrgeometer; retrieved from www.kippzonen.com/Product/17/CGR-4-Pyrgeometer on May 2014.

Koebel M., Rigacci A., Achard P. Aerogel-based thermal superinsulation: an overview; Journal of Sol-Gel Science and Technology 63 (2012) 315-339

Kolaitis D.I., Malliotakis E., Kontogeorgos D.A., Mandilaras I., Katsourinis D.I., Founti M.A. Comparative assessment of internal and external thermal insulationsystems for energy efficient retrofitting of residential. Energy and Buildings 64 (2013) 123–131

Kontoleon K.J., Bikas D.K. The effect of south walls outdoor absorption coefficient on time lag, decrement factor and temperature variations. Energy and Buildings, 39 (2007), 1011–1018

Kontoleon K.J., Eumorfopoulou E.A. The influence of wall orientation and exterior surface solar absorptivity on time lag and decrement factor in the Greek region. Renewable Energy 33 (2008) 1652–1664.

Kontoleon K.J., Eumorfopoulou E.A. The influence of wall orientation and exterior surface solar absorptivity on time lag and decrement factor in the Greek region. Renewable Energy 33 (2008) 1652–1664

Kosny J., Kossecka E. Multi-dimensional heat transfer through complex buildings envelope assemblies in hourly energy simulation programs. Energy and Buildings (2002); pp. 34:445–54.

Kosny J., Petrie T., Yarbrough D., Childs P., Syed A.M., Blair C. Nano-Scale Insulation at Work: Thermal Performance of Thermally Bridged Wood and Steel Structures Insulated with Local Aerogel Insulation.

Kossecka E., Kosny J. Effect of insulation and mass distribution in exterior walls on dynamic thermal performance of whole buildings. Proceedings Thermal Performance of the Exterior Envelopes of Buildings, 1998.

Kossecka E., Kosny J. The influence of insulation configuration on heating and cooling loads in a continuously used building, Energy and Buildings 34 (2002) 321–331.

Krauss G. Etude experimentale des transferts de chaleur entre un batiment et son environment: conception, realization, instrumentation d'une cellue test. PhD thesis, University P. & M. Curie, Paris, 1985.

Kunzel H.M. Simultaneous heat and moisture transport in building components. PhD Thesis, Fraunhofer Institute of Building Physics, 1995.

Kunzel H.M., K. Kießl, and M. Krus. 1995. Moisture in exposed building components. Proceedings of the international symposium on moisture problems in building wall, Porto, pp. 258-266.

Künzel H.M., Kießl K. 1996. Drying of brick walls after impregnation. Internationale Zeitschrift für Bauin- standsetzen 2 H.2, S., pp. 87-100

Kusuda, T. Early history and future prospects of buildings system simulation. In Proceeding of Building Simulation, IBPSA 1999.

LARET L. Contribution au développement de modèles mathématiques du comportement thermique transitoire des structures d'habitation. PhD Thesis, LIEGE University, 1980.

Mantha, P., & Arena, L. B. (2012). A Systematic Approach to Hygrothermal Modeling and Compliance With Failure Criteria Using WUFI®.5th National Conference of IBPSA-USA, Madison, Wisconsin, August 2012

Manz H., Loutzenhiser P., Frank T., Strachan P.A., Bundi R., Maxwell G. Series of experiment for empirical validation of solar gain modeling in building energy codes – experimental setup, test cell, characterization, specifications and uncertainty analyses. Building and Environment, 41 (2006), pp. 1784–1797

MARTI A., RIGNAC J.P. Méthode de résolution du système différentiel utilise par le simulateur thermique de stratege. Technical report, EDF, 1991.

MATLAB v. R2011a. The MathWorks Inc., Natick, Massachusetts: 2011. http://www.mathworks .com/

Mavromatidis L.E., EL Mankibi M., Michel P., Santamouris M. Numerical estimation of time lags and decrement factors for wall complexes including Multilayer Thermal Insulation, in two different climatic zones. Applied Energy 92 (2012) 480–491

McAdams WH. Heat transmission. 3rd edition, NewYork: McGraw-Hill (1954)

Mechri HE., Capozzoli A., Corrado V. Use of the ANOVA approach for sensitive building energy design. Applied Energy 87 (2010) 3073–83.

MODELISAR, Functional Mock-up Interface. https://www.fmi-standard.org/.

NF EN 12667. Thermal performance of building materials and products - Determination of thermal resistance by means of guarded hot plate and heat flow meter methods - Products of high and medium thermal resistance.

Nayak J.K, Sukhatme S.P., Limaye R.G., Bopshetty S.V. Performance studies on solar concrete collectors. Solar Energy, 42 (1) (1989) 45–56.

NF EN 1159-3. Advanced technical ceramics - Ceramic composites, thermophysical properties - Part 3: determination of specific heat capacity.

NF EN 1602 standard. Thermal insulating products for building applications - Determination of the apparent density.

NF EN ISO 12572. Performance hygrothermique des matériaux et produits pour le bâtiment - Détermination des propriétés de transmission de la vapeur d'eau

NF EN ISO 8130-2. Poudres pour revêtement - Partie 2 : détermination de la masse volumique à l'aide d'un pycnomètre à gaz (méthode de référence)

NF EN ISO 12571. Performance hygrothermique des matériaux et produits pour le bâtiment - Détermination des propriétés de sorption hygroscopique

Nielsen T. Simple tool to evaluate energy demand and indoor environment in the early stages of building design. Solar Energy, 2005.

Ozel M., Pihtili K. Optimum location and distribution of insulation layers on building walls with various orientations, Building and Environment 42 (2007) 3051–3059.

Ozel M. The influence of exterior surface solar absortivity on thermal characteristics and optimum insulation thickness. Building and Environment, 39 (2012), pp. 347–355

Ozel M. Thermal performance and optimum insulation thickness of building walls with different structure materials. Applied Thermal Engineering 31 (2011) 3854–3863

Pajonk G., Elalouie E., Begag R., Durant M., Chevalier B., Chevalier J.L., Achard P. UNIVERSITE CLAUDE BERNARD - LYON I, PRODUITS CHIMIQUES AUXILIAIRES ET DE SYNTHESE, ARMINES, CENTRE SCIENTIFIQUE ET TECHNIQUE DU BATIMENT. Procédé pour la fabrication d'aérogels de silice monolithiques et aérogels de silice ainsi obtenus. Inventeurs. Patent U7-B-12.940 FR, France, n° 95.08573.

Pajonk G., Elalouie E., Begag R., Durant M., Chevalier B., Chevalier J.L., Achard P.; inventors (Université Claude Bernard - Villeurbanne, Produits Chimiques Auxiliaires- Longjumeau, Armines, Centre Scientifique et Technique du Bâtiment). Process for the preparation of monolithic silica aerogels. United States Patent n° 5-795-557, August 18, 1998.

Pulsonic Anemometer ; retrieved from http://www.pulsonic.net/combo-vent/alizia-147-capteur-combine-vitesse-et-direction-du-vent/id menu-84.html on May 2014.

Reim M., Beck A., Korner W., Petricevic R., Glora M., Weth M., Schliermann T., Fricke J., Schmidt C.H. and Potter F.J. Highly insulation aerogel glazing for solar energy use. Solar Energy Vol. 72, No. 1, pp. 21–29, 2002.

Reim M., Korner W., Manara J., Korder S., Arduini-Schuster M., Ebert H.P., Fricke J. Silica aerogel granulate material for thermal insulation and daylighting. Solar Energy 79 (2005) 131–139

RICHALET V. Caracterisation energetique des bâtiments sur site. Identification de modeles dynamiques. Methodes de signature Energetique. Thèse de doctorat, INPG, 1991.

Roucoult J.M., Douzane O., and Langlet T. Incorporation of thermal inertia in the aim of installing a natural nighttime ventilation system in buildings. Energy and Buildings, 29(2) :129 – 133, 1999.

Roux J.J. Proposition de modèles simplifiés pour l'étude du comportement thermique des bâtiments. PhD thesis, INSA Lyon, 1984.

Sarak H., Satman A. The degree-day method to estimate the residential heating natural gas consumption in Turkey: a case study; Energy (2003)

Shwarz B. Heat and material transfer in outdoor wall surfaces. Thesis dissertation. University of Stuttgart (1971).

Sisman N., Kahya E., Aras N., Aras H. Determination of optimum insulation thicknesses of the external walls and roof (ceiling) for Turkey's different degree-day regions, Energy Policy 35 (2007) 5151–5155.

Soleimani Dorcheh A. Silica aerogel: synthesis, properties and characterization. Journal of Materials Processing Technology, 2007.

Spaceloft® Safety Data Sheet, Retrieved February 09, 2011, from http://www.aerogel.com/products/pdf/Spaceloft_MSDS.pdf.

Srivastava A., Hussain S.Q., Sharma B.N., Tiwari G.N. Thermal performance of ground as an inexpensive solar collector and storage system. Energy Conversion and Management, 22 (3) (1982) 197–204

Stahl Th., Brunner S., Zimmermann M., Ghazi-Wakili K. Thermo-hygric properties of a newly developed aerogel based insulation rendering for both exterior and interior applications. Energy and Buildings 44 (2012) 114–117.

Stoops J. A possible connection between thermal comfort and health, paper LBNL 55134. Lawrence Berkeley National Laboratory. University of California; 2004.

Straube J.F., Smegal J. Building America Special Research Project: High-R Walls Case Study Analysis. Research Report – 0903. Somerville, MA: Building Science Corporation (2009).

Sun C., Shu S., Ding G., Zhang X., Hu X. Investigation of time lags and decrement factors for different building outside temperatures. Energy and Buildings 61 (2013) 1–7

TAASI. www.taasi.com/apps.htm (2011, date of last access).

Taxe d'habitation, FICHIER DU LOGEMENT COMMUNAL (FILOCOM) 2009.

Theodosiou T.G., Papadopoulos A.M. The impact of thermal bridges on the energy demand of buildings with double brick wall constructions, Energy and Buildings 40 (2008) 2083–2089.

Tian W., Zuo W. Literature review and research needs to couple building energy and airflow simulation. APEC Conference on Low-carbon Towns and Physical Energy Storage, Changsha, China 2013.

Trčka, M. Co-simulation for Performance Prediction of Innovative Integrated Mechanical Energy Systems in Buildings. Thesis (PhD). Eindhoven University of Technology, Eindhoven, The Netherlands, 2008.

Trčka, M., Hensen, J. L., & Wetter, M. (2009). Co-simulation of innovative integrated HVAC systems in buildings. Journal of Building Performance Simulation, 2(3), 209-230.

Trčka, M. and Hensen, J. (2006) "Model and tool requirements for co-simulation of building performance". In: Proceedings of Proceedings of the 15th IASTED Int. Conf. on Applied Simulation and Modelling, pp. 26-28.

Trčka, M., Wetter, M. and Hensen, J. (2007) "Comparison of co-simulation approaches for building and HVAC/R system simulation", Proceedings of the Building Simulation 2007, 1418-1425.

TRNSYS, A Transient System Simulation Program, Solar Energy Laboratory, University of Wisconsin, Madison. http://sel.me.wisc.edu/trnsys/.

Tronchin L., Fabbri K. A round Robin test for buildings energy performance in Italy. Energy and Buildings, 42 (2010), pp. 1862–1877

Tsilingiris P.T. Wall heat loss from intermittently conditioned spaces- The dynamic influence of structural and operational parameters, Energy and Buildings 38 (2006) 1022–1031.

Typologie des bâtiments d'habitation existant en France. Direction de l'habitat, de l'urbanisme et des paysages (DHUP) 2007.

Ulgen K. Experimental and theoretical investigation of effects of wall's thermo- physical properties on time lag and decrement factor. Energy and Buildings 34 (2002) 273–278.

UNEP (United Nations Environment Programme), 2012. State of play of sustainable building in France 2012. Retrieved from http://www.unep.org/sbci/pdfs/SoPFrance-Final.pdf on September 2014.

Vaisala , Vaisala Hygrothermal sensor ; retrieved from http://www.vaisala.fr/fr/lifescience/ products/ probes/Pages /HMP110.aspx on May 2014

VDI Richtlinie 6020. 2001. Anforderung an Rechenverfahren zur Gebäude- und Anlagensimulation. Düsseldorf, Berlin: VDI-Verlag GmbH.

Verbeeck G., Hens H. Energy savings in retrofitted dwellings: economically viable? Energy & Building – 2004

Vijayalakshmi M.M., Natarajan E., Shanmugasundaram V., Thermal behavior of building wall elements, Journal of Applied Sciences 6 (2006) 3128-3133.

Walton, G. N. 1983. Thermal Analysis Research Program Reference Manual. NBSSIR 83-2655. National Bureau of Standards, p. 21.

Wang, Z.; Yi, L.; Gao, F. (2009). Night Ventilation Control Strategies in Office Buildings. Solar Energy; (83:10); pp. 1902-13

Wetter, M. and Haves, P., 2008. A modular building controls virtual test bed for the integration of heterogeneous systems. In: Proceedings of SimBuild, 3rd National Conference of IBPSA-USA Bekeley, CA, USA: International Building Performance Simulation Association, USA chapter.

Windsonic Gill 2D WS1 anemometer; retrieved from http://www.gillinstruments.com/products/ anemometer/windsonic.htm on May 2014.

Wong, S.L., Wan, K.K.W., Lam, T.N.T. (2010). Artificial Neural Networks for Energy Analysis of Office Buildings with Daylighting. Applied Energy; (87:2); pp. 551-557.

Wurtz E. and Ibrahim M. Bâtiment intégrant un dispositif de régulation thermique, dispositif et procédé de régulation associés. French Patent application 1359334 submitted on September 27th, 2013.

Zayane C. Identification d'un modèle de comportement thermique de bâtiment à partir de sa courbe de charge. PhD Thesis, École nationale supérieure des mines de Paris, 2011.

Zhai, Z., Chen, Q., Haves, P. and Klems, J.H. (2002) "On approaches to couple energy simulation and computational fluid dynamics programs", Building and environment, 37, 857-864.

Zhai, Z. and Chen, Q.Y. (2003) "Solution characters of iterative coupling between energy simulation and CFD programs", Energy and Buildings, 35, 493-505.

ANNEXES

Annex A: Experimental Test cell in Sophia Antipolis

- Test cell: Geometry and construction materials

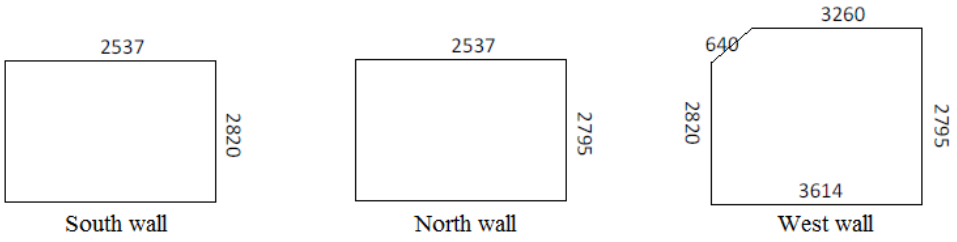

Wall	Area (m²)
South	7,15
North	7,09
East / West	11,70
Ground	9,17
south Ceiling	1,62
north Ceiling	8,27

Volume : 29,68 m^3

Fig. A1: Geometry of the Test cell in Sophia Antipolis

Table A1: Test cell construction materials thermo-physical properties

wall	material	thickness (m)	thermal conductivity ($W.m^{-1}.K^{-1}$)	specific heat ($J.kg^{-1}.K^{-1}$)	density ($kg.m^{-3}$)
south wall	plaster	0,013	0,32	800	790
	glass wool	0,16	0,041	840	12
	concrete	0,25	2,1	800	2400
east wall	plaster	0,013	0,32	800	790
	glass wool	0,16	0,041	840	12
	wooden plate	0,019	0,18	1700	780
	expanded polystyrene	0,08	0,04	1380	25
west wall (partition)	plaster	0,013	0,32	800	790
	glass wool	0,16	0,041	840	12
	plaster	0,013	0,32	800	790
north wall (partition)	plaster	0,013	0,32	800	790
	glass wool	0,16	0,041	840	12
	concrete	0,25	2,1	800	2400
	Mousse phénol-formol	0,077	0,032	1255	32
roof	plaster	0,013	0,32	800	790
	glass wool	0,16	0,041	840	12
	wooden plate	0,018	0,18	1700	780
ground	tiles	0,015	1	1000	2400
	concrete	0,15	2,1	800	2400
	expanded polystyrene	0,08	0,04	1380	25

Annex B: Experimental Test cell Hygrothermal Performance – Sensitivity of the results on some input variables

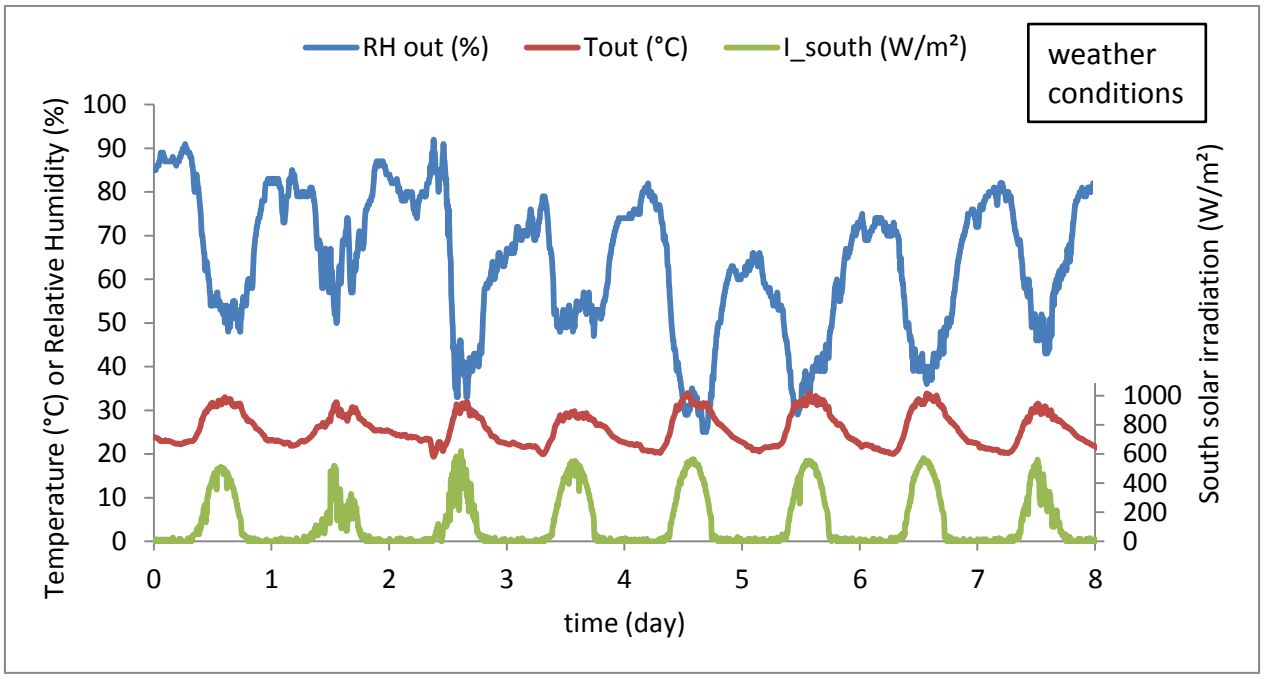

(a)

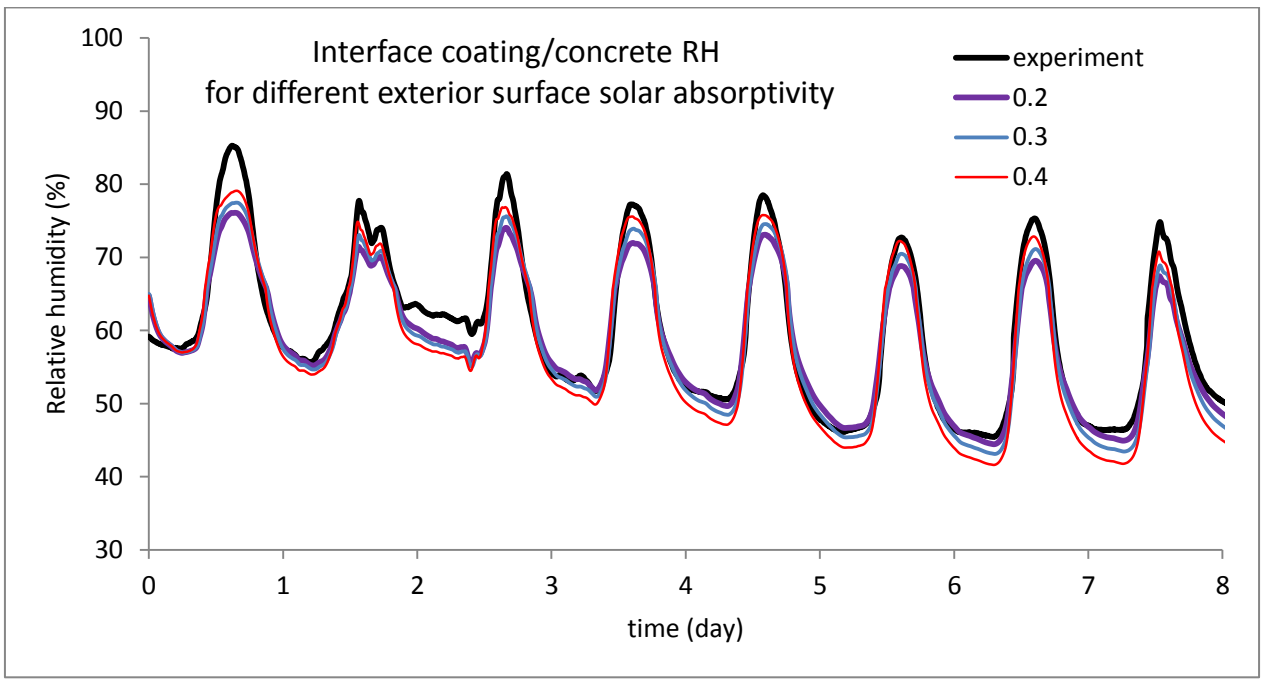

(b)

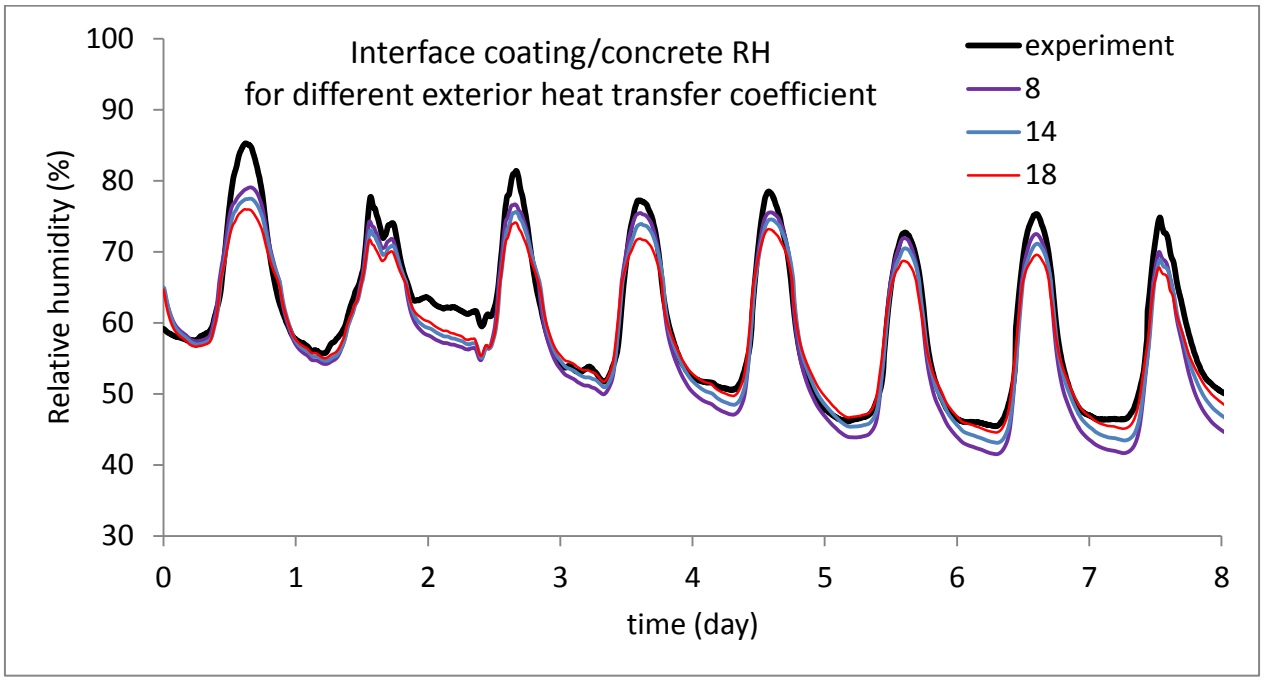
Interface coating/concrete RH
for different exterior heat transfer coefficient
experiment
8
14
18
Relative humidity (%)
100
90
80
70
60
50
40
30
0
1
2
3
4
5
6
7
8
time (day)

(c)

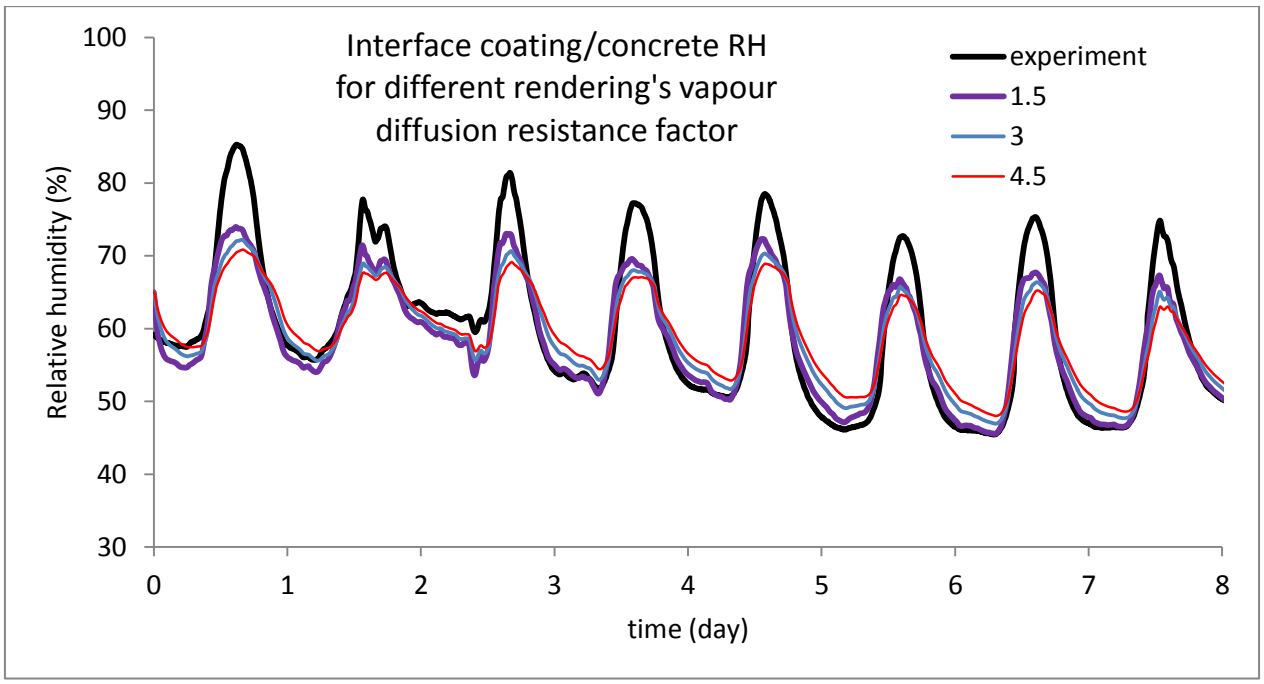
Interface coating/concrete RH
for different rendering's vapour
diffusion resistance factor
experiment
1.5
3
4.5
Relative humidity (%)
100
90
80
70
60
50
40
30
0
1
2
3
4
5
6
7
8
time (day)

(d)

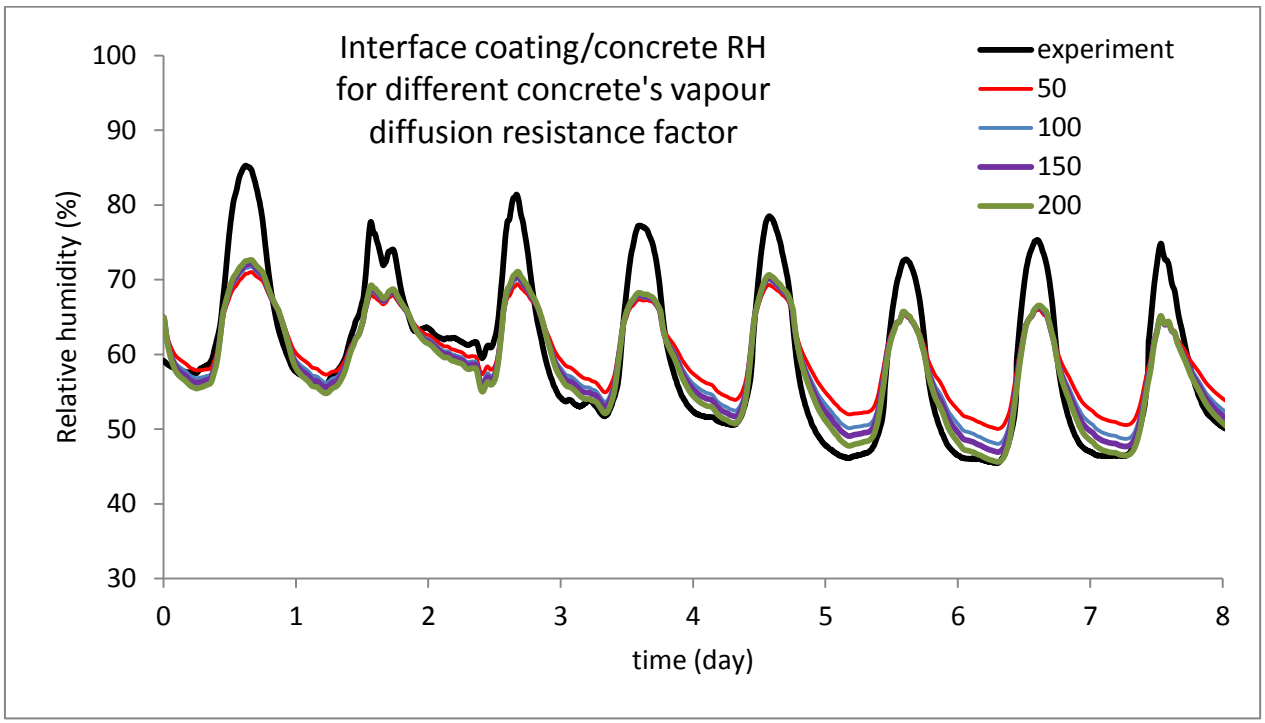

(e)

Fig. B1 (a-e) : Experimental Test cell Hygrothermal Performance – (a) weather data and (b-e) Sensitivity of the relative humidity at the interface coating/concrete for different (b) exterior surface solar absorptivity, (c) exterior heat transfer coefficient, (d) rendering's vapour diffusion resistance factor, and (e) concrete's vapour diffusion resistance factor

Annex C: INCAS Experimental House

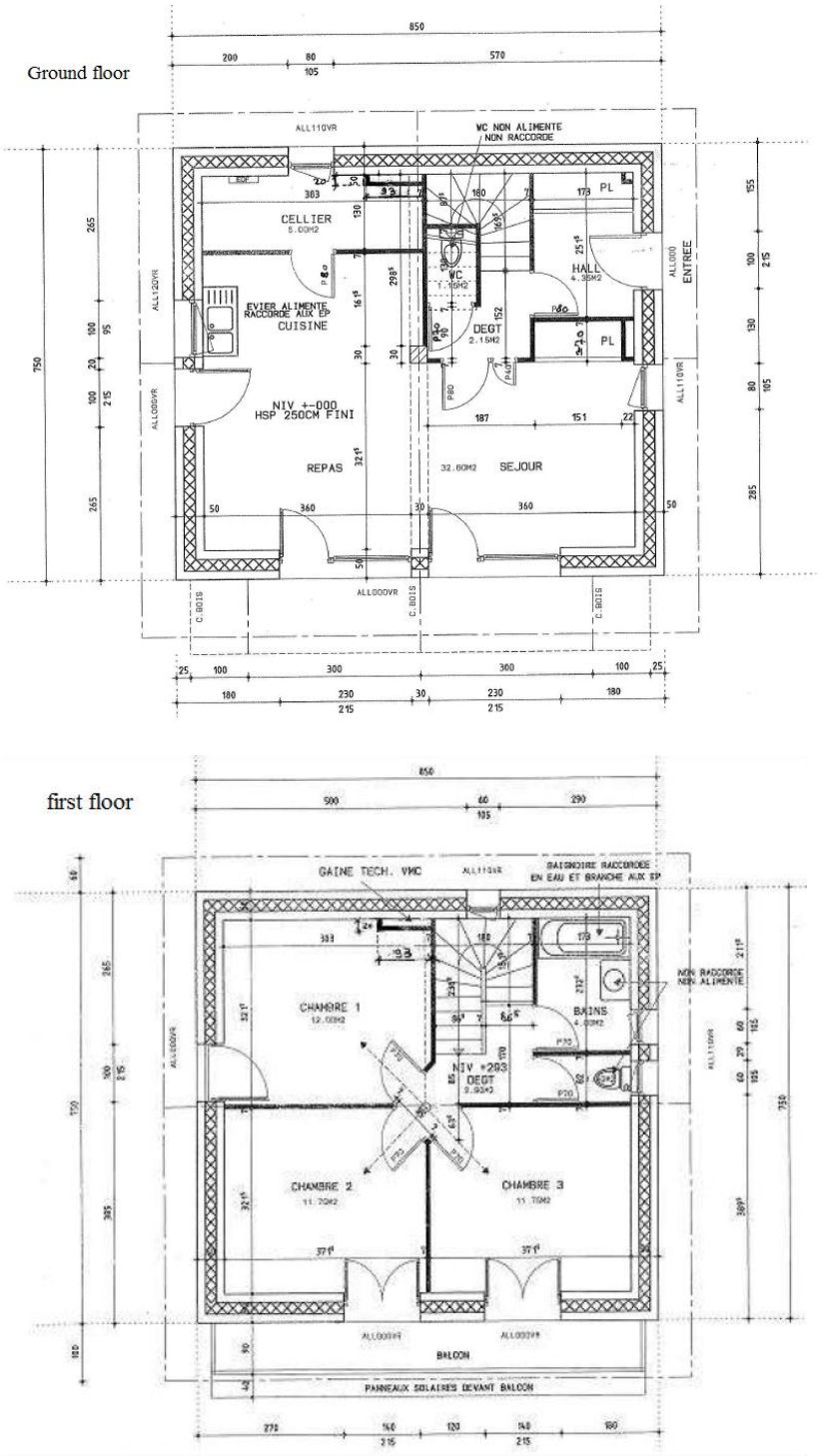

Fig. C1: Experimental INCAS house floor plans

Table C1: INCAS house construction materials properties

element	Construction	Thickness (cm)	Thermal Conductivity (W/m.K)	Specific Heat (J/kg.K)	Density (kg/m^3)
Roof	Brick tiles	1.5	0.7	1059	1700
	Wood framing	1	0.16	2400	500
Ground Stage : Floor	Extruded Polystyrene	16	0.031	1200	20
	Reinforced concrete slab	20	2	1000	2500
Ground Stage : Ceiling	Concrete Block (Hourdis)	16	1.23	648	1300
	Concrete slab	4	2	1000	2500
	Concrete screed	8	1.75	880	2200
First Stage : Ceiling	OSB	2.2	0.13	1700	650
	Glass Wool	44	0.035	840	12
Windows	Double glazed: U_value = 1.4 W/(m^2.K) Triple glazed: U_value = 1.28 W/(m^2.K)				
Exterior Walls	Brick-monomur	42	0.115	986	700
	Insulating Coating	4	0.0267	990	150

Annex D: Hygrothermal properties of the materials used in the WUFI simulations

- Basic properties

Table D1: Hygrothermal properties

	Bulk density (kg/m^3)	Porosity (m^3/m^3)	Specifi heat [J/kg.K)]	Thermal conductivity (dry – 10°C) [W/(m.K)]	Water vapour diffusion resistance factor (-)
Plaster	850	0.65	850	0.2	8.3
Polystyrene	15	0.95	1500	0.04	30
Concrete	2300	0.18	850	1.6	180
Brick	600	0.77	850	0.12	16
Aerogel based coating	156	0.98	990	0.0268	4.25
Exterior stucco	1900	0.24	850	0.8	25

- Moisture storage functions

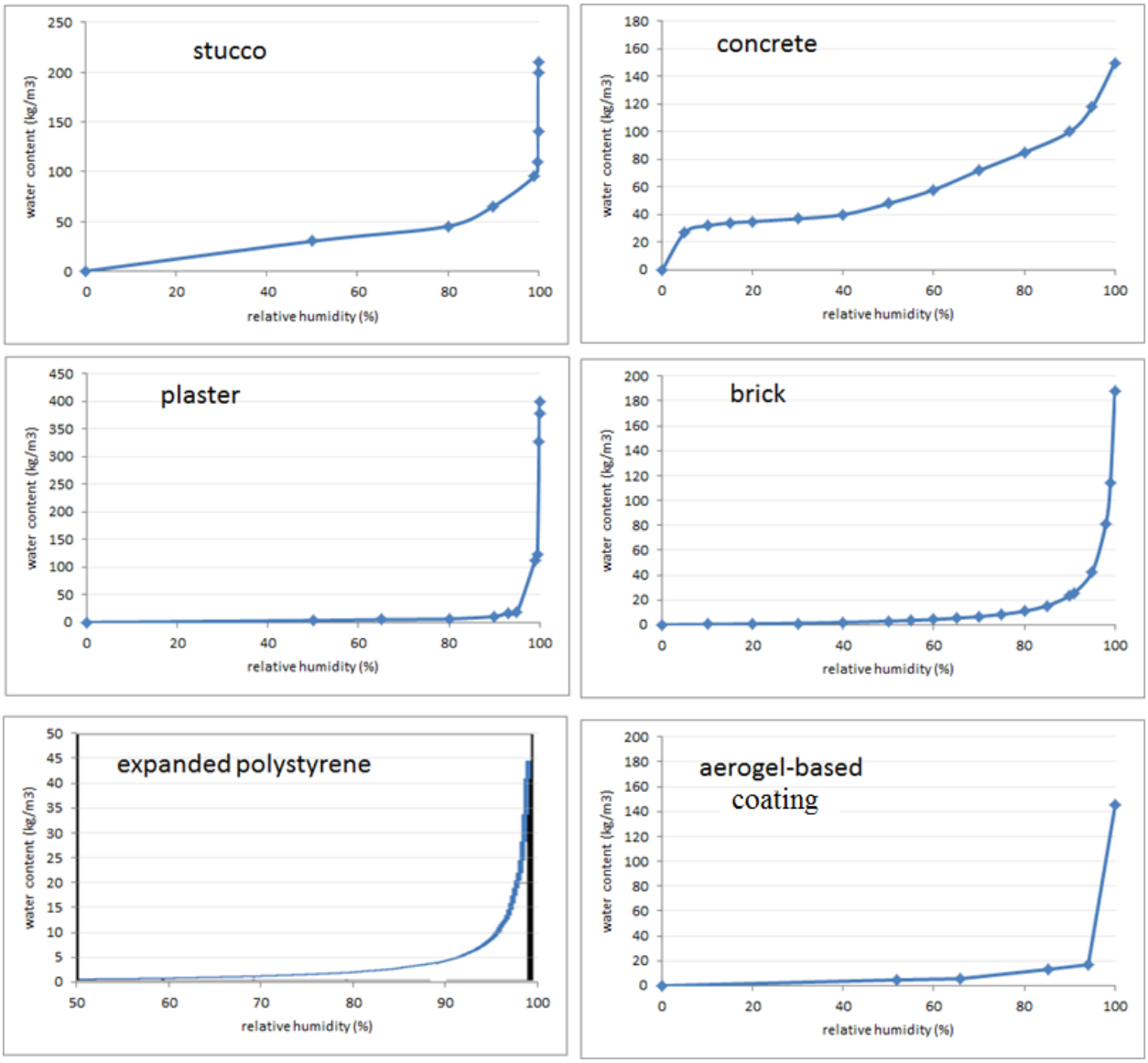

Fig. D1: Moisture storage functions for the different materials used in WUFI simulations

Annex E: Rapid Assessment Tool (RAT) Graphical User Interface

(a)

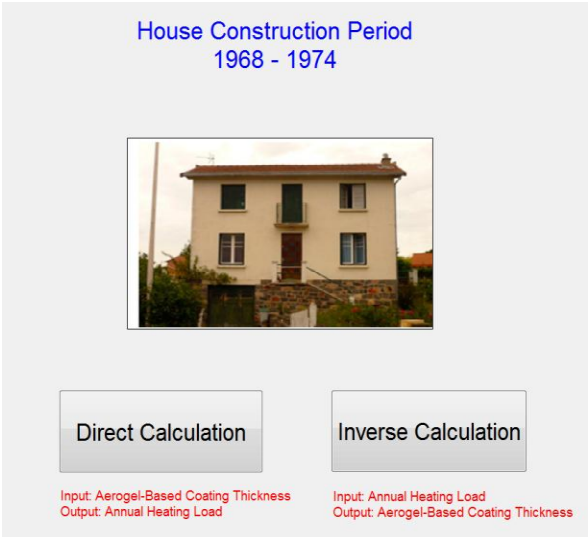

(b)

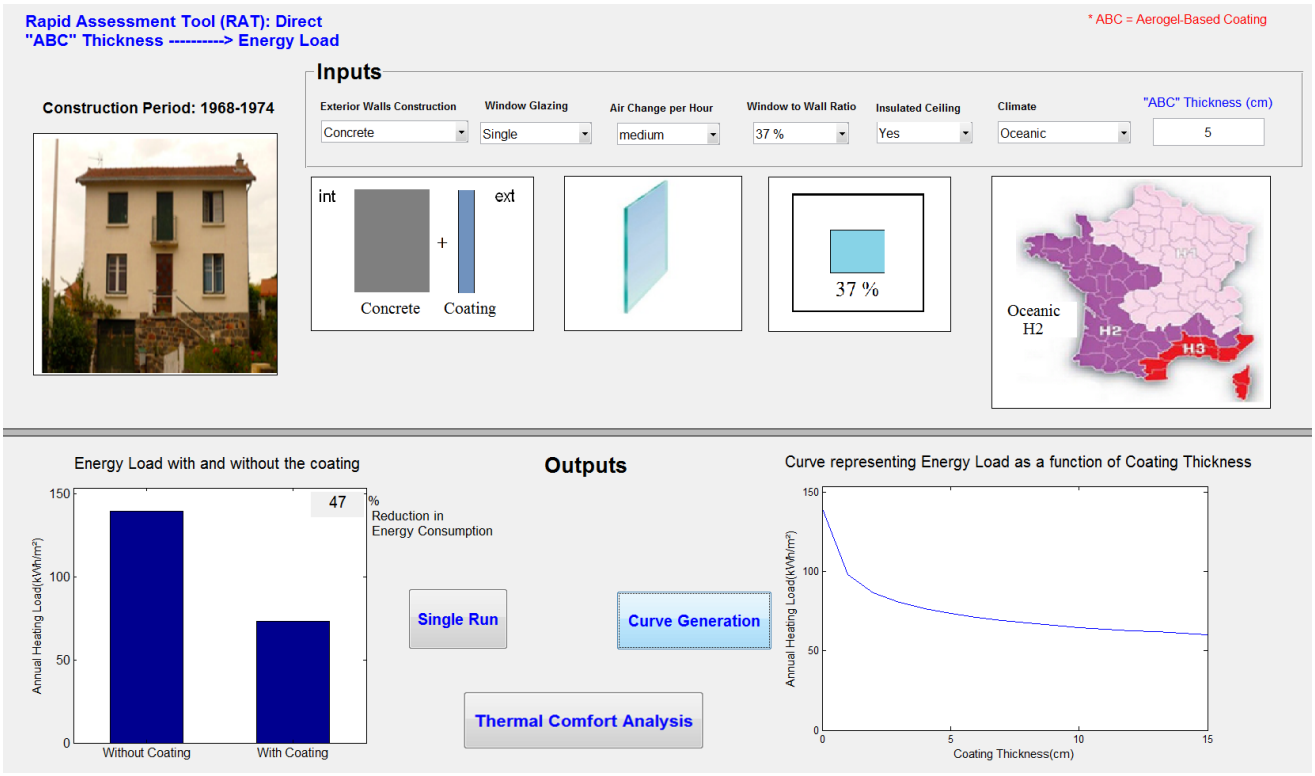
Rapid Assessment Tool (RAT): Direct
"ABC" Thickness ----------> Energy Load
* ABC = Aerogel-Based Coating
Inputs
Construction Period: 1968-1974
Exterior Walls Construction
Concrete
Window Glazing
Single
Air Change per Hour
medium
Window to Wall Ratio
37 %
Insulated Ceiling
Yes
Climate
Oceanic
"ABC" Thickness (cm)
5
int
ext
Concrete
Coating
37 %
Oceanic
H2
H1
H2
H3
Energy Load with and without the coating
Annual Heating Load(kWh/m²)
Without Coating
With Coating
47
% Reduction in Energy Consumption
Outputs
Single Run
Curve Generation
Thermal Comfort Analysis
Curve representing Energy Load as a function of Coating Thickness
Coating Thickness(cm)

(c)

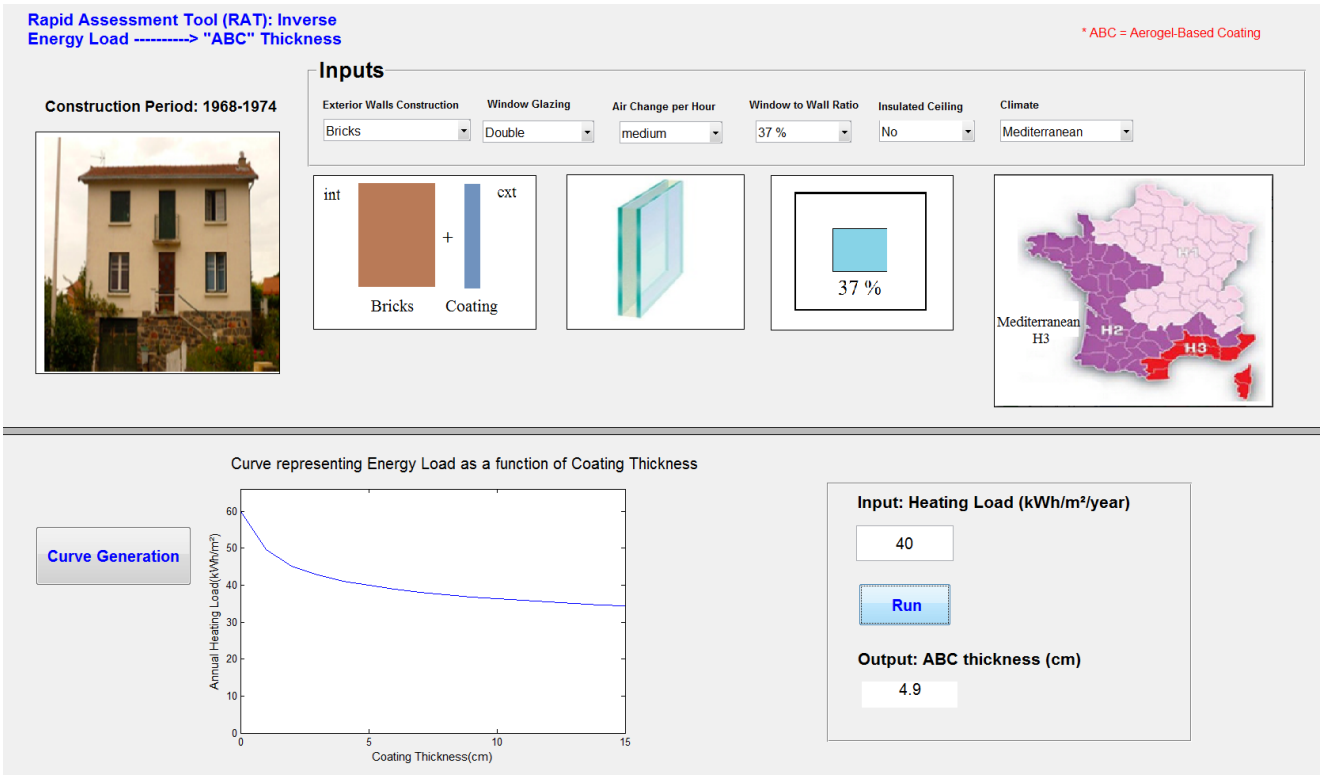
Rapid Assessment Tool (RAT): Inverse
Energy Load ----------> "ABC" Thickness
* ABC = Aerogel-Based Coating
Inputs
Construction Period: 1968-1974
Exterior Walls Construction
Bricks
Window Glazing
Double
Air Change per Hour
medium
Window to Wall Ratio
37 %
Insulated Ceiling
No
Climate
Mediterranean
int
cxt
Bricks
Coating
37 %
Mediterranean
H3
H1
H2
H3
Curve representing Energy Load as a function of Coating Thickness
Curve Generation
Annual Heating Load(kWh/m²)
Coating Thickness(cm)
Input: Heating Load (kWh/m²/year)
40
Run
Output: ABC thickness (cm)
4.9

(d)

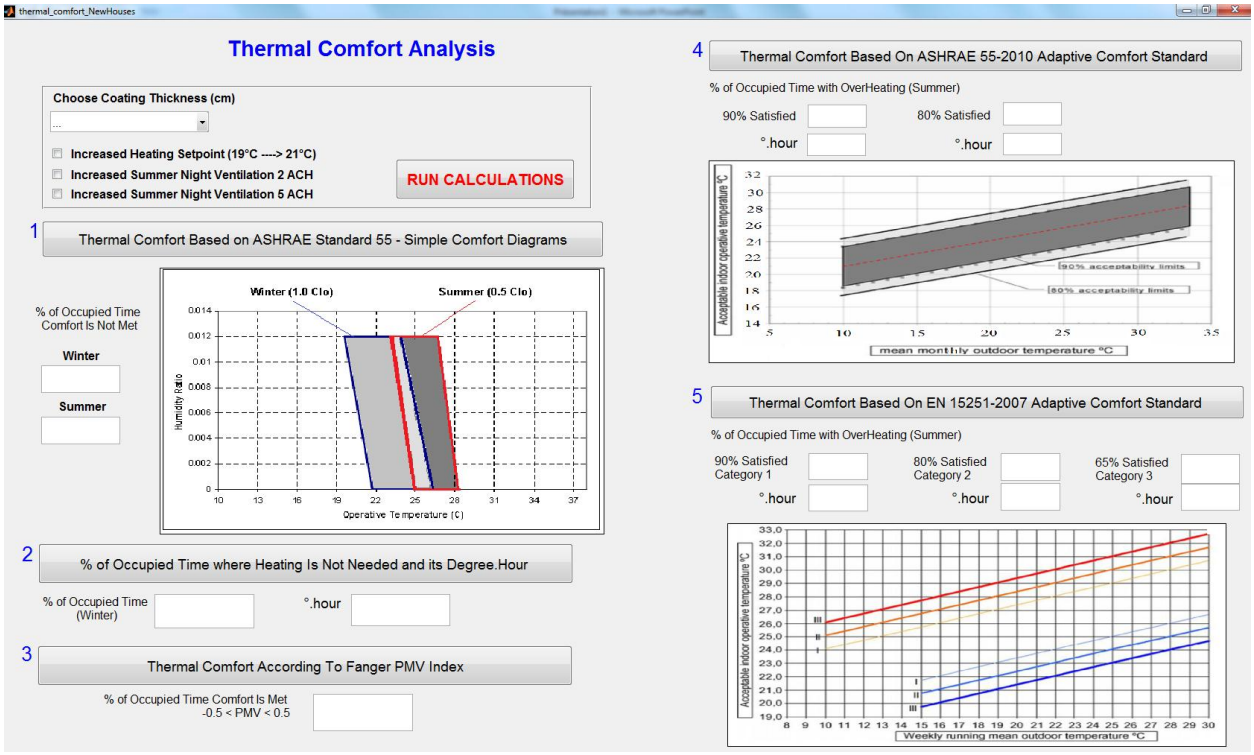

(e)

Fig. E1 (a-e): Rapid Assessment Tool screen shots

Etude de l'amélioration de la performance énergétique de bâtiments due à l'emploi d'enduit minéral à fort pouvoir isolant

RESUME : En France, le secteur du bâtiment est le plus grand consommateur d'énergie et représente environ 43% de la consommation totale d'énergie. L'isolation thermique dans le bâtiment est nécessaire afin d'améliorer son efficacité énergétique. Dans certains pays dont la France, la rénovation des bâtiments occupe une place essentielle dans la stratégie de transition énergétique. La stratégie mise en place consiste donc à renforcer l'isolation thermique des enveloppes de bâtiment et ceci en perdant le moins de surface habitable possible. Ceci justifie le fait de développer et de mettre en œuvre à l'avenir des matériaux super isolants comme les aérogels. Les objectifs de cette étude sont d'examiner le comportement thermique des bâtiments et d'étudier l'amélioration possible de leur efficacité énergétique en utilisant un nouvel enduit isolant à base d'aérogels de silice et ainsi que l'énergie solaire. Tout d'abord, la performance thermique et hygrothermique des murs extérieurs est étudiée afin de trouver la meilleure structure de ces murs. Deuxièmement, nous étudions l'évolution du confort thermique et du comportement énergétique des maisons en adoptant le nouvel enduit isolant comme isolation extérieure. Cette évolution a aussi été représentée par un modèle mathématique. On a comparé les résultats obtenus à l'aide de ces modèles avec les mesures expérimentales faites sur une maison récemment construite. Enfin, le potentiel de réduction de la charge de chauffage en adoptant un système actif dans la paroi est analysé. Ce système est proposé pour capter une partie de l'énergie solaire qui tombe sur la façade sud et qui est disponible pendant les journées non nuageuses en hiver, et la transférer vers la façade nord par l'intermédiaire de canalisations d'eau intégrées dans l'enduit isolant objet de l'étude.

Mots clés : Enduit isolant à base d'aérogels; systèmes d'isolation par l'extérieur; simulation thermique-dynamique des bâtiments; analyse hygrothermique; confort thermique; façade active

Improving the building envelopes energy performance using aerogel-based insulating mineral rendering

ABSTRACT : In France, the building sector is the largest consumer of energy and accounts for about 43% of the total energy consumption. The building sector offers significant potential for improved energy efficiency through the use of high-performance insulation and energy-efficient systems. For existing buildings, renovation has a high priority in France because these buildings represent a high proportion of energy consumption and they will be present for decades to come. Nowadays, there is a growing interest in the so-called super-insulating materials, such as Aerogels. The objectives of this study are to examine the thermal behavior of buildings and to foster energy efficiency through the use of a newly developed aerogel-based insulating coating as well as the use of renewable energy sources, specifically solar energy. Firstly, the thermal and hygrothermal performance of exterior walls having different layer composition structures are examined. Secondly, the heating energy demand as well as the risk of summer overheating is examined for different construction periods and under different climates. Also, a mathematical model is built and compared to experimental measurement of a recently built full-scale house. Finally, the potential to decrease the heating load by adopting a closed wall loop system is scrutinized. The latter is a proposed system to capture some of the solar energy falling on the south facade available during non-cloudy winter days and transfer it to the north facade through water pipes embedded in the aerogel-based coating.

Keywords : Aerogel-based insulating coating; exterior insulation systems; building energy simulation; hygrothermal assessment; thermal comfort; embedded-pipe envelopes

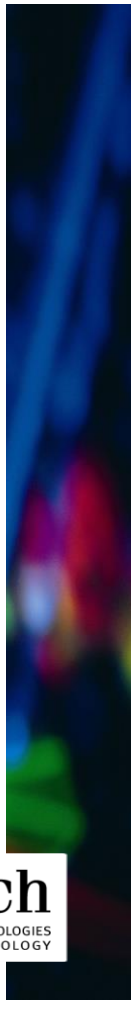

MINES ParisTech

ParisTech
INSTITUT DES SCIENCES ET TECHNOLOGIES
PARIS INSTITUTE OF TECHNOLOGY